Enhancing the Seismic Performance of Dou-Gon Systems in Traditional Timber Structures

Xie, Wenjun

Award date:
2019

Awarding institution:
University of Bath

Enhancing the Seismic Performance of Dou-Gon Systems in Traditional Timber Structures

By

Wenjun Xie

A thesis submitted for the degree of Doctor of Philosophy

University of Bath

Department of Architecture and Civil Engineering

Feb 2019

-COPYRIGHT-

Acknowledgements

First of all, I would like to express my respectful appreciation to my supervisor, Dr Wen-Shao Chang, he has supported me with research suggestions, profound structural engineering knowledge and encouragement throughout the past year of my PhD research life. I would also like to thank Dr. Giorgia Giardina for her assistance after Dr. Wen-Shao Chang left University of Bath.

Beside my supervisors, I would like to thank Prof. Yoshikazu Araki, for his patience, insightful comments and encouragement. His invaluable advice and feedback helped me improve my thesis a lot.

Special thanks to Mr. William Bazeley who organised my experiments and ensured that all machines were functioning optimally. I am also hugely appreciative to Mr. Steve Handley and Mr. Robert Dyer for manufacturing the testing specimens. The experiments would not be successful without all the support I received from the laboratory.

I would like to thank the Graduate Office who approved the two years' extension of my PhD study after I delivered my daughter which helped me to cope with stress of looking after my daughter during my PhD life.

Last but not the least, I would like to take this opportunity to express my gratitude to my family: my parents and my sister in China, my hunsband, Zhan Shi, and my daughter, Charlotte Qianran Shi, for supporting my spiritually throughout writing this thesis and my life in general.

Abstract

Traditional timber structures such as temples, traditional palace halls and estates that widely distributed in mainland China, Japan, Taiwan and various other regions of Asia are suffering from earthquakes. However, the research efforts have been scarcely seen on the techniques for enhancing the seismic performance of historic timber buildings with the Dou-Gon system. This study developed a technique to enhance the seismic performance of traditional timber buildings with the Dou-Gon system. High-strength steel bars and super-elastic alloy bars are used in this study to substitute conventional Dou-Gon system that uses wooden pegs to connect Dou and the lower structure.

In this thesis, the material characterisation of super-elastic alloy is studied by the axial quasi-static loading and dynamic cyclic loading. The results of experiments found that the Cu-Al-Mn super-elastic alloy has a great damping capacity and exceptional recentring capability. The cyclic results demonstrate that the equivalent damping ratio increases with the increase of the loading frequency. Pre-straining of the super-elastic alloy showed a better damping effect compare to the non-prestrained super-elastic alloy. However, when the self-heating temperature becomes the primary governing factor, the equivalent damping ratios slightly reduces with the increase of the loading frequency.

The research is based on the analysis of a two-layer Dou-Gon set from an ancient structure called Qinghui Hall at the Weiyuan Temple in Henan province, China. A full scaled specimen was made by glued laminated timber. Static pushover tests and dynamic shaking table tests were carried out under different loading conditions. The factors discussed in this study include vertical load imposed on the Dou-Gon system and the pre-strained levels of super-elastic bars. Analytical models have been built using the software Open System for Earthquake Engineering Simulation (OpenSEES). The parametric study has been carried out and the output acceleration spectrums have been recorded by inputting full scaled seismic waves. The results from static push over, dynamic tests and parametric study have shown that the simple technique with super-elastic alloy enhances the energy dissipation capacity, stiffness and the ultimate strength of the Dou-Gon system. Dou-Gon system with super-elastic alloy bar connections also show a better anti-seismic performance due to its constant damping behaviour and longer fatigue life. Moreover, pre-strain of super-elastic alloy bars can also increase the damping ratios of Dou-Gon system and lead to a greater energy dissipation, not only during the main earthquake shock but also for several aftershocks.

Content

List of Figures

List of Tables

Chapter 1 Introduction

1.1 Background and Motivation

1.1.1 History of traditional timber structures

Traditional timber structures such as temples, traditional palace halls and estates are widely distributed in mainland China, Japan, Taiwan and various other regions of Asia. The history of traditional timber structures can be traced back to B.C. 1300, Zhou Dynasty of China. At that time, the load-bearing structure was made of rammed earth, while timber frames were used to reinforce the structure. The relics of Mingtang (the hall for the King's sacrificial ceremony), originally built in Tang Dynasty in China, was excavated in 1986 at Luoyang, China. In contrast to the earlier structures, the restored building showed the structure was merely made of timber without using rammed earth for load bearing. This structure of Mingtang proved that people already had the mature skills to build robust timber structures during the Tang Dynasty in China.

Tailiang and Chuandou (Figure 1) are the two main classifications of oriental timber structures systems with locations both north and south of the Yangtze River, respectively. The Chuandou structure shows in Figure 1 is part of a private historical house in Taiwan. The front façade of the Main Hall of Foguang Temple in Shanxi, China illustrates Tailiang structure (Figure 1). In Tailiang timber structures, the weight of the roof is transferred from purlins to beams and then to columns. However, the columns in Chuandou timber structures are connected with purlins directly. These structures, made of timber frames, are characterised by the absence of nails and the use of mortise and tenon joints. The mortise and tenon joint shows a semi-rigid behaviour (Fang, 2001) because the natural frequency of the structure increased by strengthening mortise and tenon joints and Dou-Gon of the structure. In contrast to the mortise and tenon joint, the natural frequency stay constant when the stiffness of the roof increased as the roof is stiff enough and further reinforcement cannot change its relative stiffness significantly. King et al. (1996) also found that the mortise and tenon joint is a semi-rigid connection and is the weak point of the structure, due to the P-Δ effect. Given the various types of mortise and tenon connections in the traditional timber structures, their stiffness cannot be univocally estimated.

Figure 1 Chuandou (left) and Tailiang (right) timber structure system in real structures

The primary components of traditional timber structures are the Dou-Gon sets. The Dou-Gon sets are located between the junction of a column and beams; they support the beams and transmit the vertical loads of the upper trusses and the roof to the columns; the loads are then transferred to the foundation. A complete structural frame always consists of several sets of Dou-Gon and the Dou-Gon sets are linked by the through beams (Figure 2). The through beams can transfer lateral loads between the Dou-Gon sets and provide stability to the structure. Figure 3 shows the details of a fundamental Dou-Gon set, which consists of the elements Dou, Gong and through beams. Dou is a quadrate timber element with a cross and Gong and Ang are knuckle timber elements that can fit into the groove of the Dou. The Dou sits on the column or through beams and wooden pegs are used to connect them. (Figure 4) The traditional timber structures have an effect called 'Housing does not fall down together with the wall' (Figure 5). This is due to the fact that the traditional structures consist of timber frames: the brick walls do not bear the vertical load but provide lateral resistance and there are no structural connections between walls and the columns or beams. Dou-Gon sets make a valuable contribution to this effect. Every element of Dou-Don set is connected with each other by mortise and tenon joint or wood pegs. The movement between each element can dissipate energy during the earthquakes. The gaps between the walls and the timber frame can provide ventilation and prevent decay of the structural materials.

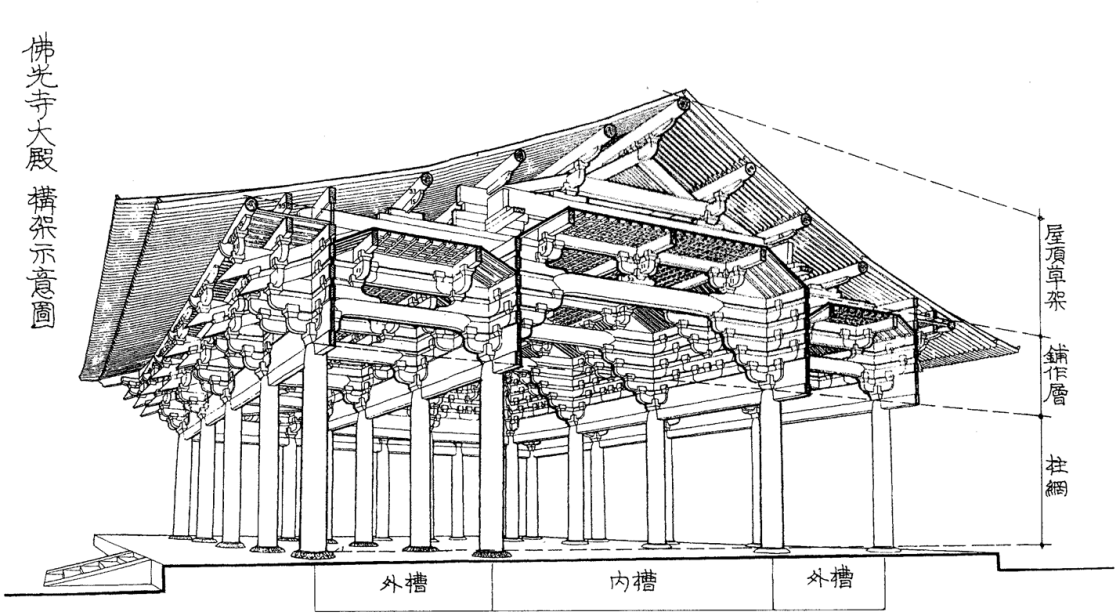

Figure 2 The framework of Nanchan Temple in Shanxi, China (Liang, 1984)

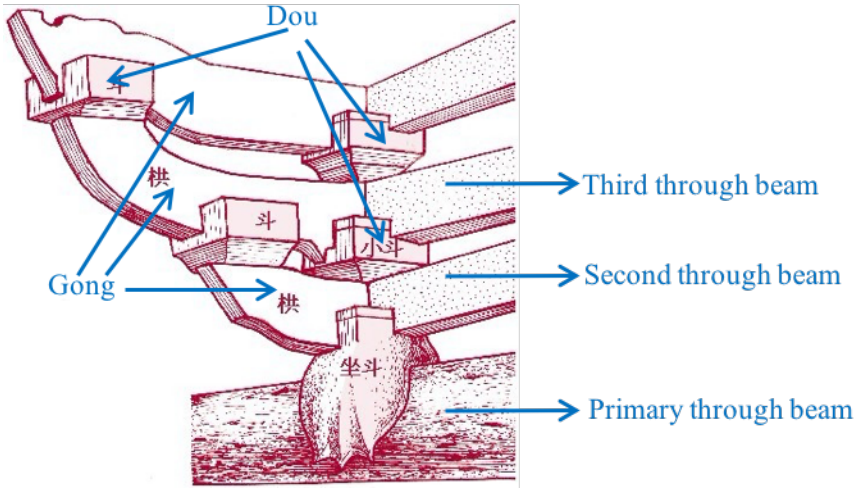

Figure 3 Details of Dou-Gon set (Chen, 2003)

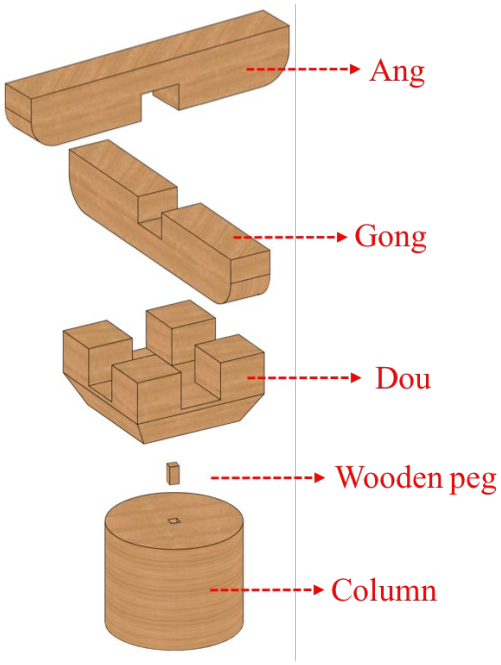

Figure 4 3D drawing of elements in Dou-Gon system


Figure 5 Feitian Hall in Yunyan Temple after earthquake (Peng, 2013)

1.1.2 Current situation of traditional timber structures

One of the existing oldest traditional timber structures in Asia, the Main Hall of Nanchan Temple was restored in 782AD in Shanxi, China. The original timber elements of the Main Hall of Nanchan Temple were weathered due to the long history. The entire structure was inclined towards the west and most elements had been serious damaged at the time when the Hall was found in 1953. The structure was damaged further by the earthquakes in 1964 and 1966 (Figure 6): beam frames had deflections towards the east, the columns were inclined forward and some tenon joints had been pulled out of the mortises. (Gao, 2011)

Figure 6 Temporary supports of Nanchan Temple after the earthquakes in 1964 and 1966 (Gao, 2011)

There are more than 600 traditional timber structures existed in China currently in which 440 of them were built between the Yuan Dynasty and Qing Dynasty (1279AD-1912AD), 99 structures were constructed in the Song Dynasty (960AD-1279AD), 5 structures were completed during the Five Dynasties period (907AD-960AD) and only 4 of the existing timber structures were built during the Tang Dynasty (618AD-907AD). These 4 structures are all located in Shanxi Province, China (Lv, 2017). The Cultural Relics Protection Law of the People's Republic of China was adopted on 19 November 1982 in China. The renovation of traditional timber structures was rarely carried out before that and both conservation works and researches are still at the initial stage at present. There is also no record for neither previous renovation methods nor follow-up assessment of the renovated structures.

Because of the great historical significance of the traditional timber structures, and the fact that most of them are located in seismic belts in Asia, these structures require protection against seismic loading. For examples, during the 1999 Chi-Chi earthquake in Taiwan, 42% of the traditional timber structures were seriously damaged and 48% collapsed, while only 10% of other building typologies were slightly damaged (Chang, 2005) (Figure 7).

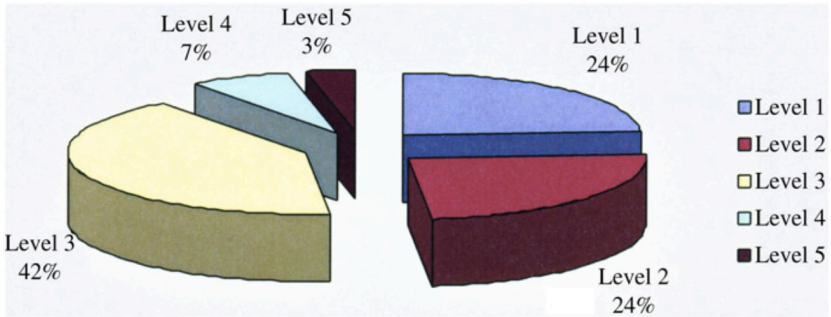

Figure 7 Level of damage of Dieh-Dou buildings after Chi-Chi earthquake (D'Ayala & Tsai, 2008)

1.1.3 Existing conservation methods

The traditional timber structures were serious damaged by earthquakes recently because the original stiffness of the structure has been weakened by several factors, such as cracks due to the environment impact, decay and weathering of the timber, as well as insects damage (Qin & Yang, 2016). The movement between mortise and tenon during the earthquake loosed the connection by breaking the tenons or pulling out the tenon joints from the mortises permanently.

There are three main reinforce methods for the traditional timber structure:

1) Repair by taking every or part of the structure apart. The tiles on the roof need to be removed first and dismantle each component from top to bottom. Reassemble the structure after repaired or replaced each damaged element. The Main Hall of Nanchan Temple was renovated by this method in 1974 and 1975 (Qi & Chai, 1980).
2) Reset the inclined, rotated or pulled out elements back to its original position without taking the structure apart and reinforce the overall structure afterwards.
3) Reinforce the entire structure without moving any components. This method can be only used for the structures without significant damage after the earthquake or enhance the structures who have not experience any earthquakes yet.

Zhang (2013) and Tian (2014) have proposed those main reinforce methods of entire structure together with four techniques which are always used for renovating individual element:

1) Reinforce by patching the damaged timber column and beam when the cracking depth is less than 1/3 and ¼ of the element's diameter, respectively. The material used for patching is depended on the width of the crack.
2) The decayed column root can be reinforced by glue new material together with the old timber column. The reinforcement material can be timber, reinforced concrete and stone depends on the decay level and location. Steel hoops need to be fitted to the column for further reinforcement.
3) Reinforce the timber element by pouring resin into the cavity when the timber is damaged by insects or decay.
4) Reinforce the mortise and tenon joints with FRP sheet. FRP has higher ratio of strength to self-weight and easier for construction. However, the stiffness of mortise and tenon joints can only be limited enhanced by FRP sheet (Xie et al., 2008).

However, the reinforce and renovation methods used in real structures were rarely seen in transcript and the efficiency of those techniques has not been proven by scientific research.

The aim of this research is to enhance the seismic performance of traditional timber structures by evaluating the efficiency of new connection systems made of contemporary materials.

1.2 Objective

The good anti-seismic performance gives traditional timber structures a life-time over thousands of years; however, their structural behaviour to resist earthquake loading is complicated and not adequately understood. The research efforts have been scarcely seen on the techniques for enhancing the seismic performance of historic timber buildings. Dou-Gon systems are the primary structural components of traditional timber structures. Re-centring capability and energy dissipation capacity are the two fundamental characteristics that Dou-Gon system have, to give historic timber buildings good seismic performance. Re-centring capability can pull the oblique structures back to centre and energy dissipate capacity will dissipate the major seismic energy. However, the conventional connectors of Dou-Gon, wooden pegs, have a low ultimate strength which cause the damages of the building during earthquakes. It is important to introduce a new technique with a contemporary material to enhance the Dou-Gon system by keeping the original re-centring capability and increasing the energy dissipation capacity and therefore to increase the ultimate strength and equivalent damping ratio of the structure. On the other hand, as the traditional timber structures are historical heritages, the changes of their appearance should be minimized. The new retrofitting technique should not be seen from the outside.

The column footing joint is another primary connection of traditional timber structure (Qin et al., 2018) and they have been damaged during the earthquakes and need retrofitting works as well. However, this research is only focused on the Dou-Gon systems, the base structure will be assumed as rigid connection and strong enough to bear all the excitations that applies on the Dou-Gon system.

The aim of this project is to mitigate the risk for traditional timber structures to be damaged in the future earthquakes by developing a suitable retrofitting technique. This project specifically address the strengthening of Dou-Gon systems. The research objectives are highlighted below:

1) To understand the original anti-seismic performance of Dou-Gon, based on the evaluation of the static and dynamic responses of Dou-Gon with conventional wooden peg connections should be studied.
2) To understand the structural performance of different types of Dou.

3) To assess the effectiveness of alternative solutions to the conventional wooden peg connections, such as high-strength steel and super-elastic alloy.
4) To understand the characteristics of the chosen reinforcement material under dynamic loadings, and in particular the effect of loading frequency, strain level and loading cycles on the dynamic performance of the material should be studied.

The research is based on the analysis of a two-layer Dou-Gon set from an ancient structure called Qinghui Hall at the Weiyuan Temple in Henan province, China (Figure 8). The Weiyuan Temple was originally built under the Sui Dynasty (581AD-618AD) and renovated during the Song, Jin, Yuan, Ming and Qing Dynasties (960AD-1912AD). The Qinghui Hall, built under the Yuan Dynasty, is a typical Tailiang timber structure where the roof weight is carried by purlins and transferred to Dou-Gon sets (Figure 9) through beams; Dou-Gon sets support the upper structure and transfer the loads to the columns and then to the foundation.

Figure 8 Qinghui Hall at Weiyuan Temple, Henan Province, China

Figure 9 Original Dou-Gon sets on Qinghui Hall at Weiyuan Temple, Henan Province, China

1.3 Outline of the thesis

The structure of this thesis is shown in Figure 10. The literature review in Chapter 2 states that Dou-Gon system is the primary structural component of traditional timber structures and provides good anti-seismic performance to the structure. However, the reinforce methods of Dou-Gon system are scarcely been seen in previous researches. Previous research also found that the weakest point of Dou-Gon system is the conventional wooden peg connections due to their low ultimate strength. The wooden pegs were always been pulled out from lower structures and made the structure unstable. Therefore, this research is going to propose a retrofitting technique with a contemporary material to enhance the Dou-Gon system. Based on the literature review on possible reinforced materials in Chapter 2, super-elastic alloy has been selected to enhance the seismic performance of the Dou-Gon set. In order to understand the dynamic behaviour of super-elastic alloy, Chapter 3 presents the material characterisation. A new connection technique is introduced in Chapter 4 and static experimentally studies of three different types of Dou with three connection mechanisms are also presented in this chapter. The strain changes under loading of base Dou analysed by Digital Image Correlation technique illustrates in Chapter 4. Chapter 5 describes the the static experiments performed on a two-layer Dou-Gon set with three connection mechanisms. The strain level of super-elastic alloy and the effect of roof weight variation under static lateral push-over loads are evaluated in both Chapter 4 and Chapter 5. Chapter 6 carries out the dynamic experiments of Dou-Gon with three connection mechanisms. The lateral excitations of scaled Northridge earthquakes and white noises are inputted to the actuator and both input and response spectrums are recorded by two accelerometers. The strain level of super-elastic alloy and dynamic performance under various roof weight are presented in Chapter 6. Base on the experimental results presented in Chapter 5, analytical models were developed by using the software Open System for Earthquake Engineering Simulation (OpenSEES), and subsequent parametric studies were performed by using several full-scale earthquake excitations (Chapter 7).

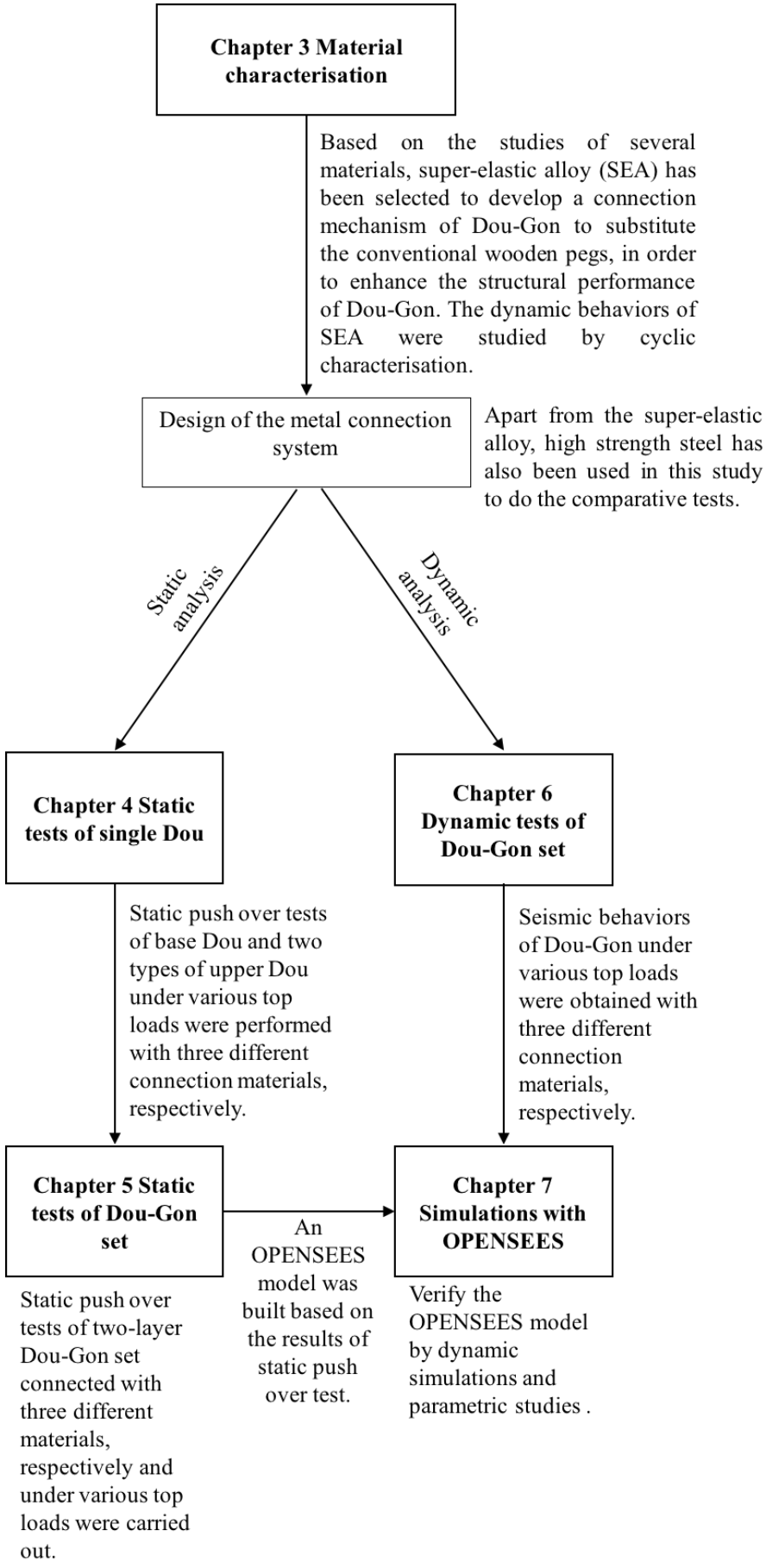

Figure 10 Structure of the thesis

Chapter 2 Literature Review

The aim of this research is to use contemporary materials to strengthen oriental historical timber structures against seismic loading. Hence, the literature review will address the performance of traditional timber structures and contemporary materials.

2.1 Conservation of traditional timber structures

2.1.1 The traditional timber structures

There are two main classifications of oriental timber structure systems, namely Chuandou and Tailiang (Guo, 1999). (Figure 11) The Chuandou system is mostly located in the region south of the Yangtze River and is used for residential houses; the Tailiang system is always used for state buildings that appear on the north side of the river. One Chuandou building consists of several parallel frames and each frame is pre-built by using Chuanfang to connect columns. Chuanfang (Figure 11) is the horizontal element that connects the columns together without taking any loads of the structure. The parallel frames are connected by purlins. No beams are used in Chuandou structures and the roof weight is transfer from purlins to columns directly. In contrast to Chuandou, beams are the important component of Tailiang structures. The roof weight is transferred from the purlins to columns through beams. The advantages and disadvantages of Chuandou and Tailiang timber structures are shown in Table 1. Later, some hybrid structures were constructed in the region south of the Yangtze River to form a spacious internal space of Chuandou timber structure.

Table 1 Comparrison of Chuandou and Tailiang timber structures

	Chuandou timber structures	**Tailiang timber structures**
Advantages	• Need smaller timber size • Better anti-seismic performance due to high integrity of the structure • Higher load-bearing capacity	• Large internal space by using longer beams and reduce the number of column
Disadvantages	• Small internal space due to high dense of column	• Big timber size needed • Less adaptability

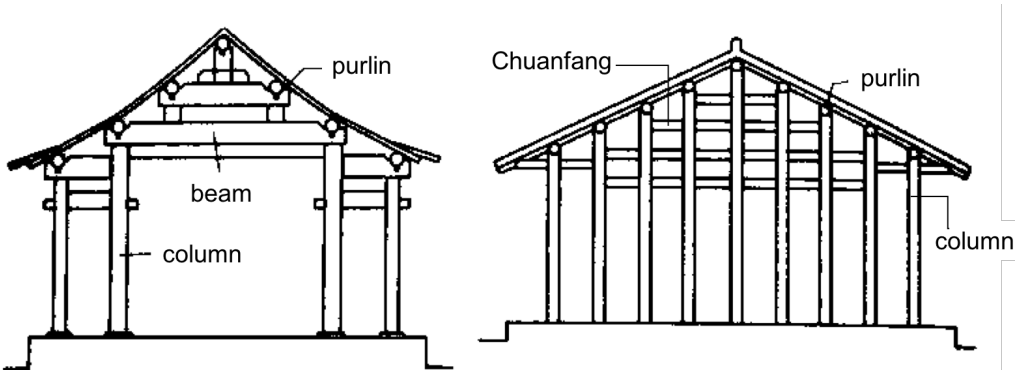

Figure 11 Tailiang (left) and Chuandou (right) timber structures

The most important units in both of Chuandou and Tailiang timber structures are the block and bracket sets, which sit on top of the columns and connect the roof frame with the columns to transmit the entire load of the upper structure to the columns. Guo (1999) stated that the block and bracket set was originally called a Puzuo in the Song Dynasty, but then transformed into a smaller decorative unit during the Qing Dynasty, when the name changed to Dou-Gon. However, this paper will refer to the block and bracket set as the Dou-Gon (Figure 12).

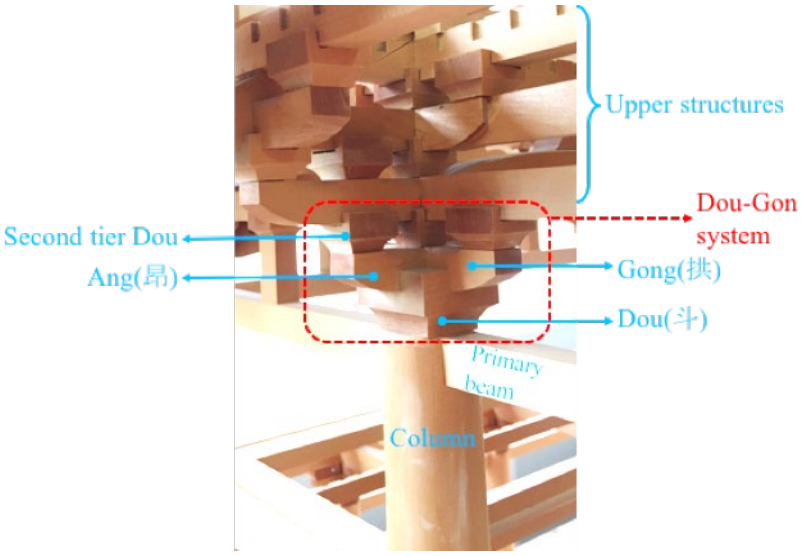

Figure 12 Dou-Gon system

The evolution of the Dou-Gon (Figure 13) can be divided into three stages (Zhou, 2007):

i. From the Western Zhou Dynasty to the Northern and Southern Dynasty (1100BC-589AD), the capital block was positioned on top of a column, whereas arched brackets were added to the block to support the purlins or the beams. Every Dou-Gon is unique compared to the others.

ii. From the Tang Dynasty to the Yuan Dynasty (618AD-1368AD), the beam or the purlin went through the Dou-Gon and constituted a horizontal frame called the 'Dou-Gon

layer'. However, the Dou-Gon set became more complicated, as the dimension of each single element had been reduced. By the end of this period, the structural function of the Dou-Gon had become less relevant, thus the roof weight was applied on the beams directly.

iii. From the Ming Dynasty to the Qing Dynasty (1368AD-1911AD), the Dou-Gon involved a sub-crust between the roof frame, beam frame and columns. The dimension of the Dou-Gon continued to reduce and became significantly more complex as Dou-Gon sets with more layers were produced. The main function of the Dou-Gon gradually turned into decoration during this period.

The original Chuandou system did not have any Dou-Gon. However, in some evolved buildings the shorter columns used Dou-Gon instead. In the Tailiang system, the Dou-Gon sets are located between the columns and beams.

In general, the Dou-Gon has three main functions (Yin & Li, 2010):

i. Located between the columns and beam frame, it transmits the load from the upper structure through the columns to the foundation.

ii. The large number of layers of Dou-Gon sets create a broad eave area and contribute to the aesthetic function of the structure through decorations.

iii. The Dou-Gon sets are the key point of the structural resistance to seismic actions. The nodes of the system are not rigid connections that contribute to the stiffness of the entire structure. During earthquakes, the Dou-Gon system will become loose without shattering; this can dispatch a large amount of energy and significantly reduce the seismic loads.

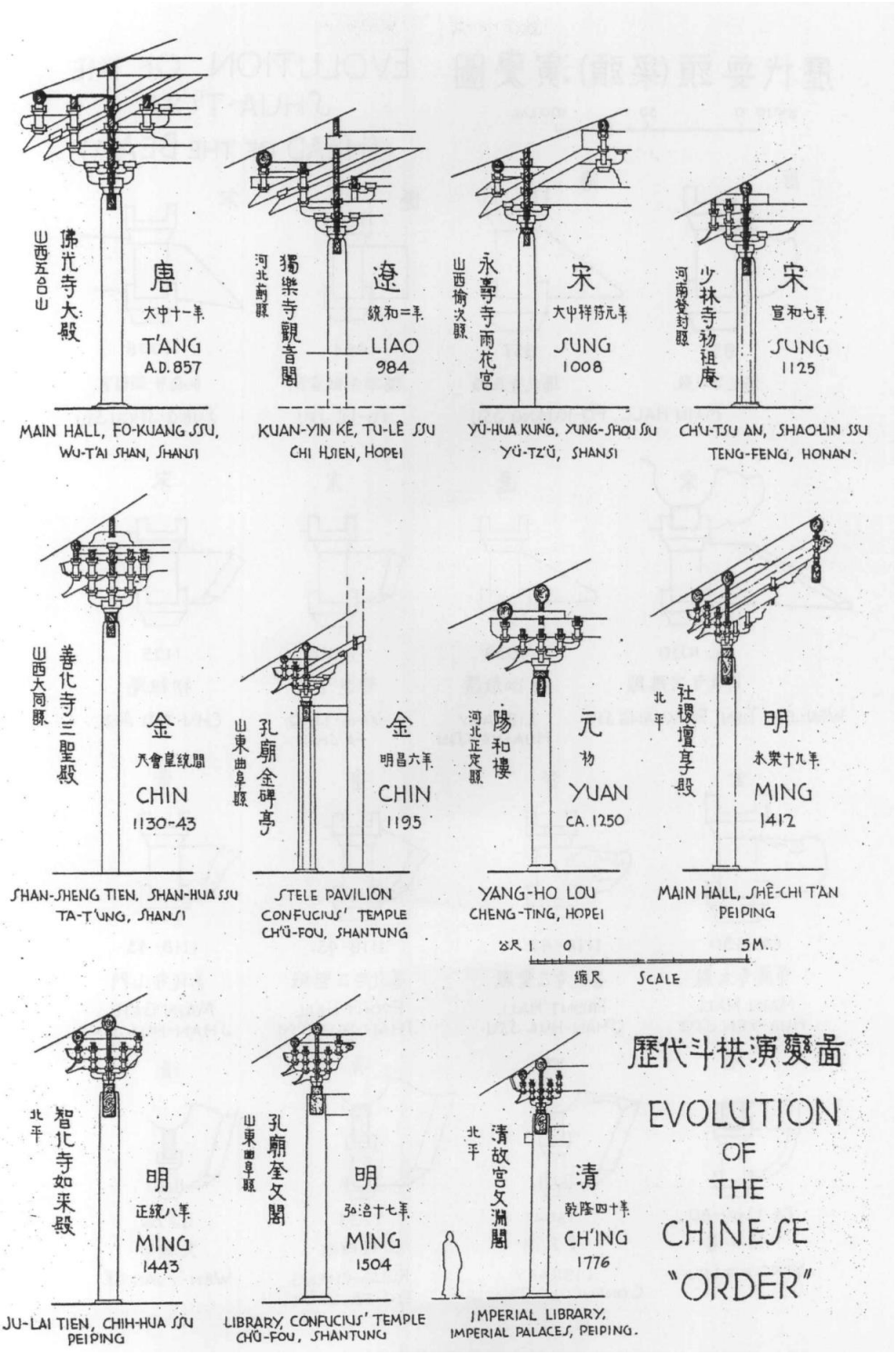

Figure 13 The evolution of Dou-Gon sets from the Tang Dynasty to the Qing Dynasty (Liang, 1984)

The great prosperity period of timber structure with Dou-Gon was from AD618 to AD191. Five main dynasties governed during that period: Tang, Song, Yuan, Ming and Qing. During the Tang, Song and Yuan Dynasties, the elements of Dou-Gon were characterised by great volumes that made the size of the Dou-Gon set nearly to half the height of the column and gave to the structure a broad eave with a maximum length of 4 meters. There were only 1 or 2 sets

of Dou-Gon sit between two columns and the Dou-Gon sets during this period always had a simple but bright colour. The Dou-Gon sets during Ming and Qing Dynasties have magnificent colour and the size of Dou-Gon reduced to a fraction of the height of the column. The number of Dou-Gon sets in-between two columns increased to 4-8. The structure then had a narrower eave with an approximate length of 1 meter.

Figure 14 The evolution of Dou-Gon sets in traditional timber structures

Figure 14 illustrated the transformation of Dou-Gon set in existing traditional timber structure from Tang Dynasty to Qing Dynasty. The information for each Dou-Gon shows in Figure 14 are listed in Table 2.

Table 2 Basic information of the Dou-Gon sets show in Figure 14

	Structure	Location	Dynasty	Year of construction
A	Main Hall of Nanchan Temple	Shanxi, China	Tang	AD782
B	Main Hall of Foguang Temple	Shanxi, China	Tang	AD857
C	Guanyin Pavilion of Dule Temple	Tianjin, China	Song	AD984
D	Sansheng Hall of Shanhua Temple	Shanxi, China	Song	About AD1123-1149
E	Dafo Hall of Guangsheng Temple	Shanxi, China	Yuan	AD1305
F	Dening Hall of Beiyue Temple	Hebei, China	Yuan	AD1347
G	Zixiao Hall of Zixiao Palace	Hubei, China	Ming	AD1412
H	Turret of The Forbidden City	Beijing, China	Ming	AD1420
I	The Summer Palace	Beijing, China	Qing	AD1888
J	The Forbidden City	Beijing, China	Qing	AD1683-1695

In summary, Dou-Gon sets were the main structural components of the structures built before the Ming Dynasty and became decorative components in structures built during Ming and Qing Dynasties. This research is focused on the structural behaviour of the Dou-Gon set, and analysed a two-layer Dou-Gon set from the Qinghui Hall that was originally built under the Yuan Dynasty.

2.1.2 Structural behaviour of Dou-Gon

An experimental study was carried out on a Dou-Gon set of an ancient timber structure (Gao et al., 2003a). The static response analysis indicated that the Dou-Gon set reduced the impact of earthquake significantly. Yu et al. (1986) performed on-site full-scale dynamic tests on the Front Tower over the North Gate of the Xi'an City Wall, the construction of which was completed in 1378. The structure has experienced two earthquakes in 1556 and 1654 without suffering any serious damage. The Tower underwent tile mounting in June 1988. Four mode vibration frequencies (Figure 15) were measured before and after the tile mounting, respectively. The locations of vibration and the level of seven sensors are illustrated in Figure 16. The results demonstrated that the frequencies decreased with the increase of the dead load, highlighting how the dynamic characteristics are highly dependent on the weight of the roof (Hayashi et al., 1998). This is confirmed by further dynamic experimental results performed on a Dou-Gon set (Zhao et al., 1999).

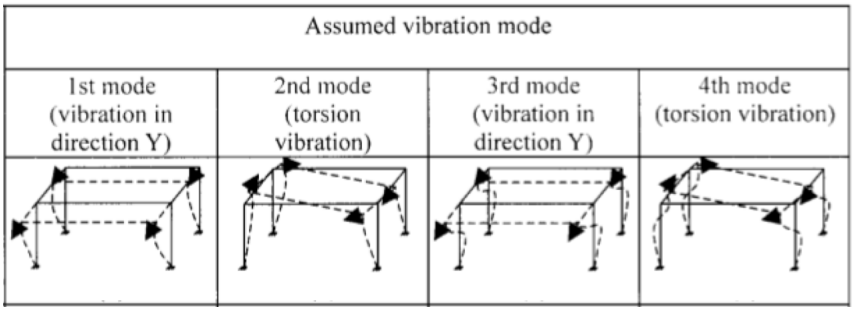

Figure 15 Four mode of vibration of the Front Tower over the North Gate of the Xi'an City Wall (Fang et al., 2001)

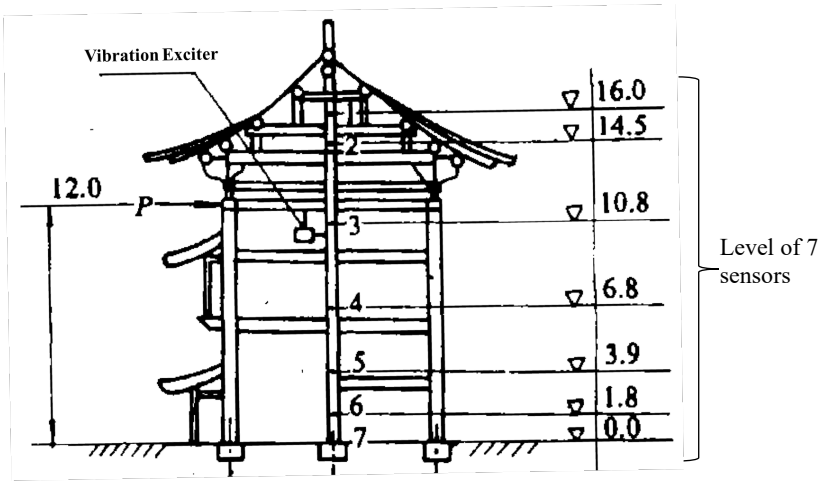

Figure 16 Elevation of the Front Tower over the North Gate of the Xi'an City Wall (Yu et al., 1986)

Two model tests consisting of a partial timber model of the Front Tower of Xi'an City Wall with a scale of 1:10 and an integral polymethyl methacrylate (PMMA) model with a scale of 1:30 were also conducted to make a comparison with the on-site test (Yu et al, 1991; Fang et al. 2001). The free vibration curve of the timber model generated a damping ratio of 5.6%. This is significantly larger than the design damping ratio of steel or concrete structures, and resulted in improved seismic performance of this structure. However, the PMMA model only provide a damping ratio of 4.1% which is ¼ lower than the timber model. This is because the PMMA model used rigid connections to substitute Dou-Gon sets and other mortise and tenon joints. It indicates that the interaction between timber components plays an important role to dissipate energy during earthquakes. A roof with a very heavy dead load can decrease the natural frequency of the structure; however, it has a relatively smaller influence on the third and fourth modes of frequency because of the smaller vibration amplitude of the top of the column. On the other hand, the heavy roof weight also creates large friction between structure members, which was the reason behind the enhancement of the structure's damping. Fang et al. (2001) also proposed that the Dou-Gon sets are semi-rigid connections because the natural frequency of the structure increased with the strengthening of the Dou-Gon. Hence, the stiffness of Dou-

Gon have significant influence on structural stiffness. The natural frequency has no significant change with the increase of the roof's stiffness, because the roof already has sufficient stiffness. The comparison of natural frequency in on-site and models tests are shown in Table 3. The 1:10 timber model has 15% difference with the on-site test in the first natural frequency due to the disparity of the connection used for the column and foundation and the second natural frequency of torsion has the difference over 40% because the timber model is a partial model. The results of PMMA model have even greater variance with on-site test result in the first natural frequency as rigid connections were applied to the PMMA model. The results also indicate that the models cannot identify the third and fourth natural frequency.

Table 3 Natural frequency in on-site and models tests of the Front Tower of the Xi'an City Wall (Fang et al., 2001)

		Assumed Vibration Mode			
Method	Roof condition	First mode, vibration in *Y*-direction	Second mode, torsion vibration	Third mode, vibration in *Y*-direction	Fourth mode, torsion vibration
On-site test	With roof dead load	1.110	1.700	2.725	3.100
	Without roof dead load	1.450	2.175	2.900	3.400
Wooden model	With roof dead load	1.280	2.220	8.670	12.85
	Tolerance	15.3%	30.6%	218.2%	314.5%
	Without roof dead load	1.460	3.100	8.310	12.68
	Tolerance	0.69%	42.5%	186.6%	272.9%
PMMA model	With roof dead load	1.400	2.070	7.410	9.750
	Tolerance	27.3%	21.8%	171.9%	214.5%
	Without roof dead load	1.790	2.350	8.020	10.110
	Tolerance	23.4%	8.0%	8.1%	226.1%

A further static test was performed by on the partial timber model of the Front Tower of Xi'an City Wall by Yu et al. (1991; 2008) in order to discover the rigidity and ductility of the structure. A constant vertical load was applied on top of the roof and the horizontal load was increased gradually until the structure failed. The load-displacement diagram (Figure 17) showed four stages of structural stiffness. The beams in the lower level were not stressed when only vertical load was applied. During the initial period of the application of the horizontal load, there was minimal displacement on the connections and the structure started to slip. This behaviour also been found by Chang et al. (2006; 2007), who demonstrated that this is due to the initial gap between the mortise and tenon. Then, the structural stiffness increased rapidly as the load increased until reaching the yield point. At this elastic period, the mortise and tenon joints began to bear the shear and flexural moments. The Dou-Gon and mortise and tenon joints at the side columns began to be pulled out as the load increased to the limitation defined as the plastic stage. Subsequently, the structural stiffness decreased under the ultimate load until the final collapse. This behaviour can be seen clearly from the hysteretic diagram of the static push over test (Figure 18). The static experiment determined that the weakest connections occur at the Dou-Gon on side columns; therefore, the Dou-Gon will be pulled out and the integrity of

the structure will ultimately be weakened. However, the material does not reach its plasticity even at the structural limit stage. In a frame structure with just mortise and tenon joints, the general failure mode is either bending or shear failure at the mortise branches (Seo et al., 1999). The rotational stiffness of mortise and tenon joint is dependent on the depth and width of tenon (Chang et al., 2004). Hayashi et al. (1998) also found that the structural deformation of timber frame with Dou-Gon is mainly caused by the deformation of base Dou and slip between each element.

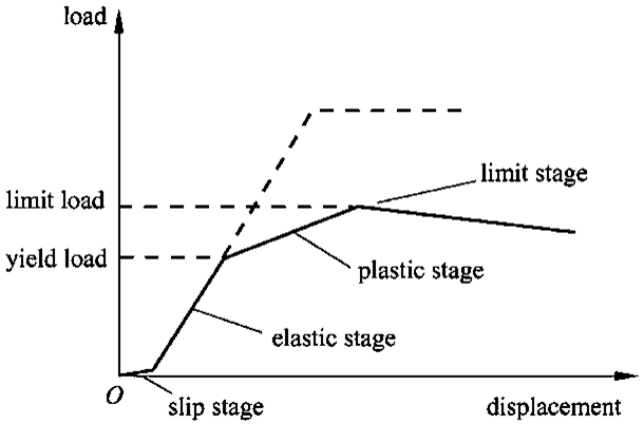

Figure 17 Failure diagram of the timber structure model (Yu et al. 2008)

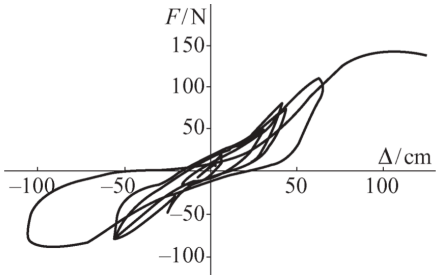

Figure 18 Hysteretic diagram of the timber model test of the Front Tower of Xi'an City Wall (Yu et al., 1991)

A Pagoda is an oriental traditional timber tower with five stories that is usually built in a temple. It also consists of a large number of Dou-Gon sets. A study on Yingxian Pagoda conducted by Lam et al. (2008) analysed the oldest pagoda in China, with an age close to 1000 years. It is located in a seismic region where over forty earthquakes have occurred, including an earthquake of 7 Richter Scale and six earthquakes over 6 Richter Scale. A total of 54 different types of Dou-Gon sets were used in Yingxian Pagoda in order to enhance the seismic performance of the structure. Nonetheless, this Pagoda requires significant restoration according to the on-site assessment (Li et al., 2005), given that structural components are damaged due to the decay of the material and they might suffering from earthquakes in the future. Chinese Academy of Culture Heritage (2013) proposed a renovation plan of Yingxian Pagoda in 2013 to enhance and protect the first and second floors of the pagoda (Figure 19)

and this plan was approved by National Cultural Heritage Administration of China on 20th March 2014 (Chinese Academy of Culture Heritage, 2014). According to the news (Chinese Academy of Culture Heritage, 2014), the construction of renovation work of Yingxian Pagoda started in December 2014. The natural frequencies of Yingxian Pagoda were measured on-site (Che et al., 2006) to be 0.6Hz (1st mode), 1.66Hz (2nd mode) and 2.93Hz (3rd mode), which are significantly less than the natural frequency of the ground soil (2.5Hz to 3.5Hz). The results suggest that the Yingxian Pagoda is a flexible structure that would be relatively safe under future seismic loading. A 1:10 model has been built by Li et al. (2004). The shaking table tests under different seismic waves highlighted that the second and third floor of Yingxian Pagoda are the weakest level of the structure and need to be enhanced urgently.

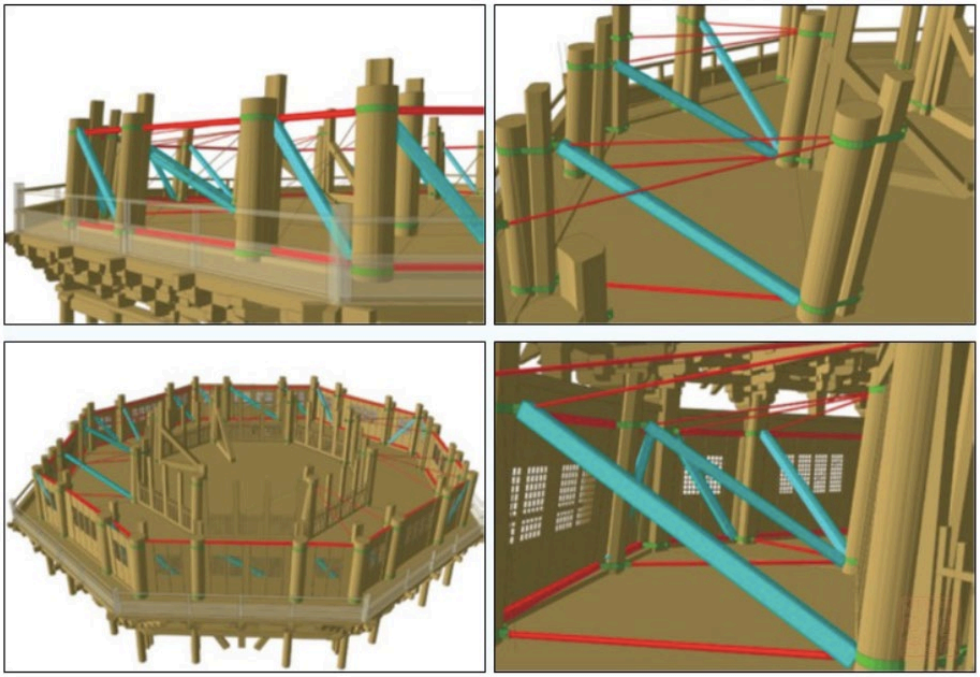

Figure 19 Illustration of renovation method of Yingxian Pagoda (Chinese Academy of Culture Heritage, 2013)

Earthquake response monitoring was performed on a newly-built timber pagoda called Tsu-Kanon in Japan (Figure 20) that was constructed with a traditional structural system (Fujita et al. 2004). Both micro tremor measurement and free vibration test were also performed on this Pagoda. The natural frequencies of vibration were 1.5Hz (1st mode), 4.2Hz (2nd mode) and 7.2Hz (3rd mode) and the average damping factor was determined to be approximately 5%. The earthquake response monitoring showed that the response amplitude of both the 2nd and 3rd modes were substantially larger than the 1st mode of vibration. The shaking table tests were performed on a 1:5 scale pagoda model in Japan (Fujita et al. 2006). A logarithmic relationship was discovered between the natural frequency of vibration and the maximum horizontal

displacement due to the non-linearity of the structure. The damping ratios are in the range of 1-8%, which is relatively high compared to other timber structures. The two Pagodas, Tsu-Kanon and the 1:5 scale model, have different sizes, designs and details, which nevertheless result in consistent vibration characteristics.

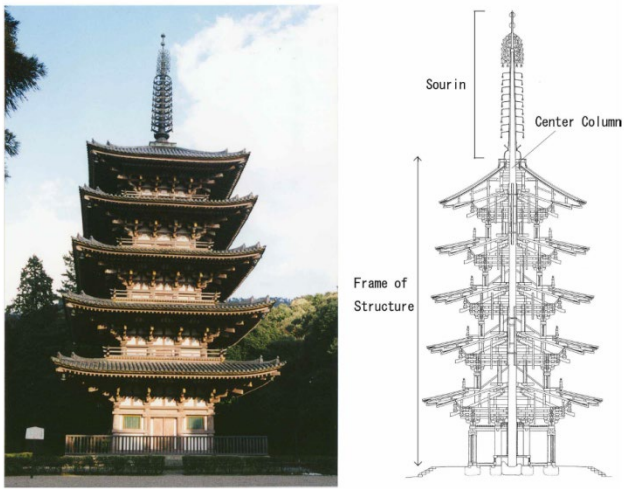

Figure 20 Example of the Section and Picture of a Five Storied Pagoda (Fujita et al. 2004)

D'Ayala and Tsai (2008) performed rotational and translational pull out tests on a Dou-Gon set with two Dou elements. Two different vertical loads of 6.5kN and 3.2kN were applied on top of the upper Dou. The results from the rotational tests indicate that the rotational stiffness of the Dou-Gon sets depends on the vertical load applied on the top. Hence, the rotational stiffness of each Dou-Gon set in a building will be different due to the different locations. During the translational pull out tests, both dovetail and flat cut connections (Figure 22(a)) were employed. When the connection was dovetailed, the translational stiffness and pull out force were not affected by the vertical load but governed by the strength of the timber, whereas the pull-out force was dependent on the vertical load with the flat cut connection (Figure 21). Both upper and lower Dou elements were not damaged in the translational pull out tests and in terms of the translational stiffness was not affected by the vertical load. Different dovetail connections also provide different structural performance, such as stepped dovetail connection and Go-Dou connection (Figure 22(b)) (Chang & Hsu, 2005). The stepped dovetail connections have greater ultimate moment capacity and more gentle stiffness degradation than Gou-Dou connections. Cyclic loading tests were conducted by Tsai (2009) and the results confirmed the conclusions gathered from the static tests. These experiments indicated that the rotational stiffness of Dou-Gon sets varies between 1.2×10^4 and 4.04×10^4Nm/rad and the translational stiffness ranges between 780 and 1,800N/mm.

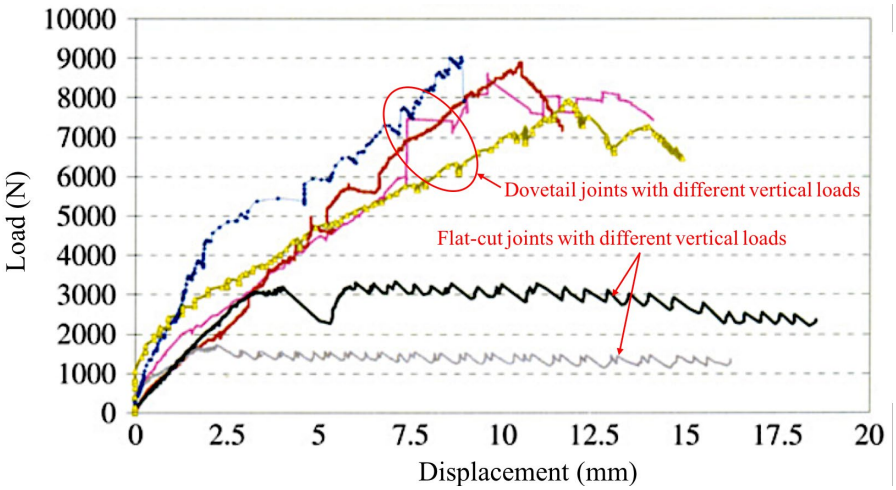

Figure 21 Pull out test results for dovetail and flat-cut joints (D'Ayala and Tsai, 2008)

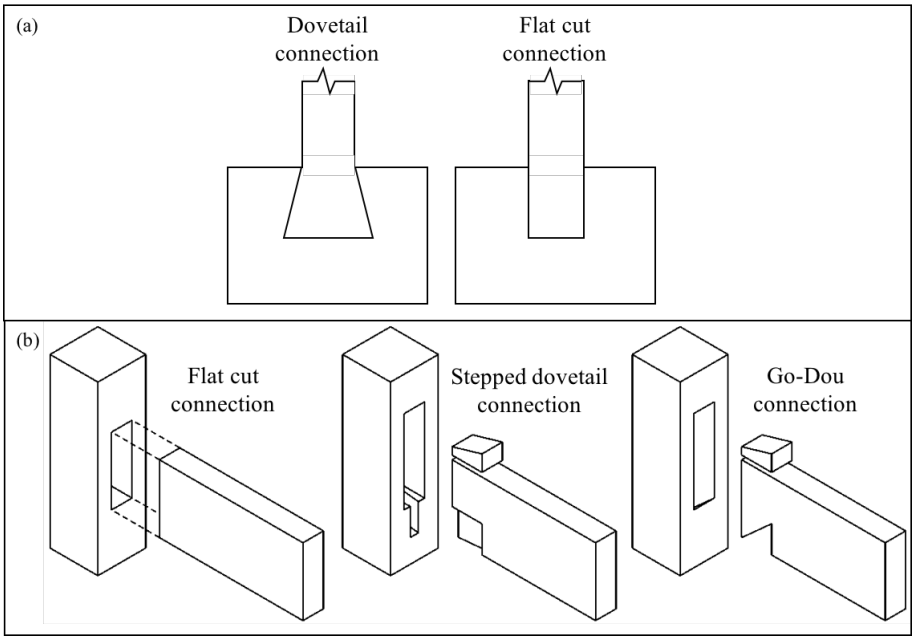

Figure 22 Four types of mortise and tenon joints (Chang & Hsu, 2005)

Based on the results of shaking table tests and static lateral loading tests of traditional timber frames with Dou-Gon sets (Suzuki & Maeno, 2006), two structural mechanisms against earthquake loadings were observed: bending moment resistances from the main beams and restoring force during column rocking. When the structure's deformation is small, the latter is the dominate resisting mechanism, while the former becomes more important as the deformation increases. This study also found that the Dou-Gon set plays an important role as it rotates in reverse proportion to the rocking of the column. Most energy are dissipated through the sliding and rotations between the occlusive element in Dou-Gon (Li et al., 2018).

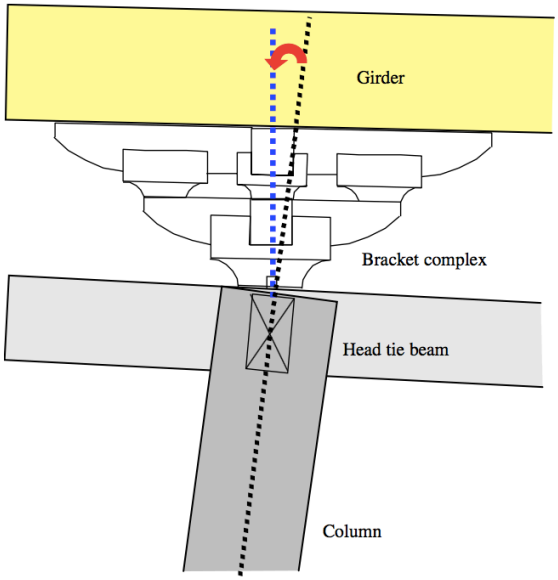

Figure 23 Rocking of column and Dou-Gon set (Suzuki & Maeno, 2006)

Both static and dynamic loading tests for four different types of Dou-Gon sets were conducted by Fujita et al. (2000). The static lateral loading tests for those four different types of Dou-Gon sets showed common characteristics:

- Load-displacement curves give a non-linear stiffness of the Dou-Gon.
- Major horizontal deformation happens to the rotation of the base Dou in the region of the initial stiffness.
- Slipping has been observed when the horizontal load exceeds the frictional capacity between the elements and this results in second stiffness.

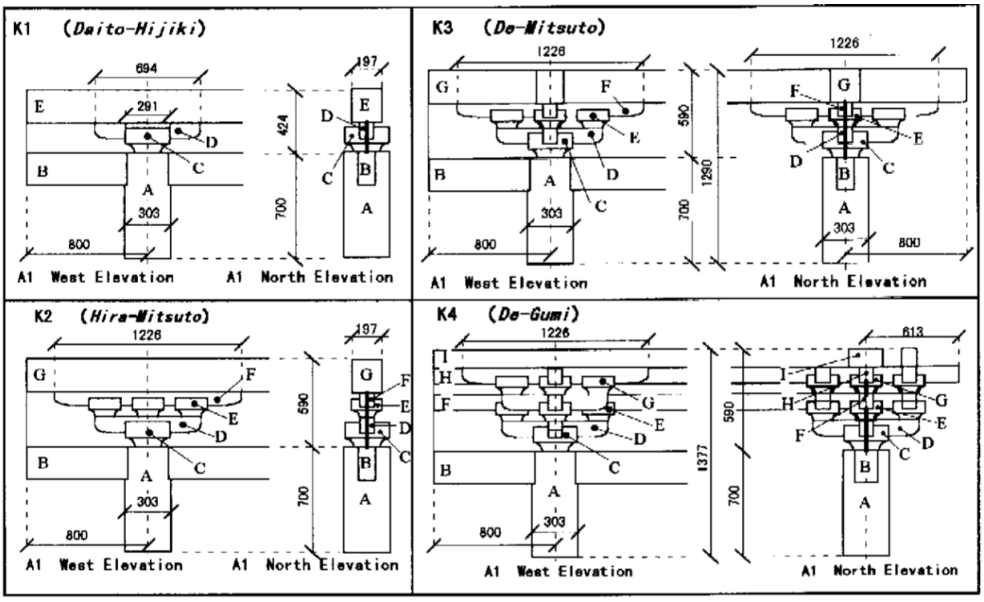

Figure 24 Elevations of 4 specimens (Fujita et al., 2000)

A slight different load-displacement model was proposed by Fujita et al. (2000) (Figure 25). The slip stage with 0 stiffness happened after the first stiffness of the rotation of base Dou. The third stiffness of Dou-Gon is provided by the rotation of second layer's Dou. This structural stiffness model can also apply to the shaking table test on ancient timber structure that completed by Zhang et al. (2011).

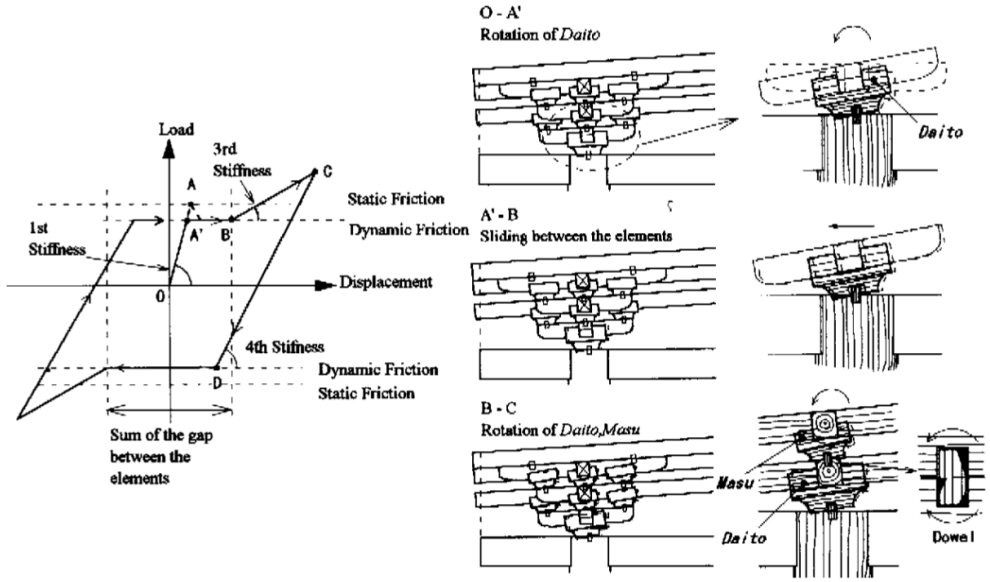

Figure 25 Non-linear model of Dou-Gon proposed by Fujita et al. (2000)

Shaking table tests have been performed for a full scale two-layer Dou-Gon set (Figure 26) by Kyuke et al. (2008). The initial stiffness of the Dou-Gon set under dynamic loadings was measured in accordance with the previous static test results (Kusunoki et al., 2005). The base Dou did the majority of the work for both rotational and sliding deformations and this behaviour has been also been demonstrated by Tsuwa et al. (2008).

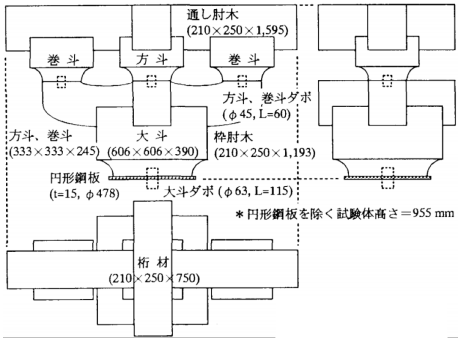

Figure 26 Two-layer Dou-Gon set tested by Kyuke et al. (2008) and Kusunoki et al., 2005

Further shaking table tests have been conducted with two semi-full scale Dou-Gon sets (symmetric and asymmetric) (Figure 27) under different vertical dead loads (Yeo et al., 2016a). The results show that the symmetric Dou-Gon set can be more easily damaged than the asymmetric one due to lower secondary stiffness at an early stage, which gives the symmetric

Dou-Gon set a larger response under seismic loadings. In general, the damage always occurred in the front base Dou first and then spread to the front-upper Dou and back elements. Although higher vertical dead loads will significantly increase the global stiffness of the structure, the larger inertia force will magnify the rocking effect and cause greater deformation. Hence, this study suggests that varying the vertical dead loads should be taken into consideration in future studies. Push-over test of the symmetric Dou-Gon set (Yeo et al., 2016b) demonstrated the great damage observed at the front-upper Dou and back-lower Gong (Figure 28) which is different with the Dou-Gon set with only one base Dou.

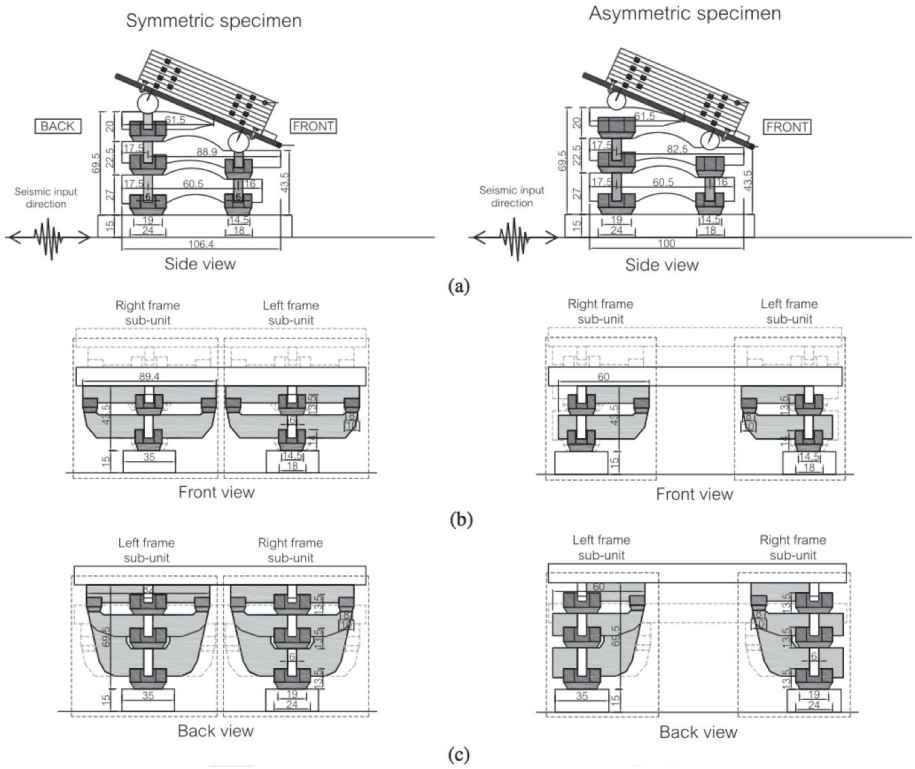

Figure 27 The (a) side view; (b) front view and (c) back view of symmetric and asymmetric Dou-Gon sets tested by Yeo et al. (2016a)

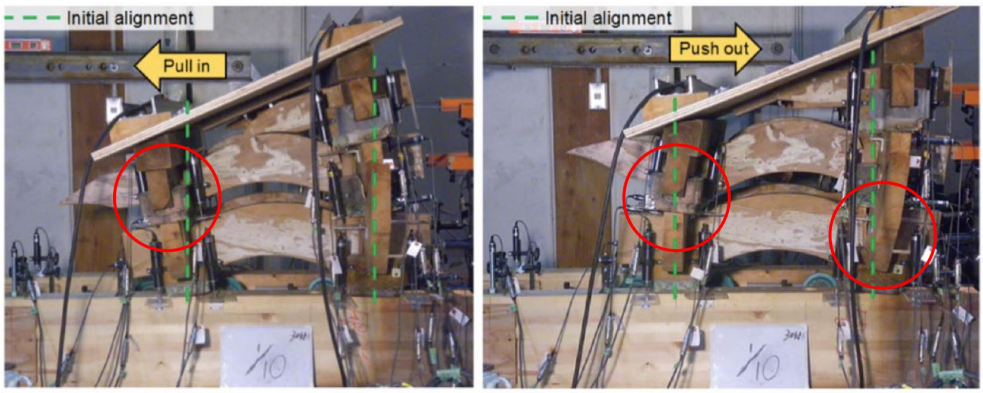

Figure 28 Deformation observed of symmetric Dou-Gon set under push over loadings (Yeo et al. 2016b)

Results from previous experiments performed on Dou-Gon sets are listed below:

- Larger roof weight can enhance the structural stiffness, but then the P-Δ effect becomes more significant and result in a great deformation. The pull out force of flat-cut joint is dependent on the vertical load. This highlights the need to evaluate the influence of the roof weight variation.
- Model materials other than timber, such as PMMA, cannot present the behaviour of traditional timber structure. Because the movement between elements of Dou-Gon or mortise tenon joints is impractical to create by other materials. Experiments on full scaled models are necessary.
- Enhancing the stiffness of the Dou-Gon can increase the global structural stiffness.
- The push over test performed on the frame with Dou-Gon sets indicates that the failure of the structure happens when the Dou-Gon is pulled out, but the connection material never reaches the plasticity during the test. Changing the connection between the Dou-Gon and the lower structure to prevent the Dou-Gon from being pulled out can increase the structural stiffness.
- The Dou-Gon has non-linear stiffness. But the load-displacement models proposed by different researchers has slight discrepancy.
- The base Dou takes the most deformation of Dou-Gon set with only one base Dou. Different damage patterns can be observed in various Dou-Gon sets (Figure 24, Figure 26 and Figure 27)

2.1.3 Simulation of Dou-Gon

A Dou-Gon set modelled as a rotational spring was firstly proposed by Fujita et al. (1999, 2000,2001). A mechanical model was developed by Yeo et al. (2016b) and compared with the static test results of the full-scale Dou-Gon specimen. The model was designed to estimate the global load-deformation behaviour of the entire structure. The results indicated that the force-deformation relationship is highly dependent on the stiffness of the rotational spring and the dead load. The yield rotational angle and the yielding moment of the bearing block members increase with the increasing of the dead load. However, because each rotational stiffness is assumed to be bi-linear, the model is only valid for estimating the first and second stiffness. Therefore, further evaluation of the failure criterion for each member is required to predict the ultimate stage of the entire structure.

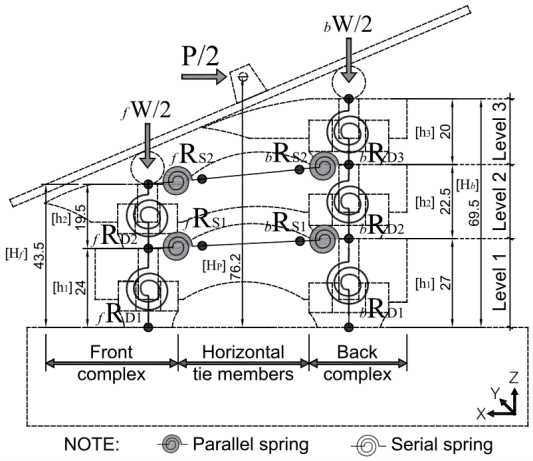

Figure 29 Globle rotational spring model proposed by Yeo et al. (2016b)

The finite element method (FEM) was employed to simulate the traditional timber structure with Dou-Gon sets. FE model program Structural Analysis for Ancient Timber Structures (SAFATS) was developed by Fang et al. (2001b). The behaviour of both Dou-Gon sets and mortise and tenon joints in a structure were simulated by a semi-rigid connection element (SRCE) with zero mass and dimensionless. The natural frequencies of the first and second modes obtained by SAFATS were the same as those of the partial timber model. The natural frequencies of the third and fourth modes exhibited significant differences to the experimental results but were closer to the results from the on-site tests. Furthermore, the natural frequencies of the fifth and sixth modes obtained by SAFATS were similar to the third and fourth modes' natural frequencies obtained from the PMMA model. This was due to the fact that the third and fourth modes were related to the plane bending deformation of the Tower, but the model tests were unable to provide such flexibility and there were no constraints in the real structure during the on-site test.

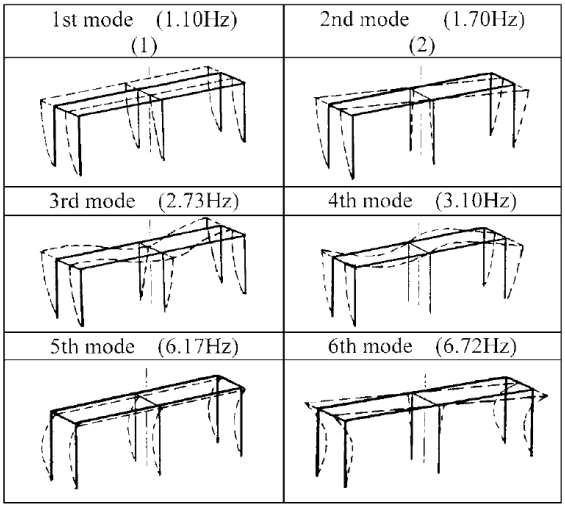

Figure 30 Vibration Modes of Front Tower over North Gate of Xi'an City Wall (Fang et al. 2001b)

Fang et al. (2001b) also determined that the semi-rigid connections of Dou-Gon sets and mortise and tenon joints can improve the structure's anti-seismic ability by reducing the internal forces by one-third compared to the seismic response of a structure with all rigid connections. Furthermore, the damping ratio of the structure has a considerable influence on the seismic response, whereby the deformation and internal forces of the structure will decrease when the damping ratio increases. However, maintenance of the connection by bracing or strengthening might reduce the damping capability of the structure, which requires significant attention.

Tsai and D'Ayala (2011) used ALGOR© to build 2D finite element numerical models to simulate a traditional timber structure. Each connection was simulated by three parallel elements, which comprised one rigid element, one translational spring and one rotational spring to connect the two nodes. The models indicate that the outer part of the frame suffered more damage than the central part. Furthermore, the analyses demonstrated that the critical failures consisted of a combination of pull out and rotational failures, while neither of them had material failure. Those findings are consistent with the experimental results from the research that done by Yu et al. (1991; 2008). An assessment and strengthening strategy flow chat has also proposed by Tsai and D'Ayala (2011). However, further analysis of the old strengthening method of Dou-Gon is necessary, as well as the definition of new strengthening methods.

Simulation results of Dou-Gon from previous studies also verified that Dou-Gon can be assumed as semi-rigid joint. Hence, rotational springs were applied to the models to simulate Dou-Gon sets. The seimi-rigid connections provide the structure with a much better damping ratio than the one offered by the rigid connections. Therefore, this research aims to develop a new connection technique to substitute conventional connections of Dou-Gon sets and reduce the damping ratio of the structure.

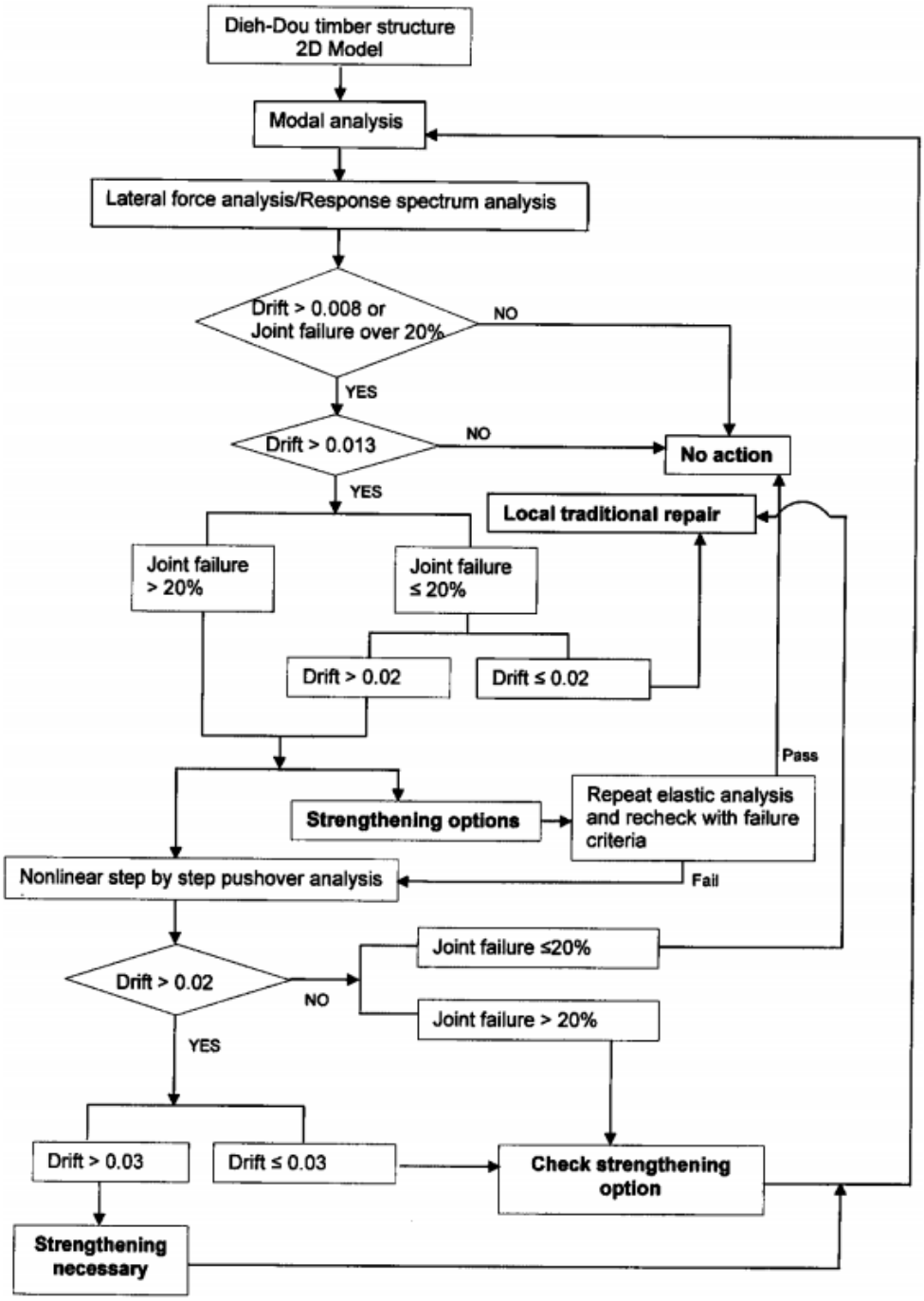

Figure 31 The assessment and strengthening strategy proposed by Tsai and D'Ayala (2011)

2.1.4 Principles for the preservation of historical structures

The historical structures which have experienced several earthquakes without severe damage, demonstrate a certain level of seismic resistance. Modern materials can be used to increase the tensile resistance and bonding once the traditional means of the buildings is completely understood (Feilden, 1982).

The International Council on Monuments and Sites (ICOMOS) has adopted the Principles for

the Preservation of Historic Timber Structures (1999). This is intended to protect and preserve timber structures due to their long lasting cultural presence in terms of explaining the principles and practices involved in their construction and preservation. These guidelines recommend that any intervention is based on thorough investigations and assessments including records of the condition of the structure and its components, as well as accurate diagnosis of any decay or structural failure. The intervention should follow the nature of the historical structure and also needs to be reversible; at a minimum it should not impede or prejudice future preservation work. Significant caution should be applied when using contemporary materials, where the materials' durability and structural behaviour in addition to the construction techniques need to be satisfactorily proven over a sufficiently long period.

China initiated the process of developing a national inventory and assessment of heritage sites in 1950 and over 300,000 sites were reported that needs to be reinforced or protected. The Principles for the Conservation of Heritage Sites in China (2004) was issued by China ICOMOS in 2002 and subsequently revised in 2004. It outlines the conservation processes, conservation principals and conservation interventions for heritage sites in China. The Principals represent the professional guidelines for heritage conservation and preservation and specify criteria for the evaluation of all conservation work.

2.2 Study on possible materials

In order to use contemporary material to substitute the conventional wooden peg connections, three different materials, namely aluminium alloy foams, low-yield-strength steel and shape memory alloy, were investigated in this section.

2.2.1 Aluminium alloy foam

The foam material made with aluminium alloys (Figure 32) has very high energy absorption, which can accommodate large plastic strains. The tensile and compression tests undertaken by McCullough et al. (1999) found that aluminium alloy foam is ductile in compression but more brittle in tension. The stress-strain behaviour of aluminium alloy also proves that it is an anisotropic and inhomogeneous material for which the yield strength in the longitudinal direction is greater than in the transverse and through-thickness directions.

Figure 32 Aluminium alloy foams

A pilot test was conducted in this project and demonstrated that the aluminium alloy foam can only absorb energy during permanent deformation. It can be observed from Figure 33 that the material only dissipated energy in the first cycle under displacement control and the test machine was running idle after 43 cycles. This means that it is a one-off material and cannot satisfy the requirements for this project.

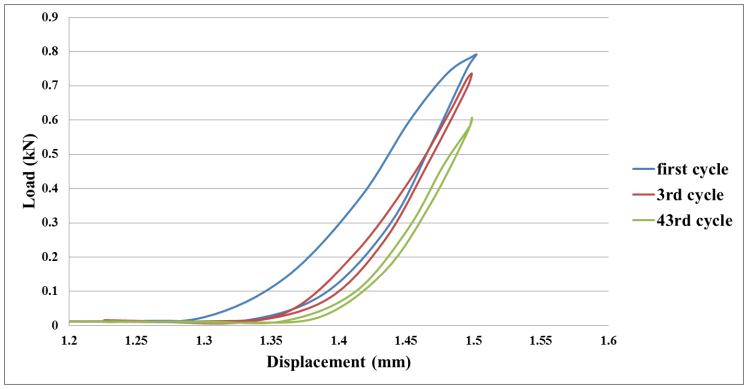

Figure 33 Load-displacement curve of aluminium alloy foams in cyclic shear test

2.2.2 Low-yield-strength steel

The low-yield-strength steel 100 (LYS100) has a yield strength of 100N/mm^2 and is widely used for shear panel dampers to dissipate energy. This material exhibits good ductile performance, and has a large deformation capacity, which produces a large energy dissipating capacity and good low-cycle fatigue performance. Both static and dynamic cyclic loading shear tests were conducted by Zhang et al. (2012) with four strain levels ranging between 20% an 50%. The static tests giving the spindle hysteretic curves and the dynamic tests with frequencies of 0.5Hz and 1Hz demonstrated that the hysteretic curves have a rectangular shape (Figure 34). The damping forces increased from approximately 400kN to 600kN in the first two cycles for all specimens, remained constant in the static tests and then dropped rapidly in the dynamic tests. Tanaka and Sasaki (2000) also performed static cyclic loading tests on 16 shear panel dampers (made by LYS100) with different width-thickness ratios and observed that the

dampers have better hysteretic performance when the width-thickness ratio is less than 40. Tension-compression cyclic tests were conducted by Dusicka et al. (2007) on LYS100 dog-bone specimens with 7 different strain levels ranging from 1% to 7%. The specimens under 1% and 2% strain amplitudes have about 700 and 150 cycles respectively, whereas the others failed within 5 to 50 cycles. However, the first two cycles of the hysteresis loop illustrated that the maximum stress of these cycles is approximately double the maximum stress in the first quarter cycle.

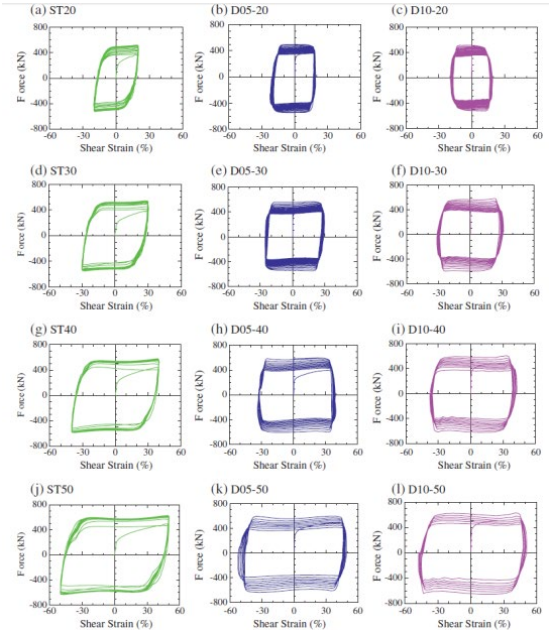

Figure 34 Static and dynamic force-shear strain hysteretic curves (Zhang et al. 2012)

All experiments on LYS100 demonstrated that although the hysteresis loops (Figure 34) showed excellent energy dissipation performance, the materials experience permanent deformation after the first quarter cycle and failure occurs after a small number of cycles. Figure 34 also shows that the material needs over 400kN force to re-centre- after the material deforms to dissipate a large amount of energy. Because both re-centring and energy dissipation behaviours are needed for the renovation of historical buildings, LYS100 is not a suitable material for this project.

2.2.3 Super-elastic alloy (SEA)

Shape memory alloy (SMA) is a metallic material with two main crystal structures, martensite and austenite which depends on temperature and external stress. The former phase is the low temperature phase whereas the latter one is the high temperature phase. There are four temperatures referring to the phase transformation, M_f, M_s, A_s and A_f in an ascending order. M_s

and M_f are the start and finish temperature points of the martensite phase and A_s and A_f are the start and finish transformation temperatures from martensite phase back to austenite phase. (Janke et al. 2005) SMA is regarded as smart material because of its two remarkable mechanisms, the shape memory effect and pseudoelastic effect (or superelasticity effect). SMA is well-known for its shape memory effect. The crystal structure of SMA will transfer from twinned martensite to detwinned martensite by applying external stress in the temperature range of M_s and M_f under shape memory effect. If heat the temperature above A_f, the crystal structure will become austenite phase. Reversely, it will come back to its original phase after reduce the temperature below the M_s. However, if the material is always in the environment with a temperature above A_f, the interconversion between the twinned martensite and austenite phases will occur under loading-unloading condition and this is referred as pseudoelastic effect of SMA and this type of SMA is called super-elastic alloy (SEA). SMA can obtain a large elastic strain up to 8%. (Omori and Kainuma, 2013) The nature of SMA was schematized in Figure 35.

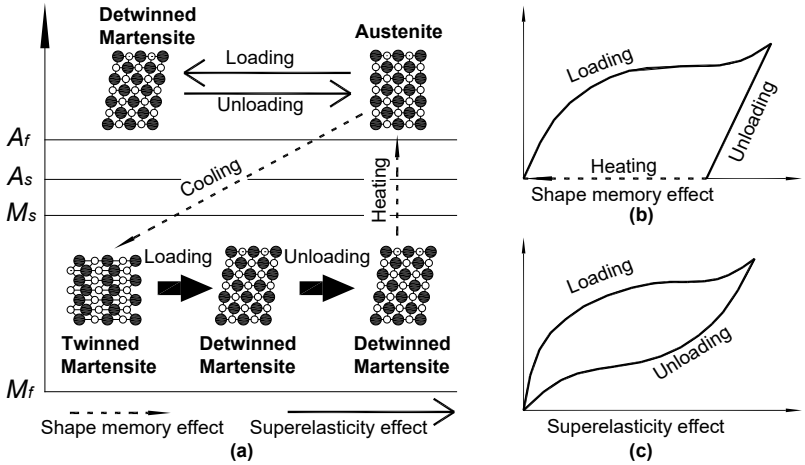

Figure 35 the different phases of SMA in different temperature, and its relation with the shape memory and pseudoelasticity effects (Chang & Araki, 2016)

The ductility of Cu-Al-Mn SMA has been studied by Sutou et al. (2008). The results show that the maximum super-elastic stress increase with increasing ratio of mean grain diameter and the diameter of specimen (d/D) (Figure 36) and the Cu-Al-Mn SMA has superelasticity effect up to 7.5% strain level.

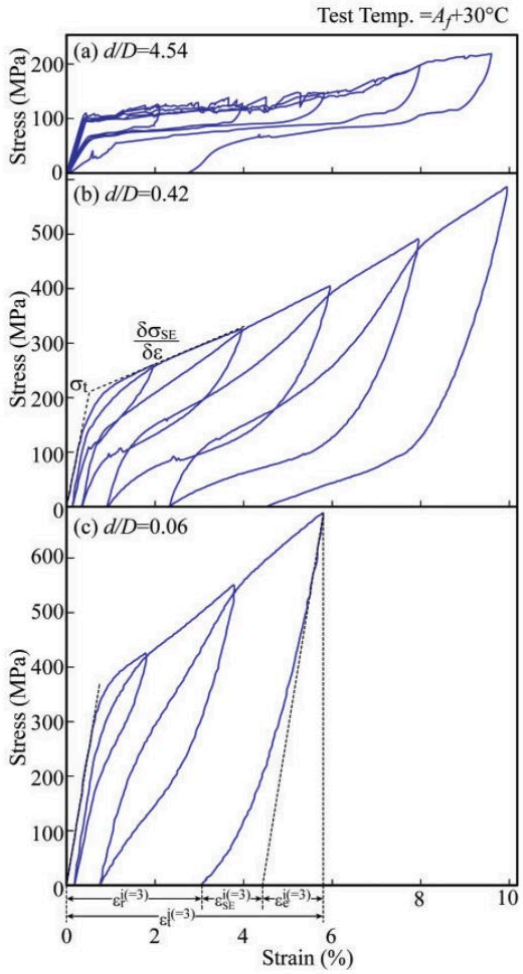

Figure 36 Cyclic stress-strain curve obtained from Cu-Al-Mn SMA at temperature of A_f+30ºC (Sutou et al., 2008)

2.2.3.1 Applications of super-elastic alloy

The applications of SMA can be classified into active control, passive control and hybrid control schemes (Saadat et al. 2002). Active control schemes use the shape memory effect of SMA, which is the temperature-induced phase transformation and it can always be used as an actuator. The pseudoelastic effect of SMA accommodates the passive control scheme due to the stress-induced phase transformation. Under the active control scheme, SMA is not able to dissipate energy, but can give restoring forces to the system. The SMA has a larger damping capacity during the martensite phase in comparison to the austenite phase (Song et al. 2006); however, heating is required to restore it back to its initial shape. On the other hand, SMA has small residual strain after loading under passive control scheme; thus, the strong re-centring force can restore the structure's original position.

SEA are widely used for the vibration control of structures and energy dissipation mechanisms such as dampers. Thomson et al. (1995) conducted an experiment using a cantilever beam with

a tip mass and used SEA wires to constrain the end of the cantilever by pre-straining the wires to lie within the hysteresis loop. The results showed that the presence of SEA wires can augment the structural damping by a factor of 6 and accomplish frequencies of dynamic response that are close to the first mode natural frequency of the structure. Three inner hysteresis loop models (Figure 37) were proposed, where the first two were based on linear approximate stress-strain curve and the other one was based on an experimental stress-strain curve of Ni-Ti wire. The inner loop of the first model has linear elastic with the same Young's modulus of the outer loop until reaching the yield strength. The second model (Muller and Xu, 1991) has a trigger line that lies diagonally across both inner and outer loops and the boundaries of the inner loop are parallel to the outer loop. The inner loop of the last model is equivalent to sections of the outer loop displaced along the strain axis. Model three shows the best agreement with the experimental results, whereas model two provides approximate damping that can be added to the structure due to the SEA wires.

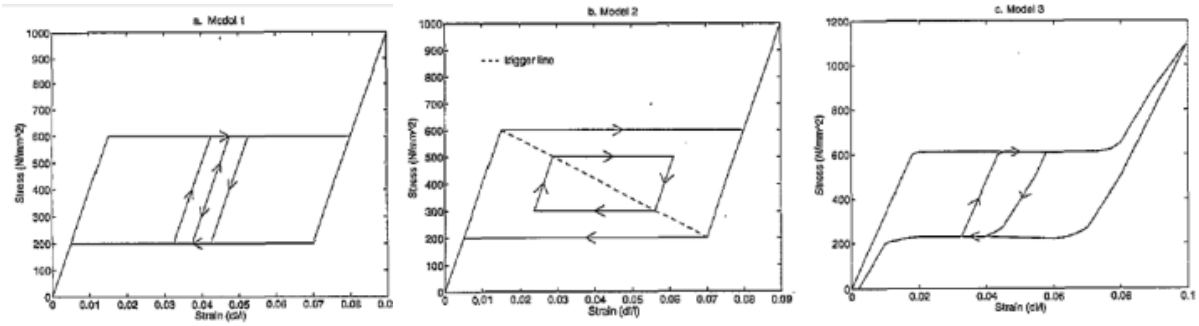

Figure 37 Theoretical inner hysteresis loops (Thomson et al. 1995)

Han et al. (2003) developed a damper device constructed of two steel bars with a diameter of 7mm and length of 582mm in addition to an SEA wire with a diameter of 0.75mm and length of 250mm. Eight of the dampers were installed in a two-metre high steel frame structure. The experimental data showed that the controlled structure had a significantly faster vibration decay speed compared to the uncontrolled structure (Figure 38). Numerical simulation by FEM also found that the damper with SEA wires exhibited an excellent seismic response under an El-Centro earthquake wave. Tamai and Kitagawa (2002) also proposed an SEA-based anchor bolt of a column base and SEA bracing as the anti-seismic component of the frame structure. An SEA seismic isolation system that can carry a maximum force of 600kN maximum force and a supplemental recentring force of 200 KN was produced by Dolce et al. (2001), which was installed in a small building in Italy. The building underwent a free oscillation test with 150mm displacement. The S. Giorgio Church Bell-Tower in Italy, which was seriously damaged by an earthquake in 1996, was rehabilitated using SEA devices (Indirli et al. 2001). An investigation

of this tower showed that it experienced no damage after another earthquake that occurred in 2000 with the same epicentre and a similar magnitude to. All the applications of SEA stated above present excellent energy dissipation, large restoring forces and good acceleration reduction. Two passive seismic control devices with pre-strained SEA (Figure 39(c))were presented by Dolce et al. (2000): a special bracing for frame structures and isolation devices for buildings and bridges (Figure 39). Full-scale model tests on the two types of devices not only showed good energy dissipation, self-centring capabilities and high stiffness for small displacements, but also extraordinary fatigue resistance, long-term reliability and high durability.

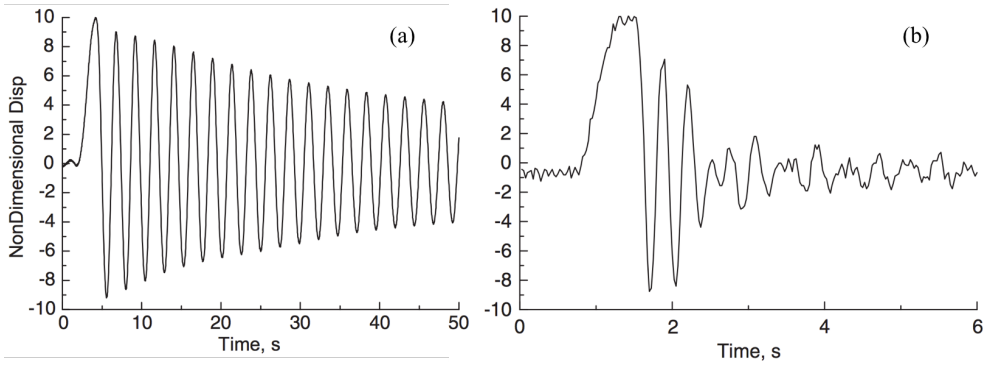

Figure 38 Vibration decay history of (a)the uncontrolled frame; (b) the frame with the SMA dampers (Han et al., 2003)

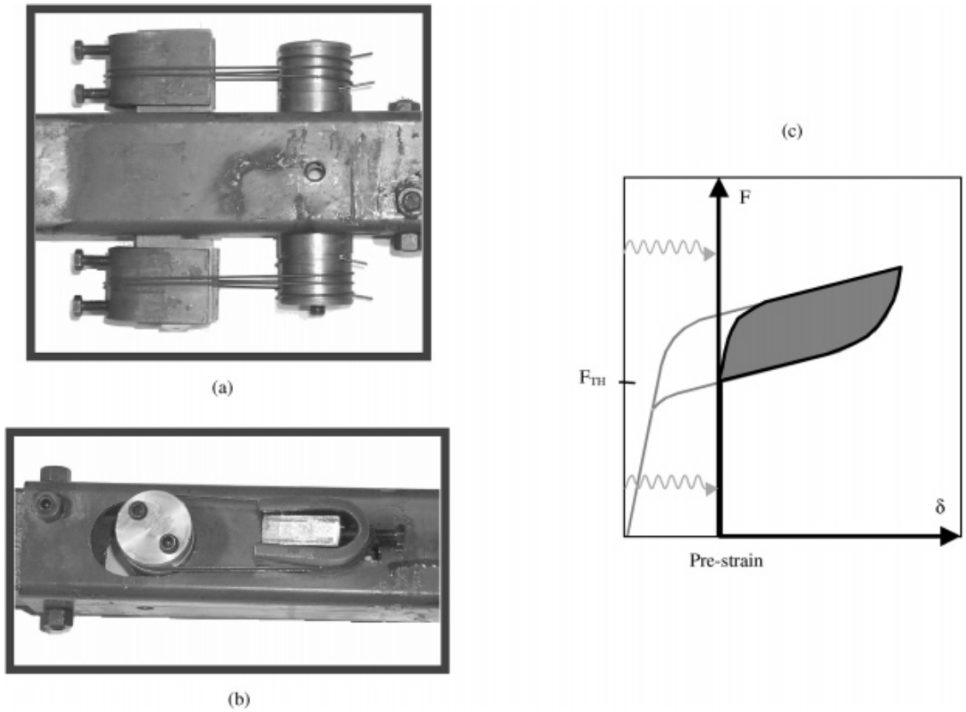

Figure 39 Re-centring group based on austenite superelastic wires: (a) top view; (b)lateral view; (c) effects of pre-strain (Dolce et al., 2000)

2.2.3.2 Mechanical behaviours of super-elastic alloy

The ambient temperature is a governing factor of the phase transformation of shape memory alloy. Apart from the previously mentioned four phase transformation temperatures, M_s, M_f, A_s and A_f, the ultimate temperature required to induce super-elastic deformation, M_d, was introduced by Miyazaki et al. (1990). The SMA exhibits the super-elasticity when the ambient temperature is between A_f and M_d (Janke et al., 2005). The shape memory effect governs the material behaviour if the ambient temperature is lower than M_f (Figure 40).

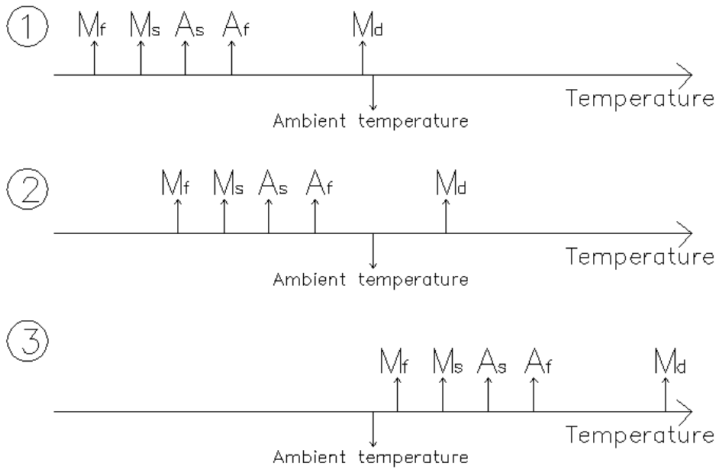

Figure 40 (1) Plastic deformation; (2) superelasticity; (3) shape memory effect or martensitic damping (Huang, 2017)

Miyazaki et al. (1986) conducted another experiment on Ni-Ti SEA under three different temperatures of 284.6K, 298.5K and 308.5K. The highest temperature will give a larger critical stress for inducing the martensite phase (Figure 41), while a smaller hysteresis loop will be achieved (Figure 42). The same trend has been also observed in the copper-based SEA that tested by Araya et al. (2008). Cu-Al-Be SEA were tested under ambient temperatures of 6°C, 20°C and 50°C for a strain amplitude of 2.2%. The result clearly indicated that the four transformation stresses with in one full loading cycle increased with the ambient temperature and then the equivalent damping ratio decreased with the increase of ambient temperature.

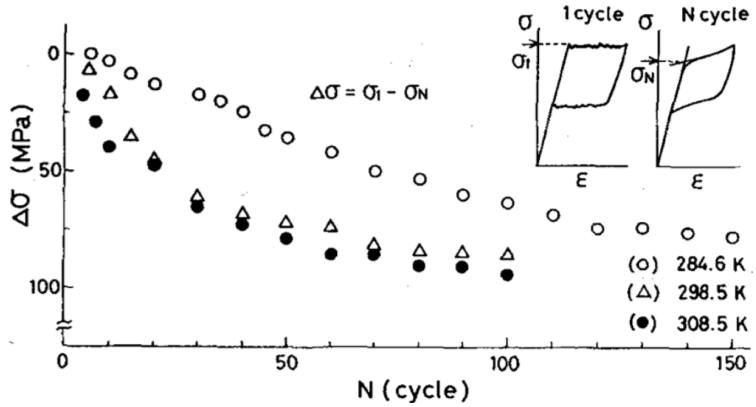

Figure 41 Effect of cyclic deformation of critical stress for inducing martensites at various temperatures (Miyazaki et al., 1986)

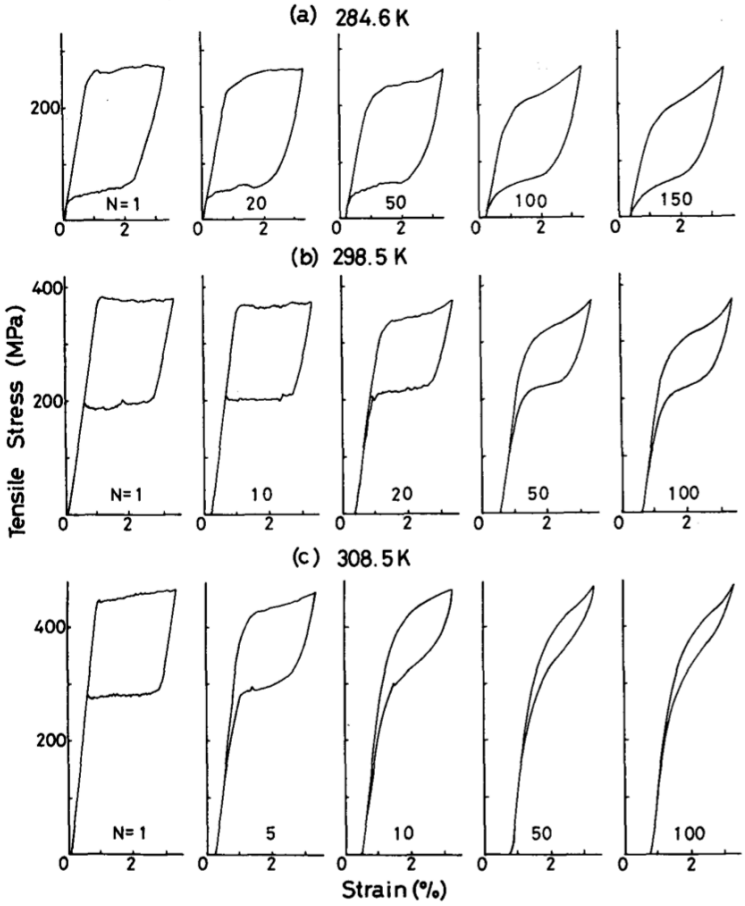

Figure 42 Effect of cyclic deformation on stress-strain curve at various temperature (Miyazaki et al., 1986)

Tension-compression cyclic tests were conducted on NiTi SEA bars with a diameter of 6.7mm by Liu et al. (1999). The tests were performed with three strain amplitudes: 1%, 2% and 4%. The stress-strain curves (Figure 43) showed different behaviours in tension and compression, with the material reaching higher compressive stress than tensile stress under the same strain amplitude. A plateau of stress-strain curves was observed under the tensile loadings, while strain hardening appeared earlier under compressive loadings in comparison to tensile loadings,

with no plateau. Consequently, an asymmetric hysteretic loop can be obtained for the SEA.

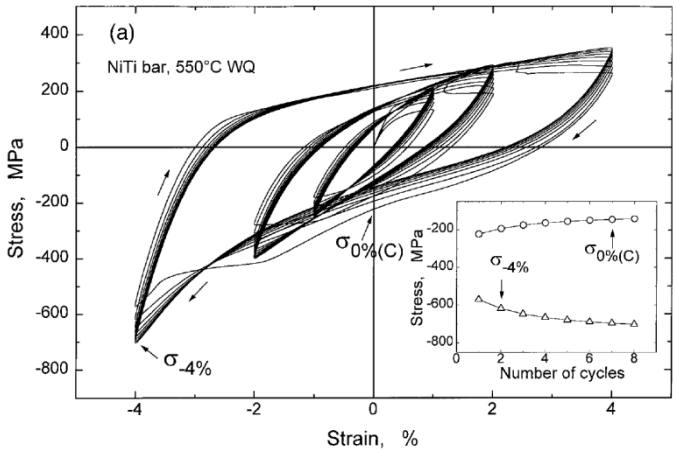

Figure 43 Stress±strain curves of a NiTi SMA under tension±compression cyclic deformations (Liu et al. 1998)

Investigations of the deformation in the pseudoelasticity characteristics of Ni-Ti SEA have been conducted by numerous researchers. Tensile cyclic tests on Ni-Ti wires with an A_f of 276K at room temperature were conducted by Miyazaki et al. (1981). The specimens had a diameter of 0.35mm and a gauge length of 30mmh. The tests results indicated that the strain hysteresis loop decreased as the number of cycles increased (Figure 44). This is due to the cyclic loading effect on SEA. When the number of loading cycle increases, the dissipated energy, strain energy, residual strain and phase transformation stress do not remian stable (Kawaguchi et al., 1991). The stress-strain curve (Figure 44) also shows a plateau after the elastic deformation, which the phase of the material transitioned to the martensitic and then the stiffness rose again due to strain hardening. The curve that occurs before strain hardening is defined as stage one of deformation, which is followed by stage two. The width of the plateau decreases when the number of cycles is increased. After 100 cycles, the tensile load was applying on the material until stage two started, hence another plateau appeared. This phenomenon means that the deformation of Ni-Ti SEA at stage one is inhomogeneous.

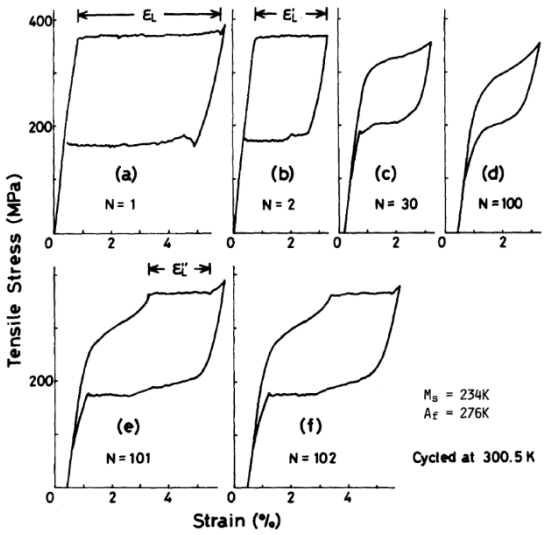

Figure 44 Effect of cyclic deformation on stress-strain curves (Mizayaki et al. 1981)

However, DesRoches et al. (2004) found that the mechanical behaviours tend to stabilise along with the loading cycles and this is defined as cyclic stabilisation of SEA. Miyazaki et al. (1986) indicated that the residual strain, critical stress for induce martensites and the strain hysteresis remain steady with increasing number of loading cycles. He explained that this effect is cause by the work hardening due to the introduction of dislocations in the martensitic phase during cyclic deformation. Cyclic stabilisation was also suggested by Soul et al. (2010). The residual strain increased and dissipated energy of a 2.46 mm diameter Ni-Ti SEA wire decreased rapidly during the first 10 loading cycles and tends to be stable after 20 loading cycles (Figure 45). Similar outcome was proposed by Liu et al. (1999) based on the tension-compression cyclic test of Ni-Ti SEA bars. The material exhibited greater damping capacity with larger strain amplitude, but this decreased with the number of cycles and became stable after around 15 cycles.

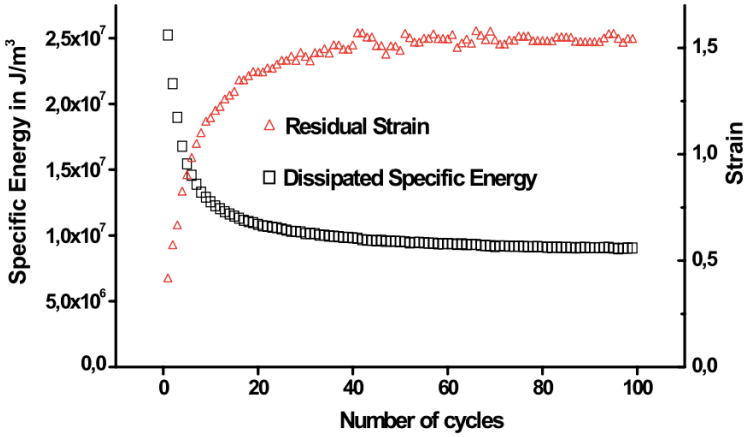

Figure 45 Evolution of the dissipated energy and residual strain during the 100 training cycles (Soul et al., 2010)

Hence, the ‘training’ treatment is recommended to give SEA stable mechanical behaviours before application (Miyazaki et al., 1986). In order to stabilise the material, Dolce and Cardone (2001) suggested that all SEA samples need to experience 10 loading cycles ‘pre-training’ with 7% strain amplitude at 0.02Hz loading rate. The residual strain and equivalent damping ratio of SEA are considered remain constant after the ‘pre-training’.

DesRoches et al. (2004) conducted tensile cyclic tests on Ni-Ti SEA with four different diameters (from 1.8mm to 25.4mm). The SEA wires exhibited relatively higher strength and significant higher equivalent viscous damping than the SEA bars. The equivalent viscous damping defines the energy dissipation capability, which is equal to the area of the hysteresis loop divided by the product of π and the strain energy of an entire cycle. The equivalent viscous damping had a linear increase when the strain amplitude was less than 5% and it was slightly reduced when the strain amplitude reached more than 5% (Figure 46) (Dolce and Cardone, 2001). Moreover, the martensite Ni-Ti showed significantly higher damping capacity than the austenite Ni-Ti. Nevertheless, DesRoches et al. (2004) found that the residual strain increased with the cyclic strain amplitude.

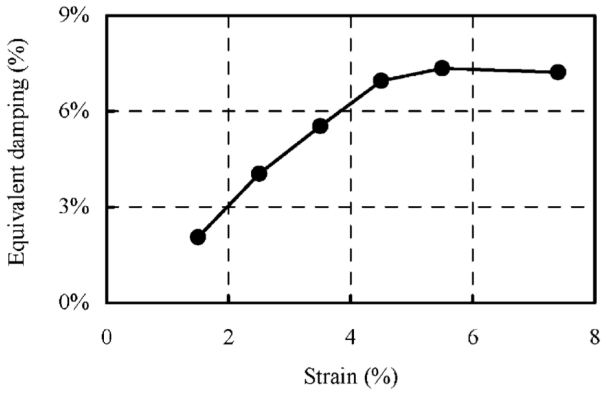

Figure 46 The equivalent damping ratio influent by strain amplitude (Dolce and Cardone, 2001)

Many researchers have proved that the damping capacity is affected by the loading frequencies. Tensile cyclic tests were performed on SEA bars with a composite of Cu-Al-Mn by Araki at al. (2012) under three different frequencies of 0.001Hz, 0.5Hz and 1Hz. The results showed that the maximum damping capacity occurred under quasi-static loading while the loading frequency was 0.001Hz and there was no significant change between the loading frequencies of 0.5Hz and 1Hz. However, only three cycles were analysed in this experiment. Dolce and Cardone (2001) found that the equivalent viscous damping decreased from 0.02Hz loading frequency and remained relatively stable after 0.2Hz loading frequencies. There was a slight increase from 1Hz to 4Hz loading frequencies. The secant stiffness has the contrary trend to

the equivalent damping ratio (Figure 47). Based on the experiments conducted by Wolons et al. (1998), the energy dissipation experienced a rapid decrease during the initial stage of the loading frequencies increase (less than 1Hz) and it approached a stable level at around 10Hz loading frequency. The energy dissipation capacity was found to be 50% of the low loading frequency at a loading frequency of 10Hz. Qian et al. (2013b) developed a passive damper with Ni-Ti SEA wires for structural vibration control. The test results indicated that the equivalent viscous damping decreased from 0.01Hz loading frequencies and was not sensitive to loading frequencies above 0.5Hz. Gencturk et al. (2014) also reported that the equivalent viscous damping of copper-based SEA had a significant decrease from the quasi-static loading rate to 1Hz loading frequency, while it had negligible change with the increased loading frequencies from 1Hz to 15Hz. The reason for the damping capacity decrease with the rising of loading frequency might because the inverse transformation stress increased more than the transformation stress when the loading frequency increased (DesRoches et al., 2004; Qian et al., 2013a). Hence the hysteresis loop becomes narrower and results in the decrease of the equivalent damping ratio (Figure 48). The other reason for the frequency effect is the temperature increase during the cyclic loading due to the self-heating (DesRoches et al., 2004; Soul et al., 2010) which refers to the damping ratio is lower at higher temperature (Araya et al., 2008). DesRoches et al. (2004) also indicated that the loading frequency will not effect on the residual strain which needs further study on.

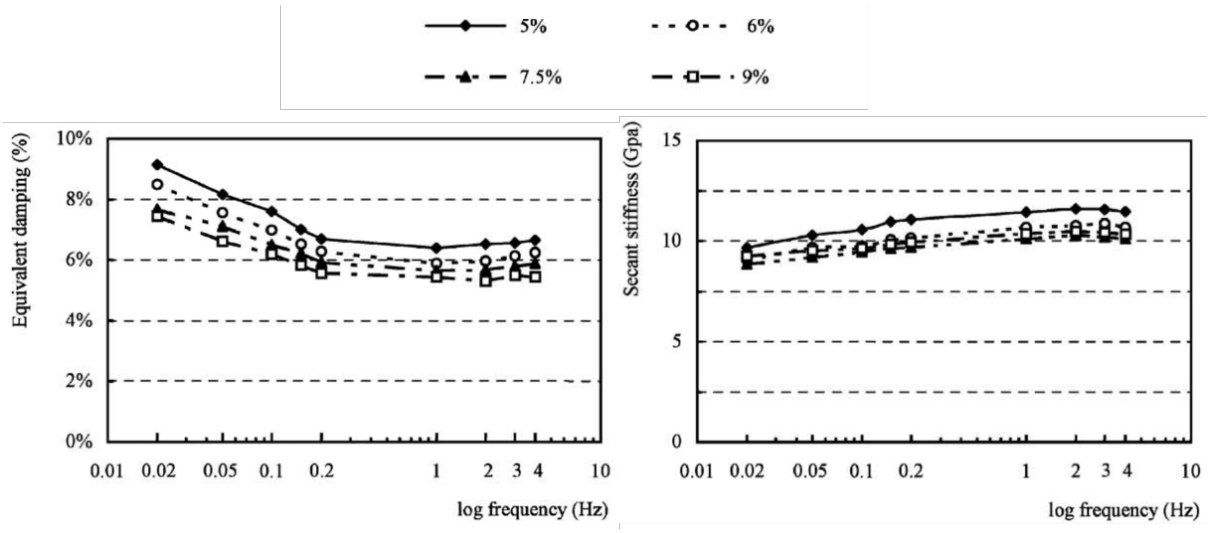

Figure 47 Cyclic tensile tests on pre-tensioned superelastic wires: mechanical behaviour as a function of strain amplitude and frequency of loading (Dolce & Cardone, 2001)

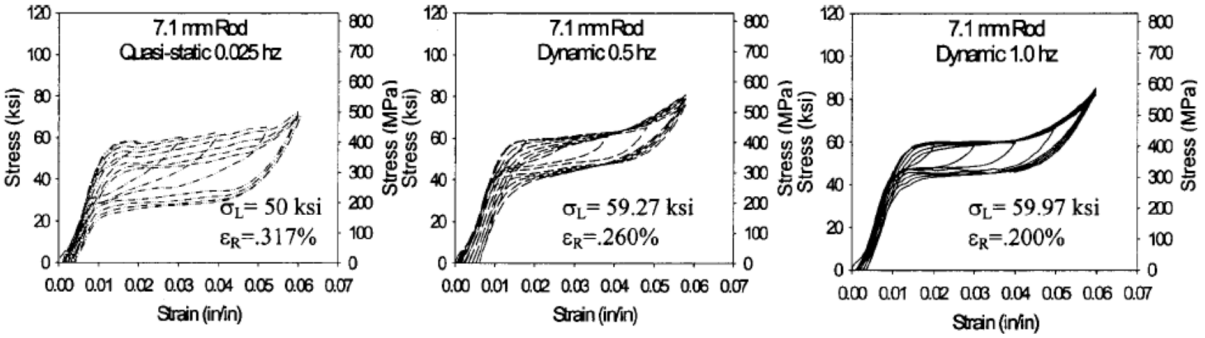

Figure 48 Comparison of static and dynamic loading on 7.1 mm diameter shape memory alloy bar (DesRoches et al., 2004)

Instead of having a stable equivalent damping ratio under dynamic loading frequency that found by Araki at al. (2012), Dolce and Cardone (2001), Wolons et al. (1998), Qian et al. (2013b) and Gencturk et al. (2014), Piedboeuf and Gauvin (1998) claimed that the dissipated energy and equivalent viscous damping decreased with the increasing frequencies after 0.1Hz (Figure 49). Both the maximum energy dissipation capacity and equivalent viscous damping occurred around 0.1Hz based on the results of tensile tests conducted on Ni-Ti wires with a diameter of 0.1mm. Soul et al. (2010) also demonstrated similar finding.

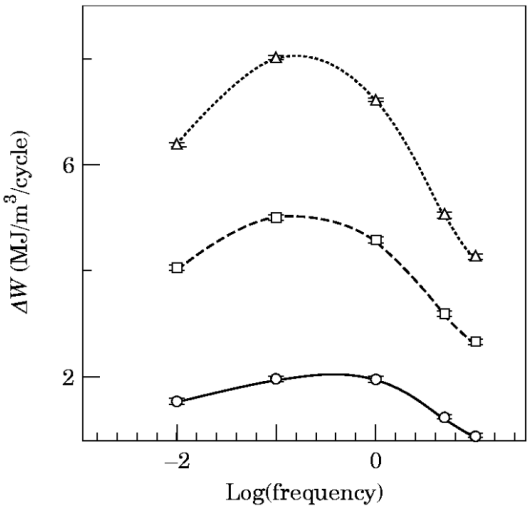

Figure 49 Variation of the average values of the dissipated energy at 2% (——), 3% (- - - -) and 4% (……) of strain level (Piedboeuf and Gauvin, 1998)

Tensile cyclic tests were performed on Ni-Ti SEA bars by Choi et al. (2010). The result (Figure 50) shows that under static loading, the material has a residual strain up to 2.5%, but it was insensitive to the loading rate. The residual strain increased with the number of loading cycles under dynamic loading and remained constant after approximately 250 cycles. In fact, this finding is contrary to others. It might because the inconsistent manufacture process gives the material different mechanical properties which means that the material is not stable at current stage.

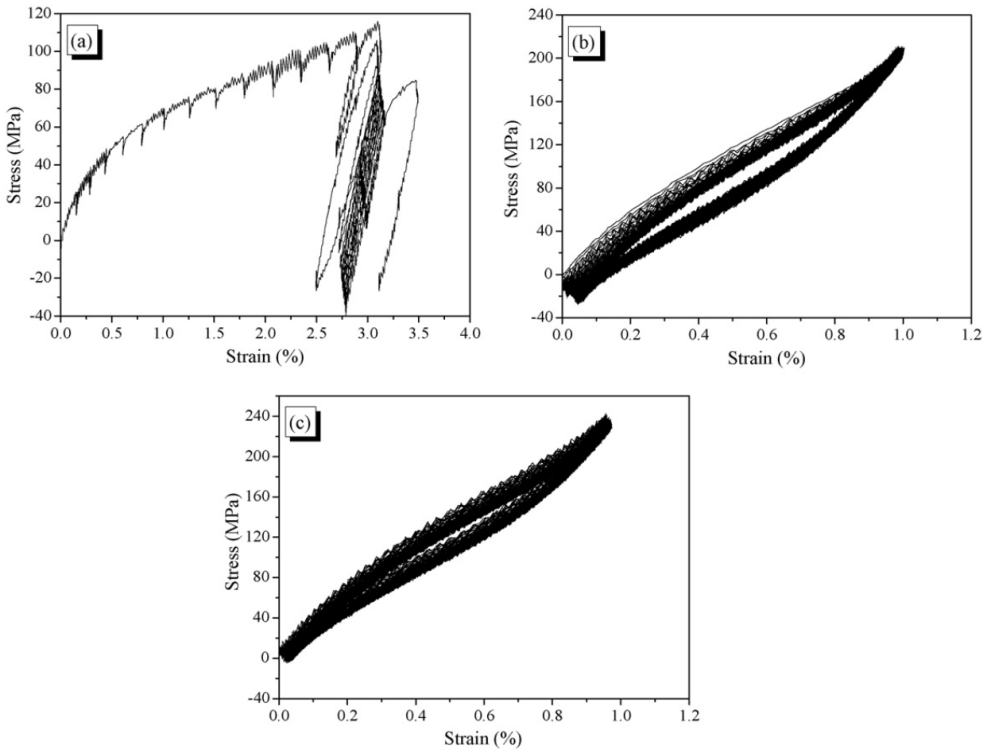

Figure 50 Hysteretic curves of SEA bar under (a) Static loading, (b) dynamic loading with the first 500 cycles, (c) dynamic loading with the second 500 cycles (Choi et al., 2010)

The fatigue behaviour of Cu-Al-Be SEA and Ni-Ti SEA under the effects of an earthquake as well as for lifetime were analysed by Torra et al. (2009). The cyclic tests for both types of SEA indicated that the Cu-Al-Be SEA is sufficient for sustaining the earthquake effect with larger deformations for a shorter time, while Ni-Ti SEA is more appropriate for damping the small deformations over a long period, which works for around 500,000 cycles.

The understanding of copper SEA remains limited and only a minimal amount of research has investigated the alloy. The mechanical behaviours of super-elastic alloy will change with different compositions and manufacturing processes. Regrading to the literature review in this section, the super-elasticity property examined by Choi et al. (2010) is found not stable, and a large residual strain under static loading appears. Therefore, a complete characterisation of SEA in terms of loading rate and strain level should be carried out. The findings from the literature review presented in this section are summarised below:

- ‘Pre-training’ is needed before application of SEA due to the cyclic stabilisation effect of the material.
- The damping capacity of Ni-Ti SEA changes with the strain amplitude. The previous application of SEA demonstrated that the pre-strain of SEA can contribute to the

damping capacity of the structure. Therefore, the strain effect with and without pre-strain of copper-base SEA needs to be evaluated.

- Loading frequency and number of loading cycles will change the mechanical behaviour of SEA. Structures always suffer earthquakes because of the cyclic loading and various frequencies of earthquakes. Hence, both effects need to be analysed.
- Self-heating will cause the decrease of the damping capacity of SEA due to the temperature effect. It might be the reason for equivalent damping ratio drops with the increasing of loading cycles.

In order to use the SEA in traditional timber structures to enhance the seismic performance of the structures, the energy dissipation and recentring capabilities of SEA need to be understood by conducting static and dynamic experiments with various strain amplitude under different frequencies.

Chapter 3 Material Characterisation

Based on the studies of several material previously, super-elastic alloy (SEA) has been chosen to enhance the anti-seismic performance of traditional timber structures in this study. To investigate the mechanical properties of SEA bars under dynamic loading, cyclic tensile tests for non-prestrained and pre-strained Cu-Al-Mn SEA bars were performed. The stress-strain curves, secant stiffness and equivalent damping ratios were analysed and the temperature of some of the pre-strained samples was recorded.

3.1 Samples set up

The shape memory alloys used in this study are polycrystalline and superelastic Cu-Al-Mn super-elastic alloy bars with a diameter of 12mm, provided by Furukawa Techno Material Co., Ltd., Japan. The chemical composites of the Cu-Al-Mn SEA bars as measured by a Scanning Electron Microscope are Cu=81.84wt%, Al=7.43wt% and Mn=10.73wt%. The transformation temperature, A_f, is -39℃; much lower than the normal ambient temperature that gives a stable superelastic behaviour to the material.

The samples were prepared according to British Standard EN ISO 6892-1:2009, the original gauge length of the Cu-Al-Mn SEA bars was set to be 50mm and the total length of the sample was 160mm, which includes the transition area (10mm) and 50mm at both ends for the grip (Figure 51). The diameter of the gauge had been machined down to 9mm in diameter, which can give highest strength to the connection without any failure at the transition area. All samples performed 5 quasi-static tensile cycles with a loading rate of 1mm/min to the strain level higher or equal to that of cyclic tests, referred to as 'pre-training', in order to stabilise the material, as shown in Figure 52. The material began transfer from elastic to superelastic deformation at around 1% strain level with a transformational stress of 240MPa. The transformation from martensite back to austenite during unloading was at around the same strain level as loading and the residual strain was less than 0.05%.

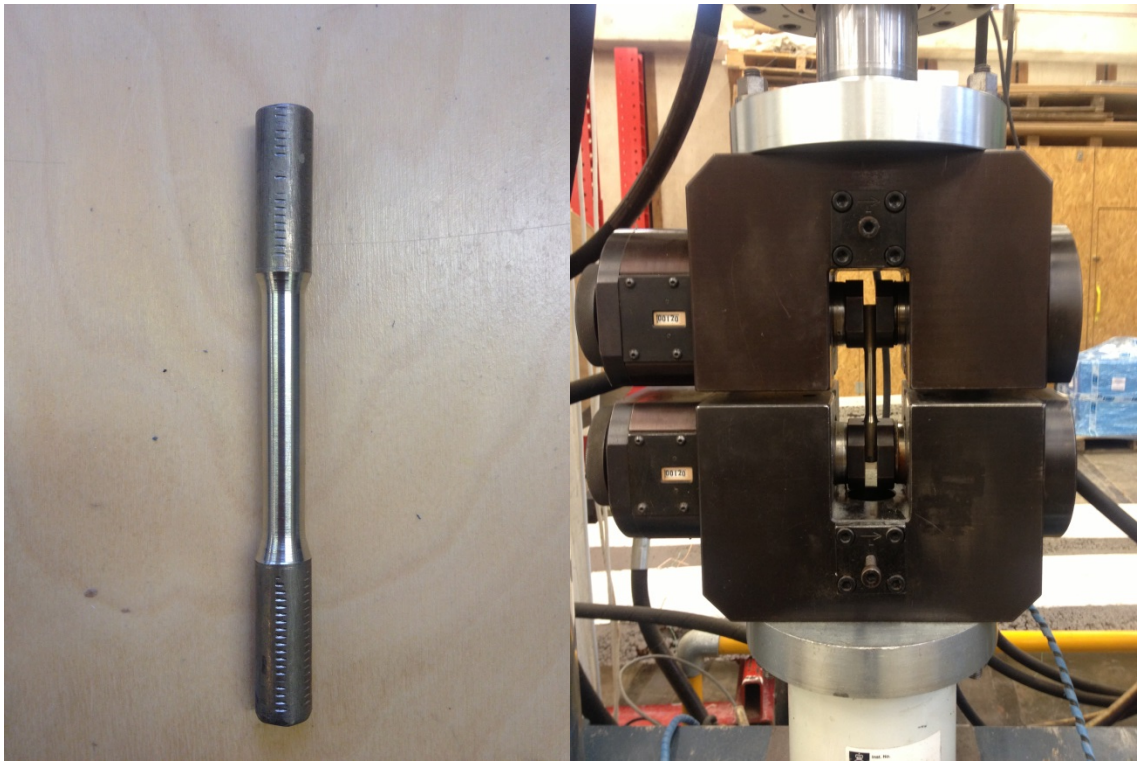

Figure 51 Experimental test machine and sample

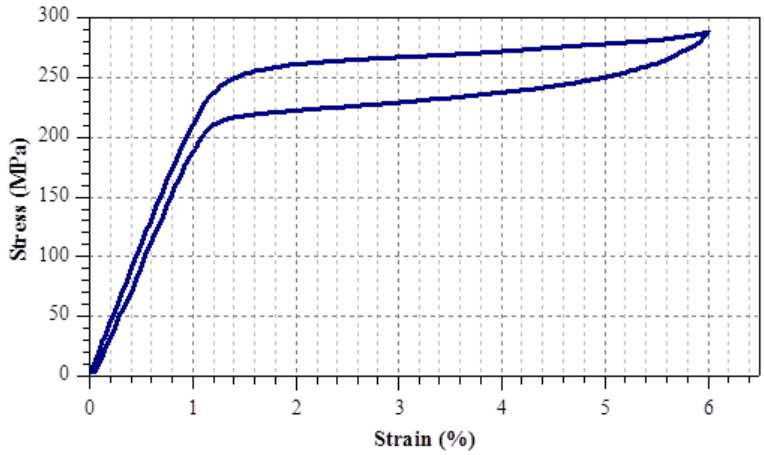

Figure 52 The stress-strain curve of quasi-static tests with 6% strain amplitude

A pre-strain can be applied to the super-elastic alloy bar by applying an axial tensile force onto the bar. This will change the initial crystal structure of the connection bar to detwinned martensite and theoretically jump over the initial elastic stage and dissipate energy more quickly.

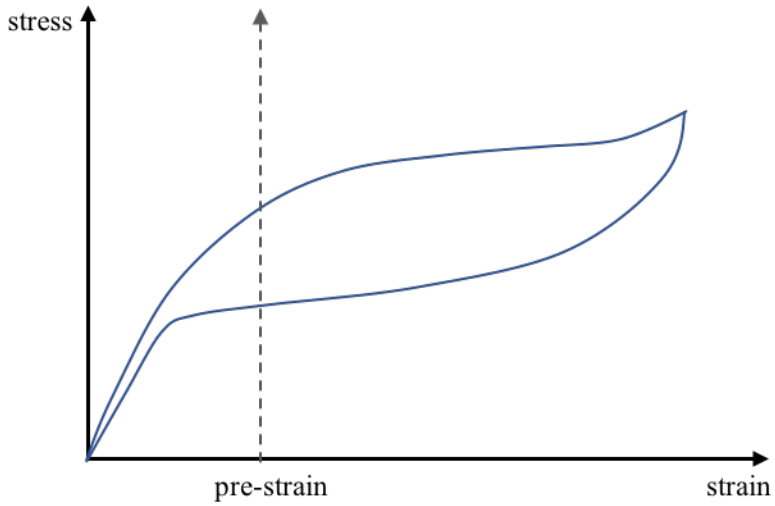

Figure 53 Schematic of pre-strain of super-elastic alloy

3.2 Experimental programme

The Dartec 100kN Universal Testing Frame with hydraulic clamps was used for the tensile tests. The tests were controlled by displacement. The displacements and loads were recorded by data logger. The experimental programme of cyclic tensile tests for both non-prestrained and pre-strained is summarised in Table 4. There is no test for the 4% strain level under 8Hz loading frequency since the displacement exceeded the test machine's limit under that loading frequency. For the pre-strained cyclic tensile tests, the samples were pre-strained to 2% and 4% strain with the cyclic amplitude of ±1% and ±2% strain, respectively. Different loading frequencies were applied to the samples in order to understand the hysteretic behaviour changes with the loading frequency. When SEA are been used in anti-seismic dampers, the fatigue life of the material needs to overcome 1000 working cycles (Torra et al., 2015). Hence, a total of 1000 cycles of fatigue was imposed to all the cyclic tests so as to understand changes to its mechanical properties. The temperatures of samples P5 and P6 were recorded during the tests.

Table 4 Experimental tests conditions

Frequency	**Non-prestrain**		**Pre-strained**		
	2%	4%	1-3%	3-5%	2-6%
1Hz	N1	N5	P1	P3	P5*
2Hz	N2	N6			
5Hz	N3	N7	P2	P4	P6*
8Hz	N4				

*NOTE: The temperature of sample was recorded during the test for further investigation.

3.3 Experimental results and discussion

3.3.1 Non-prestrain cyclic tensile tests

The energy dissipation capacity of a material can be estimated by the equivalent damping ratios, which can be calculated using the equation below (Priestley, 1996):

$$\xi_{eq} = \frac{A_h}{4\pi A_e} \quad (1)$$

where A_h is the area inside the hysteresis loop that represents the energy dissipated per cycle and the area A_e represents the equivalent linear elastic strain energy.

The stress-strain curve for non-prestrain cyclic tensile tests during the10^{th}, 300^{th}, 600^{th} and 1000^{th} cycles of each sample are illustrated in Figure 54 and Figure 55. The stress-strain curves of sample N1 that was tested with 2% strain amplitude and 1Hz frequency did not change significantly with loading cycles. For samples N2, N3 and N4, the maximum stress of a single loading cycle increased with the loading cycles, because the material had entered the martensitic hardening stage. This phenomenon can be seen from Figure 56(b) where the secant stiffness increases with the loading cycles. The secant stiffness increase rate of sample N3 was much quicker than for other samples due to the material discrepancy caused by the different cold work and annealing treatment undertaken by the manufacturer for each bar. Because the microstructure of material might have unrecoverable transmutation under 5Hz and 8Hz frequencies and the Young's modulus has changed for the unloading period, the unloading curve will intersect with the loading curve giving the hysteresis loop an '8' shape, as shown in Figure 54 (samples N3 and N4).

The changing of equivalent damping ratio with the loading cycles is illustrated in Figure 56(a). The equivalent damping ratios of the sample with 2% strain level and 1Hz loading frequency (sample N1) remained constant during the 1000 cycles' tests and the equivalent damping ratio of sample N5 rose initially and then remained unchanged after 300 cycles, while the equivalent damping ratios of other samples generally decreased due to the self-heating of the material. Nevertheless, there was a rise in sample N7 during 400 to 650 cycles. It can be seen from Figure 55 that the hysteresis curve of the 600th cycle has covered a larger area than the 300th cycle since the unloading curve has changed. The possible reason for this might also be unrecoverable transmutation of the material's microstructure and the Young's modulus of unloading having been altered.

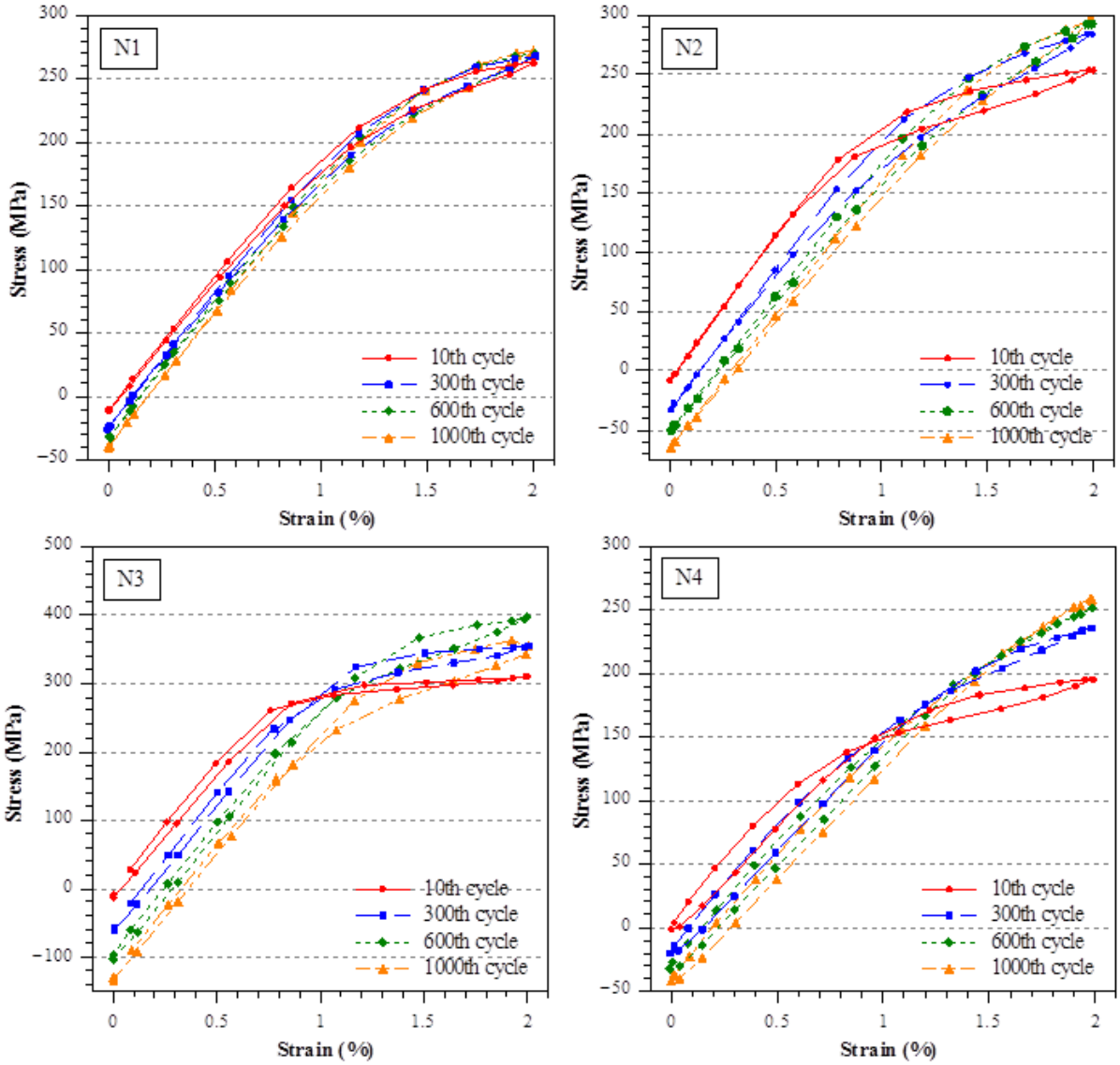

Figure 54 Hysteresis curves of non-prestrained Cu-Al-Mn SEA bars with 2% strain

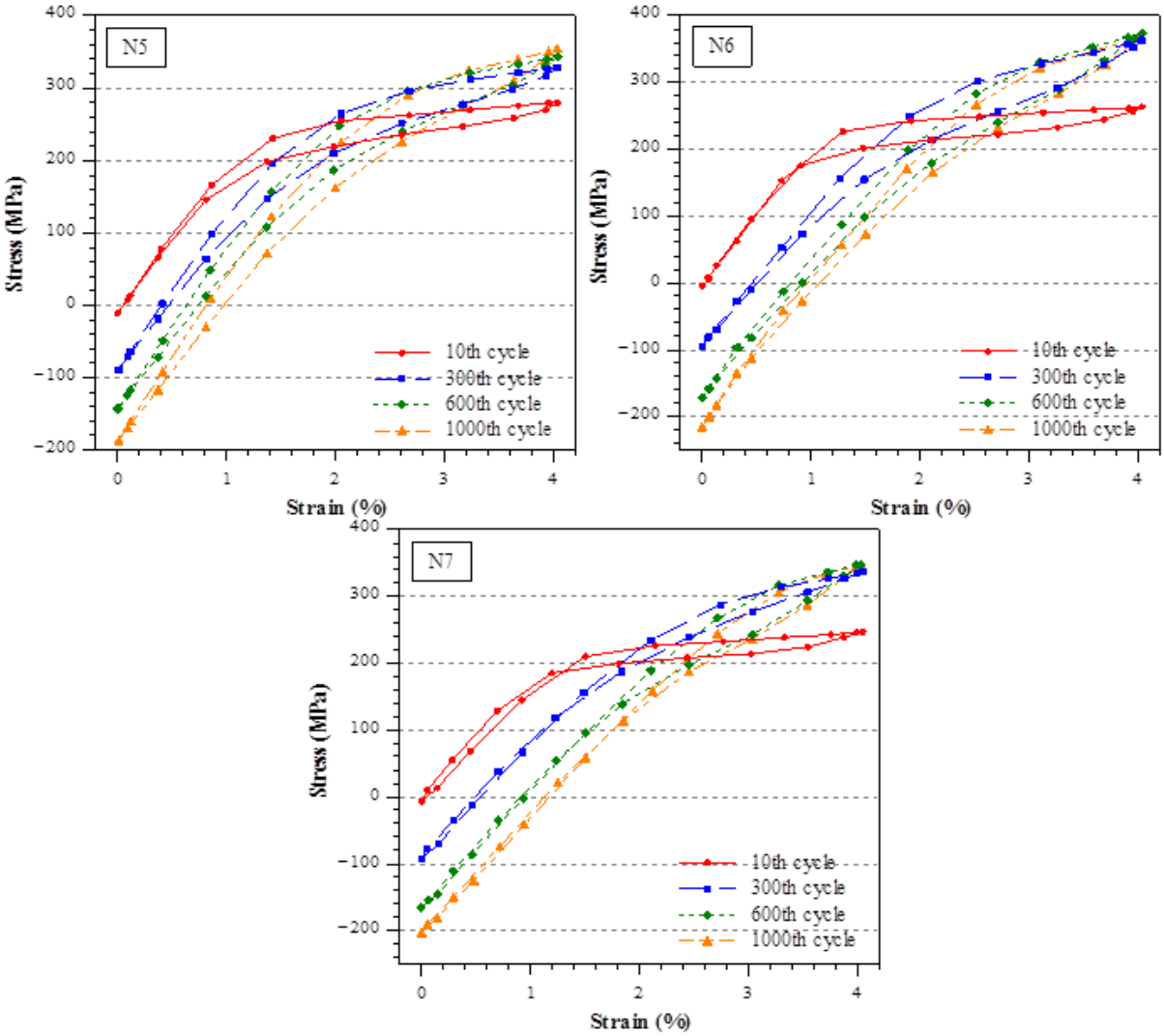

Figure 55 Hysteresis curves of non-prestrained Cu-Al-Mn SEA bars with 4% strain

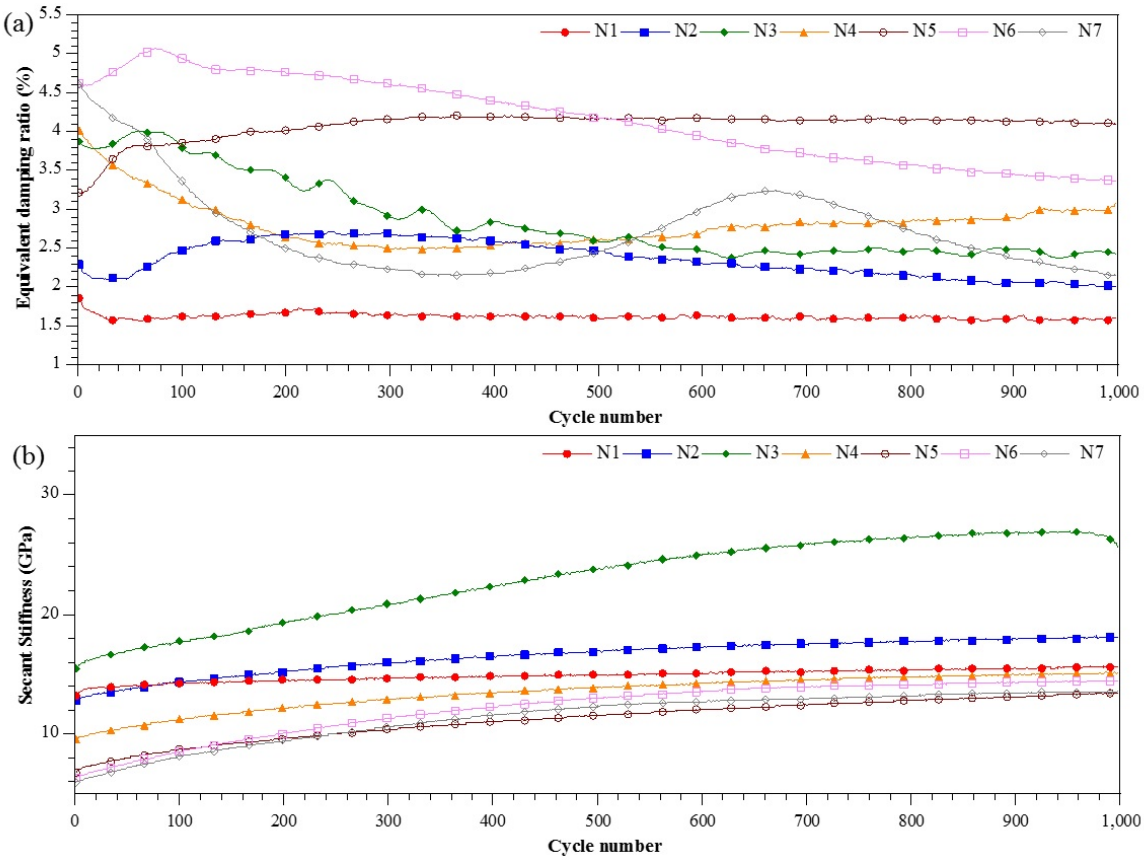

Figure 56 (a) Equivalent damping ratio (b) Secant stiffness changes with loading cycles for non-prestrained cyclic tensile tests.

For the samples with 4% strain amplitude, material completely performed the superelastic deformation with the hardening of the material becoming more dominant. The residual strains of the tests with 2% strain amplitude after 1000 loading cycles were around 0.3%, while it increased to approximate 1% for 4% strain amplitude tests. Table 5 presents the equivalent damping ratio increases with the increase of loading frequency with 2% strain amplitude, while this growth does not occur in the cases at 4% strain level. This is because the self-heated temperature becomes a noticeable effect of sample N6 and N7 due to both larger pre-strained amplitude and higher loading frequency. The equivalent damping ratio of sample N7 decreased rapidly after 700 cycles due to the dramatic rise in temperature by self-heating.

Table 5 Equivalent damping ratio for non-prestrained samples in the 10^{th} and 1000^{th} cycles.

	2%		4%	
	10^{th} cycle	1000^{th} cycle	10^{th} cycle	1000^{th} cycle
1Hz	1.71%	1.58%	3.20%	4.09%
2Hz	2.20%	2.05%	4.61%	3.37%
5Hz	3.58%	2.47%	4.57%	2.16%
8Hz	3.96%	3.02%	N/A	N/A

3.3.2 Pre-strained cyclic tensile tests

Figure 57 shows the stress-strain curves for each pre-strained tensile sample during 10^{th}, 300^{th}, 600^{th} and 1000^{th} loading cycles. The maximum stress of a single loading cycle increases with the number of loading cycles and the minimum stress decreases with the number of loading cycles or even drops below zero, which means the SEA bar has experienced compression. The increment of maximum stress of a single loading cycle during 1000 loading cycles with 1Hz loading frequency is relatively smaller than that with 5Hz loading frequency, which indicates that martensitic hardening becomes more significant when it experiences higher loading frequency. Samples P1, P5 and P6 have experienced the compression. Compression caused buckle of the materials which reduced the fatigue life of SEA and failure of the bars occurred along the grain boundary. The fatigue life of all test samples will not be discussed further in this study since they are not cracked or snapped during 1000 loading cycles. For both non-prestrained and pre-strained samples, the residual strain becomes more significant with a larger strain level but independent of the loading frequency, which is consistent with previous research. (DesRoches & Smith, 2004)

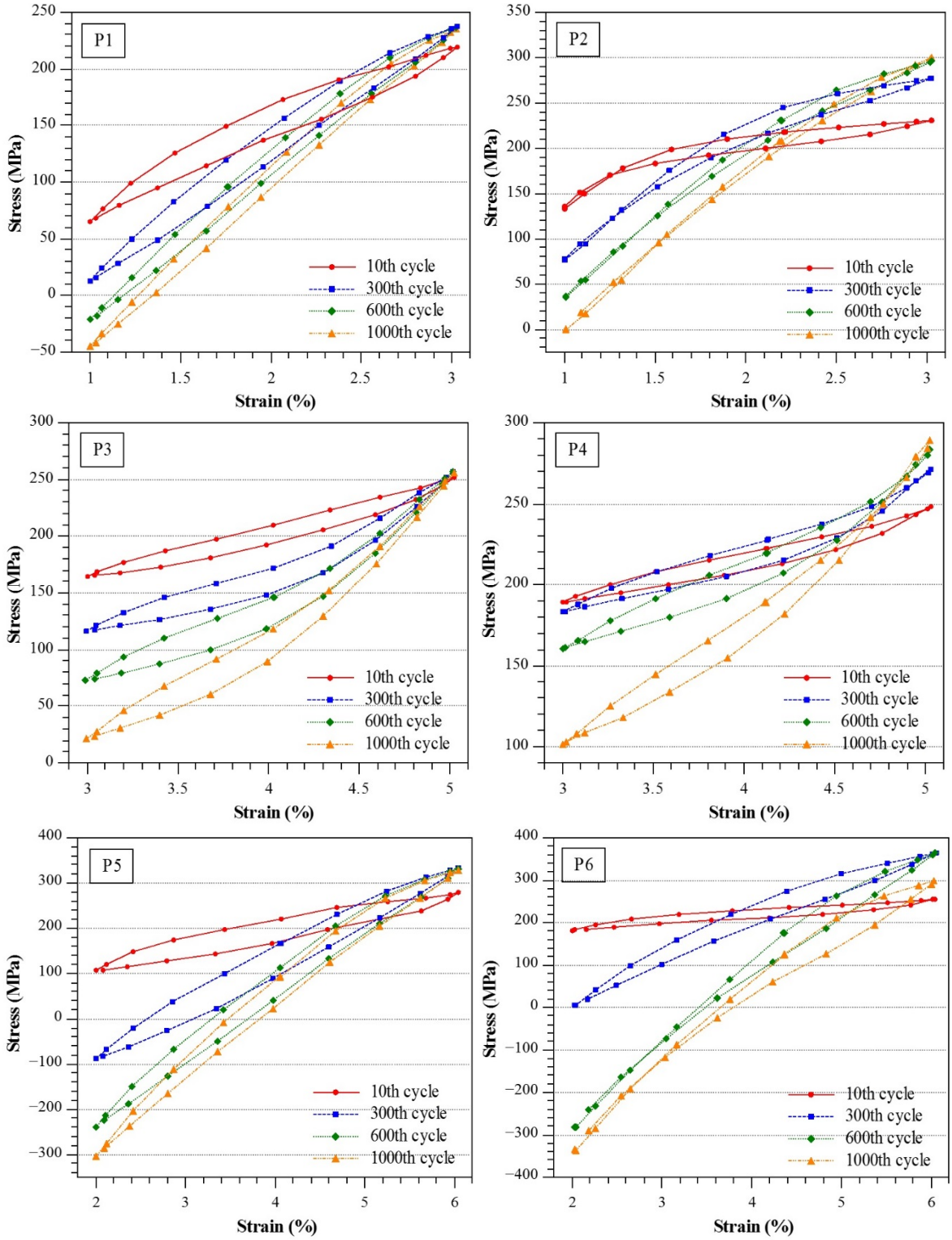

Figure 57 Hysteresis curves of Cu-Al-Mn SEA for pre-strained cyclic tensile tests

The hysteresis curves of the 10th cycle with pre-strained samples under different frequencies and strain levels are illustrated in Figure 58. It can be observed that the sample cycles between 2-6% strain levels with 1Hz frequency and has produced the largest area inside the hysteresis curve, which implies the largest energy dissipation capacity.

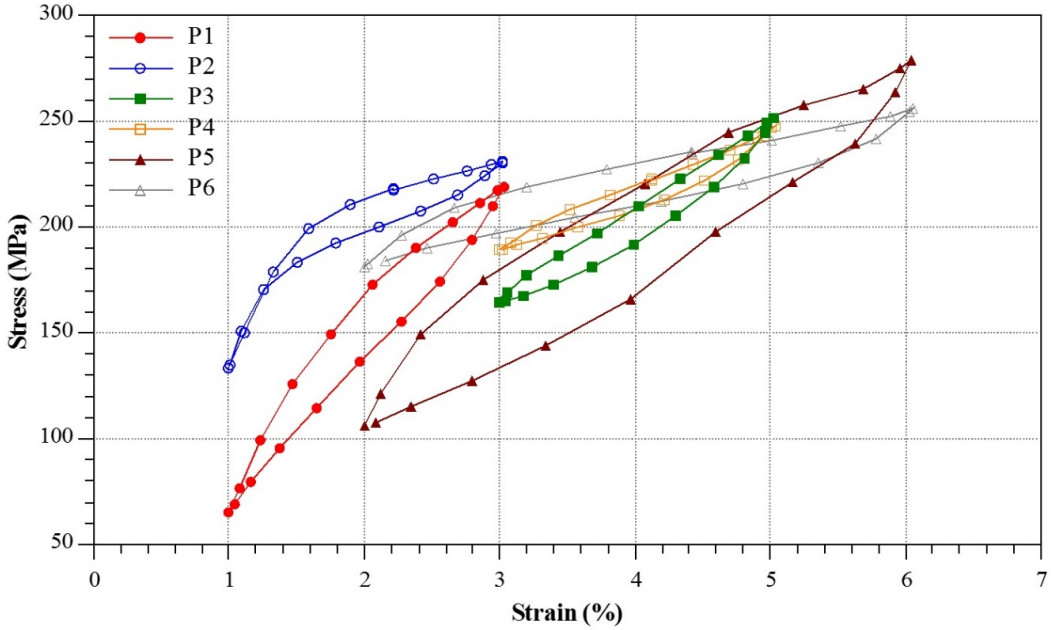

Figure 58 Comparison of the10th cycle's hysteresis curve between each sample

The equivalent damping ratio varies from the 10th to 1000th cycle under different experimental conditions, as summarised in Table 6. The samples tested with 3-5% strain level have higher damping capacity than those with 1-3% strain level, since the material reaches super-elastic deformation at 1.2% strain level. The table also shows remarkably high values of equivalent damping ratio with 2-6% strain level at more than 13%. By comparing the results with the non-pre-strained tests, samples with pre-strain exhibited much higher damping capacity and even decayed drastically after 1000 cycles of loading.

Table 6 Equivalent damping ratio for pre-strained samples in the 10th and 1000th cycles.

	1-3%		3-5%		2-6%	
	10th cycle	1000th cycle	10th cycle	1000th cycle	10th cycle	1000th cycle
1Hz	8.71%	3.40%	8.93%	4.73%	13.70%	4.35%
5Hz	6.18%	0.59%	8.65%	3.50%	13.17%	2.86%

Figure 59 indicates that the equivalent damping ratio and secant stiffness changes with the number of loading cycles. The equivalent damping ratio drops quickly during first 300 cycles and remains almost constant after 700 cycles. It stands to reason that samples P5 and P6 have higher equivalent damping ratios than other samples as they were cycled between larger strain amplitudes. Under the same strain level, higher loading frequency gives a smaller equivalent damping ratio.

Since the material starts to transfer from elastic to superelastic deformation at around 1% strain, samples P3-P6 should have lower initial secant stiffness than sample P1 and P2. However,

sample P2 also shows relative lower initial secant stiffness, which may be due to the diversity between each sample. The secant stiffness of hysteresis curve increases substantially with the number of loading cycles. The possible reasons for this behaviour are that stress grows with the number of loading cycles due to the martensitic hardening of the material and that the residual strain rises as well and this needs a restoring force to compress the sample back to its original position. In sample P6, the secant stiffness rose from 2GPa to 17GPa.

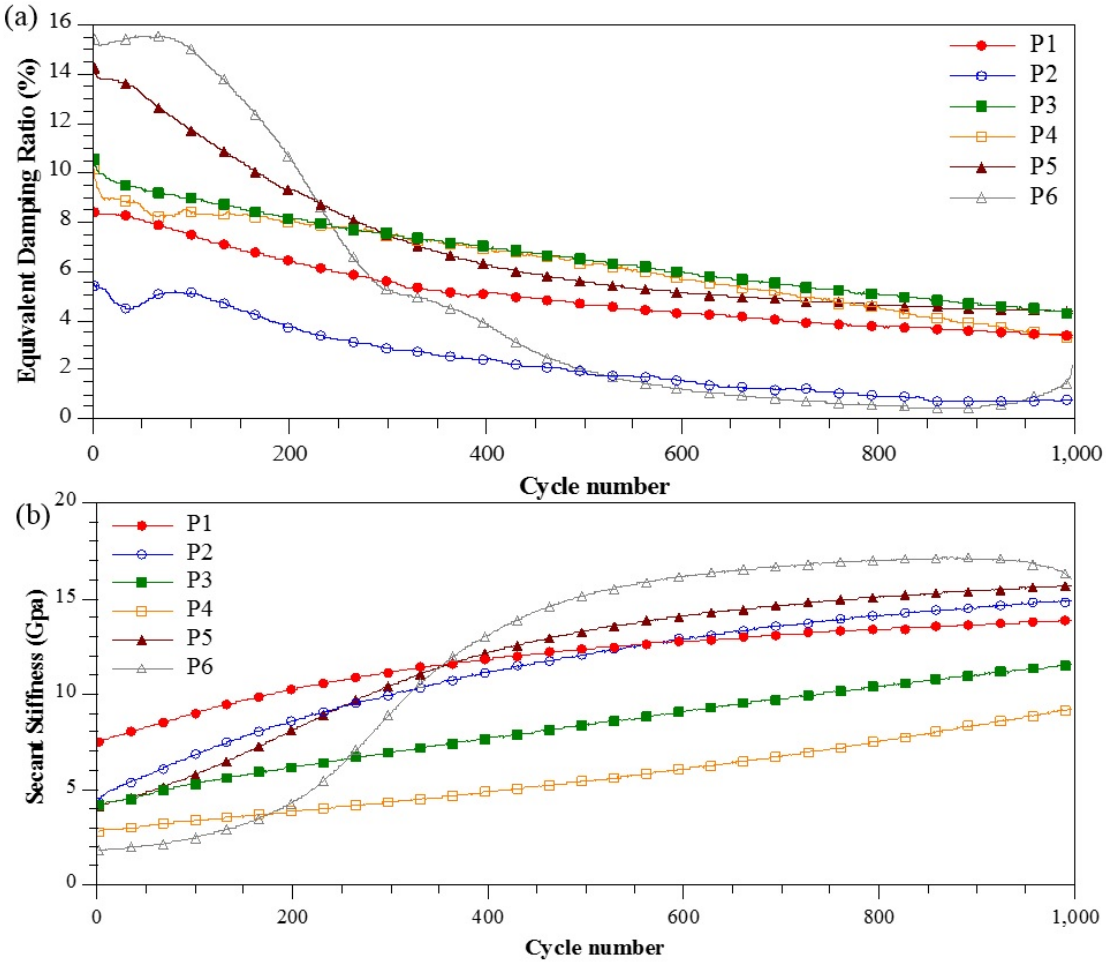

Figure 59 (a) Equivalent damping ratio (b) Secant stiffness changes with loading cycles for pre-strained cyclic tensile tests

3.3.3 Interaction between temperature, damping and loading frequency

As the latent heat of phase transformation cannot be dissipated fast enough, this results in the self-heating of the material during the tests (DesRoches & Smith, 2004; Soul et al., 2010). The temperature of the SEA sample will increase with the increase of the loading frequency due to self-heating (DesRoches et al. 2004). The thermo-mechanical properties of SEA have been investigated (Shaw & Kyriakides, 1995) and show that the self-heating of SEA will increase the austenite to martensite transformation stress and decrease the stress required for

transformation of martensite to austenite. The stress-strain curve of unloading will intersect with loading for non-prestrained cyclic tensile tests, but this will not occur in pre-strained cyclic tensile tests due to the material being always located in the phase transformation stage.

According to previous research investigations by others (Strnadel et al., 1995; Chang et al., 2006; Niitsu et al., 2011), critical transformation stress and secant stiffness diminishes as the experimental ambient temperature decreases. Moreover, it has been found that the equivalent damping ratio decreases while increasing the experimental ambient temperature (Araya et al., 2008; Andrawes & DesRoches, 2007; Dolce & Cardone, 2001). Gencturk et al. (2014) presented the loading rate dependency of super-elastic Cu-Al-Mn SEA bars. The samples were tensioned for 5 cycles of 5% at 1Hz to 15Hz loading frequency and results demonstrated that the equivalent damping ratio decreased with the increase of loading frequency. The reason for this behaviour is due to the self-heating temperature increase with the loading frequency increase. Other research has been presented by Moroni et al. (2002), where Cu-Zn-Al-Ni SEA bars were under axial tests with ±1.5% strain amplitude. The work showed that loading frequency has limited influence on damping properties. However, the range of the loading frequency was between 0.5 to 2Hz and, moreover, the samples were tested in tension-compression to a strain level up to 1.5%.

The results of non-prestrained cyclic tensile tests indicate that the differences in behaviours of SEA between this study and previous research might be the different strain amplitudes chosen and different compositions of the materials. For the tests with 2% strain amplitude, the materials were not always located in phase transformation stage and hence the latent heat of phase transformation is not a primary governing factor here. For the tests under 4% strain amplitude at 1Hz loading frequency, the materials still have enough time to dissipate most of the latent heat. Gencturk et al. (2014) stated that the number, size and orientation of grain are the important factors affecting material behaviours.

However, the self-heating induced temperature change of material will influence the equivalent damping ratio and secant stiffness of pre-strained SEA bars. During pre-strained cyclic tensile tests, the materials were always located in phase transformation stage and self-heating temperature became significant. The results also show that the equivalent damping ratios on pre-strained SEA bars might have a slight reduction with the increase of loading frequency. This is because higher loading frequency will induce greater self-heating temperature with martensitic material and then reduce the equivalent damping ratios.

The effects of fatigue on samples N1 to N6 were found to be negligible during 1000 loading cycles, yet were found to be a great influence on other samples with the result that the equivalent damping ratios reduced a great deal with the loading cycles on samples N7 and P1 to P6. These behaviours are also affected by the self-heating temperature.

Figure 60 illustrates the self-heating temperature changes with the number of loading cycles for samples P5 and P6. The temperature of sample P5 increases from 28℃ to nearly 70℃ at about the 300th cycle and remains constant after that. The temperature of sample P6 rises to a peak value which is over 150℃ at around the 600th cycle and then reduces gently after 800 cycles.

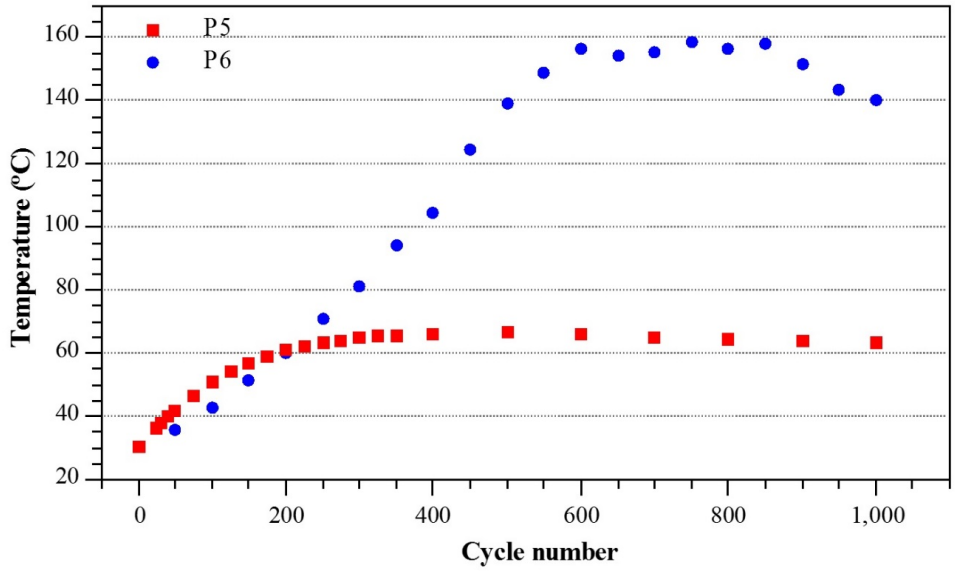

Figure 60 Self-heating temperature changes with loading cycles for samples P5 and P6

The changes in both equivalent damping ratio and secant stiffness with number of loading cycles of sample P6 are relatively greater than that of other samples by reason of the variance in temperature. The equivalent damping ratio of sample P6 has dramatically reduced from the 100th to 600th loading cycle since the material has been self-heated to nearly 160℃ during that period. The relations between equivalent damping ratio, secant stiffness and self-heating temperature of samples P5 and P6 are demonstrated in Figure 61. It clearly shows that the equivalent damping ratio decreases and the secant stiffness increases with the increase of self-heating temperature.

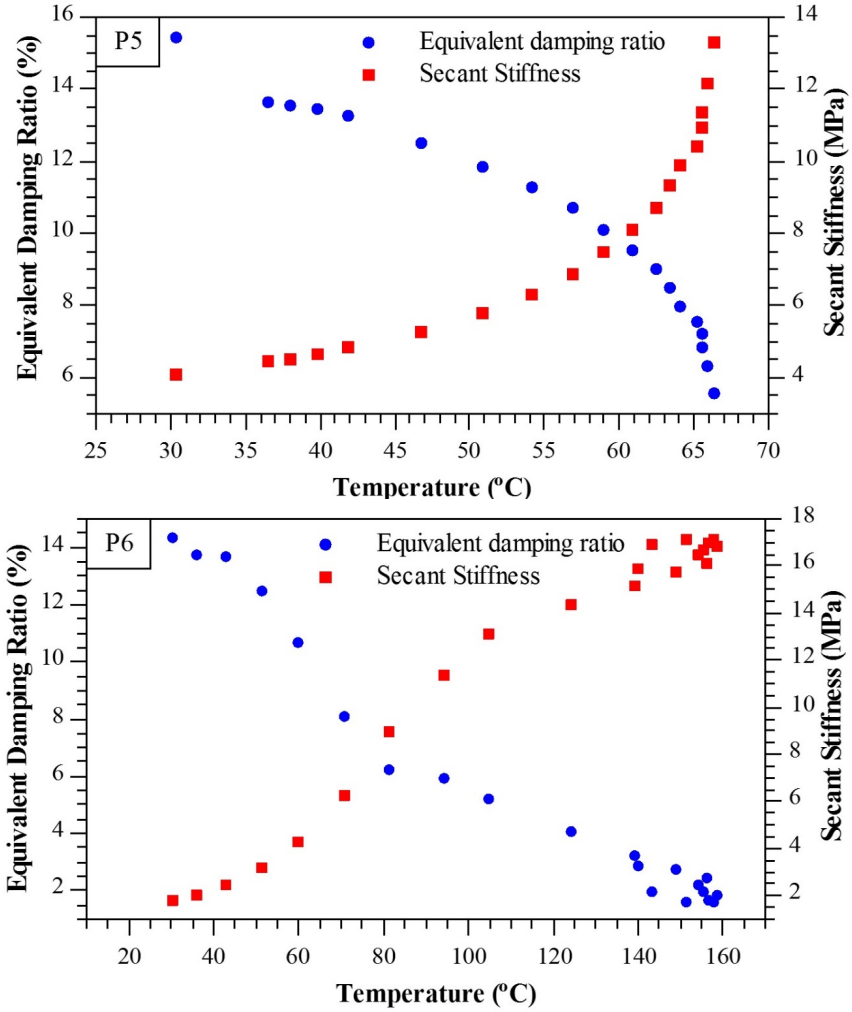

Figure 61 Relationship among equivalent damping ratio, secant stiffness and self-heating temperature of samples (a) P5 and (b) P6

3.4 Conclusion

Due to the unstable behaviours of super-elastic alloy from different supplier, the material characterisation of Cu-Al-Mn super-elastic alloy bar that used in this research need to be done. However, the results have shown a highly consistency with previous researches. The quasi-static tensile test of super-elastic alloy bar indicated that the transformation from elastic to pseudo-elastic deformation happened at 1.2% strain level and no residual strain has been noticed. The residual strain has been discovered during the cyclic tests and increased with the increasing of loading frequency and amplitude. Due to the martensitic hardening of super-elastic alloy, secant stiffness increased with the loading cycles. The equivalent damping ratio is higher with higher loading frequency until the self-heating temperature becomes to the primary governing factor and a small reduction of the equivalent damping ratio can be seen. Pre-straining of super-elastic alloy gave higher equivalent damping ratio within the first 1000

loading cycles and dropped to same level with the non-prestrain super-elastic alloy after 1000 loading cycles due to the rapid increase in the self-heating temperature. This finding suggest that super-elastic alloy can provide Dou-Gon a good damping ratio especially with pre-strain. However, further experiments of Dou-Gon with super-elastic alloy bar connections are needed.

Chapter 4 Static Tests of Single Dou

This Chapter introduces a series of static tests for the single Dou (two types of 2nd level Dou and base Dou) shown in Figure 62. The whole set of Dou-Gon system (Figure 62) is originally from an ancient structure in Henan province in China. Previous researches show that conventional wood peg connections have low stiffness and strength, and would be pulled out from the peg hole by the horizontal loads. There are many means and methods that can be used to increase the seismic resistance of a structure. Re-centring force can pull the oblique structures back to centre and energy dissipation capability will dissipate the major seismic energy. Figure 63 shows a stress-strain curve that illustrates the ideal solution comprised of these two effects. To resist the seismic activities, the traditional structures should have the ability to dissipate the large amount of seismic energy, self-centring force and increase the stiffness of the structure. Super-elastic alloy has been applied to this study due to its re-centring capability, energy dissipation capacity which is demonstrated in Chapter 3 and it has much higher stiffness than wood as well.

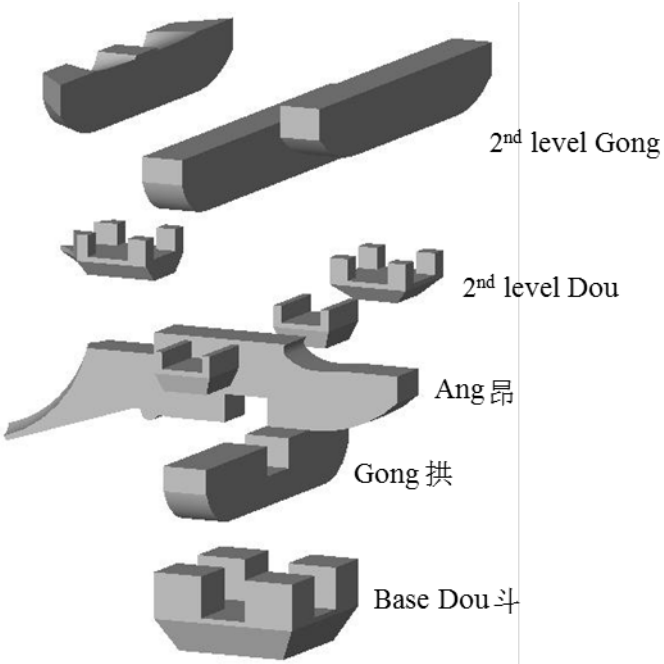

Figure 62 Details of Dou-Gon system that used in this study

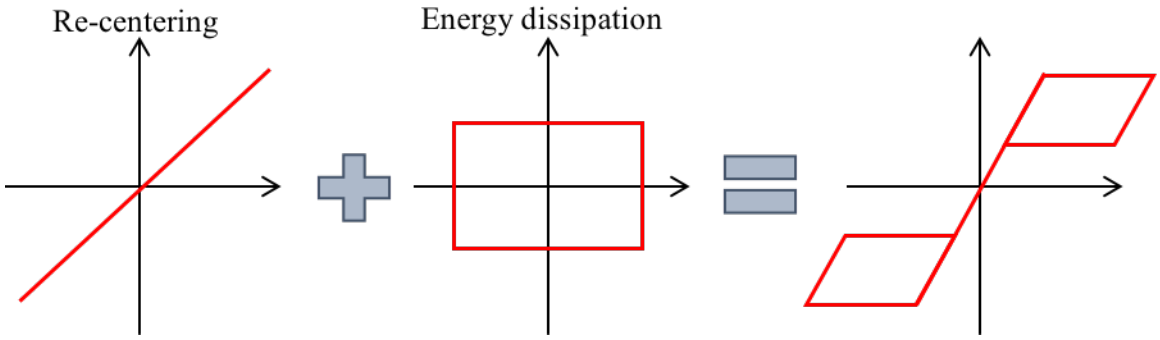

Figure 63 The re-centring and energy dissipate capabilities

Half of the material presented in Chapter 4 has been published in the *International Journal of Architectural Heritage* under the title 'Enhancing the seismic performance of historic timber buildings in Asia by applying super-elastic alloy to a Chinese complex bracket system', and the other half of the content has been published in the *World Conference on Timber Engineering (WCTE) 2016* under the title 'Employing super-elastic alloy to enhance the damping and re-centring capacity of a single bracket unit in traditional temples in Asia'.

4.1 Static tests of upper level Dou

4.1.1 Specimens preparation

Two full-scaled models that imitate the two different shapes 2nd level Dou were made by GL28h (Table 7). The top plans and elevations of both Dou are shown in Figure 64.

Table 7 Mechanical properties of glulam GL28h, MPa

Mean modulus of elasticity in bending ($E_{0,mean}$)	12600
Mean modulus of elasticity perpendicular to grain ($E_{90,mean}$)	420
Bending strength ($f_{m,k}$)	28
Tension strength parallel to grain ($f_{t,0,k}$)	19.5
Compression strength parallel to grain ($f_{c,0,k}$)	26.5
Compression strength perpendicular to grain ($f_{c,90,k}$)	3.0

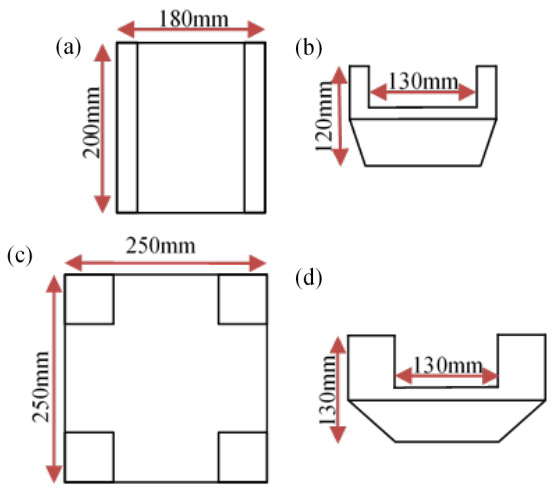

Figure 64: (a)Top plan of Dou A (b)Elevation of Dou A (c)Top plan of Dou B (d)Elevation of Dou B

The Dou were connected to a timber block with the dimensions of 400×250×200mm by three different materials (wood peg, high strength steel bar and super-elastic alloy bar), respectively. The timber block was fixed by two 20 mm threaded bolts to the strong floor which can be assumed as rigid base.

For the metal bar connections, an inserted connector with threads was fix into the timber block by epoxy. A hole has been drilled through the centre of both Dou to install the metal bar. A 50mm diameter washer was used to bear the pre-strain load. The ball joint gave a pin joint on top end of the metal bar allowing the Dou to rotate. The set-up and detail drawing of the mechanism can be seen in Figure 65 and Figure 66.

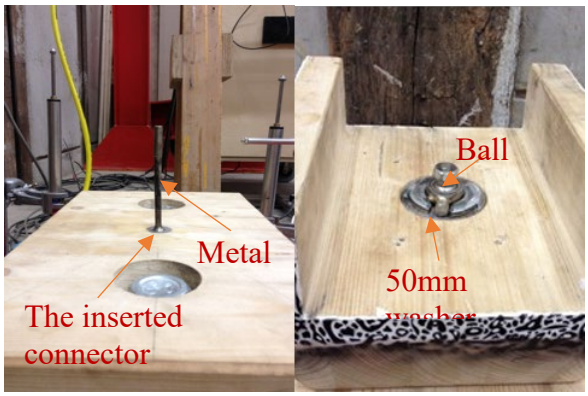

Figure 65: Set up of the metal bar connection

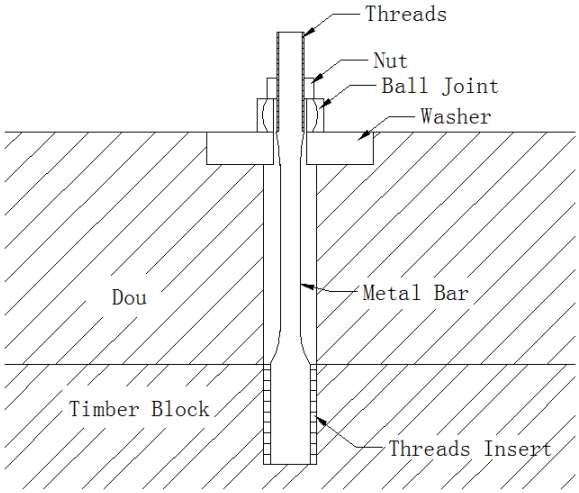

Figure 66: Details drawing of metal bar connection

4.1.2 Materials for the connection

The Dou and the timber block were connected by a wood peg, high strength steel bar or a super-elastic alloy bar (Figure 67).

Figure 67: The materials of three different connections

4.1.2.1 Wood peg connection

Wood pegs are the conventional connections used in the traditional timber structures to connect the components in the Dou-Gon system. Dovetail and flat cut are two different wood peg connections (Figure 68). When the connection is dovetailed, the rotational stiffness and pull out force are not affected by the vertical load, whereas the pull out force is dependent on the vertical load with the flat cut connection (D'Ayala &Tsai, 2008). In this research, flat cut wood peg connection has been employed. The width of wood pegs was one fifth the width of the groove. The size of the cuboid wood peg is 26×26×52mm. A cubic hole with width of 26mm were chiselled out in both bottom of the Dou and top of the timber block to install the wood peg.

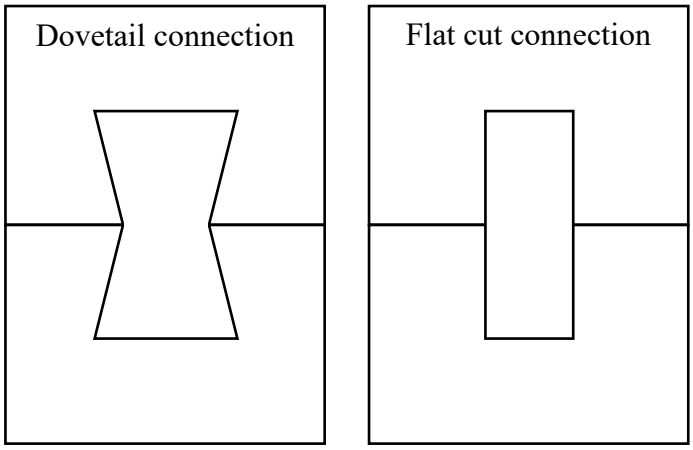

Figure 68 Dovetail and flat cut connections

4.1.2.2 Super-elastic alloy bar connection

To enhance the structural behaviour of the Dou-Gon system, a super-elastic alloy bar has been employed to replace the wood peg connection. The nature of super-elastic alloy bar is described in Chapter 2.2.3. Not only the super-elastic alloy bars but also high strength steel bars have been used to replace the wood peg connection as a comparative parameter because should it be a real project they are likely to be used due to their strength and easy accessibility. The tensile stress-strain curves of both high strength steel bar and SEA bar are illustrated in Figure 69. The high strength steel bar has an ultimate tensile strength of 720MPa and SEA bar has the ultimate tensile strength of 200MPa. The ultimate tensile strength of high strength steel bar is much higher than the SEA bar. But it was fractured at 3.6% strain. The SEA bar was pulled to 7% strain and there is negligible residual strain after unloading.

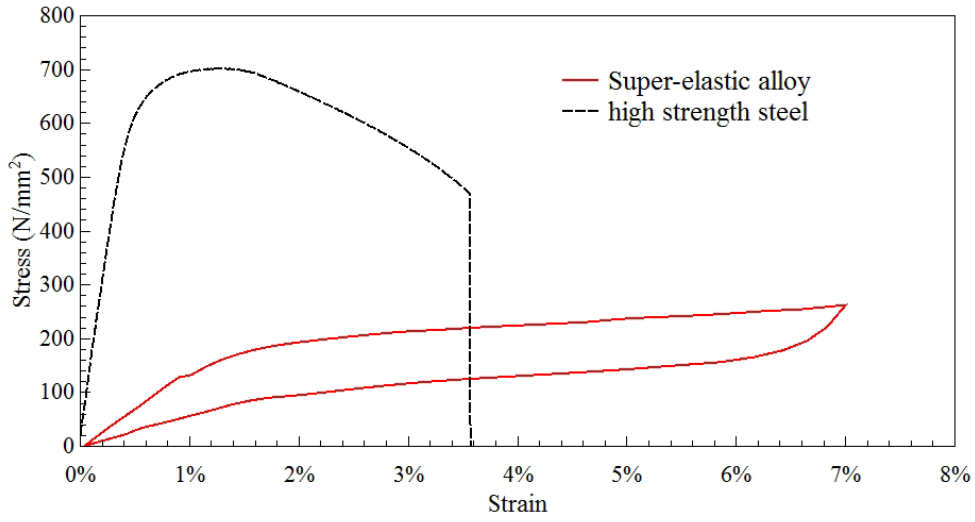

Figure 69 Stress-strain curves of metal bars

The diameter of original metal bar is 12mm. The gauge diameter has been machined down to 6mm and length is 60 mm for both high strength steel and super-elastic alloy bars. 8mm and

12mm threads are applied on top and bottom ends of the metal bars, respectively. (see Figure 67)

4.1.3 Experimental programme

To simulate the weight of the roof that supported by the Dou-Gon system, the vertical loads of three different load levels (1kN, 1.75kN and 2.5kN) have applied on top of the specimen which were comprised of steel blocks and plates. The specimen was rotated around point A (Figure 70) by applying a lateral load at a height of 200 mm to the bottom surface of Dou A and Dou B (Figure 64) using a jack. It recovered to its original position when the lateral load was released. The trajectory of the specimen which rotates to 0.1 radians and recovers to its original position is defined as one loading cycle. The specimens were tested under static cyclic loadings. Four vertical LVDTs were used to record the rotation of the Dou, and two horizontal LVDTs were used to record the horizontal displacement of the specimen (Figure 70). There were six cases of the experiments which are listed in Table 8.

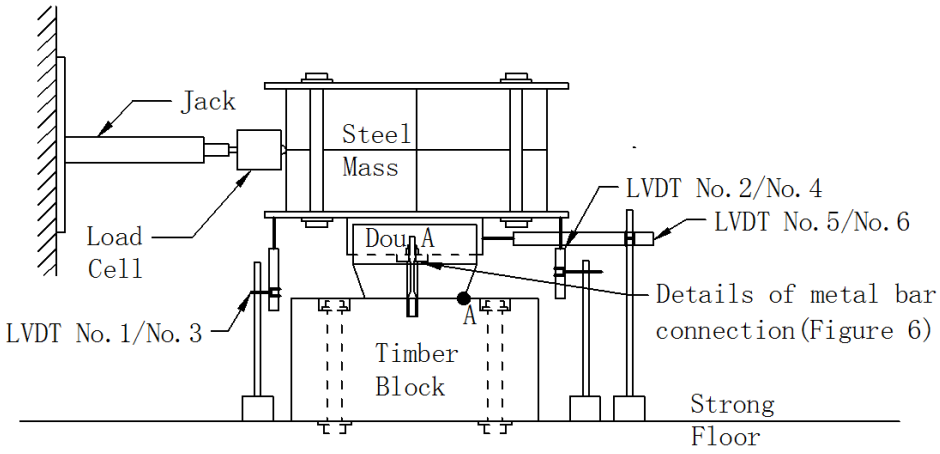

Figure 70: Loading apparatus

Table 8: Experimental cases

CASE 1	Dou A under 1kN vertical loads
CASE 2	Dou A under 1.75kN vertical loads
CASE 3	Dou A under 2.5kN vertical loads
CASE 4	Dou B under 1kN vertical loads
CASE 5	Dou B under 1.75kN vertical loads
CASE 6	Dou B under 2.5kN vertical loads

In addition to the non-prestrain condition for both metals, the super-elastic alloy bars have also been pre-strained by stretching along the axis to 1%, 3% and 5% strains using a nut. Table 9 has listed all the tests have been done.

Table 9: Experimental conditions

Connection materials	**1kN**	**1.75kN**	**2.5kN**

Wood peg	1 cycle	1 cycle	1 cycle
High strength steel bar	5 cycles	5 cycles	5 cycles
Super-elastic alloy bar	5 cycles	5 cycles	5 cycles
Super-elastic alloy bar with 1% pre-strain	5 cycles	5 cycles	5 cycles
Super-elastic alloy bar with 3% pre-strain	5 cycles	5 cycles	5 cycles
Super-elastic alloy bar with 5% pre-strain	5 cycles	5 cycles	5 cycles

4.1.4 Results and discussion

4.1.4.1 Elememt Dou with conventional wood peg connection

The specimens with wood peg connections have been tested for one loading cycle with 0.2 radians rotation. The hysteresis loops for both Dou A and Dou B (Figure 71 and Figure 72) illustrated the non-linear stiffness of the Dou with conventional wood peg connection. Three stages stiffness of the structure could be discovered from the hysteresis loops. The first stiffness is the elastic stage in which it has slightly rise with the vertical loads. It entered to the plastic stage with the second stiffness when the lateral loads bigger than the yield load of the structure. The ultimate strength and the second stiffness of the Dou has increased significantly with the vertical loads. Dou A and Dou B behaved the same but Dou A has a higher ultimate strength than Dou B. Most of the lateral loads were overcoming the dead loads and then start to drop after the lateral loads reach limit load of the structure. The wood peg has been pull out from the chiselled hole and then the Dou stuck in the hole after lateral loads removed. The Dou tipped over finally by the lateral loads which matches the previous research (Yu et al. 2008). Higher vertical loads would make a greater contribution to the P-Delta effect which results in a lower third stiffness of the Dou. The Dou tips over at a smaller rotational angle with higher vertical loads. Dou A has slightly higher ultimate strength than Dou B when using wood peg connection.

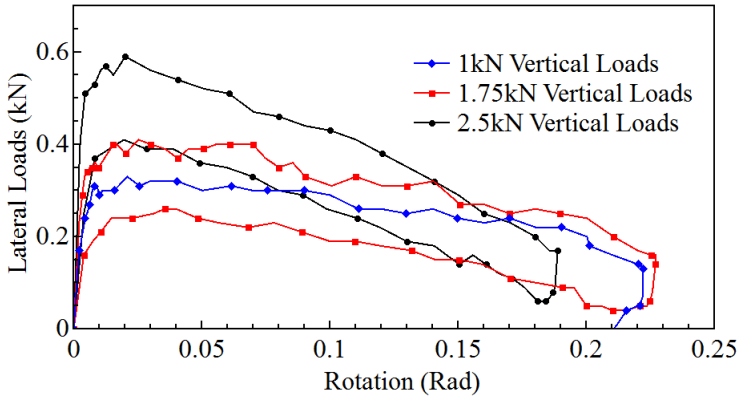

Figure 71: The hysteresis loops of Dou A with wood peg connection

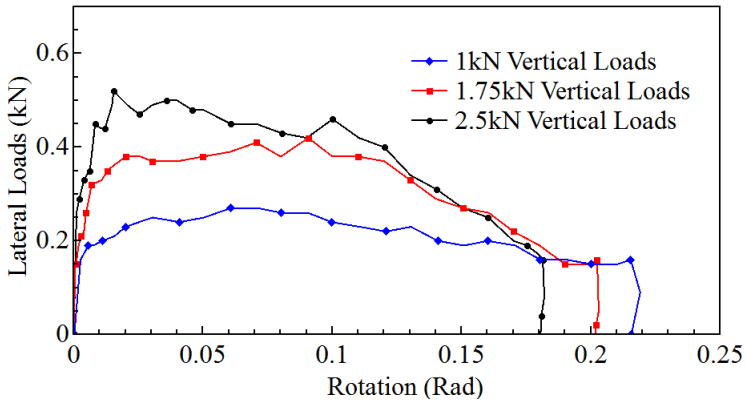

Figure 72: The hysteresis loops of Dou B with wood peg connection

4.1.4.2 ELEMENT DOU WITH HIGH STRENGTH STEEL BAR CONNECTION

Both Dou with high strength steel bar connection have been tested for 5 loading cycles with 0.1 radians rotation. Figure 73 and Figure 74 have shown the hysteresis loops for Dou A and Dou B, respectively. Generally, the structures have two stages of stiffness which entered from elastic to plastic deformation when the Dou has about 0.05 radians rotation. The high strength steel bar connections can dissipate a big amount energy in the first loading cycle, and have permanent deformations after that. The strength of the steel became less than 10% of its original ultimate strength. The ultimate strength of the structure is independent to the vertical loads.

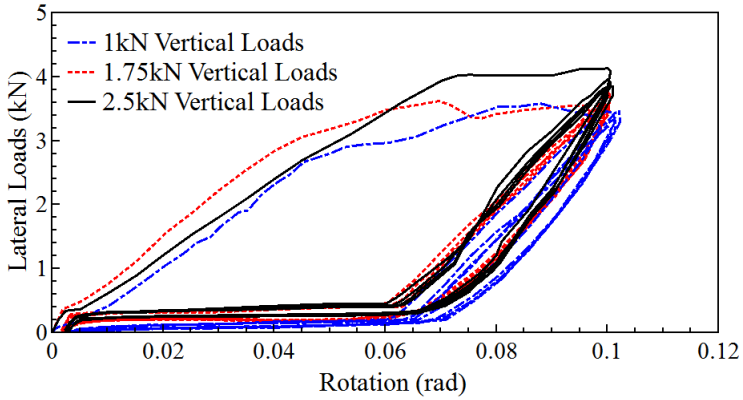

Figure 73: The hysteresis loops of Dou A with high strength steel bar connection

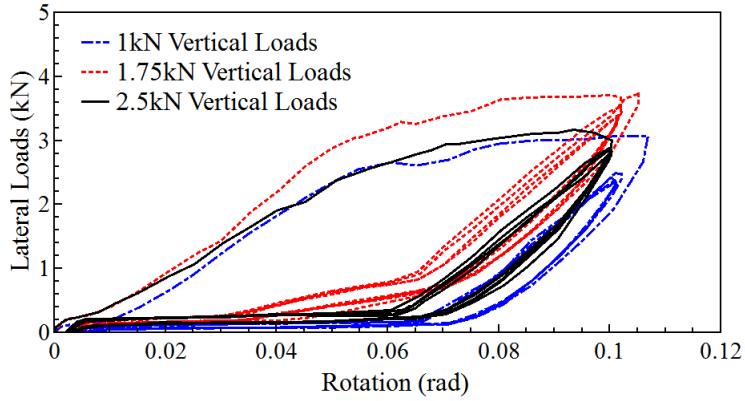

Figure 74: The hysteresis loops of Dou B with high strength steel bar connection

Figure 75 and Figure 76 clearly showed that both Dou have a high equivalent damping ratio around 30% in the first loading cycle. They have dramatic reductions to 5% at second loading cycle and decrease steadily and gently after that. The equivalent damping ratios are independent to the vertical loads that applied onto the structures when connected with a high strength steel bar. Dou A and Dou B has insignificant differences in ultimate strength and equivalent damping ratio when connected by high strength steel bar.

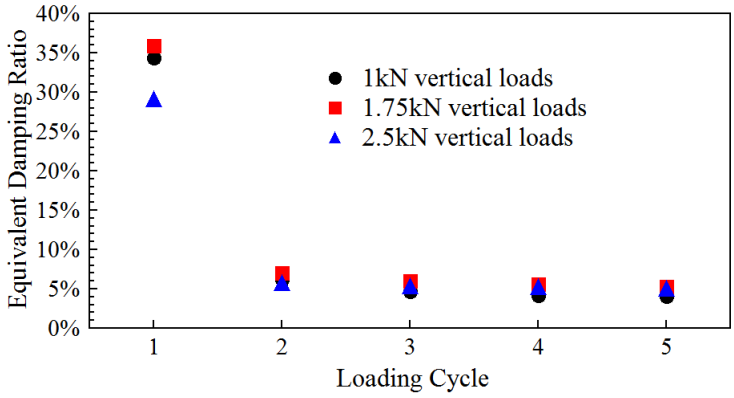

Figure 75: Equivalent damping ratios of Dou A with high strength steel bar connection

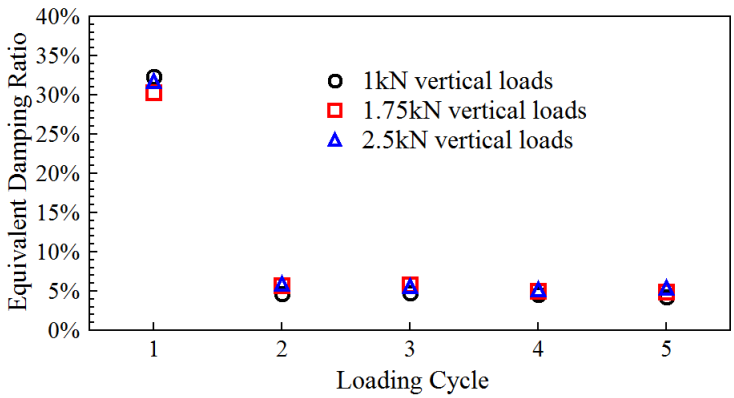

Figure 76: Equivalent damping ratios of Dou B with high strength steel bar connection

4.1.4.3 Element dou with super-elastic alloy bar connection

Figure 77 and Figure 78 illustrated the hysteresis loops of Dou A and Dou B with super-elastic alloy bar connection under three different vertical loads. They have experienced 0.1 radians rotation for five loading cycles. There is no significant change in the hysteresis loops within five loading cycles. This indicates that the energy dissipation capacity of Dou with super-elastic alloy bar connection almost remains the same. Four stages of stiffness of the structures could be gathered from the hysteresis loops. The first two stiffness of the Dou A happened within 0.01 radians rotation and entered to the super-elastic stage when the Dou has approximate 0.04 radians rotation. For Dou B, the structure transited to the super-elastic stage at 0.05 radians rotation. The loops of Dou B are smaller than Dou A.

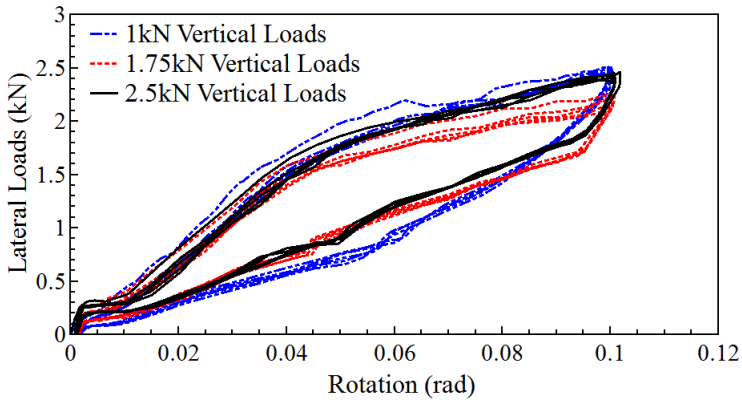

Figure 77: The hysteresis loops of Dou A with super-elastic alloy bar connection

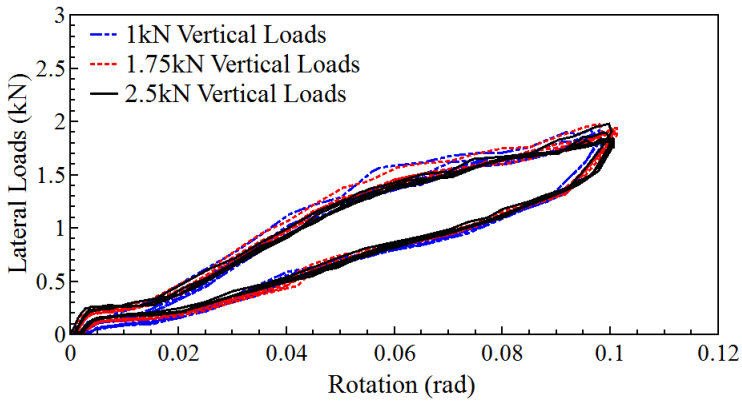

Figure 78: The hysteresis loops of Dou B with super-elastic alloy bar connection

The equivalent damping ratios of Dou A and Dou B with super-elastic alloy bar connection have reduced marginally from the first to the second loading cycle. And then remain constant in the second to fifth loading cycles. Figure 79 also demonstrated that the equivalent damping ratios decreases with increasing vertical loads that applied on top of Dou. It means that a heavier roof will give a lower equivalent damping ratio of Dou A and Dou B. Dou A has a better energy dissipation capacity than Dou B.

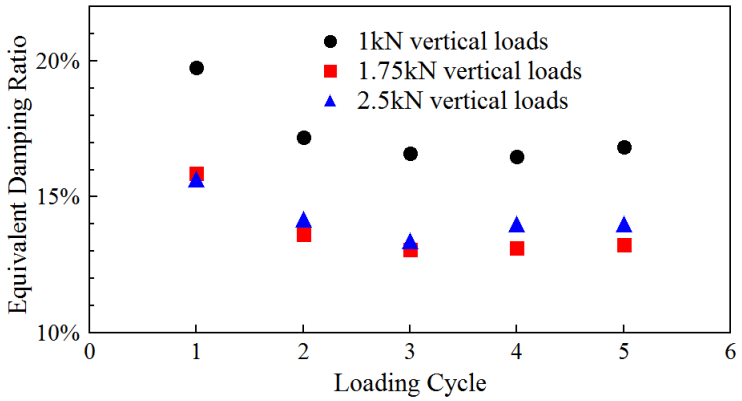

Figure 79: Equivalent damping ratios of Dou A with super-elastic alloy bar connection

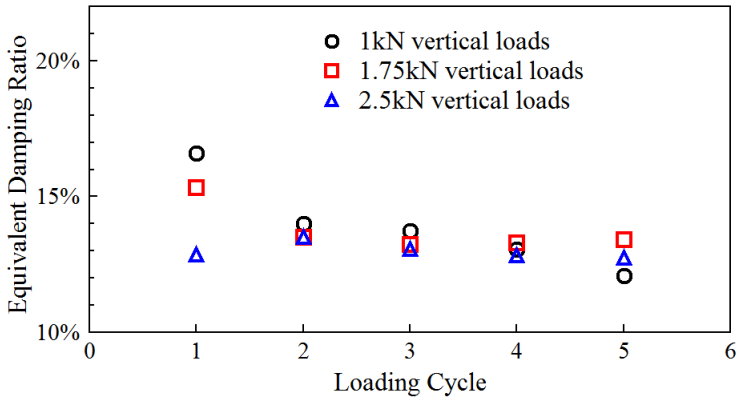

Figure 80: Equivalent damping ratios of Dou B with super-elastic alloy bar connection

4.1.4.4 Comparison of connections with three different materials

From the results shown above, it can be clearly seen that Dou with metal bar connections have a greater ultimate strength than Dou with conventional wood peg connections. The Dou with conventional wood peg connections reached the limit load at the Dou with only 0.02 radians rotation and the structure stiffness started to drop until the wood peg has been pulled out from the chiselled hole. Finally, the structure collapsed.

Figure 81 illustrated that Dou A with high strength steel bar connection in the first loading cycle has the highest elastic stiffness and the possible ultimate load is about 10 times the conventional wood peg connection. This ultimate load is nearly double of that with the super-elastic alloy bar connection. The area within the hysteresis loop of Dou A with high strength steel bar connection is much larger than that with the other two connections in the first loading cycle. This indicates that the most energy was dissipated during this period. However, in the second loading cycle, the stiffness of Dou A with high strength steel bar connections reduced dramatically to a value that even lower than the Dou with conventional wood peg connection. No significant change could be obtained in both stiffness and ultimate strength of Dou with super-elastic alloy bar connection from first to second loading cycles.

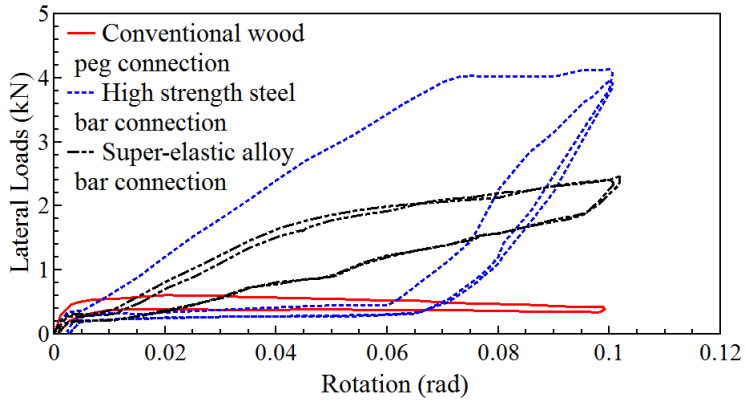

Figure 81: The hysteresis loops of Dou A with three different connections under 2.5kN vertical loads

Element Dou with high strength steel bar connection can get 35% equivalent damping ratio in the first loading cycle but drop to 5% after the second loading cycle since the permanent deformations of the steel bar. Over 15% equivalent damping ratios could be get by the element Dou with super-elastic alloy bar connection in the first loading cycle and they have insignificant reduction in the second loading cycle. The equivalent damping ratio of the structure could always stay above 12% in the first five loading cycles when connected with a super-elastic alloy bar.

Several aftershocks usually occur after the main shock has passed in an earthquake which requires the connections having stable damping ratio to dissipate energy during the aftershocks

as well. The high strength steel bar connections have very low equivalent damping ratio and small resistance to the Dou during the aftershocks since they would have had permanent deformations in the main shock. Thus, the super-elastic ally bar connection is a better substituent of the conventional wood peg connection.

4.1.4.5 The effects of super-elastic bar connections with different levels of pre-strain

The previous material tensile tests have indicated that pre-strain of the super-elastic alloy could get a higher ultimate strength and dissipate more energy than the non-prestrain materials. Thus, pre-straining has been applied to the super-elastic alloy bar connection of element Dou.

Figure 82 to Figure 87 have illustrated how the hysteresis loops change with the pre-strain level of super-elastic alloy bar in six cases. The pre-strain gives the structure a higher initial elastic stiffness than non-prestrain conditions. So the structure could dissipate more energy when the rotation is less than 0.04 radians. Element Dou with pre-strained super-elastic alloy bar connection has two stages of stiffness, while non-prestrain conditions have four stages of stiffness. The super-elastic alloy bar already sits in the super-elastic deformation range when it has been pre-strained, while it needs to undergo the elastic deformation firstly without pre-strain. In case 1, case 2 and cases 4 to 6, there is no significant increase in the ultimate strength of the structure when the super-elastic alloy bar has 1% pre-strain. But perceptible growth in the ultimate strength of the structure can be seen when the super-elastic alloy bars have been pre-strained to 3 and 5 percentage strains. The increase in vertical loads has no noticeable effect on the structures.

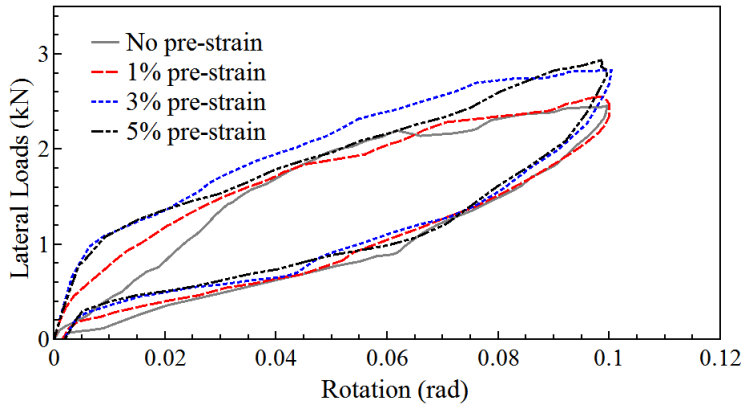

Figure 82: The hysteresis loops of Dou A with super-elastic alloy bar connection under 1kN vertical loads

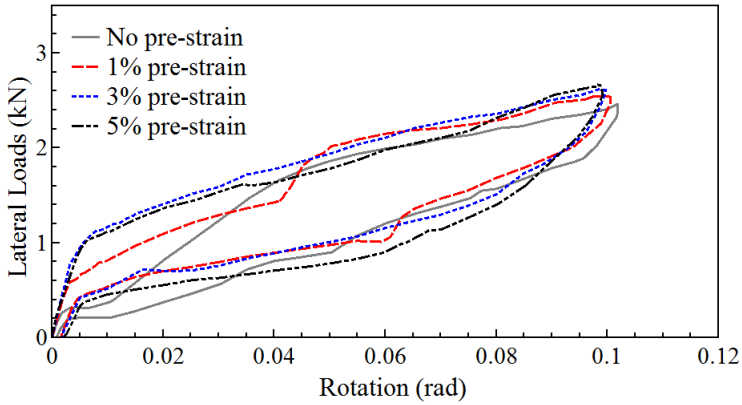

Figure 83: The hysteresis loops of Dou A with super-elastic alloy bar connection under 1.75kN vertical loads

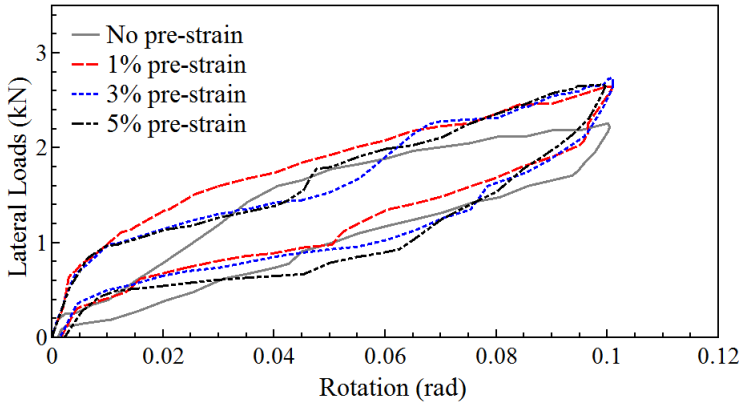

Figure 84: The hysteresis loops of Dou A with super-elastic alloy bar connection under 2.5kN vertical loads

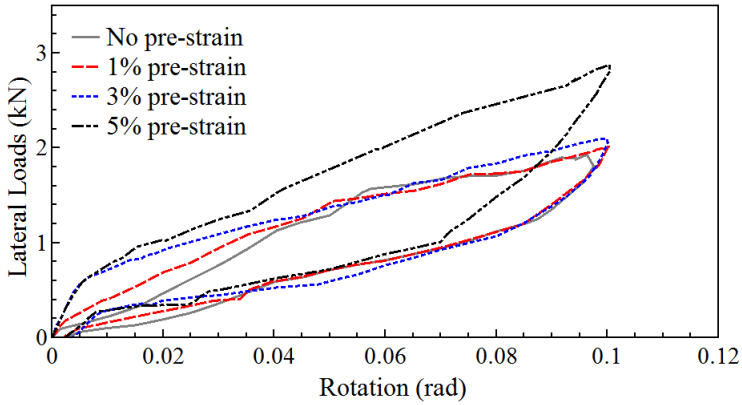

Figure 85: The hysteresis loops of Dou B with super-elastic alloy bar connection under 1kN vertical loads

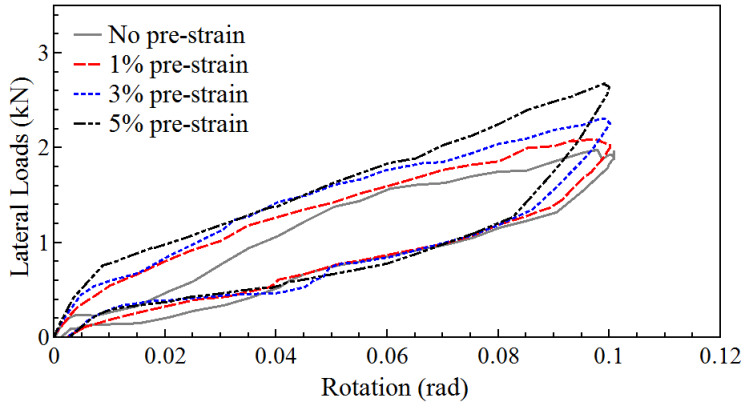

Figure 86: The hysteresis loops of Dou B with super-elastic alloy bar connection under 1.75kN vertical loads

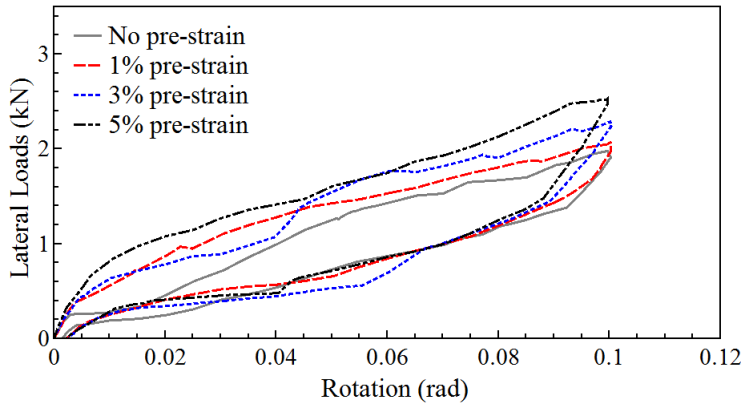

Figure 87: The hysteresis loops of Dou B with super-elastic alloy bar connection under 2.5kN vertical loads

The increase in the pre-strain level of the super-elastic alloy bars will not result in a steady growth of the equivalent damping ratios for neither Dou A or Dou B. Only in case 3 and case 4, the equivalent damping ratios of the structure have a tiny reduction when the super-elastic alloy bar has been pre-strained to 1% strain. There were significant increases in the equivalent damping ratios of the structure with 3% pre-strain super-elastic alloy bar connection except case 2. In all cases, the equivalent damping ratios of the structure increase when the pre-strain level of super-elastic alloy bars increase to 5% strain. In general, the pre-strain of super-elastic alloy bar can give a higher equivalent damping ratio of Dou A and Dou B.

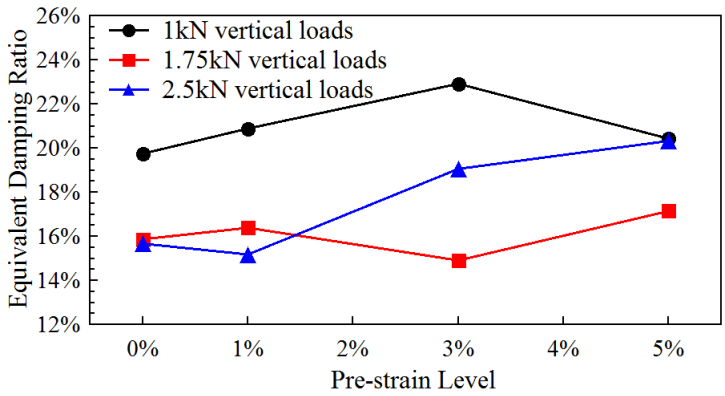

Figure 88: Equivalent damping ratios of Dou A with pre-strained super-elastic alloy bar connection

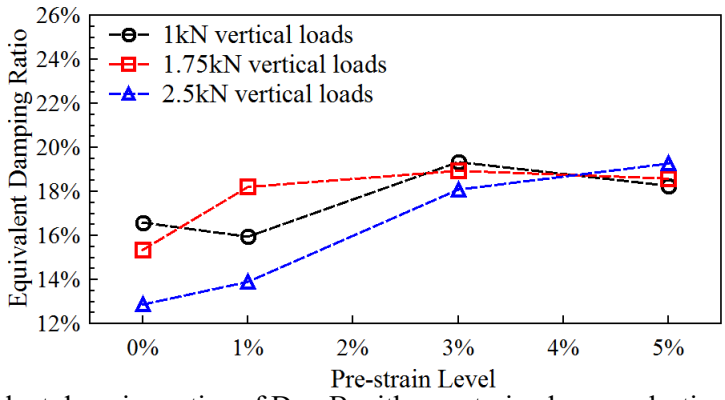

Figure 89: Equivalent damping ratios of Dou B with pre-strained super-elastic alloy bar connection

4.2 Static tests of base Dou

4.2.1 Specimen preparation

The base Dou is the Dou that sits on the top of a column in structures. The base Dou was made by glulam of the strength class GL28h as well (Table 7) and its dimensions are illustrated in Figure 90. It was connected by three different materials (wood peg, high strength steel bar and SEA bar) to a timber block with the dimensions of 400x400x200mm (Figure 91). The timber block was fixed by two 24mm threaded bolts to the strong floor. One Gong and one Ang were fitted in the groove of the base Dou (Figure 92). A pallet with several wood bricks (shaded area in Figure 96) was fixed at their bottom to the top of the base element to fit the irregular top surface of the base Dou system. Several concrete blocks were pre-casted and put onto pallet to apply the vertical loads to the system.

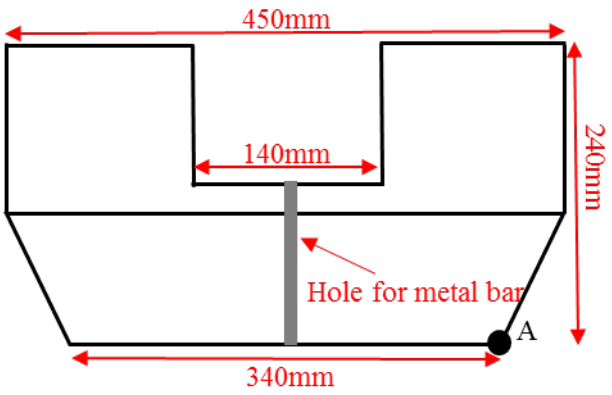

Figure 90 The section of base Dou

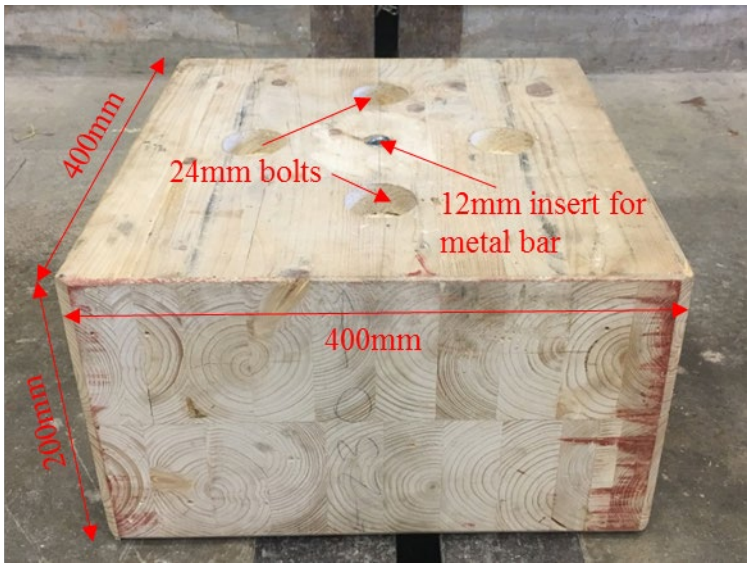

Figure 91 The timber block that fix the base Dou to the ground

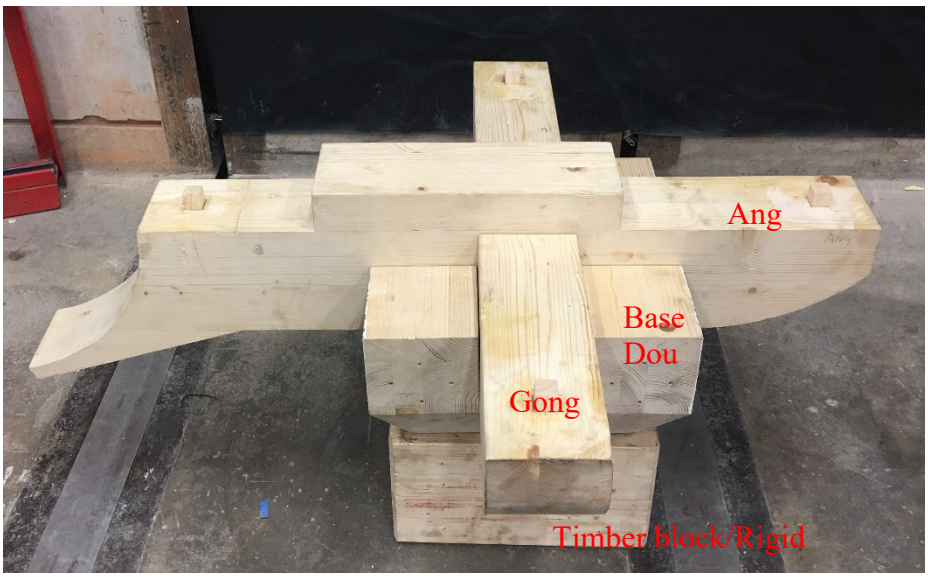

Figure 92 Dou-Gon set up without loads

A 12mm threads insert (Figure 93a) was fixed into the timber block with epoxy resin. A vertical hole was pre-drilled at the centre of the base Dou. Either high strength steel or SEA bar with threads was installed through the vertical hole of the base Dou and connected to the insert. A

square steel plate with length of 100mm was embedded into the top surface of the base Dou to bear the pre-load applied to the bar and prevent damaging of the timber. A ball joint was installed at the top of the bar to remove the rotational restraint from the connection system. A nut was introduced to fix the connection system and provide pre-loading to the connection system in some cases. Details of the metal bar connecting technique can be seen from Figure 5b and 5c.

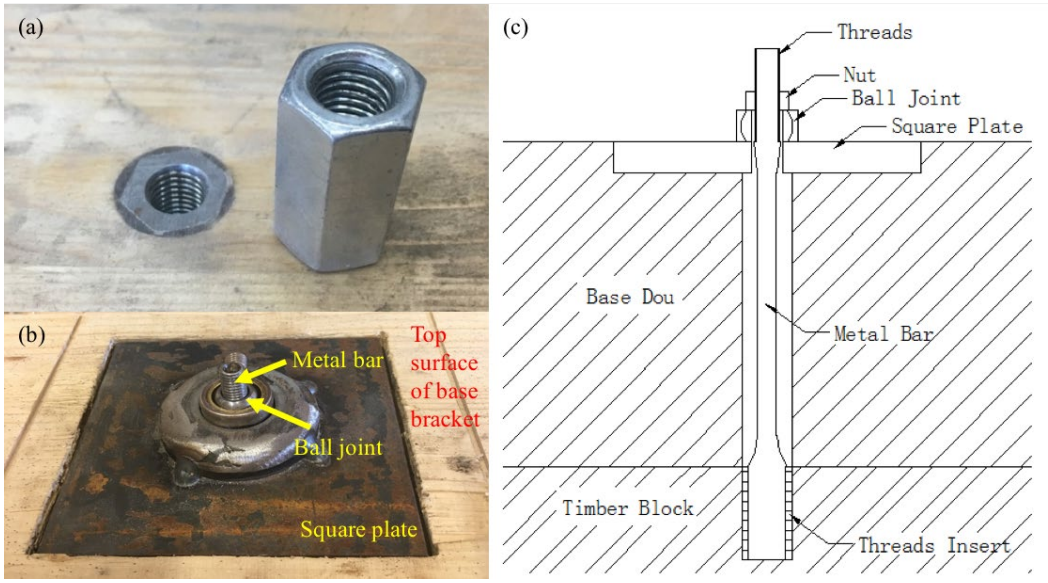

Figure 93(a) 12mm threads insert; (b) Square plate and ball joint; (c) Details of metal bar connection

4.2.2 Materials for the connection

Flat cut wood peg connection (Figure 68) was employed to the base Dou as well. The timber grade of the peg is the same as Dou-Gon. The width of the wood pegs used in this research is one fifth of the width of the groove and the dimensions are 28x28x56mm. Cubic holes with the width of 28mm were chiselled out in both bottom of the Dou and top of the timber block respectively to install the wood peg (Figure 94).

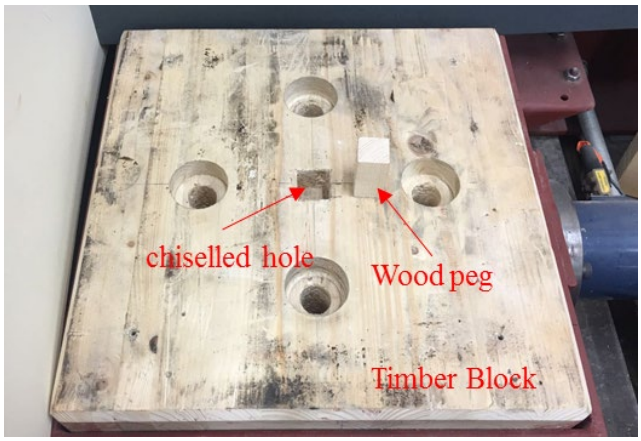

Figure 94 Wood peg and chiselled hole

Super-elastic alloy bar was used to instead of the wood peg connection and high strength steel bar as a comparative parameter (Figure 95). Both materials have an initial diameter of 12mm. The length of the specimens is 160mm. There are M8 and M12 threads at the two ends of the specimens as shown in Figure 95. The middle part of the specimens was machined down to 6mm diameter to reduce the risk that Dou will be damaged by the large pre-strain load. The length of the reduced section part is 105mm. The stress-strain curves of both SEA and high strength steel bars are shown in Figure 69.

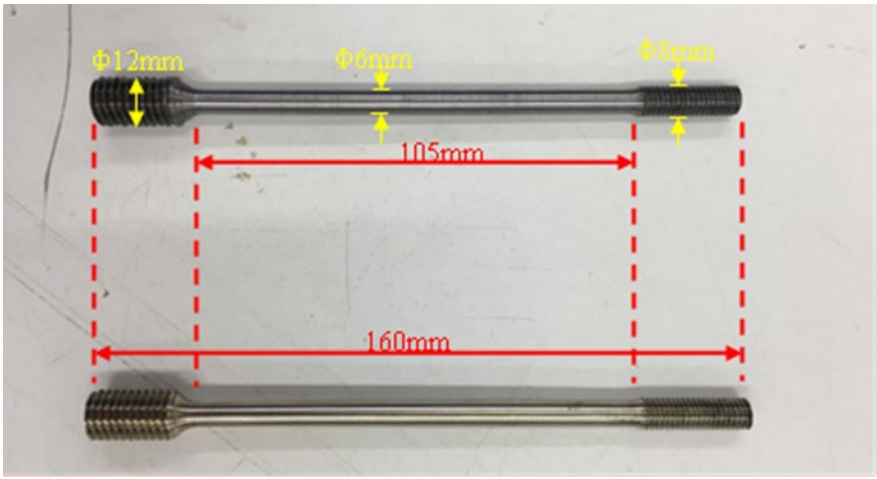

Figure 95 High strength steel bar (top) and SEA bar (bottom)

4.2.3 Experimental programme

To simulate the weight of the roof supported by the Dou-Gon system, the vertical loads of three different load levels (4kN, 7kN and 10kN) were applied to the top of the specimen using concrete blocks. The specimen was rotated around point A in Figure 90 by applying a lateral load at a height of 500mm to the bottom surface of the base Dou (Figure 96) using a hydraulic jack. It recovered to its original position when the lateral load is released. The trajectory of the specimen which rotates to a certain point with prescribed radian (θ) and recovers to its original position is defined as one loading cycle. The specimens were tested under static cyclic loadings. Four vertical LVDTs (No 1 to 4) were used to record the rotation of the Dou and two horizontal LVDTs (No. 5 and 6) were used record the horizontal displacement of the specimen as depicted in Figure 96. The radians (θ) are worked out by the differences in measurements (ΔL) between LVDT 1&2/3&4.

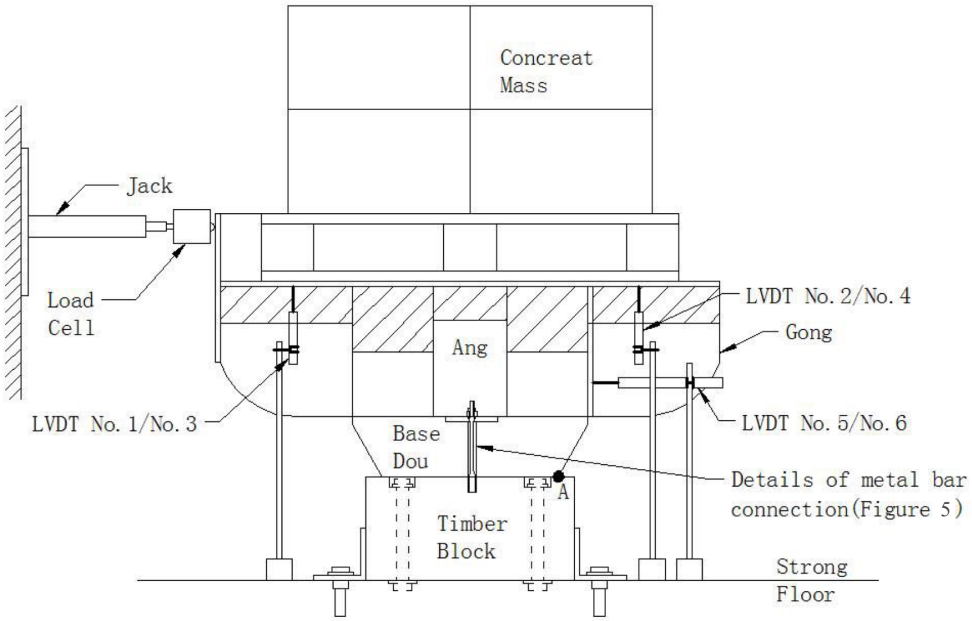

Figure 96 Loading apparatus and instrumentation used

In addition to the non-prestrain conditions, the Cu-Al-Mn SEA bars were pre-strained by stretching along the bar axis at 1%, 3% and 5% strains using a nut. The SEA bar with 1% pre-strain condition was tested under three different vertical loads 4kN, 7kN and 10kN. The SMA bar with 3% and 5% pre-strain conditions was tested under 10kN vertical load only. Table 10 lists all the test conditions.

Table 10 Experimental conditions

Vertical Loads (kN) / Connector Material	4kN	7kN	10kN
Wood Peg	✓	✓	✓
High Strength Steel Bar	✓	✓	✓
SMA Bar	✓	✓	✓
SEA Bar with 1% pre-strain	✓	✓	✓
SEA Bar with 3% pre-strain			✓
SEA Bar with 5% pre-strain			✓

Generally, all specimens were rotated up to when ΔL is 80mm with 10mm increment. The specimens with steel bar connection experienced 3 loading cycles when ΔL equals to 60mm and was loaded 10 cycles in total. For the specimens with SEA bar connection, it was loaded 2 cycles at ΔL =70mm when the SEA bar has 0% pre-strain under 10kN vertical loads and only 1 loading cycle for each prescribed rotation with other SEA bar connection conditions. The specimens with wood peg connections were tested for only one loading cycle with θ=10%. The actual setup can be seen in Figure 97.

Table 11 Loading conditions

ΔL(mm)	High Strength Steel Bar Connections	SEA Bar Connection with 0% pre-strain under 10kN vertical load	Other SEA Bar Connections
10	1 cycle	1 cycle	1 cycle
20	1 cycle	1 cycle	1 cycle
30	1 cycle	1 cycle	1 cycle
40	1 cycle	1 cycle	1 cycle
50	1 cycle	1 cycle	1 cycle
60	3 cycles	1 cycle	1 cycle
70	1 cycle	2 cycles	1 cycle
80	1 cycle	1 cycle	1 cycle

Figure 97 The test setup of Dou-Gon with 10kN dead load

4.2.4 Results and discussions

4.2.4.1 Base Dou system with conventional wood peg connector

The specimens with wood peg connectors have been tested for one loading cycle with θ=10%. The hysteresis loops (Figure 98) illustrated the non-linear restoring force of the Dou-Gon system with conventional wood peg connector. Three stages of stiffness could be discovered from the hysteresis loops, the elastic, plastic and limit stages (Yu et al., 2008). The elastic stage has a high stiffness which is independent of the vertical loads. The applied lateral load increases rapidly until reaching the yield point. At the plastic stage, the wood peg connection began to bear the shear and flexural moments and was pulled out from the chiselled hole as the lateral load increased to reach the limit rotation. The ultimate strength and the second stiffness of the base Dou system increased significantly with the vertical loads. Higher vertical loads made a

greater contribution to the P-Delta effect which results in a lower limit stiffness of the base Dou system. The restoring force of the structure with wood peg connection can be calculated as:

$$\mathbf{F} = \frac{\mathbf{P}\times\cos\boldsymbol{\theta}}{\mathbf{L}\times\mathbf{H}}(\mathbf{aL} - \mathbf{2a^2} - \mathbf{2ah}\times\tan\boldsymbol{\theta} - \frac{\mathbf{h^2}\times\tan^2\boldsymbol{\theta}}{\mathbf{2}}) \quad (2)$$

where P is the vertical load, L, H, a and h are illustrated in Figure 99.

The equation also expresses that the restoring force will increase with increasing the vertical load applied on the top of the Dou-Gon system. The restoring force curve obtained using the restoring force model is shown in Figure 98 when the vertical load is 10kN.

The energy dissipation is the energy loss per loading cycle which is represented by area enclosed by each hysteresis loop. The energy dissipation of Dou-Gon with a wood peg connection (Table 12) has a significant rise when the vertical loads increased from 4kN to 7kN and remain constant when the vertical loads reached 10kN. The base Dou system with conventional wood peg connection shows a full re-centring capability as expected because the system came back to its original position without any sliding after unloading.

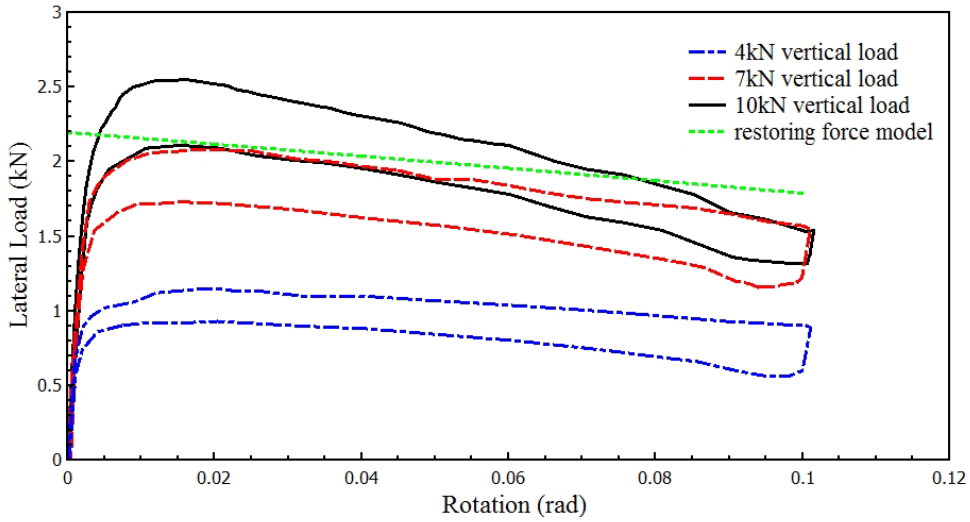

Figure 98 The first cycle hysteresis loop of Dou-Gon with wood peg connection

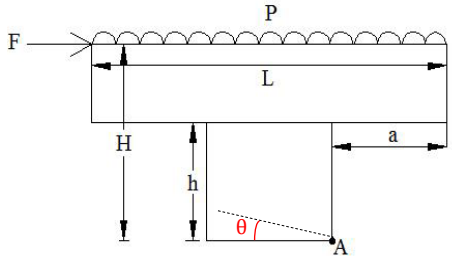

Figure 99 Simplified model of the structure and loadings

Table 12 The energy dissipation of Dou-Gon system with a wood peg connection

Vertical Loads (kN)	4	7	10
Energy dissipation (N.rad)	23.8	34.7	34.9

4.2.4.2 Behaviour of base Dou system with different vertical connectors

The hysteresis loops of the Dou-Gon system with connectors made of 3 different materials and under 3 different vertical loads are illustrated in Figure 100 to Figure 102. The figures clearly show that the Dou-Gon itself already has a good re-centering capability with wood peg connector and the re-centring force was given by the vertical loads representing the heavy roof weight. Such re-centering characteristics are also seen in the literature (Suzuki, 2006; Yu, 2008).

The base Dou system with SEA bar connection has experienced four stages stiffness. The first two stiffness are the stiffness of the timber structure since there was little gap between the structure and the connection system. The lateral load needs to overcome the vertical loads until the SEA bar starts to work. So, the third and fourth stiffness are the stiffness of the entire system. The restoring force curves reproduce the base Dou system with SEA bar connection and showed a good matching with the experimental results for 4kN and 7kN dead load levels, while ayield load higher than the experimental yield force was observed for the 10kN dead load. The restoring force of the structure with SEA bar connection can be calculated as:

$$\mathbf{F} = \frac{\mathbf{P}\times\cos\boldsymbol{\theta}}{\mathbf{L}\times\mathbf{H}}\left(\mathbf{aL} - \mathbf{2a^2} - \mathbf{2ah}\times\tan\boldsymbol{\theta} - \frac{\mathbf{h^2}\times\tan^2\boldsymbol{\theta}}{\mathbf{2}}\right) + \frac{\mathbf{k_1}(\frac{\mathbf{L}}{\mathbf{2}}-\mathbf{a})^2\sin\boldsymbol{\theta}}{\mathbf{H}} \quad (3)$$

when $\theta \leq 0.59\%$;

$$\mathbf{F} = \frac{\mathbf{P}\times\cos\boldsymbol{\theta}}{\mathbf{L}\times\mathbf{H}}\left(\mathbf{aL} - \mathbf{2a^2} - \mathbf{2ah}\times\tan\boldsymbol{\theta} - \frac{\mathbf{h^2}\times\tan^2\boldsymbol{\theta}}{\mathbf{2}}\right) + \frac{\boldsymbol{k_2}(\frac{\boldsymbol{L}}{\mathbf{2}}-\boldsymbol{a})^2\sin\boldsymbol{\theta}+\boldsymbol{A}(\frac{\boldsymbol{L}}{\mathbf{2}}+\boldsymbol{a})}{\boldsymbol{H}} \quad (4)$$

when $\theta > 0.59\%$. k_1 and k_2 are the tensile stiffness of SEA bar.

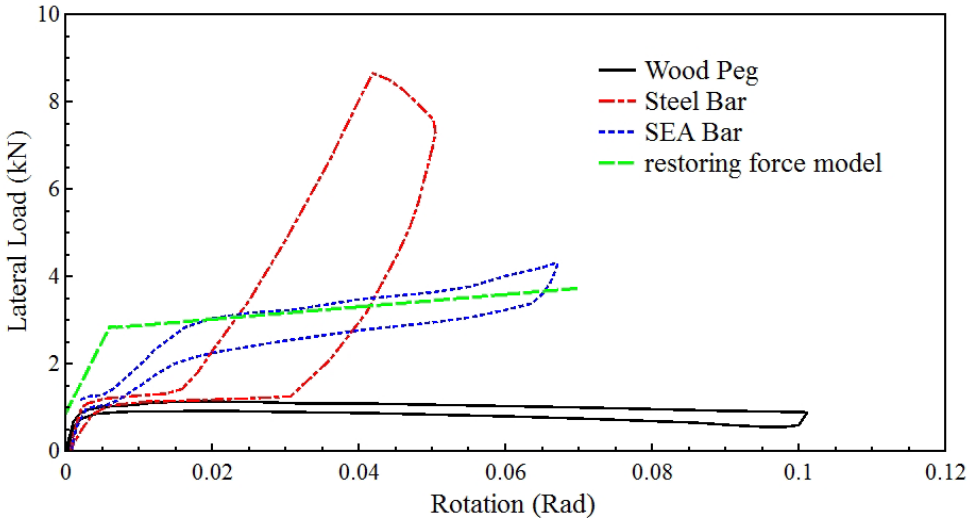

Figure 100 The second cycle hysteresis loops of Dou-Gon under 4kN dead load

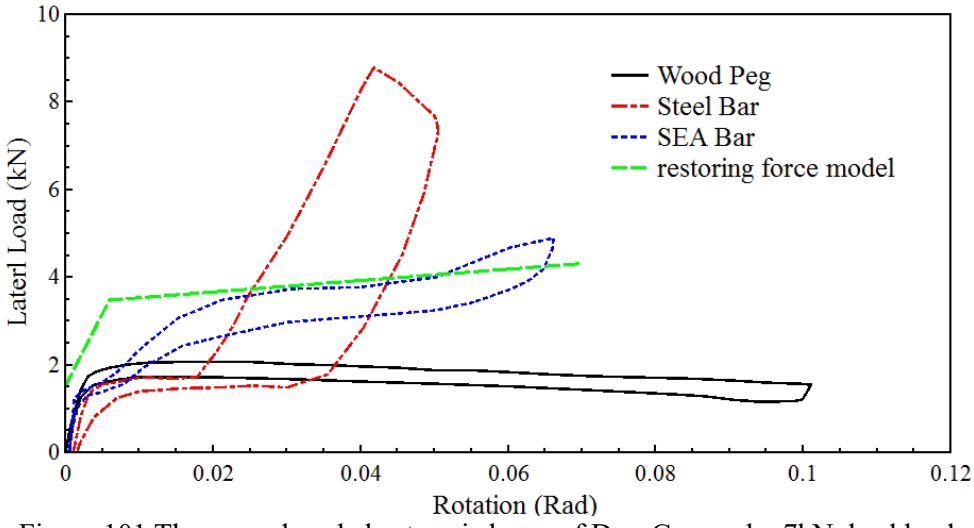

Figure 101 The second cycle hysteresis loops of Dou-Gon under 7kN dead load

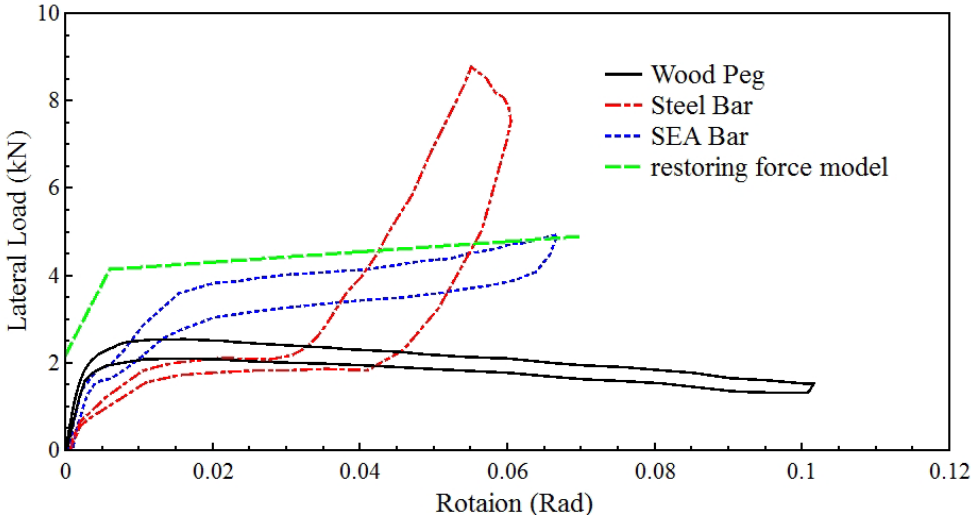

Figure 102 The second cycle hysteresis loops of Dou-Gon under 10kN dead load

In general, the base Dou system with a high strength steel bar connection has a higher ultimate strength than those with wood peg or SEA bar connectors, and it has greater secant stiffness as well. The reason for the atypical shape of base Dou system with high strength steel bar connection are illustrated in Figure 103a. The high strength steel bar connection dissipated more energy than SEA bar connection in the first loading cycle. However, in the second loading cycle, before the Dou-Gon with high strength steel connection reaches the ultimate strength, it needs to undergo a stage with very low tangent stiffness because the steel bar has already experienced several loading cycles with smaller rotational angle. The low stiffness comes from the structure itself. The high strength steel bar has permanent deformations and with low stiffness after first loading cycle called pinching effect. The energy dissipation of SEA bar connection has negligible difference between the first two loading cycles. The Dou-Gon with high strength steel bar connection was subjected to 3 loading cycles at ΔL =60mm. The areas

in the hysteresis loops significantly reduced during the 2nd and 3rd loading cycles (Figure 104). The high strength steel bar fractured before the specimen reached ΔL=80mm. On the other hand, 2 loading cycles were applied to the Dou-Gon system with SEA bar connection at ΔL=70mm. During the loading cycles, the shape of hysteresis loops almost remains unchanged (Figure 104).

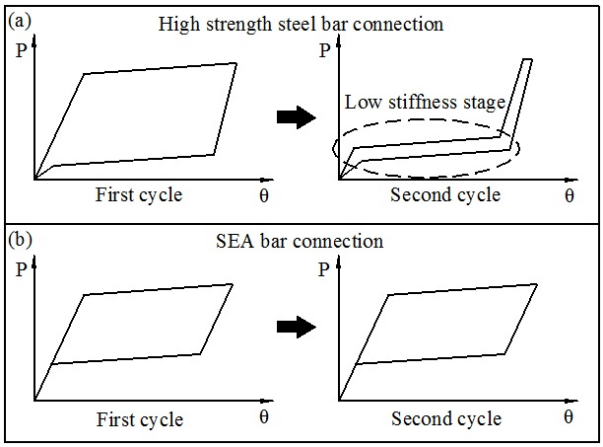

Figure 103 Schematic illustration of first two loadings cycles of Dou-Gon connects by (a) high strength steel bar and (b) SMA bar

The equivalent damping ratio of high strength steel bar connection when ΔL=70mm dropped from 6.35% to 2.66% and 1.40% at the 2nd and 3rd loading cycles, respectively. The SEA bar connection gave 4.13% and 4.08% equivalent damping ratios during the 2 loading cycles at ΔL=70mm as shown in Figure 105. The high strength steel bar connection can only provide high equivalent damping ratio in the first loading cycle and fractured after few loading cycles. The SEA bar connection can give a consistent equivalent damping ratio and better fracture behaviour since there is no fracture has been gathered during the non-prestrain tests.

The high strength steel bar connection has permanent deformation after each loading cycle, which reduces damping capacity while the SMA bar connection gives a consistent damping behaviour to the Dou-Gon system. Several aftershocks happen after the main shock in an earthquake. This requires the Dou-Gon system has stable damping ratio to dissipate energy during the aftershocks as well. The high strength steel bar connections provide low equivalent damping ratio and small resistance to the Dou-Gon during the aftershocks since they would have permanent deformations after the main shock. And the SEA bar connections can give consistent damping behaviour and dissipate energy persistent in both main shock and aftershocks.

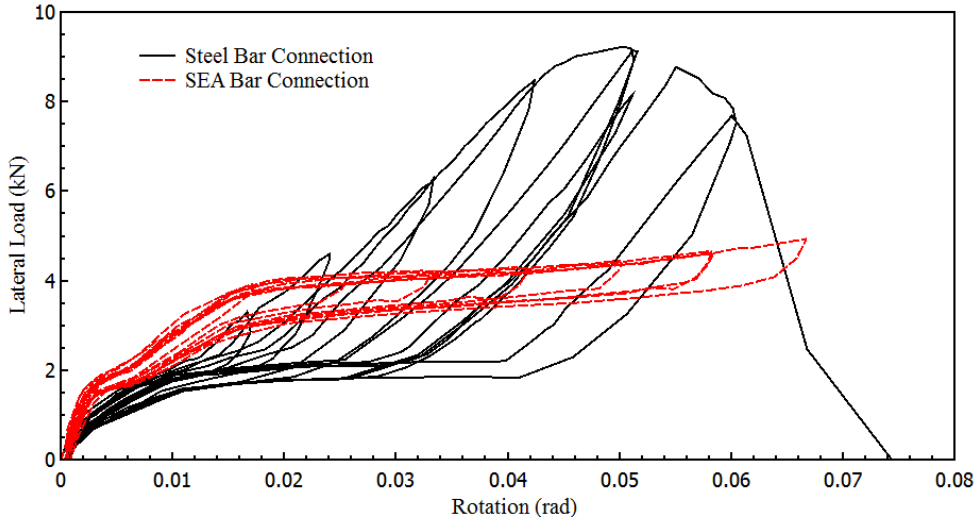

Figure 104 Hysteresis loop histories of both high strength steel bar and SMA bar connections under 10kN vertical loads

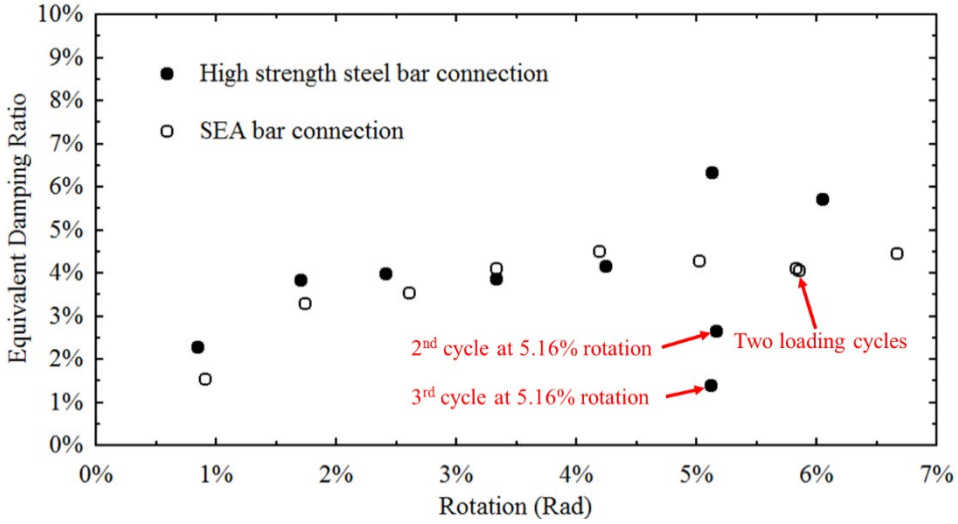

Figure 105 Equivalent damping ratios of both high strength steel bar and SMA bar connections under 10kN vertical loads

4.2.4.3 The effects of SMA bar connector with different levels of pre-strain

Previous research works showed that the pre-strain of SEA bars will give to the materials a larger energy dissipation capacity. In this research, the SEA bar connections was pre-strained to 1%, 3% and 5% strain levels, aiming at a higher damping ratio of the base Dou system.

Figure 106 illustrates that the SEA bar connector without pre-strain has experienced three stages of stiffness variation before the SEA enters the martensitic phase. So, it can only dissipate little amount of energy during small rotations. The shape of hysteresis loop of SEA bar with 1% pre-strain was not too much different from the one without pre-strain but change to the martensitic phase quicker. Because the pre-strain eliminates any possible slack between the structure and the connection system, and SEA bar starts to work from the beginning of

loading. The ultimate strength increased with the increase of the pre-strain level. The lateral load started to rise again after 4.5% radians for the SEA bar connection with 3% pre-strain. Because the SEA material is at its martensitic phase when it was pre-strained to 5% strain level. The second stiffness of SEA bar connection with 5% pre-strain is much higher than others and the lateral load increased to nearly 7kN when ΔL=70mm which gives a much better damping capacity than others. However, the SEA bar with 5% pre-strain fractured when the structure tried to reach 80mm in ΔL.

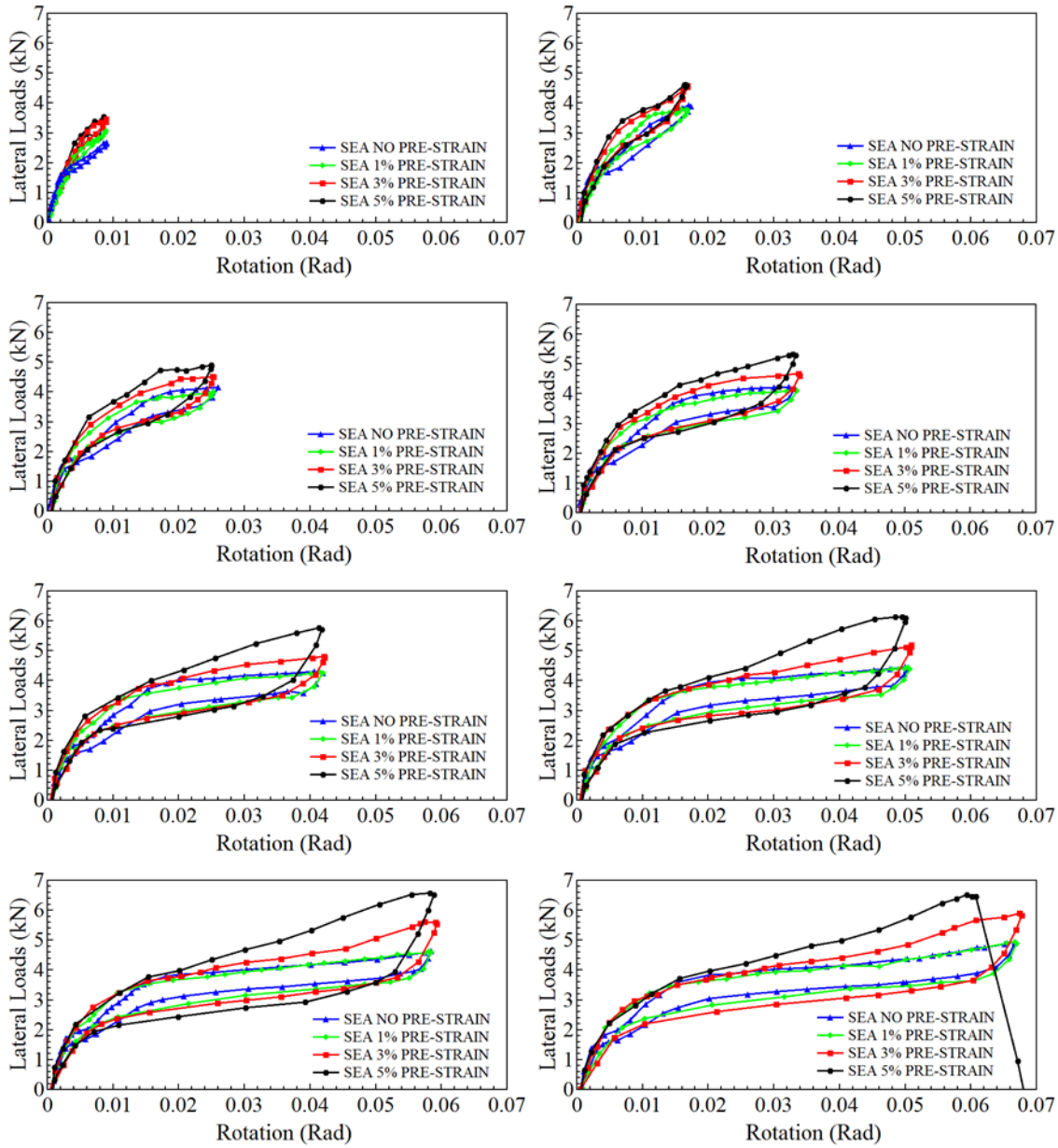

Figure 106 The hysteresis loops of Dou-Gon with SEA bar connection under 10kN dead load

Figure 107 and Figure 108 show that, under 4 and 7 kN vertical loads, SEA bar connectors with 1% pre-strain gave higher equivalent damping ratio than non-prestrain ones during small

prescribed rotation and become closer when θ increases. The equivalent damping ratio of high strength steel bar connector increases with the increasing of ΔL and SEA bar connector gives a constant equivalent damping ratio when ΔL≥20mm. The SEA bar connector with 1% pre-strain have slightly larger equivalent damping ratio than the one without pre-strain. When ΔL <40mm, the high strength steel bar connector has a higher equivalent damping ratio than the SEA bar connector without pre-strain but lower than the SEA bar connector with 1% pre-strain. They have the similar equivalent damping ratio when ΔL=40mm. Under ΔL equals to 50mm and 60mm, the high strength steel bar connection gives much higher equivalent damping ratios than other two connectors, but there are dramatic declines after the first cycle. The fracture strain of the high strength steel bar was tested to be $3.7x10^4$με. The high strength steel bar connections fractured when the base Dou system trying to reach 70mm of ΔL in both loading conditions. The behaviour was almost the same with 10kN vertical loads. No fracture happens to the SEA bars during the tests under 4kN and 7kN vertical loads which shows a longer fatigue life than high strength steel bar.

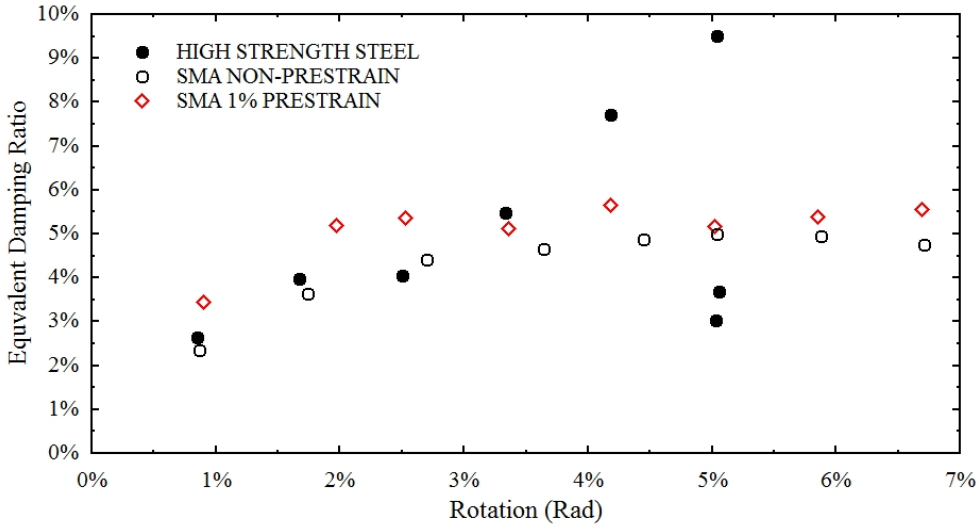

Figure 107 Equivalent damping ratios of Dou-Gon under 4kN dead loads

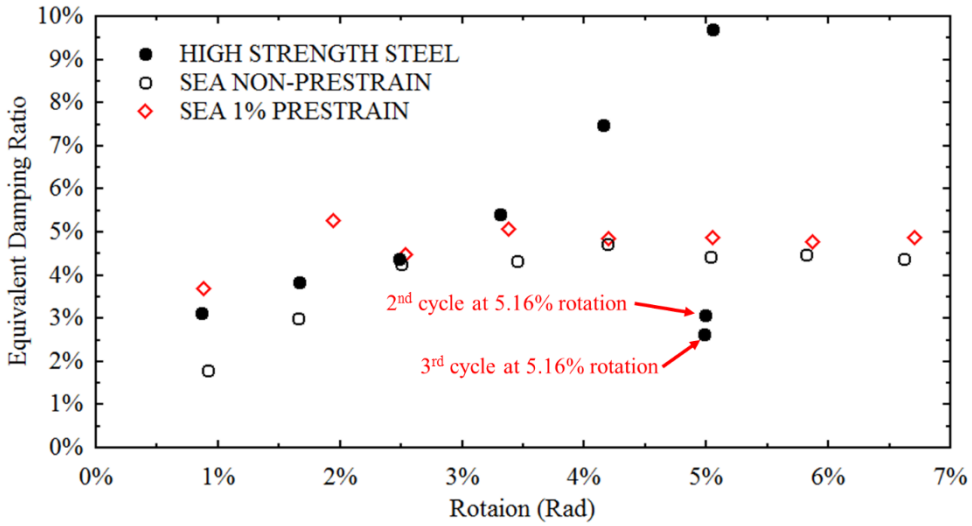

Figure 108 Equivalent damping ratios of Dou-Gon under 7kN dead loads

Under 10kN vertical loads, Figure 24, the equivalent damping ratios of SEA bar connectors with pre-strain were always larger than the ones without pre-strain. The equivalent damping ratio is increased as the pre-strain level increased. The SEA bar connector with 5% pre-strain gave the highest damping ratio under 10kN vertical loads but fractured when ΔL=80mm. The equivalent damping ratio of SEA bar connector with 3% pre-strain increases when ΔL<40mm and remain constant after that. The SEA bar connector with 5% pre-strain has a rapid increase when ΔL<30mm and rise steadily after a plateau of ΔL is between 30mm and 50mm.

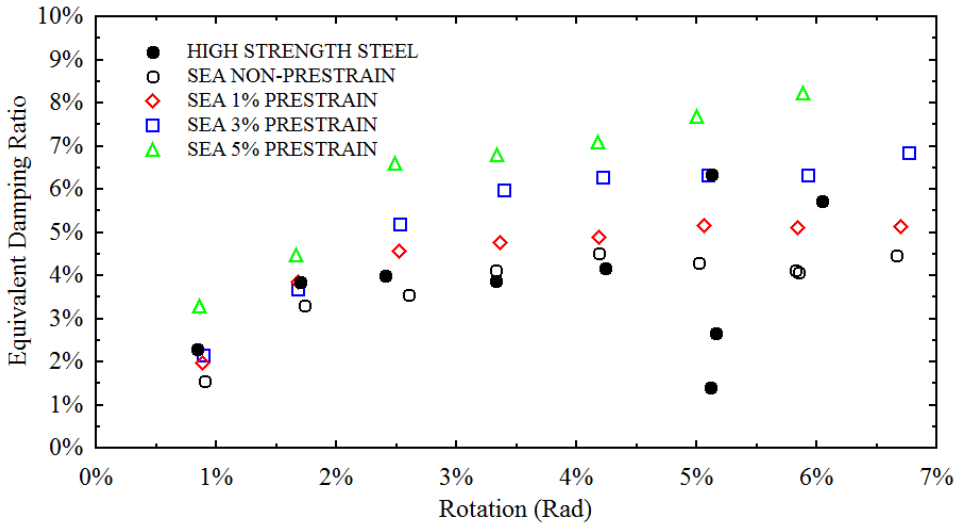

Figure 109 Equivalent damping ratios of Dou-Gon under 10kN dead loads

4.2.5 Deformations of base Dou

In previous researches, the Dou-Gon system always been assumed as rigid bodies. To understand and proof this, digital image correlation (DIC) techniques have been used in this

research to measure the strain of the base Dou. The vertical surface of base Dou was painted by white painting and a random speckle pattern has been chose to paint on top of the white background (Figure 110). A reference photo was taking before the lateral load applies and deformed photos were taking when base Dou rotates to prescribed radians.

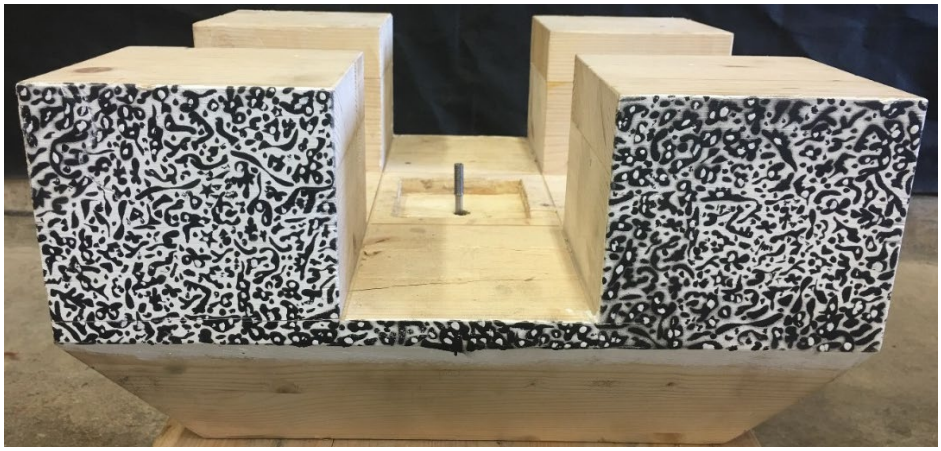

Figure 110 The random speckle pattern for DIC

The digital image correlation techniques (DIC) can work out the strain changes of the specimens under loadings. Any small amount of deformations of the specimens can be detected by the DIC. The following 4 pictures illustrate how the surface strain of base Dou changes from zero rotation to 6.77% radians with wood peg, steel and SMA connections. New connection materials have been used in these tests.

Figure 111 The DIC result for the base Dou connected by a wood peg connection

Figure 112 The DIC result for the base Dou connected by a steel bar connection

Figure 113 The DIC result for the base Dou connected by a SMA bar connection with 1% prestrain

Figure 114 The DIC result for the base Dou connected by a SMA bar connection with 3% prestrain

When the base Dou rotated to 6.77% radians, the right-hand side of the Dou is under compression and the left-hand side is under tension. With a conventional wood peg connection, the entire right hand side of the Dou was under approximately 0.5% compressive strain and the contact surface of the Dou and Gong was experienced relative high compressive strain which is up to 3.5% strain. And also the upper-right corner of the left hand side of the Dou shows a maximum 1.5% tensile strain. For the base Dou connected by a steel bar, the compression side of the Dou shows a similar behaviour compare with the Dou with a wood peg connection.

However, there is no sign on the left-hand side that indicates the Dou is under tension. There is no tension can be detected from both conditions of the Dou with SMA connections as well. For the Dou-Gon system connected by a SMA bar with 1% pre-strain, the maximum compression that the Dou has experienced is about 1% strain. When the pre-strain of SMA bar has increased to 3% strain level, the maximum compressive strain that can be noticed by the DIC is less than 0.5%.

4.3 Conclusions

Both high strength steel bar and super-elastic alloy bar are used to instead of conventional wood peg connection here. Static push over tests have been done to Dou A, Dou B and base Dou in this chapter. The strength of the structure has significant increase when use either metal bar connection. The ultimate strength and equivalent damping ratio of the structure with high strength steel bar connector is much higher than other types of connector, but only in the first cycle. The equivalent damping ratio has a dramatic decrease from the second loading cycle when using high strength steel bar. Super-elastic alloy bar connection can give the structure a consistent damping performance and longer fatigue life than high strength steel bar. The pre-strain of super-elastic alloy bar can give a relative higher equivalent damping ratio of Dou A and Dou B under higher vertical loads. For base Dou, the equivalent damping ratio increases significantly with the pre-strain level of the super-elastic alloy bar.

Furthermore, the results of DIC demonstrated that the base Dou with a conventional wood peg connection will experience both compression and tension during rotation and would have permanent deformation which need to be considered. The base Dou can be assumed as a rigid body when using pre-strained super-elastic bar connection since the material is still within the elastic deformation range.

Chapter 5 Static Tests of Two Layers Dou-Gon System

Static push-over tests of individual Dou were described in Chapter 4. This chapter reports push-over experiments conducted on Dou-Gon systems with two layers. The tests were conducted with conventional wooden peg connections and two metal connections (high strength steel and super-elastic alloy). The results were used to build the models for Open System for Earthquake Engineering Simulation.

The content of Chapter 5 has been submitted for review in the journal of *Engineering History and Heritage*: 'Static experimental study of two-layer Dou-Gon system by using super-elastic alloy as a connection material'.

5.1 Experimental method

A full-scale replica of a two-layer Dou-Gon system, which duplicates a historical building in Henan Province in China, was made of glued laminated timber. The conventional connections of Dou and the lower structure were wooden pegs. The tests involved using high strength steel and a super-elastic alloy to replace the wooden pegs to improve the seismic performance of the Dou-Gon system. Push-over tests were then conducted where the lateral loads were applied using a hydraulic jack. The displacements and rotations of components of the Dou-Gon system were measured by 18 LVDTs. Moment versus rotation curves were then obtained to evaluate the seismic performance.

5.1.1 Dou-Gon specimen and structure set up

This two-layer Dou-Gon system consisted of 11 individual components including the timber block that represents the top of a column. The lower layer comprised a base Dou, one Gon, and one Ang. The upper layer comprised 4 small Dou, 3 Gons, and one Ang. Each Dou was connected to the lower structure by a flat cut wooden peg (Figure 68). The pull-out force will change along with the dead load when a flat cut connection is used. The dimensions of the wood pegs were 28 x 28 x 56mm for the base Dou connection and 26 x 26 x 52mm for the upper layer Dou connections.

The timber block that represents the top of the column was fixed to the strong floor by two 24mm threaded bolts. Two angle plates were also fixed to the strong floor to prevent the timber block from sliding.

The two-layer Dou-Gon system was placed on top of the block in sequence (Figure 115). Gong and Ang were fitted in the grooves of Dou and bonded together. Five Dous were connected to the lower structures by wooden pegs or metal bars. Cubic holes with a width of 28mm were chiselled out for the wooden pegs in both the bottom of base Dou and the top of the timber block while 26mm width holes were chiselled out in the bottom of four upper Dou and the top of the corresponding elements.

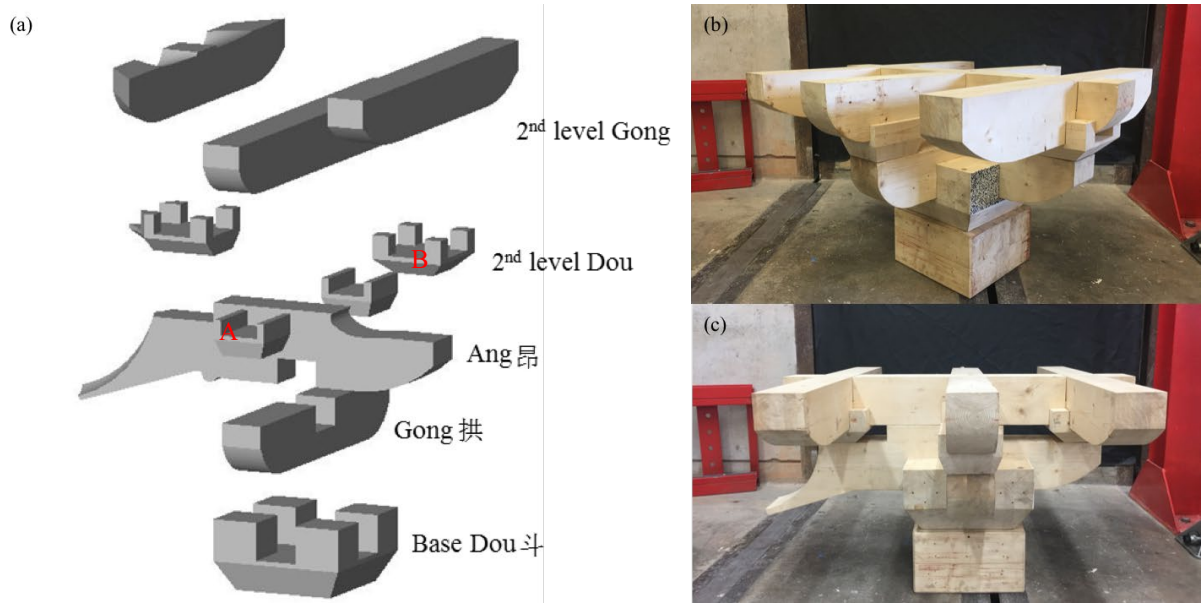

Figure 115 (a) 3D exploded view drawing of Dou-Gon; (b) and (c) Dou-Gon set up without dead loads

As shown in Figure 65, Figure 66 and Figure 93, a simple system was developed for the metal bar connections. 12mm thread inserts were fixed into the timber block, first level Gong, and Ang using epoxy resin (Figure 93a). The metal bar was placed first and inserted through the centre of the Gon along a pre-drilled vertical hole. A 100mm square steel plate and 50mm diameter washers were then embedded in the top surface of the base Dou and upper level Dou respectively to prevent damage to the timber caused by axial loads from the bar. A ball joint was then placed on top to remove the rotational restraint and provide a pin joint to the connection system. The top end of the connection system was fixed by a nut, which in some cases gives the pre-strain load to the super-elastic bar. This connection system is shown in detail in Figure 66 and Figure 93c.

Eight LVDTs (No. 1 to 8) were attached to the first level Gong and Ang to measure the sliding displacements and rotations of four upper level Dou. Two sets of four LVDTs (No. 9 to 16) were placed vertically to measure the total rotations and base Dou rotations, respectively. The radian of each rotation was calculated by the differences in the measurement of LVDTs on the

left and right sides, as shown in Figure 116. Two horizontal LVDTs (No. 17 and 18) measured the horizontal sliding displacement of both base Dou and the entire structure. A pallet was fixed on top of the Dou-Gon to house the concrete blocks and simulate the vertical load exerted on the structure. The lateral loads were applied by a hydraulic jack fixed onto the wall. The vertical distance from the loading point to the bottom level of base Dou was 700mm. The setup details for this structure are shown in Figure 116.

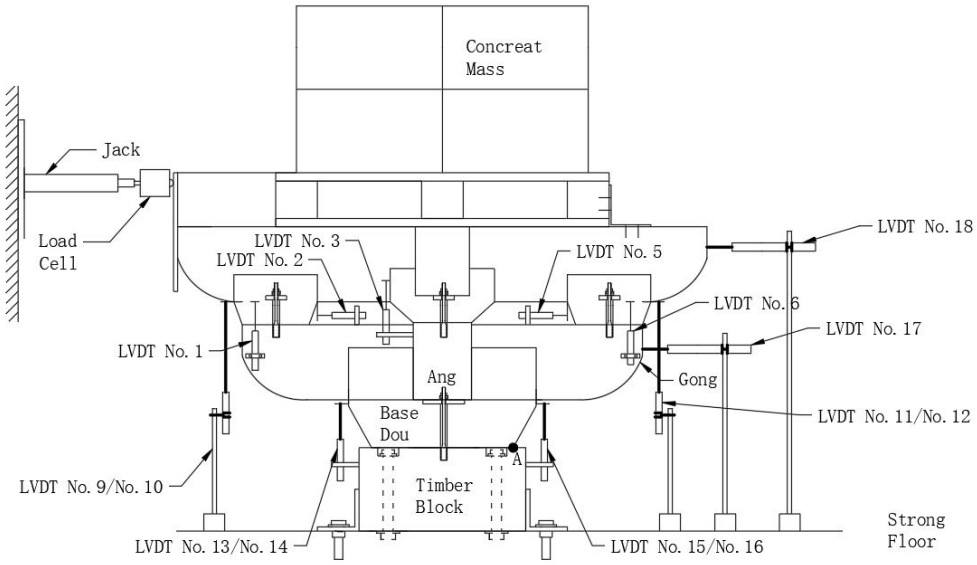

Figure 116 Loading apparatus and instrumentation

5.1.2 Test programme

For historic buildings, the weight of the roof plays a very important role in the structure and can often vary. To simulate this, 400kg, 700kg, and 1000kg weights were applied to the top of the structure to explore how the weight of the roof changes the behaviour of the structure.

As listed in the test protocol (Table 13), three different materials connecting the Dou and the lower elements under three weight levels were applied. One loading cycle was defined as the trajectory of the Dou-Gon system that rotates to a certain point with a prescribed radian and recovers to its original position. The three prescribed radians were 0.05, 0.06 and 0.07 and the Dou-Gon system loaded 3 cycles for each radian. Thus, there were 9 loading cycles in total for each test.

The super-elastic alloy bars were also pre-strained to 1% and 3% strain levels using the nut of the connection system. The pre-strained connection conditions were only tested at a weight of 1000kg.

Table 13 Test protocol

Test No.	Material for Connection	Weights on top	Pre-Strain
1	Wooden Peg	400kg	N/A
2	Wooden Peg	700kg	N/A
3	Wooden Peg	1000kg	N/A
4	Steel Bar	400kg	N/A
5	Steel Bar	700kg	N/A
6	Steel Bar	1000kg	N/A
7	SEA Bar	400kg	None
8	SEA Bar	700kg	None
9	SEA Bar	1000kg	None
10	SEA Bar	400kg	1%
11	SEA Bar	700kg	1%
12	SEA Bar	1000kg	1%
13	SEA Bar	400kg	3%
14	SEA Bar	700kg	3%
15	SEA Bar	1000kg	3%

5.2 Results and discussion

5.2.1 Dou-Gon set with conventional wooden peg connections

The results of the Dou-Gon set with conventional wooden peg connections can be illustrated using moment versus rotation curves. The curves in Figure 117 represent three stages of stiffness under a 1000kg roof weight. The first is a high elastic stage with a stiffness of 900kNm/rad. During the second, plastic stage the wooden peg of base Dou starts to pull out from the chiselled hole. The structure then begins to tip over and the lateral load is then decreased during the third stage of stiffness, the limit stage. Because the Dou-Gon has a good re-centring capability, the structure then rotated back to its original position without significant residual displacement after the lateral loads were removed.

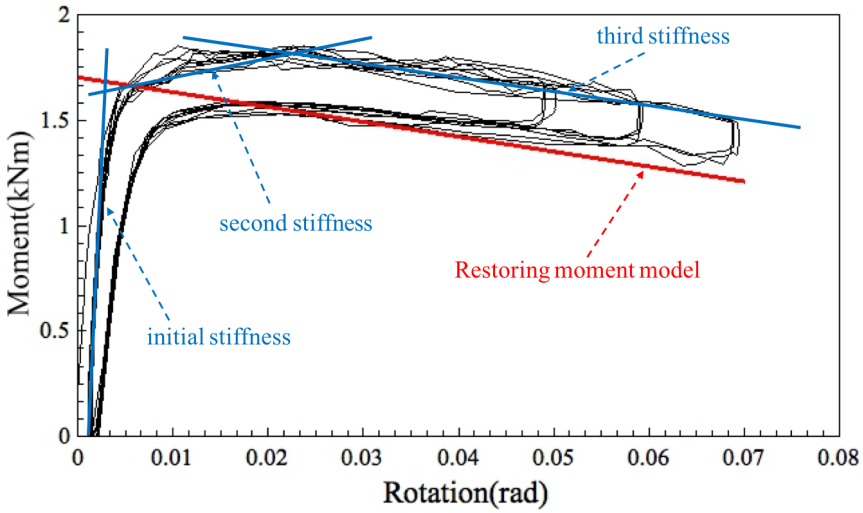

Figure 117 Hysteresis loops of Dou-Gon set with wooden peg connections at a weight of 1000kg

The restoring moment of the Dou-Gon set can be calculated using the equation:

$$\mathbf{M} = \frac{\mathbf{W \times g \times \cos\theta}}{\mathbf{2000L}}(\mathbf{L^2 - 2aL - 2LH \times \tan\theta}) \quad (5)$$

where W denotes the weight on top of the structure. Other parameters are illustrated in Figure 118.

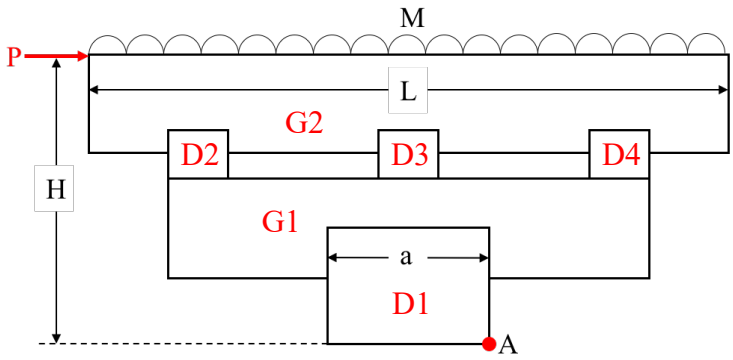

Figure 118 Simplified model of the structure and loadings

The second level of the structure was assumed to be a rigid frame as there were four Dou connected to the lower structure which restrained the movement of the upper lever structure. The restoring moment model at a weight of 1000kg is shown in Figure 117. The stiffness was virtually the same for both the model and the test results. The difference in level occurs because, in a practical situation, the upper level structure gives a constant moment to the entire Dou-Gon set.

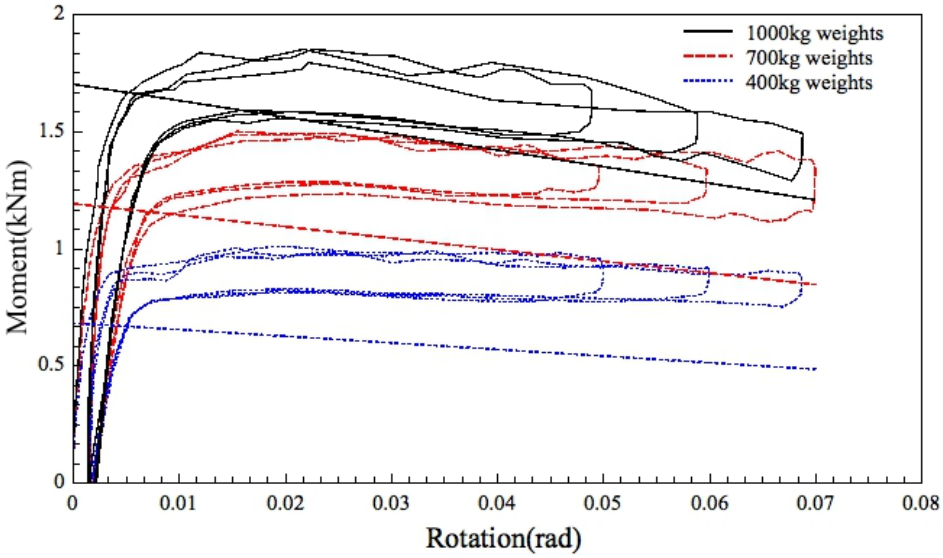

Figure 119 Hysteresis loops of Dou-Gon set with wooden peg connections under different weights

Only the hysteresis loops in the first loading cycle with the same rotation angle are shown in Figure 119 because there was negligible change at a weight of 1000kg (Figure 117). The ultimate strength of the Dou-Gon set with wooden peg connections increased significantly with

the weight on top. The higher weight on top of the structure will also increase the impact of the P-Delta effect resulting in a lower limit of stiffness of the Dou-Gon set. This is shown clearly in Figure 119 when the weight increased to 1000kg. Therefore, a heavier roof means there is a higher risk of tipping for a historical timber structure with conventional wooden peg connections.

5.2.2 Dou-Gon set with metal bar connections

In this research, two metallic materials, high strength steel and super-elastic alloy, were substituted for the wooden pegs. The vertical loads and the loading schemes remained the same.

The Dou-Gon set with high strength steel bar connections still retained a good self-centring capability. It recovered to its original position after the lateral loads were removed, even when the steel bars were yielded or fractured. The area within the hysteresis loops of the first loading cycle was much larger than in the other two loading cycles (Figure 103). This demonstrated that the Dou-Gon set with high strength steel bar connections dissipated a large amount of energy in the first loading cycle and exhibited a substantial decrease in the next two loading cycles under the same rotation angle. This is because the steel bar entered its plastic stage and showed permanent deformation during the first loading cycle. With the vertical load, there is no significant change in the ultimate strength of the Dou-Gon set with high strength steel bar connections

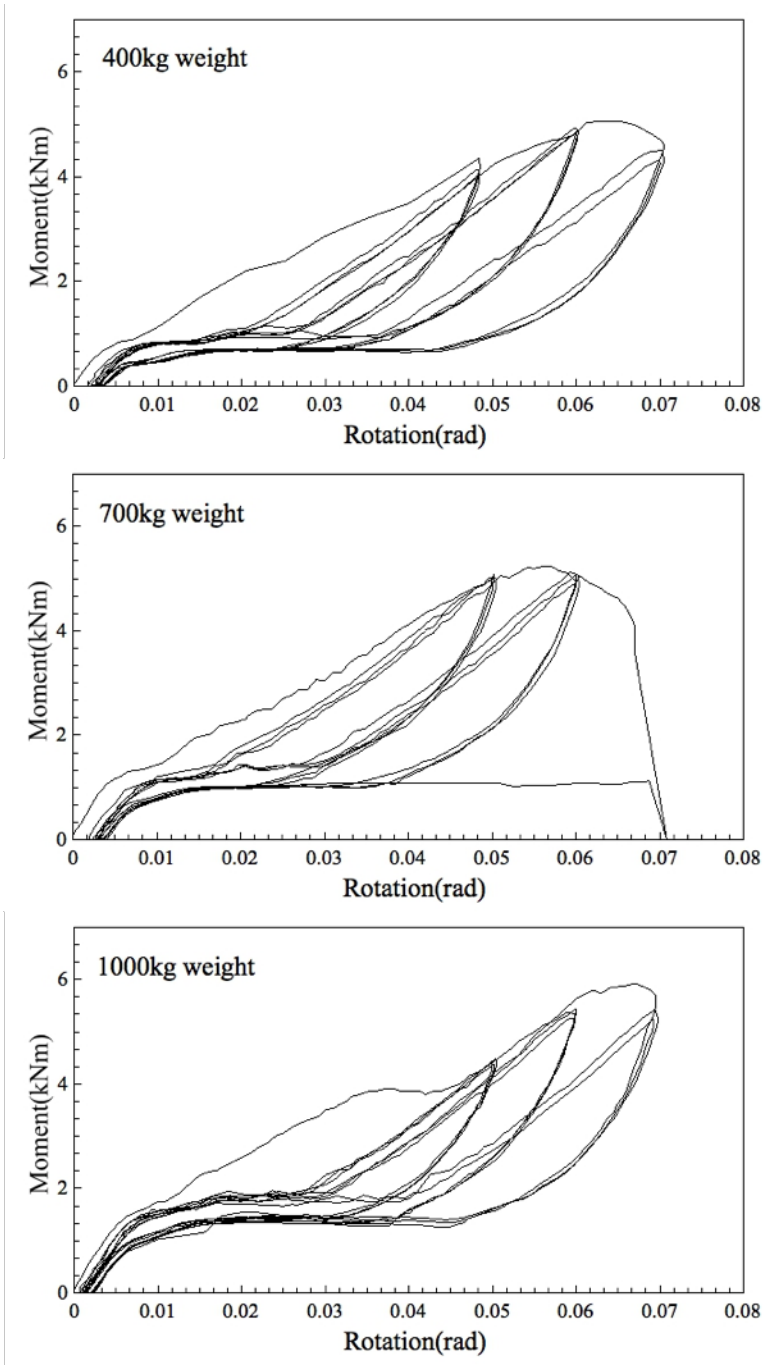

Figure 120 Hysteresis loops of Dou-Gon set with high strength steel bar connections

The super-elastic alloy bar connections give the Dou-Gon set a lower ultimate strength than the high strength steel bar connections, however, this is still much higher than for conventional wooden pegs. The Dou-Gon set experienced four stages of stiffness. The first two stages relate to the stiffness of the Dou-Gon itself while the third and fourth stages come from the super-elastic alloy bars. The shapes of the hysteresis loops under the same rotation angle remain almost the same due to the super-elasticity of the super-elastic alloy bars. The ultimate strength of the Dou-Gon set with super-elastic alloy bar connections increases significantly with the

weight on top. A heavier roof will therefore give higher ultimate strength to the Dou-Gon set. The stiffness of the Dou-Gon does not vary with the weight of the roof.

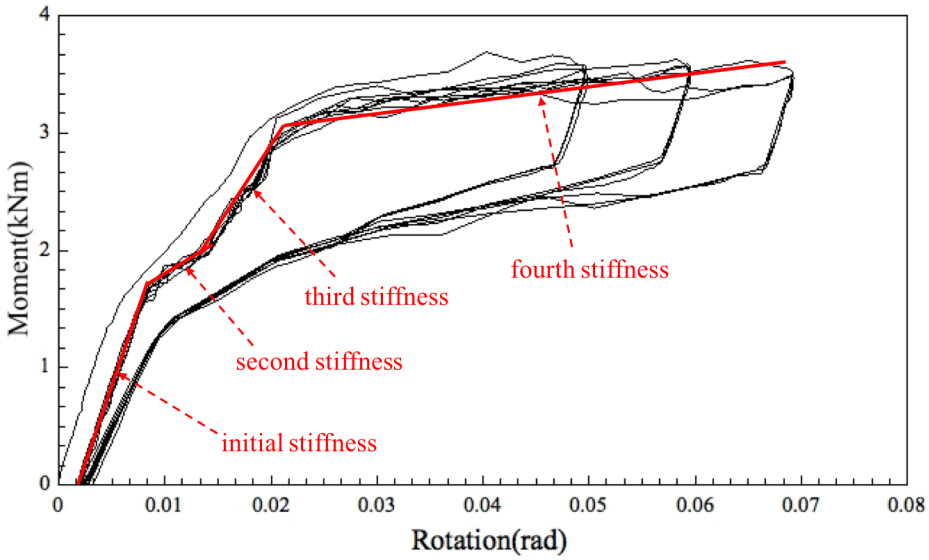

Figure 121 Hysteresis loops of Dou-Gon set with super-elastic alloy bar connections at a weight of 1000kg

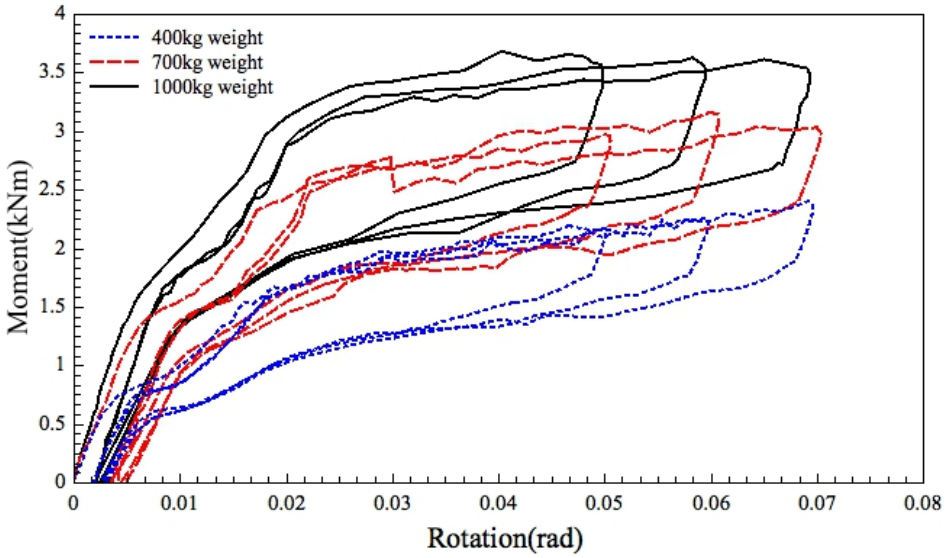

Figure 122 Hysteresis loops of first cycle of each rotation step for Dou-Gon set with super-elastic alloy bar connections

As Figure 123 shows, the second stiffness of Dou-Gon with high strength steel bar connections matched the stiffness of Dou-Gon with conventional wooden peg connections. The high strength steel bars did not exert any effort on the structure at this stage as the material experienced permanent deformation after the first loading cycle and must undergo the low stiffness stage, which is almost zero, from the second loading cycle (Figure 103). However, there was no notable change in the first and subsequent loading cycles when using the super-elastic alloy bar.

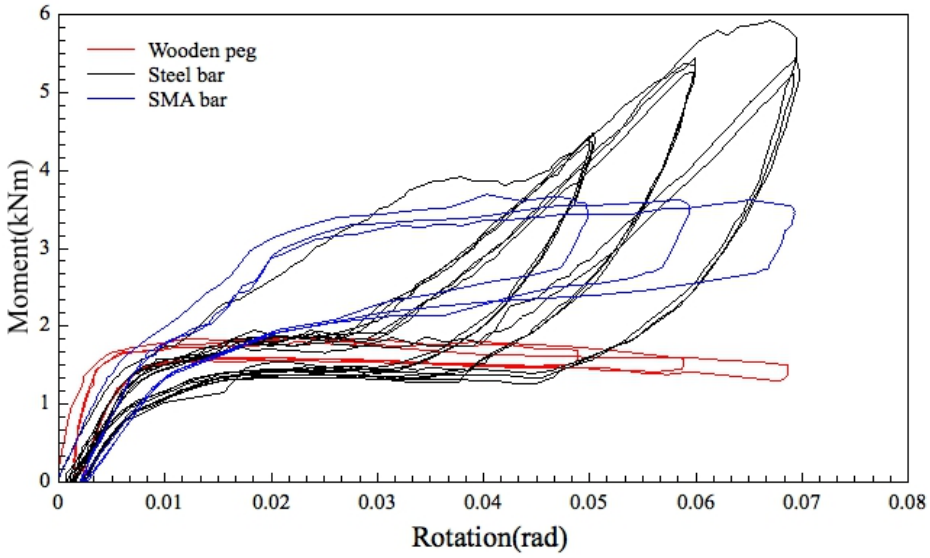

Figure 123 Comparison of three different connection materials at a weight of 1000kg

The Dou-Gon with high strength steel bar connections gave equivalent damping ratios ranging from 5% -10% in the first loading cycle which reduced to 4% - 6% in the second and third cycles. The super-elastic alloy gave equivalent damping ratios between 7% and 10% with a slight decrease in the second loading cycle (but still higher than 7%) which remained the same in the third loading cycle. These data are presented in Figure 124 and the condition for each test is shown in Table 13. It is possible that, when using a high strength steel bar, the equivalent damping ratio rises when the rotation angle increases. However, the steel will be fractured easily as it already has a permanent deformation, as shown in test 5. There was no indication that the equivalent damping ratios changed with the rotation angle of Dou-Gon when super-elastic alloy bar connections were used.

An earthquake always gives the structure more than one loading cycle and there are several small aftershocks that structures need to overcome. A super-elastic alloy is therefore more suitable for seismic applications than high strength steel because the latter will be damaged during a major earthquake and can provide neither sufficient stiffness nor good damping for the structure when it is subjected to small aftershocks.

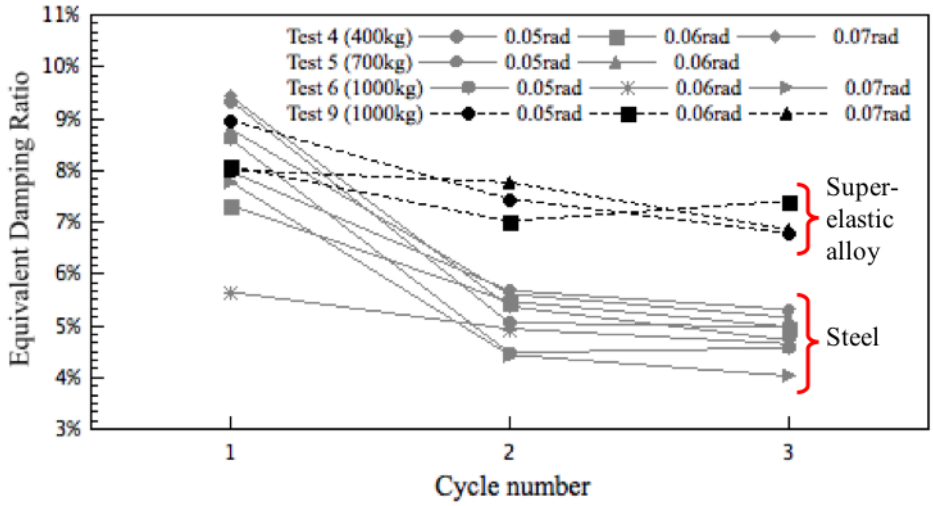

Figure 124 Equivalent damping ratios change with loading cycle

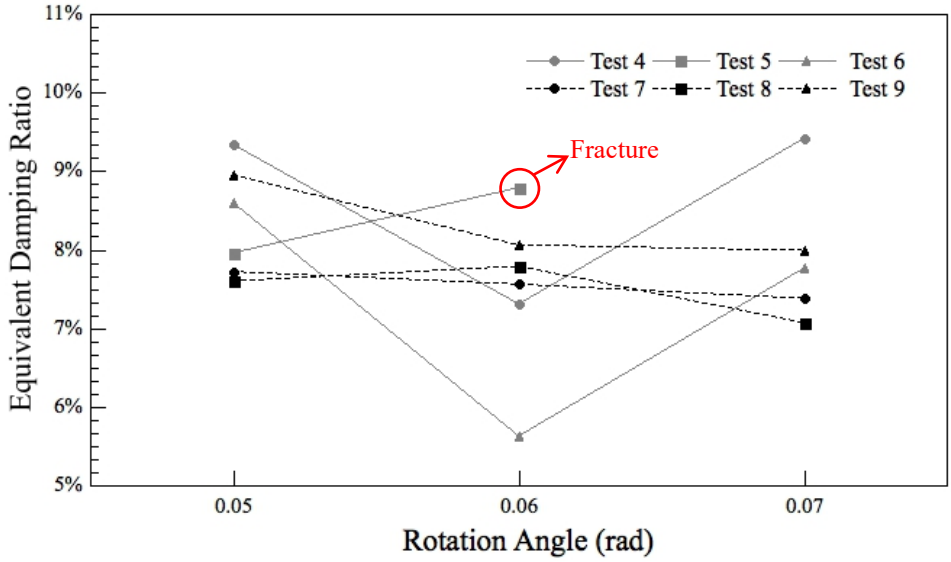

Figure 125 Equivalent damping ratios change with roof weight

5.2.3 Effects of pre-strained super-elastic alloy

The material tests and single Dou tests all show that the pre-strain of super-elastic alloy could provide a better damping ratio and dissipate more energy. In this research, the pre-strain levels of 1% and 3% were also applied to the super-elastic alloy bar connections.

The equivalent damping ratio of "no pre-strain" loading cases (tests 7-9) already showed a high equivalent damping ratio ranging from 7% to 9% (Figure 125). Figure 127 also shows that "no pre-strain" loading cases gave a higher equivalent damping ratio than the pre-strain loading cases. However, the hysteresis loops show that the 3% pre-strain loading cases dissipated more energy and have higher stiffness than both "no pre-strain" and 1% pre-strain cases. The "no pre-strain" loading cases gave a high equivalent damping ratio under rotations of more than

0.05 radians. They reached the super-elastic stage and the material then showed the super-elasticity effect until the Dou-Gon set rotated to 0.02 radians. The Dou-Gon set only retains its original stiffness and the elastic stiffness of super-elastic alloy under small displacements. The pre-strain of the super-elastic alloy allows the material to have initial super-elasticity and to dissipate a certain amount of energy, even under small displacements.

There are two possible reasons why a two-layer Dou-Gon set under "no pre-strain" loading cases gave a higher equivalent damping ratio than pre-strain loading cases. The first is that pre-strain loading cases have a higher final stiffness than "no pre-strain" cases. A higher moment is therefore needed to achieve the same rotation angle. Hence, A_e, the maximum elastic strain energy in one loading cycle used to calculate the equivalent damping ratio, will be higher and thus the final equivalent damping ratio will be smaller. The other reason may be that the top layer consists of several components and the movements between these can also dissipate energy. However, the pre-strain of the upper tie connections bound the components tightly together and resisted any movement between them. Therefore, the pre-strain on the super-elastic alloy connection of base Dou and the upper layer is the area that requires further investigation.

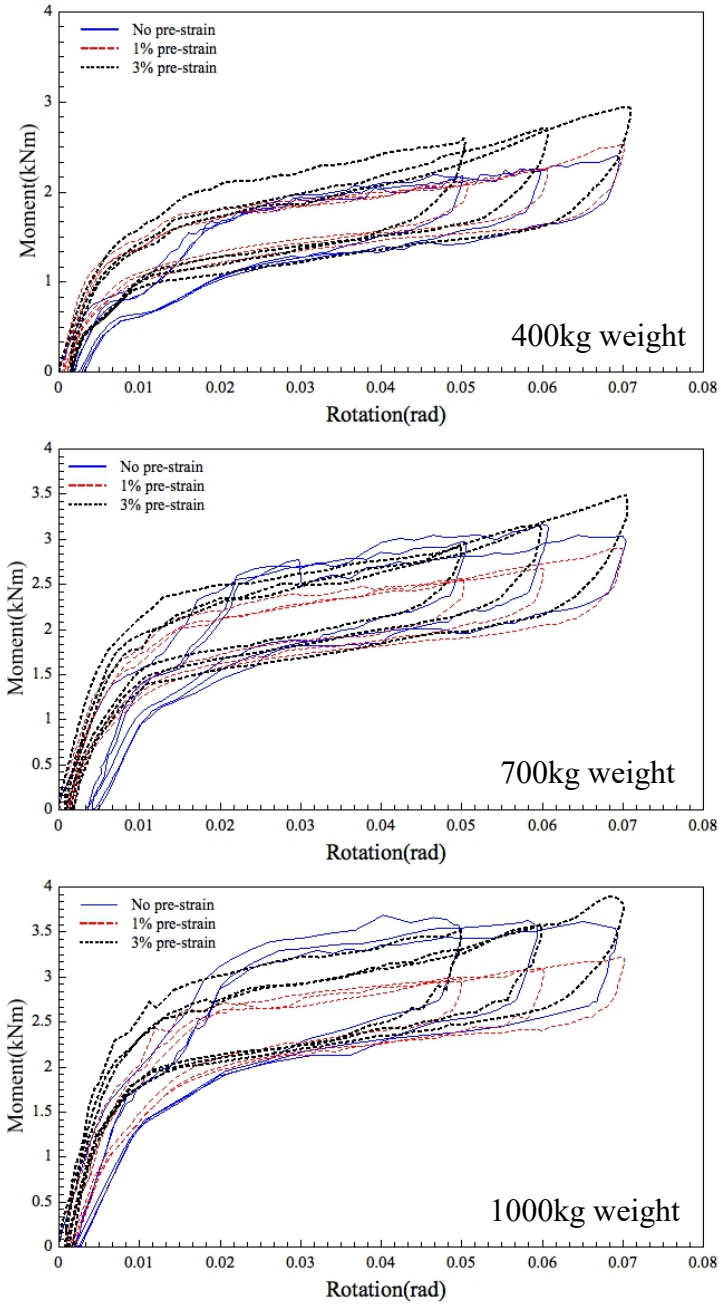

Figure 126 The effect of the pre-strain level of the super-elastic alloy on hysteresis loops of Dou-Gon set under different top loads

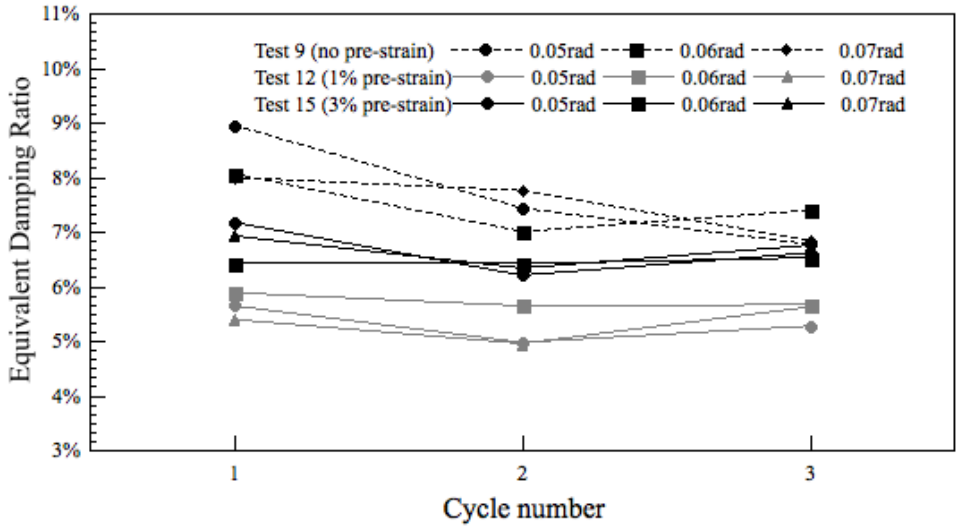

Figure 127 Equivalent damping ratios change with the pre-strain level of super-elastic alloy

Like the "no pre-strain" loading cases, the ultimate strength increases with the top loads applied on the Dou-Gon set in the pre-strain loading cases. The 3% pre-strain of the super-elastic alloy gave a slightly greater ultimate strength than the 1% pre-strain. There are only two stages of stiffness in the Dou-Gon set with 1% pre-strain super-elastic alloy connections. Three stages of stiffness can be observed in the 3% pre-strain loading cases. The structure entered its third stage of stiffness when it was rotated more than 0.05 radians because the super-elastic alloy transferred to its elastic deformation of detwinned martensite.

The equivalent damping ratio of 3% pre-strain loading cases is always higher than 1% pre-strain loading cases. The equivalent damping ratio of the latter ranges from 5% to 7% and the former from 6% to 9%. The equivalent damping ratio slightly decreases in the second and third loading cycles under 3% loading cases but not in the 1% loading cases. The equivalent damping ratio is also independent of the rotation angle of the Dou-Gon set with pre-strain super-elastic alloy bar connections.

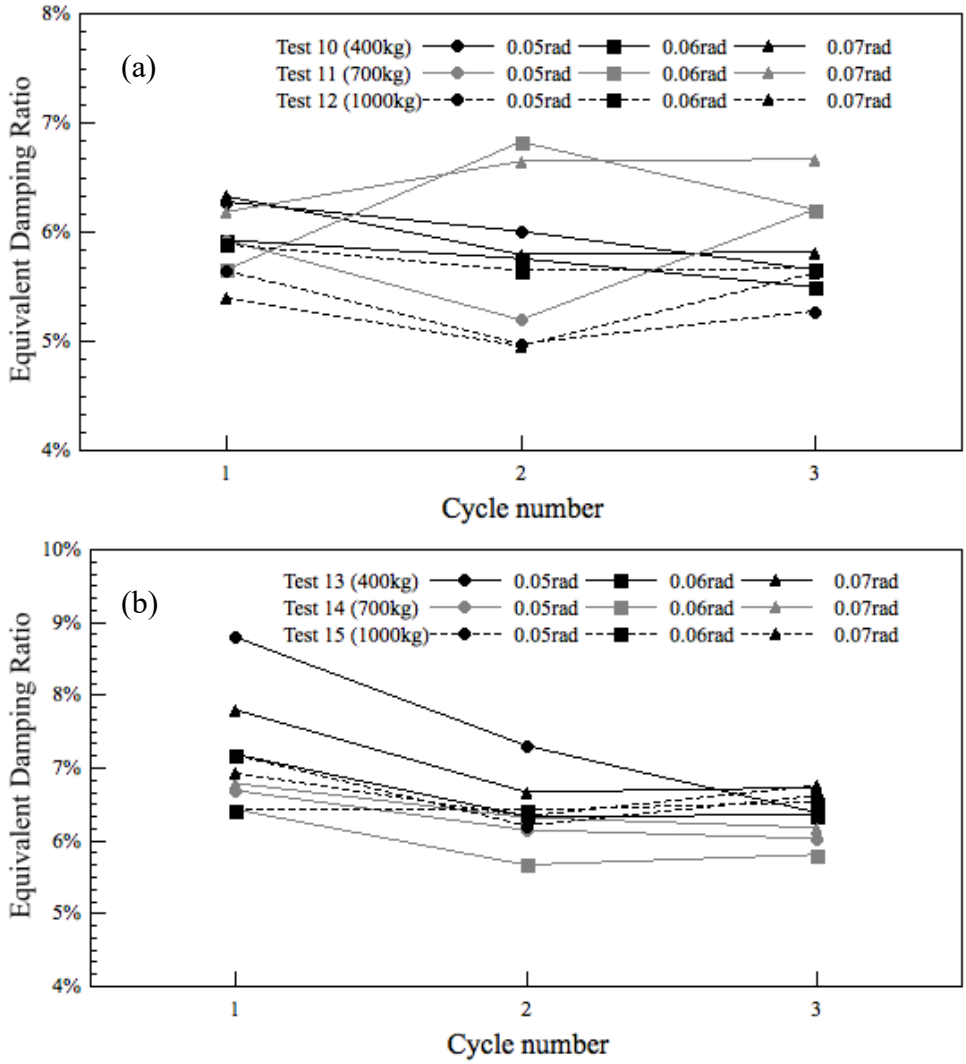

Figure 128 The effect of top loads on the equivalent damping ratio of Dou-Gon with super-elastic alloy pre-straining to (a) 1% strain level; (b) 3% strain level

5.3 Conclusion

The push-over tests of two-layer Dou-Gon system have been done in this chapter. Increasing of roof weight can significant increase the ultimate strength of Dou-Gon system with conventional wood peg connections. Same outcomes as Chapter 4 have been found in this chapter, higher ultimate strength is achieved by both metal bar connections than wood pegs. The system with super-elastic alloy bar connections has a consistent high damping ratio and high strength steel bar connections can only dissipate large amount of energy in the first loading cycle due to the permanent deformation of the material. Four stages of stiffness were observed in the "no pre-strain" loading cases of a Dou-Gon system with super-elastic alloy bar connections. 3% pre-strain level of the super-elastic alloy bar provide the two-layer Dou-Gon system with a higher equivalent damping ratio.

Chapter 6 Dynamic Tests of Two Layers Dou-Gon System

The static tests results show that the stiffness of the Dou-Gon system was enhanced by using metal bars instead of conventional wooden peg connections. The super-elastic alloy bar connections exhibit stable behaviour under several loading cycles and the pre-strain of the bar can provide an improved damping capacity. This chapter proceeds with dynamic experiments by inputting the scaled Northridge earthquake spectrum.

The content of Chapter 6 has been submitted for review in the journal of *Proceedings of the Institution of Civil Engineers - Civil Engineering*: 'Dynamic experimental and parametric studies of two-layer Dou-Gon system by using super-elastic alloy as a connection material'.

6.1 Experimental method

The dynamic tests were performed with a full-scale two-layer Dou-Gon system. It is a replica of a historical timber building from Henan Province in China and was constructed with glued laminated timber due to the limited access to large sectioned sawn timber. The dynamic rig was designed and built in the Structural Lab at the University of Bath. It was fixed on a strong floor and a dynamic actuator was connected to one end of the rig. Two accelerometers were attached to the base and the top of the Dou-Gon system to record the input and output accelerations, respectively. The input accelerations were used to compare with the input data in order to validate the accuracy and reliability of the tests.

6.1.1 Design of dynamic rig

A rig was designed and constructed into which the Dou-Gon system was placed. It consisted of two main parts, namely the track and the trolley. The track, which had channel sections on each side, was secured to the strong floor by four M24 bolts and two M24 bars were attached to each end of the track to maintain the space between the two sides of the track. The trolley had an inner space with the dimensions of 400*400*200mm in which the timber block was fitted. It sat on the track with 4 lower wheels, 4 upper wheels and 4 side bearing wheels.

6.1.2 Structure set up

The Dou-Gon system comprised three parts: the base block, lower layer and upper layer. The base block represented the column top of the structure. The lower layer had three components the base Dou, one Gong and one Ang. The upper layer had four Dou, three Gong and one Ang.

The conventional connection that connected the Dou and the lower elements was a wooden peg with a flat cut. The remaining elements were connected by cross-lap joints (Figure 129).

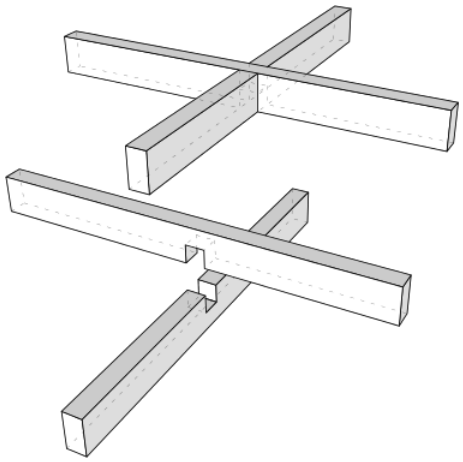

Figure 129 The cross-lap joint

The base block was placed into the rig and then fixed by several screws followed by the lower and upper layers of the Dou-Gon. Concrete blocks were positioned on top of the structure in order to apply a dead load. Two straps were tied to the concrete blocks and the top structure perpendicular to the moving direction to stop any movements between the weights and the Dou-Gon system. An additional two safety straps were tied loosely around the Dou-Gon system to hold the specimen and dead loads along the moving direction and were locked onto the hook that was attached to the 10-ton overhead gantry crane to prevent the structure from collapsing during the tests. An accelerometer was fixed to one end of the platform to record the actual input accelerations and another was fixed to the side surface of the upper Ang to record the reactive accelerations of the Dou-Gon system. The actuator was fixed by four M12 bolts to the other end of the trolley.

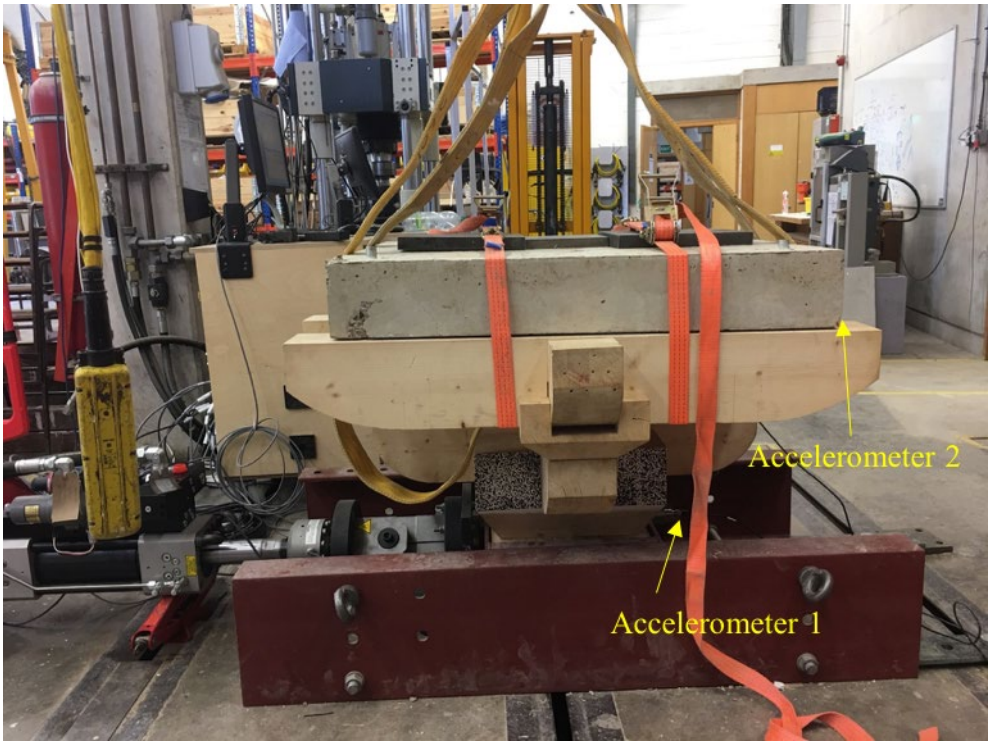

Figure 130 Test set-up

6.1.3 Test programme

Three sets of dead loads made of concrete and steel blocks were placed on top of the Dou-Gon system, loading 4kN, 7kN and 10kN, respectively. The chosen seismic wave was the Northridge earthquake. The actuator used for the tests was an Instron 3690 series 100kN pedestal base hydraulic actuator, which was controlled by one channel of an Instron 8800 controller with Wavematrix software. The maximum stroke of the actuator was 150mm on both ends from the central point. The original Northridge earthquake spectrum was converted to displacements before being imported to the actuator. Based on the Code for the seismic design of buildings (Ministry of Construction of the People's Republic of China, 2010), the accelerations of the original Northridge earthquake spectrum need to be scaled by the equation:

$$\mathbf{a_0(t_i)} = \frac{\mathbf{a_{0,max}}}{\mathbf{a_m}}\mathbf{a(t_i)} \tag{6}$$

where $a_{0,max}$ is the maximum design acceleration, a_m is the maximum acceleration of the recorded earthquake spectrum and t_i is the time coordinates of the real earthquake spectrum.

The time coordinates also need to be scaled by the equation:

$$\mathbf{t_{0,i}} = \frac{\mathbf{T_g}}{\mathbf{T}}\mathbf{t_i} \tag{7}$$

where T_g is the characteristic period of the site, and T is the characteristic period of the selected seismic response spectrum.

The Code for the Seismic Design of Buildings (Ministry of Construction of the People's Republic of China, 2010) also defines the relationships between frequent earthquakes, rare earthquakes and the local basic seismic intensity (I_0) as: I_0-1.55degree ≤ intensity of frequent earthquake < I_0 and I_0+1degree ≤ intensity of rare earthquake.

The original structure is in Huixian, Henan, China. The values of $a_{0,max}$ and T_g found in the Code for the seismic design of buildings (Ministry of Construction of the People's Republic of China, 2010) are 70cm/s^2 and 0.35s for frequent earthquakes and 400cm/s^2 and 0.40s for rare earthquakes.

Tests were also conducted by inputting white noise to calculate the damping of the Dou-Gon system. Five different amplitudes of white noise (25mm/s^2, 50mm/s^2, 75 mm/s^2, 100 mm/s^2 and 125 mm/s^2) were applied to determine whether the damping would change with the amplitude.

The three different connection materials that were used in the tests were conventional wooden pegs, high strength steel bars and super-elastic alloy bar connections. The super-elastic alloy bars were also pre-strained to strain levels of 1% and 3%. According to the results from the static tests, the equivalent damping ratios of "no pre-strain" loading cases are higher than pre-strain loading cases; hence, further dynamic tests were conducted. The super-elastic alloy bar used in the lower layer of the Dou-Gon system was pre-strained to a strain level of 3% and the other four super-elastic alloy bars used in the upper layer of the Dou-Gon system had no pre-strain applied in order to compare with the 3% pre-strain condition to evaluate whether pre-strain of the upper layer super-elastic alloy bars prevented the movements between the elements and reduced its own energy dissipation capability.

Table 14 Dynamic test protocol: comparison between different material under various dead loads

Test number	Connection material	Pre-strain conditions	Dead loads	Input data
1	Wooden peg	N/A	400kg	White noise
2(a,b)				Seismic wave
3			700KG	White noise
4(a,b)				Seismic wave
5			1000KG	White noise
6(a,b)				Seismic wave
7	High strength steel bar	N/A	400kg	White noise
8(a,b)				Seismic wave
9			700KG	White noise
10(a,b)				Seismic wave
11			1000KG	White noise
12(a,b)				Seismic wave

13	Super-elastic alloy bar	0%	400kg	White noise
14(a,b)				Seismic wave
15			700KG	White noise
16(a,b)				Seismic wave
17			1000KG	White noise
18(a,b)				Seismic wave
19		1%	400kg	White noise
20(a,b)				Seismic wave
21			700KG	White noise
22(a,b)				Seismic wave
23			1000KG	White noise
24(a,b)				Seismic wave
25		3%	400kg	White noise
26(a,b)				Seismic wave
27			700KG	White noise
28(a,b)				Seismic wave
29			1000KG	White noise
30(a,b)				Seismic wave
31		3% of the lower layer	400kg	White noise
32(a,b)				Seismic wave
33			700KG	White noise
34(a,b)				Seismic wave
35			1000KG	White noise
36(a,b)				Seismic wave

6.2 Results and discussion

6.2.1 Dou-Gon set with conventional wooden peg connections

The Dou-Gon system with conventional wooden peg connections was tested under seismic waves 6 times with different dead loads. The test conditions are shown in Table 15.

Table 15 Test protocol of wooden peg connections

Test no.	Dead loads	Input seismic wave
2a	400kg	Frequent earthquake
2b		Rare earthquake
4a	700kg	Frequent earthquake
4b		Rare earthquake
6a	1000kg	Frequent earthquake
6b		Rare earthquake

The results of the structure subjected to the scaled Northridge Earthquake are shown in Figure 131 and Table 16. The response curve of the structure under the frequent earthquake wave has no significant change with the rise of the dead loads. When the amplitude of the input seismic wave increases, the higher dead loads give the structure a better stability. According to the

maximum response acceleration and RMS, the structure has an even better seismic behaviour under the rare earthquake wave than the frequent wave.

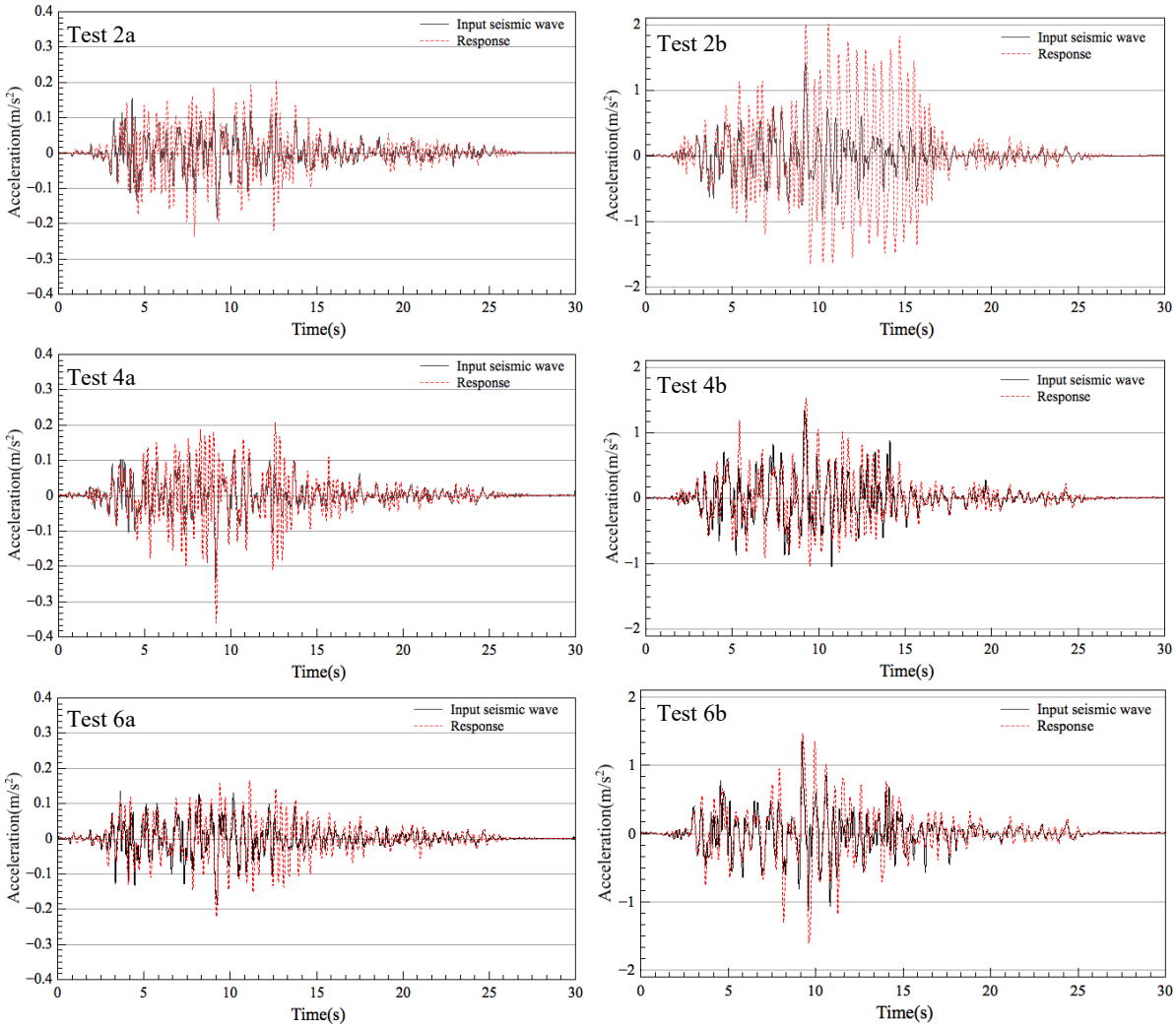

Figure 131 The results of the Dou-Gon system with wooden peg connections subject to scaled Northridge Earthquake

Table 16 Maximum response acceleration and RMS of Dou-Gon system with wooden peg connections subject to the scaled Northridge Earthquake

Case no.	2a	2b	4a	4b	6a	6b
a_{max}(m/s^2)	0.237	2.012	0.362	1.528	0.223	1.618
Increment%	27.1%	42.3%	52.6%	14.7%	18.4%	19.3%
RMS(m/s^2)	0.052	0.555	0.056	0.296	0.047	0.312
Increment%	46.9%	141.4%	65.6%	20.1%	40.1%	38.9%

White noise with different amplitudes (25mm/s^2, 50mm/s^2, 75mm/s^2, 100mm/s^2 and 125mm/s^2) was used to determine the dynamic properties of the structural system under different levels of excitation.

The damping ratios of the Dou-Gon system are determined by Half Power Bandwidth method (Saidi et al., 2006; Singh and Nanda, 2012) (Figure 132). Half power bandwidth is defined as

the ratio of the frequency range between the two half power points to the natural frequency at this mode. The damping ratio (ψ) is then evaluated using the half-power bandwidth expression as given by:

$$\psi = \frac{\omega_2 - \omega_1}{2\omega_n} \tag{8}$$

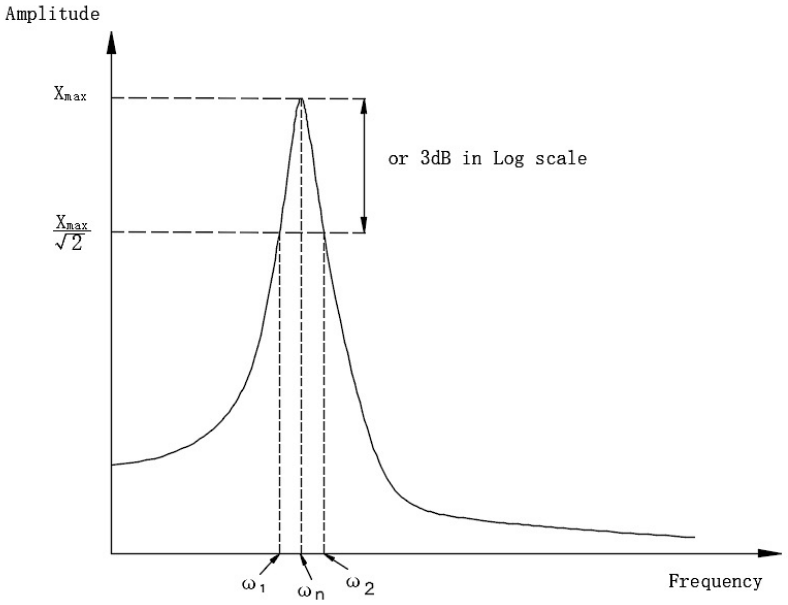

Figure 132 Half-power band width method for damping determination

The results are illustrated in Figure 133. The Dou-Gon system with conventional wooden peg connections has a damping ratio in the range of 2.5% to 5%, which corresponds to the findings of previous research. The damping ratio increased with the vibration amplitude under a dead load of 400kg and an increase can be seen from the 700kg dead load condition. There is no significant evidence to indicate that the damping ratio is dependent on the dead loads, which concurs with the previous studies conducted by Fujita. However, the Dou-Gon system have many different combinations and the specimen used in this research is not the same with the one Fujita used. It might cause the contrary behaviours of Dou-Gon.

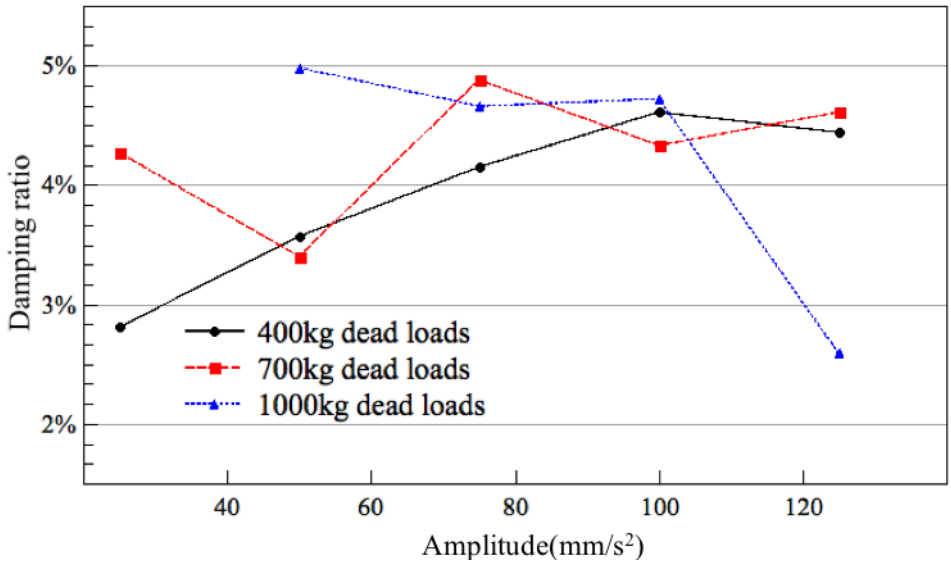

Figure 133 Damping ratios of Dou-Gon with wooden peg connections

6.2.2 Dou-Gon set with metal bar connections

Super-elastic alloy has been chosen to substitute wooden pegs due to its super-elasticity, which can dissipate energy without causing permanent deformation of the material itself. High strength steel bars were also chosen in this study as comparative specimen. The Dou-Gon systems with each connection material were tested under three different dead load weights and both frequent and rare earthquake waves were inputted.

Table 17 Test protocol of high strength steel bar and super-elastic alloy bar connections

Test no.	Material	Dead loads	Input seismic wave
8a	High strength steel	400kg	Frequent earthquake
8b			Rare earthquake
10a		700kg	Frequent earthquake
10b			Rare earthquake
12a		1000kg	Frequent earthquake
12b			Rare earthquake
14a	Super-elastic alloy	400kg	Frequent earthquake
14b			Rare earthquake
16a		700kg	Frequent earthquake
16b			Rare earthquake
18a		1000kg	Frequent earthquake
18b			Rare earthquake

The results for the Dou-Gon with two metal bar connections are illustrated in Figure 134 and Figure 135. Both tests under 1000kg dead loads have a higher overlap ratios of response and input curves than the lower dead loads test conditions.

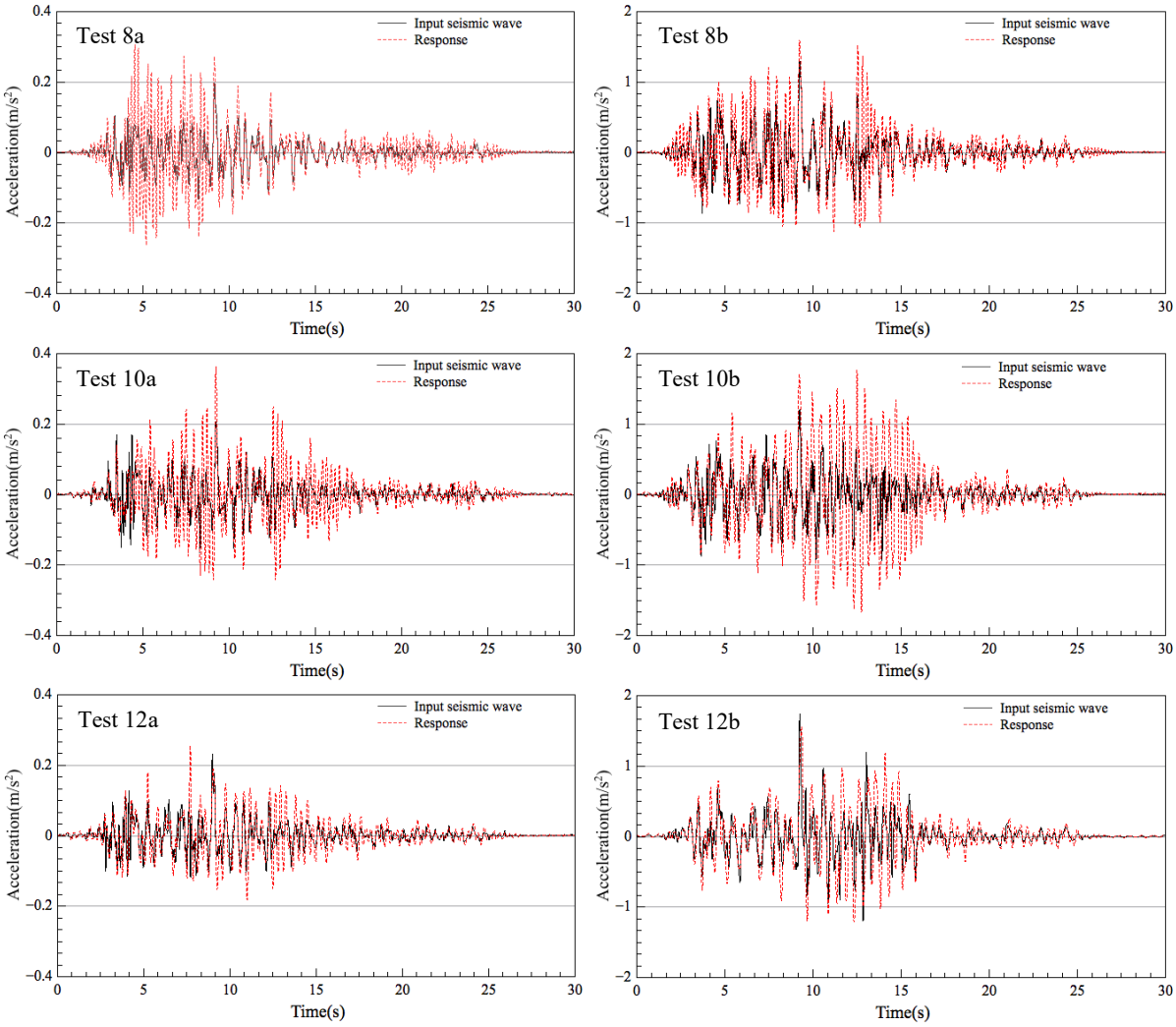

Figure 134 The results of the Dou-Gon system with high strength steel bar connections subject to scaled Northridge Earthquake

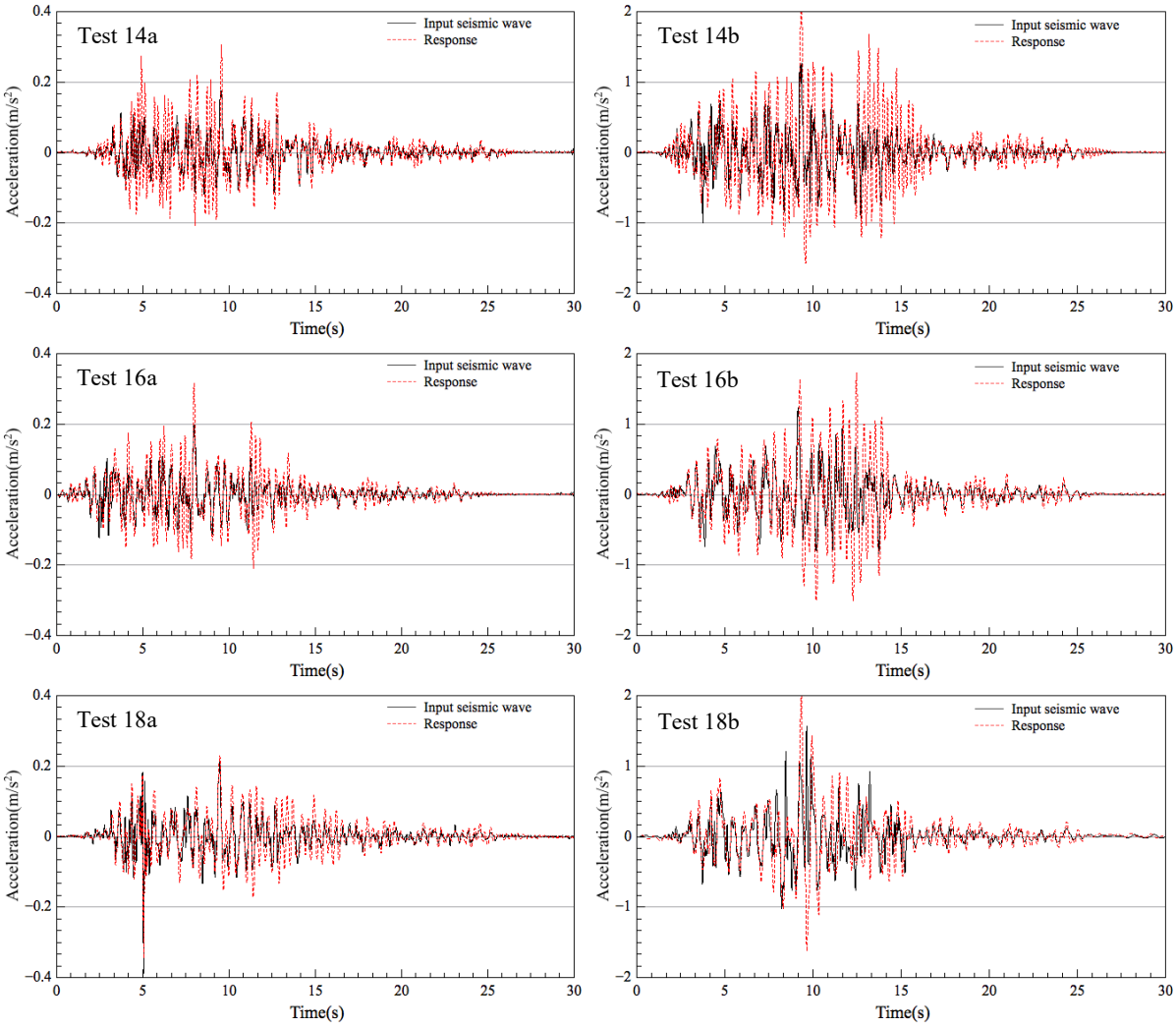

Figure 135 The results of the Dou-Gon system with super-elastic alloy bar connections subject to scaled Northridge Earthquake

A significant reduction in maximum acceleration and RMS can only be observed with the high strength steel bar connection when the dead load was 1000kN. It is a reasonable assumption that using high strength steel bars as a substitute for the wooden pegs can improve the anti-seismic performance of the structure due to the fact that real structures of heavy roofs. The tests associated with the super-elastic alloy bars have revealed a slightly different trend. The increments for both maximum acceleration and RMS decreased with the increasing of the dead loads when the super-elastic alloy was used as the connection material in the Dou-Gon system. In contrast to the specimen using conventional wood pegs, the heavier roof weight could provide the structure a better anti-seismic stability when the metal bar is used as the connection material.

Table 18 Maximum response acceleration and RMS of Dou-Gon system with high strength steel bar and super-elastic alloy bar connections subject to scaled Northridge Earthquake

Case no.	8a	8b	10a	10b	12a	12b
$a_{max}(m/s^2)$	0.305	1.590	0.363	1.757	0.255	1.564

Increment%	55.3%	20.8%	76.4%	45.9%	10.8%	-9.7%
RMS(m/s^2)	0.064	0.352	0.067	0.483	0.049	0.342
Increment%	95.3%	52.8%	82.0%	108.2%	43.3%	47.8%
Case no.	14a	14b	16a	16b	18a	18b
a_{max}(m/s^2)	0.305	2.077	0.314	1.720	0.346	2.004
Increment%	75.9%	64.2%	57.7%	39.9%	-11.3%	28.5%
RMS(m/s^2)	0.055	0.428	0.052	0.387	0.050	0.309
Increment%	67.0%	84.6%	57.6%	72.8%	35.3%	29.0%

The damping ratios of the Dou-Gon system with different types of metal bars have been calculated from the data obtained from the white noise tests with different amplitudes. The damping ratios of the Dou-Gon with high strength steel bar connections are in the range of 2-4.5%, while the ratios ranged between 1-5% with super-elastic alloy bar connections. Figure 136(a) demonstrates that the damping ratios are independent to both the dead loads and amplitudes when high strength steel bars are used as the connection material. When the super-elastic alloy bar was applied to the Dou-Gon system, the damping ratios gradually increased as the amplitudes increased under dead loads of 400kg and 700kg, whereas they largely remained constant under the 1000kg dead load. A heavier dead load can also give the structure a greater damping ratio when super-elastic alloy bars are used as the connection material.

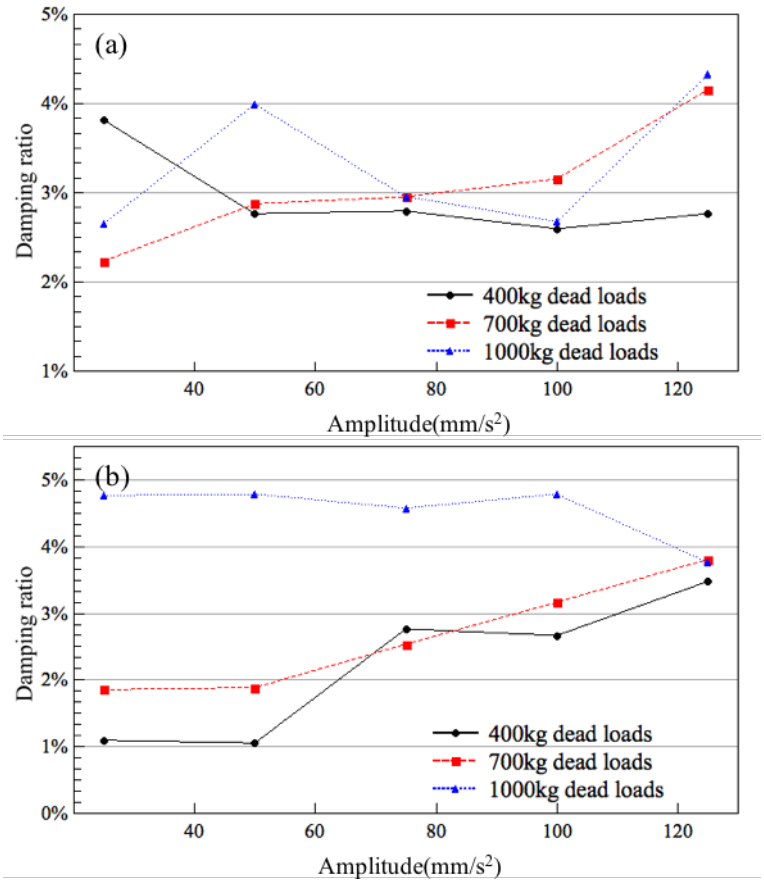

Figure 136 Damping ratios of Dou-Gon with (a)high strength steel bar connections; (b)super-elastic alloy bar connections

It can be clearly seen from Figure 137 that the conventional wooden peg connections gave the Dou-Gon system a higher damping ratio than other two metal bar connections under dead loads of 400kg and 700kg. When the dead load was increased to 1000kg, the super-elastic alloy bar gave the structure similar damping ratios to the wooden pegs. The damping ratio of the Dou-Gon with wooden peg connections under 1000kg dead loads and 125mm/s^2 input excitation experienced a dramatic drop and was significantly lower than the damping ratio of the Dou-Gon with the other two metal bar connections. The wooden pegs tended not to connect the Dou-Gon tightly; hence, they have more movement during an earthquake, which results in higher damping ratios. Additionally, since the limitations of the actuator and the considerably higher yield strength of metal bars in comparison to wooden pegs, both the high strength steel bar and super-elastic alloy bar are still deformed in the elastic range practically, which causes the damping ratios of the Dou-Gon with wooden pegs to be generally higher than the system with metal bars.

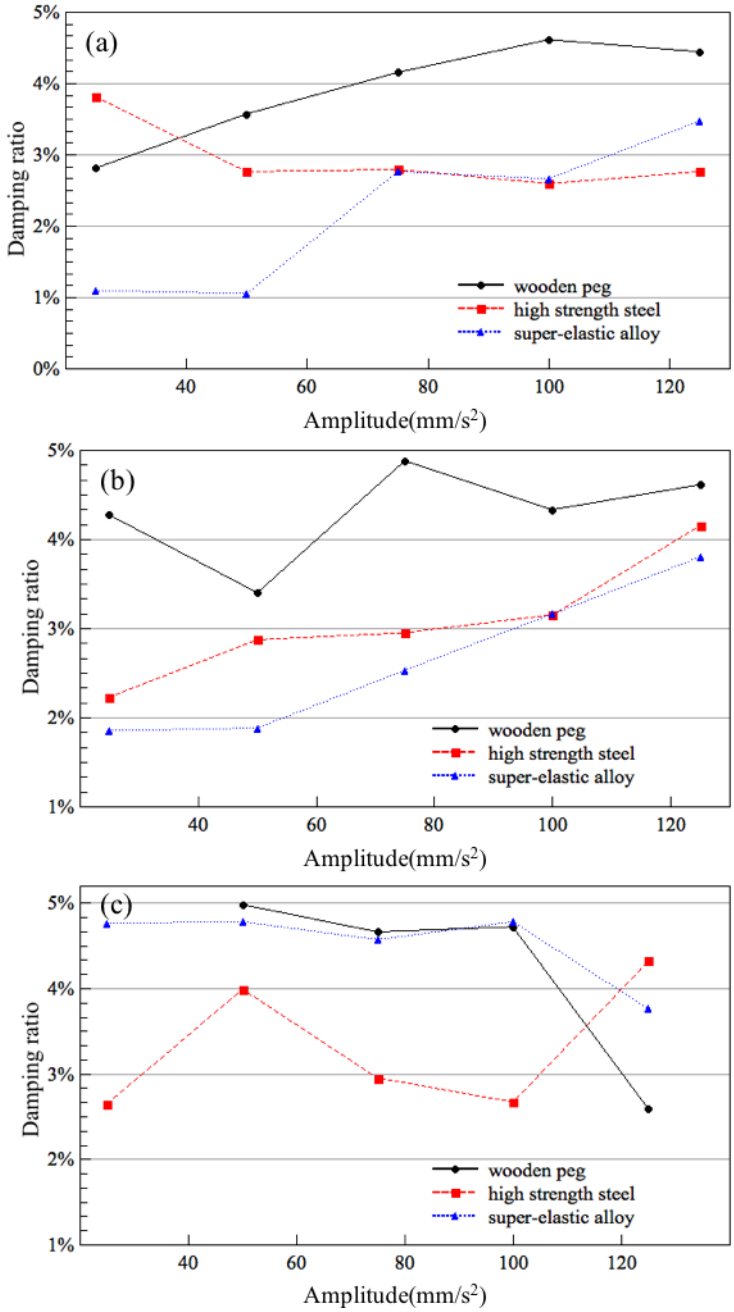

Figure 137 Damping ratios of Dou-Gon with different connections under dead loads of (a)400kg; (b)700kg; (c)1000kg

6.2.3 Effects of pre-strained super-elastic alloy

The results from the previous series of tests prove that the metal bar connections were still deformed in their elastic deformation range. The pre-strain of the super-elastic alloy can drag the material to its plastic deformation range before any external forces are applied. In this chapter, experiments were conducted on the Dou-Gon with pre-strained super-elastic alloy bar connections. The super-elastic alloy bars were pre-strained to strain levels of 1% and 3%. As the static tests show that the equivalent damping ratios of the “no pre-strain” loading cases were higher than pre-strain loading cases, additional tests in which the super-elastic alloy bar

in the lower layer was pre-strained to 3% and the rest of the bars in upper layer remained non-prestrained were conducted. Three different dead load weights were applied and both seismic waves and white noises were inputted into the structure.

Table 19 Test protocol of Dou-Gon with pre-strained super-elastic alloy bar connections

Test no.	Pre-strain condition	Dead loads	Input seismic wave
20a	1%	400kg	Frequent earthquake
20b			Rare earthquake
22a		700kg	Frequent earthquake
22b			Rare earthquake
24a		1000kg	Frequent earthquake
24b			Rare earthquake
26a	3%	400kg	Frequent earthquake
26b			Rare earthquake
28a		700kg	Frequent earthquake
28b			Rare earthquake
30a		1000kg	Frequent earthquake
30b			Rare earthquake
32a	Lower layer 3%	400kg	Frequent earthquake
32b			Rare earthquake
34a		700kg	Frequent earthquake
34b			Rare earthquake
36a		1000kg	Frequent earthquake
36b			Rare earthquake

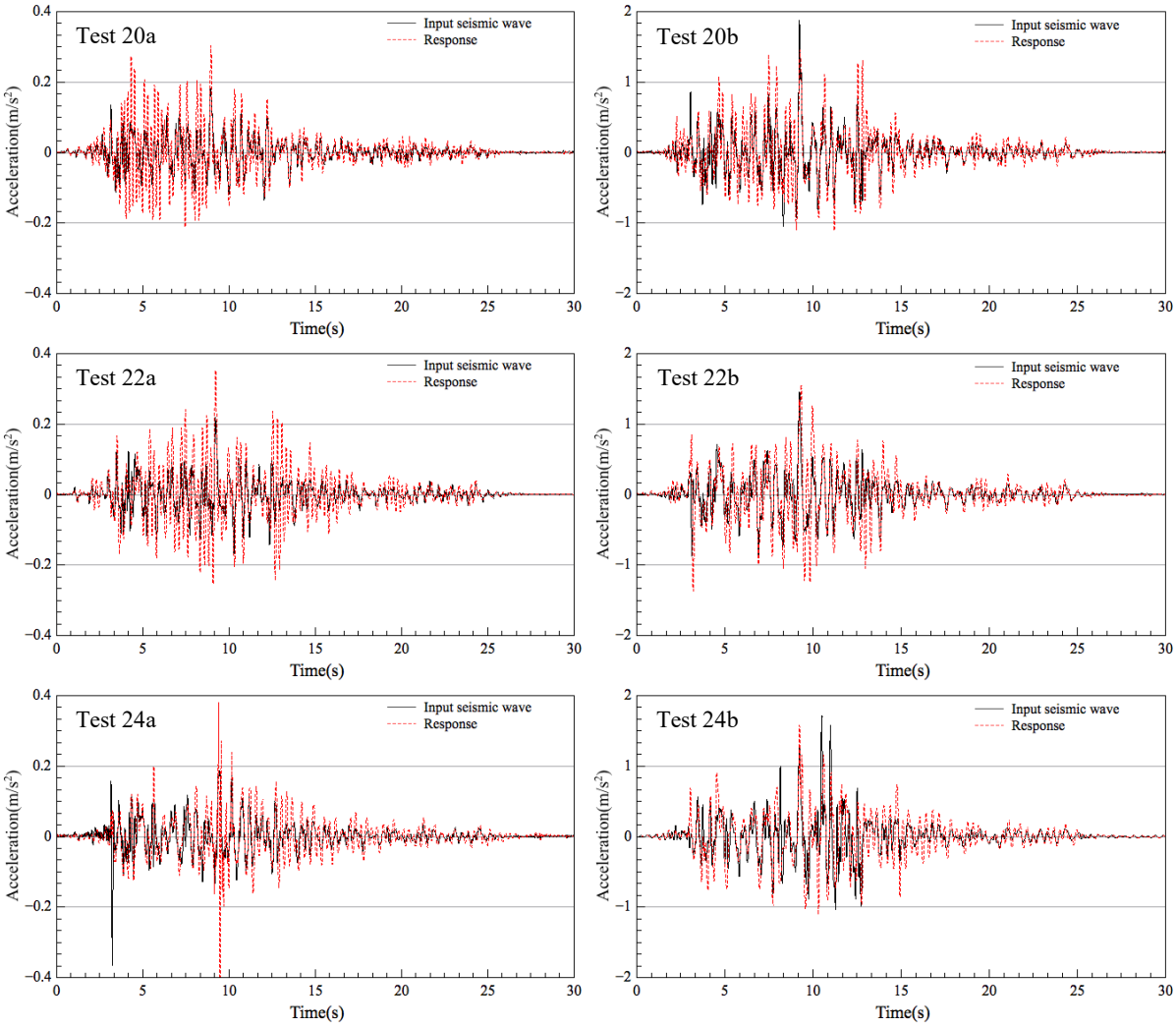

Figure 138 The results of the Dou-Gon system with 1% pre-strained super-elastic alloy bar connections subject to scaled Northridge Earthquake

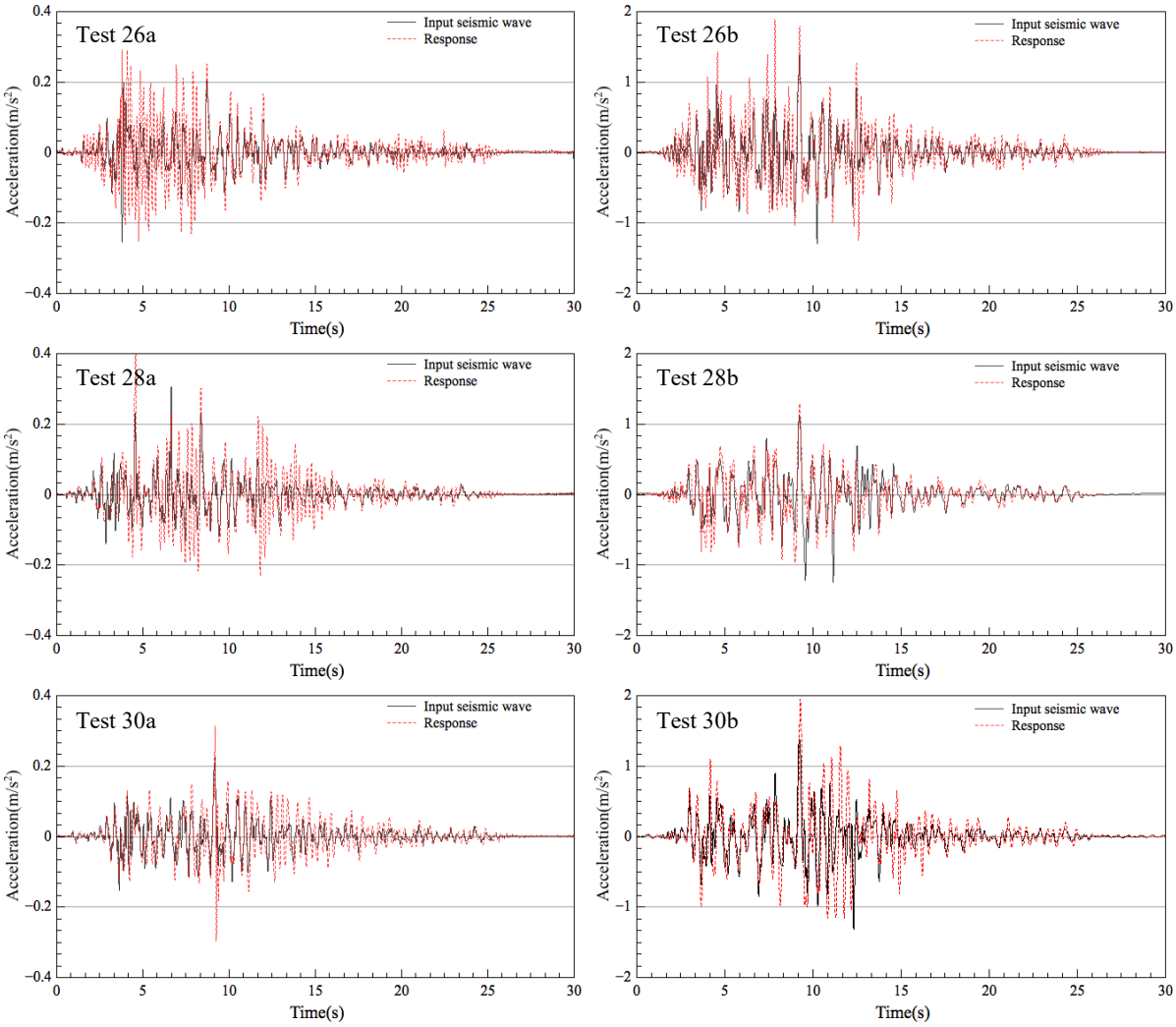

Figure 139 The results of the Dou-Gon system with 3% pre-strained super-elastic alloy bar connections subject to scaled Northridge Earthquake

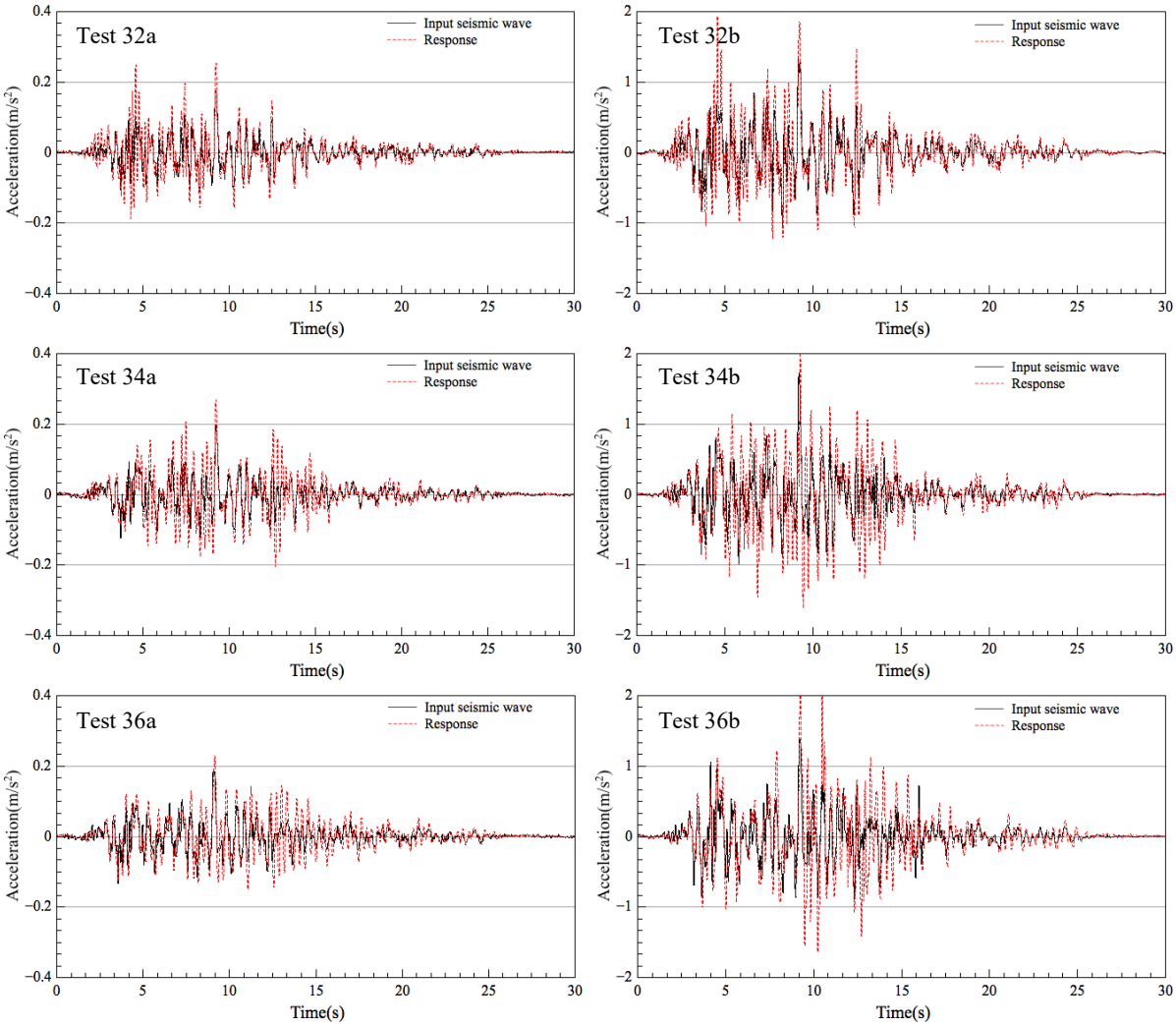

Figure 140 The results of the Dou-Gon system with super-elastic alloy bar connections in which only the base layer has been pre-strained to 3% strain level subject to scaled Northridge Earthquake

Compare to the non-prestrained conditions, the increments of maximum accelerations and RMS are less significant when the super-elastic bars were pre-strained under rare earthquakes waves and higher under frequent earthquakes waves. It might because rare earthquakes waves have bigger amplitude which induce the effect of pre-strain better. The super-elastic alloy bars were still within the elastic deformation range and the stiffness is lower with pre-strain than non-prestrained loading cases. The super-elastic alloy bars with 3% pre-strain level gave Dou-Gon less increments in the response RMS of acceleration than the 1% pre-strain level, which means that a higher pre-strain level can provide the structure better anti-seismic performances. Further evidence can be seen from the following white noise input tests.

Releasing the pre-strain of the upper layer can provide a small reduction in the response RMS of acceleration under frequent earthquakes, but is not be effective under rare earthquakes. No trend can be observed to indicate that the seismic responses of the structure are dependent on the dead loads when the pre-strained super-elastic alloy bars are used as the connection material.

Based on these results, it can be concluded that wooden peg connections in the upper layer of the Dou-Gon set can dissipate energy themselves better than the pre-strained super-elastic alloy bar connections under frequent earthquake waves. However, the conventional wood peg connections dissipate energy by the movements (rotation and deformation) between each element during the earthquakes. Consequently, great permanent deformations and damages of elements could be occurred after the shocks. The structure becomes weaker and weaker after few earthquakes and has a higher risk of damage and collapse in the future without any enhancement. However, as the wood pegs cannot connect each element tightly, it is still necessary to use super-elastic alloy bars here. The pre-strained super-elastic alloy bars become more capable when the displacements increase, such as when the structure is overcoming the rare earthquakes.

Table 20 Maximum response acceleration and RMS of Dou-Gon system with pre-strained super-elastic alloy bar connections subject to scaled Northridge Earthquake

Case no.	20a	20b	22a	22b	24a	24b
$a_{max}(m/s^2)$	0.301	1.444	0.351	1.551	0.625	1.569
Increment%	66.2%	-22.9%	60.3%	6.52%	70.9%	-8.4%
RMS(m/s^2)	0.057	0.305	0.065	0.316	0.054	0.288
Increment%	71.1%	33.4%	82.8%	46.6%	41.9%	19.8%
Case no.	26a	26b	28a	28b	30a	30b
$a_{max}(m/s^2)$	0.290	1.877	0.499	1.287	0.312	1.947
Increment%	14.3%	35.6%	63.6%	2.84%	38.7%	41.6%
RMS(m/s^2)	0.060	0.313	0.061	0.238	0.049	0.301
Increment%	68.0%	33.7%	62.2%	7.74%	28.5%	24.9%
Case no.	**32A**	**32B**	**34A**	**34B**	**36A**	**36B**
$a_{max}(m/s^2)$	0.253	1.928	0.268	2.074	0.229	2.318
Increment%	41.9%	45.4%	36.3%	20.3%	23.6%	68.9%
RMS(m/s^2)	0.044	0.338	0.051	0.378	0.048	0.385
Increment%	41.4%	40.2%	55.9%	52.1%	25.0%	55.1%

In general, the damping ratios of the Dou-Gon system with non-prestrained super-elastic alloy was between 1-5%. This increased to 2-5.5% and 2-7% when the super-elastic alloy bars were pre-strained to strain levels of 1% and 3%. The damping ratio was higher when super-elastic alloy was pre-strained to 3%. The behaviour of the damping ratios of the Dou-Gon with super-elastic alloy bar connections increased with the dead loads applied and became more significant when the pre-strain level increased, which can be seen from Figure 136(b) and Figure 141. This is unique behaviour that can only be observed in Dou-Gon systems with super-elastic alloy bar connections, but not in systems with conventional wooden pegs or high strength steel bar connections. When the Dou-Gon was under a dead load of 400kg (Figure 142(a)), there was no significant difference in the damping rations when the pre-strain level of the super alloy

elastic bars was between 1% and 3%. Figure 142(c) shows that the 3% pre-strain level gave the structure much higher damping ratios than other two conditions when the dead load increased to 1000kg. An increase in the damping ratios can be observed from the results for the Dou-Gon with both non-prestrained and pre-strained super-elastic alloy bar connections with the increase of the amplitudes and this behaviour cannot be found when either wooden pegs or high strength steel bars were used.

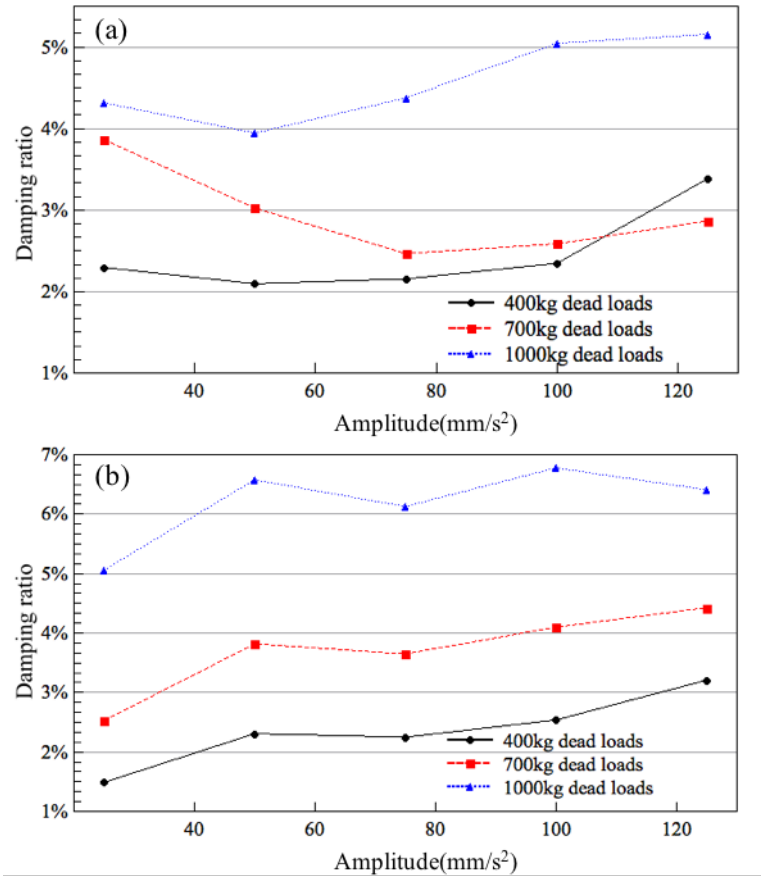

Figure 141 Damping ratios of Dou-Gon with (a)1% and (b)3% pre-strained super-elastic alloy

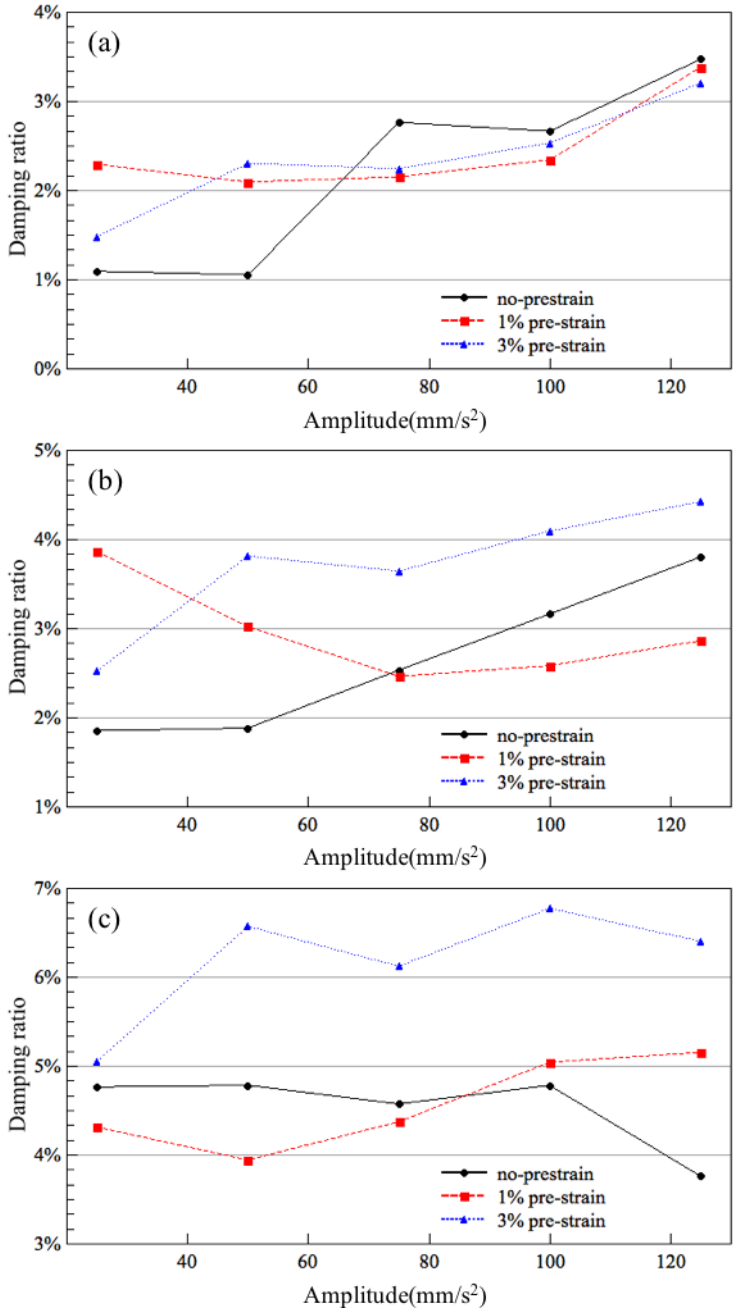

Figure 142 Damping ratios of Dou-Gon with different pre-strain level under dead loads of (a)400kg; (b)700kg and (c)1000kg

6.3 Conclusion

The seismic behaviour of a Dou-Gon is more sensitive to roof weight when a metal bar is used as the connection material than conventional wood pegs and a heavier roof will improve the stability of the structure. By assessing the response maximum acceleration and RMS, the higher pre-strain level of the super-elastic alloy bar can provide the structure a better anti-seismic performance under rare earthquake conditions. There is no significant evidence to show that the damping ratio is dependent on the dead loads when conventional wooden pegs and high strength steel bar connections were used in the Dou Gon. Nevertheless, a heavier roof can give

the structure a much higher damping ratio of 4-5% with super-elastic alloy bars, and when these bars are pre-strained to 3%, the damping ratios increase to 6-7%, which are significantly higher than those without pre-strain and those specimens using conventional wooden peg connections.

Chapter 7 Modelling and Parametric Studies

The content of Chapter 7 has been submitted for review in the journal of *Proceedings of the Institution of Civil Engineers - Civil Engineering*: 'Dynamic experimental and parametric studies of two-layer Dou-Gon system by using super-elastic alloy as a connection material'.

To understand and compare the seismic performance of using super-elastic alloy bars to replace the conventional wooden peg connections in the Dou-Gon system, it is important that a parametric study is conducted. A model has been built using Open System for Earthquake Engineering Simulation (OpenSEES) software. The Dou-Gon system has been simplified and assumed as a system with a single degree of freedom (Figure 143) which was proposed by (Gao et al., 2003b). The stiffness, k, and damping, c, are evaluated based on the static pushover tests of the Dou-Gon system.

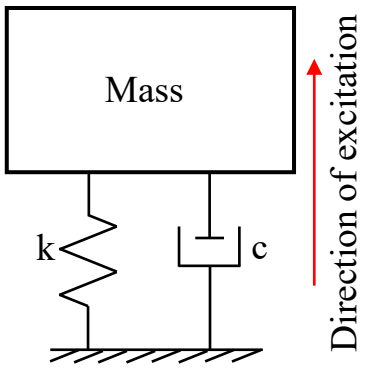

Figure 143 The single degree of freedom model

The results from the static pushover tests indicate that the high strength steel bar connections gave the Dou-Gon high ultimate strength and good energy dissipation capacity, but only in the first loading cycle and it has a high risk of fracture. Therefore, it is not suitable to use high strength steel in the structure to resist earthquakes. Super-elastic alloy bar connections have good seismic performance since they provide the structure higher ultimate strength in comparison to conventional wooden peg connections and provide a stable damping capability. Hence, only Dou-Gon sets with conventional wooden peg connections and super-elastic alloys connections have been modelled in this study.

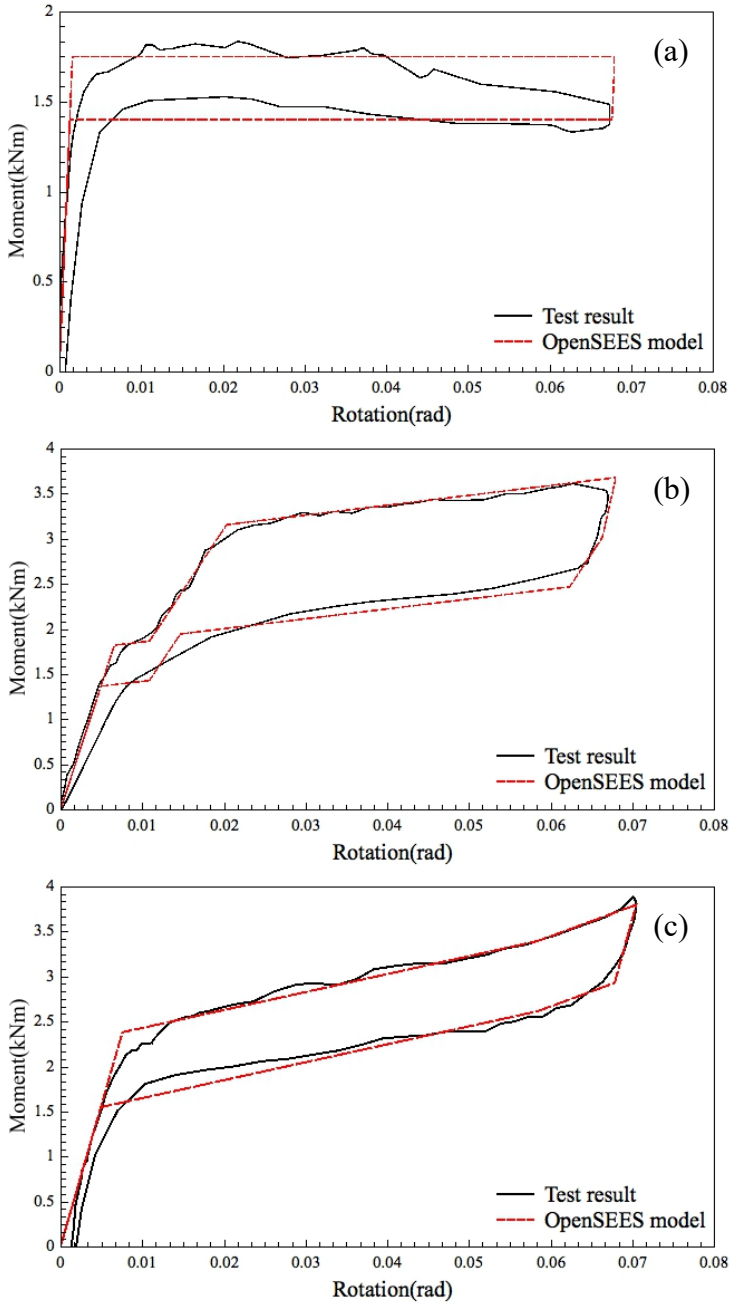

Figure 144 Comparisons of hysteresis loop between test results and OpenSEES model for Dou-Gon under 10kN dead load with connections of (a)wooden peg; (b)super-elastic alloy; (c)super-elastic alloy with 3% pre-strain

The upper layer of the Dou-Gon has been assumed as rigid body since there are four Dou, one Gong and one Ang restraining each other. The entire Dou-Gon set was simplified as a cantilever axial spring with two to four axial stiffness depending on the connections. As shown in Figure 144(a), the model of the Dou-Gon with conventional wooden peg connections has two stiffnesses. The Dou-Gon model with super-elastic alloy connections with and without pre-strain has three and four stiffnesses, respectively (Figure 144(b&c)). The flexural stiffness has been set as infinite to combine with the axial behaviour into one section, which means there

is no P-M interaction. The rotation of the Dou-Gon in the experiment has been transferred to axial extension in this model. The equivalent damping ratio of both the experiment and model are listed in Table 21, where they both have an error within 3%.

Table 21 Comparison of equivalent damping ratio between experiment and OpenSEES model

	Wooden peg	Super-elastic alloy	Super-elastic alloy with 3% pre-strain
Experiment	6.19%	7.99%	6.75%
OpenSEES model	6.22%	7.76%	6.84%

The acceleration responses for both experiment and model are illustrated in Figure 145. The Dou-Gon model with super-elastic alloy bar connections corresponds better with the experimental results than with conventional wooden peg connections. This is possibly due to the large number of small movements between each element when using conventional wooden pegs, as the connection material and these movements cannot be simulated by the single degree of freedom model.

The experiments have shown that the Dou-Gon with super-elastic alloy bar connections produced higher maximum acceleration but lower RMS than the system with wooden peg connections. The OpenSEES modelling shows a similar trend but the super-elastic alloy with 3% pre-strain has the lowest a_{max}. The peak response frequency of the Dou-Gon with wooden peg connections and super-elastic alloy bar connections without pre-strain are 1.55Hz and 1.53Hz, respectively, which are very close. The Dou-Gon with super-elastic alloy bar connections with 3% pre-strain has a peak response frequency of 2.20Hz, which is higher than the other two. This demonstrates that pre-straining the super-elastic alloy bar will increase the stiffness of the structure. This can also be seen from the OpenSEES modelling results.

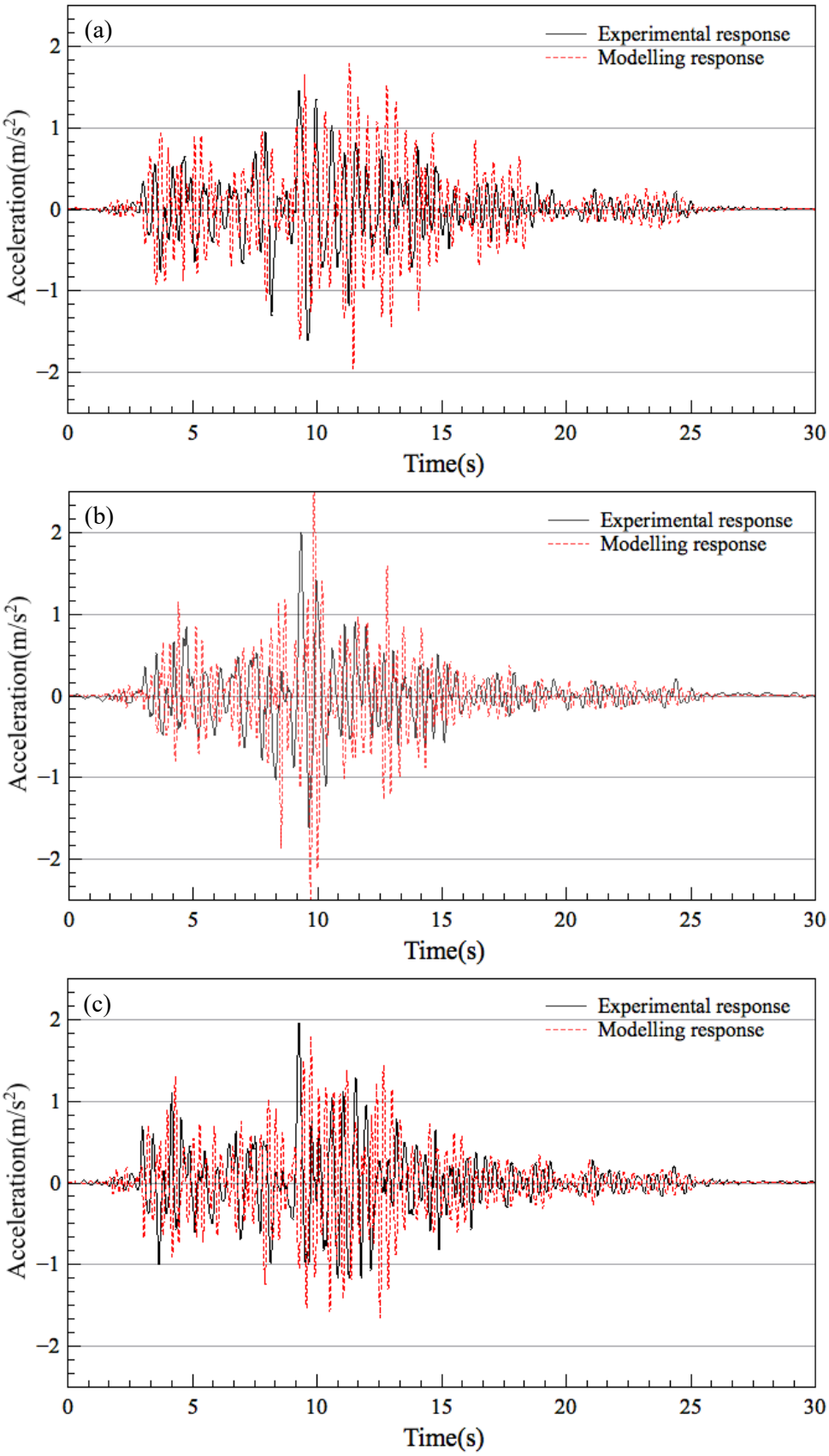

Figure 145 OpenSEES results of Dou-Gon with (a)wooden peg; (b)super-elastic alloy bar; (c)3% pre-strained super-elastic alloy bar connections under 10kN dead loads

Table 22 Comparison between the experimental results and OpenSEES modelling results

Case no.		a_{max} (m/s^2)	RMS (m/s^2)	Peak response frequency (Hz)
6b	Experiments	1.618	0.312	1.55
	Modelling	1.959	0.418	1.73
18b	Experiments	2.004	0.309	1.53
	Modelling	2.809	0.380	1.75
30b	Experiments	1.947	0.301	2.20
	Modelling	1.775	0.388	2.35

The parametric study was conducted with a OpenSEES model with three inputted full-scale seismic waves, namely the Northridge earthquake, Kobe earthquake and ElCentro earthquake. The acceleration responses are illustrated in Figure 146-Figure 148. The acceleration response has a smoother shape when using super-elastic alloy bar than wooden peg connections and a 3% pre-strain can provide an even more stable response shape. This behaviour is also because the use of super-elastic alloy bar connections with pre-strain can reduce the small movements between each element, which are significant when using wooden peg connections. The three graphs also show that when the excitation ended, the amplitude of the acceleration reduces marginally quicker when using super-elastic alloy bars with 3% pre-strain in comparison to the other two connections, which means that the super-elastic alloy bar connections with 3% pre-strain could improve the damping in the structure.

No significant difference in RMS can be observed between each connection material under any full-scale seismic wave. The peak response frequency increases when super-elastic alloy bars are used to substitute the conventional wooden pegs and increase when pre-strain is applied to the super-elastic alloy bars.

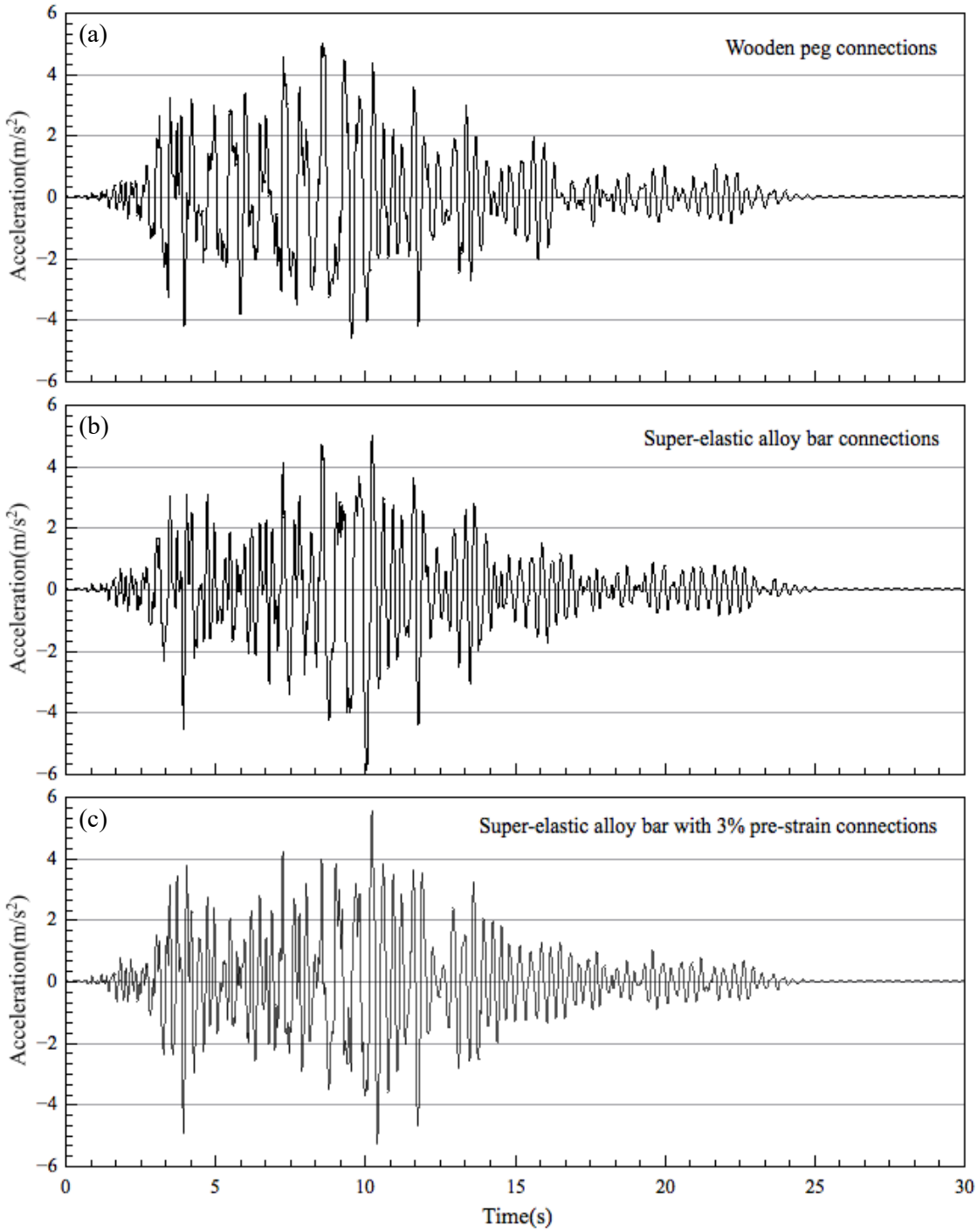

Figure 146 OpenSEES modelling results with full scale Northridge earthquake

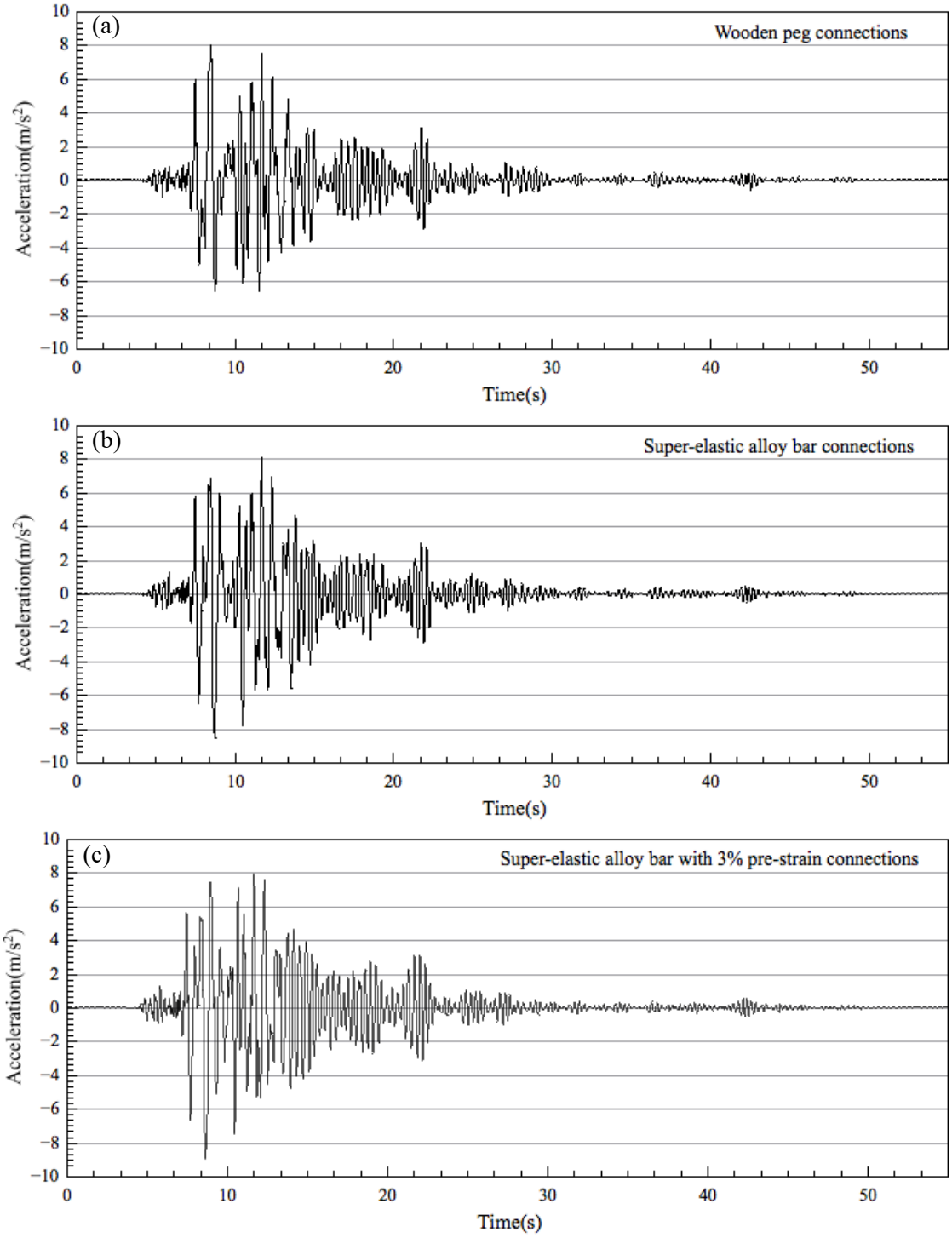

Figure 147 OpenSEES modelling results with full scale Kobe earthquake

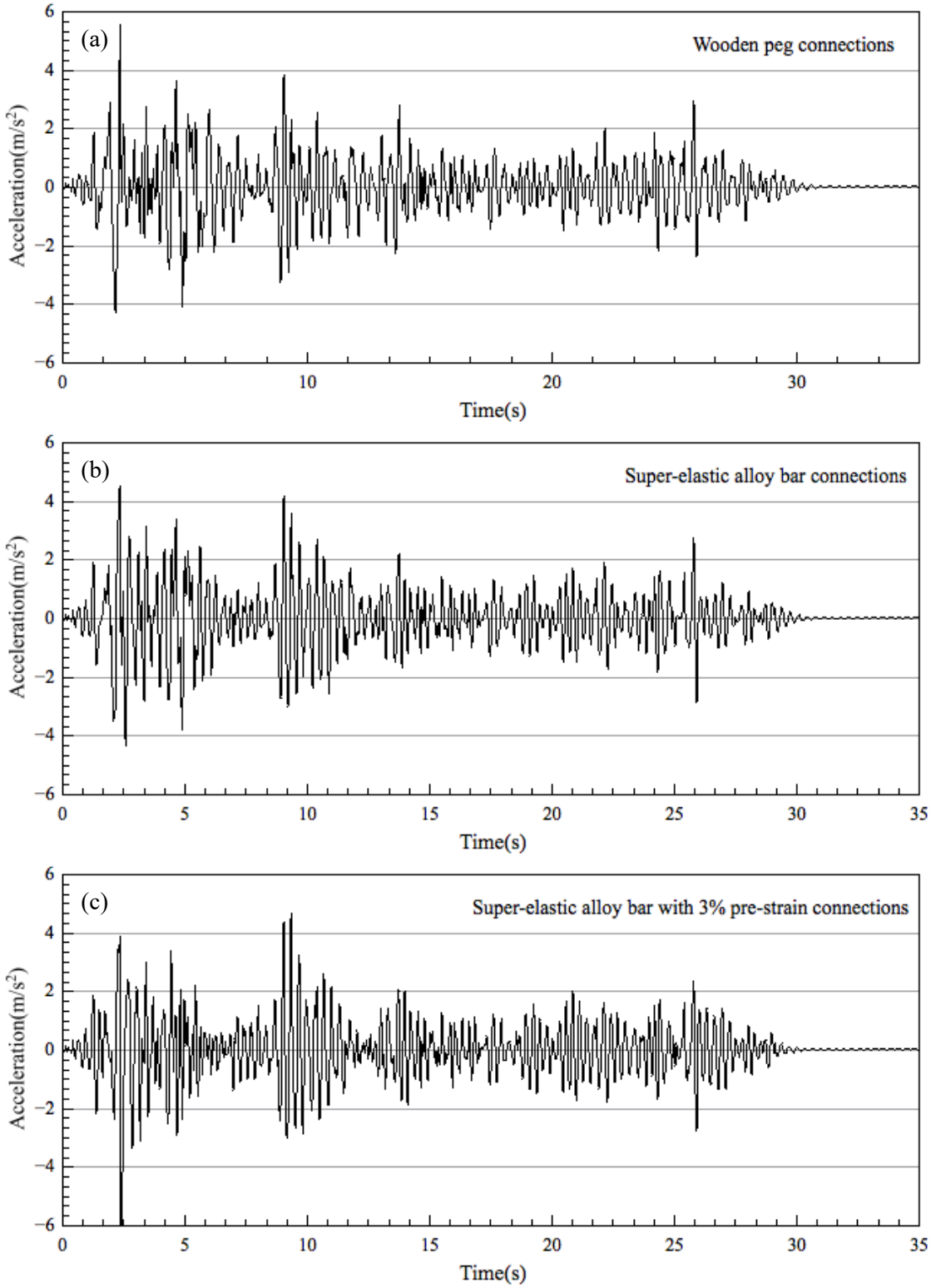

Figure 148 OpenSEES modelling results with full scale ElCentro earthquake

Table 23 Peak response frequency of OpenSEES model under three full scaled earthquake excitations

Connection materials	Northridge earthquake	El centro earthquake	Kobe earthquake
Wooden Peg	1.63Hz	2.52Hz	1.02Hz
Super-elastic alloy bar	2.3Hz	2.9Hz	1.22Hz

Super-elastic alloy bar with 3% pre-strain	2.7Hz	3Hz	1.45Hz

Table 24 RMS of OpenSEES model under three full scaled earthquake excitations

Connection materials	Northridge earthquake	El centro earthquake	Kobe earthquake
Wooden Peg	1.55m/s^2	0.864m/s^2	1.51m/s^2
Super-elastic alloy bar	1.48m/s^2	0.896m/s^2	1.67m/s^2
Super-elastic alloy bar with 3% pre-strain	1.47m/s^2	0.897m/s^2	1.75m/s^2

Chapter 8 Conclusion and Future Work

8.1 Conclusion

The Dou-Gon system is the primary structural element of historic timber buildings in Asia; it is located on top of a column and transfer the upper loads to the column. Building with the Dou-Gon system perform well under seismic loads, since they can dissipate significant amount of energy due to the sliding between wood elements and the yielding of wood elements in compression perpendicular to the grain. They also have a good re-centring capability: the heavy roof provides the Dou-Gon with a re-centering force. However, such buildings have still been severely damaged by earthquakes, and therefore require enhancement of their seismic performance. In this research, a technique has been developed to enhance the seismic performance of Dou-Gon systems by using super-elastic alloy and high strength steel bars to substitute the conventional wood peg connection of Dou and lower structure. The Dou-Gon specimen used in this research is duplicated from Qinghui Hall at Weiyuan Temple in Henan Province, China.

To use super-elastic alloy in seismic resistant structures, the material hysteresis behaviours under cyclic tension needed to be investigated. Therefore, non-prestrained and pre-strained 9mm diameter Cu-Al-Mn super-elastic alloy bars were tested under cyclic tension for 1000 cycles at frequencies of 1Hz to 8Hz. The non-prestrained tensile tests were performed with 2% and 4% strain amplitudes. In the pre-strained tests, the materials have been pre-strained to 2% and 4% strain level, performing cycles of ±1% and ±2% strain amplitudes respectively.

- The quasi-static test with 0.00417Hz loading frequency shows that the material starts to transfer from elastic to pseudoelastic deformation at around 1.2% strain level. The residual strain for the quasi-static test is negligible.
- All cyclic tensile tests have indicated that the secant stiffness increases with the loading cycles due to the martensitic hardening of the material and the increase of the residual strain. Bigger residual strain could be observed for both higher loading frequency and larger strain amplitude and this will result in the compressive deformation during the tests.
- The cyclic results demonstrate that the equivalent damping ratio increases with the increase of the loading frequency if the material does not transfer to martensite completely or there is enough time for most of the latent heat to release. However, when

the self-heating temperature becomes the primary governing factor, the equivalent damping ratios slightly reduces with the increase of the loading frequency.

- Pre-straining of the super-elastic alloy showed a better damping effect compare to the non-prestrained super-elastic alloy. The equivalent damping ratio of non-prestrained super-elastic alloy remains constant for the first 1000 loading cycles. In contrast, the equivalent damping ratio of pre-strained super-elastic alloy suddenly decreases after 100 loading cycles because of the rapid increase of the self-heating temperature, while the equivalent damping ratio of pre-strained super-elastic alloy after 1000 cycles still shows values similar to the ones of the non-prestrained super-elastic alloy.

Pushover tests have been performed on two types of upper-layer Dou (Dou A and Dou B) and the base Dou with three different connectors (wood peg, high strength steel bars and super-elastic alloy) under 4kN, 7kN and 10kN vertical loads.

- For Dou A and Dou B, both high strength steel bar and super-elastic alloy bar connections increase the strength of the structure significantly. The high strength steel bar connections dissipate a large amount of energy and has over 35% equivalent damping ratios in the first loading cycle. After that, because of the permanent deformations of the high strength steel bar, the strength of the structure suddenly reduce to a value that is even lower than the one from the conventional wood peg connection. The Dou with super-elastic alloy bar connections have lower ultimate strength and stiffness than the high strength steel bar connection in the first loading cycle. However, the hysteresis loops of Dou with super-elastic alloy bar connections have insignificant changes in the first 5 loading cycles. The element Dou with super-elastic alloy bar connection in the first loading cycle can achieve an equivalent damping ratio over 15% and always stay above 12% in the first 5 loading cycles. Thus, the equivalent damping ratios of Dou with super-elastic alloy bar connections remain constant and can provide a stable energy dissipation capacity during seismic activities. The Dou have good re-centring capability when connected with both high strength steel bar and super-elastic alloy bar connections.
- Pre-straining of the super-elastic alloy bar connection can give to the structure a higher initial stiffness than the non-prestrained super-elastic alloy bar connection, which can dissipate more energy under small rotations. The ultimate strength increases when the super-elastic alloy bar is pre-strained to 3% and 5% strain level. In general, the pre-

strain of super-elastic alloy bar can give a relative higher equivalent damping ratio of Dou A and Dou B.

- The lateral load that applies on the base Dou system with conventional wood peg connection is mainly overcoming the vertical loads, so the ultimate strength of the base Dou system increases with the weight of the roof. The high strength steel bar connection has a much higher ultimate strength than other types of connections, but only in the first loading cycle. For the second and third loading cycles, the equivalent damping ratio has a dramatic reduction. A consistent damping performance can be achieved by using the SEA bar connector. The pre-strain of the SEA bar gives a higher equivalent damping ratio to the base Dou system. The equivalent damping ratio increases with the pre-strain level of the SEA bar. When the SEA bar has been pre-strained to 5% strain level, the equivalent damping ratio reached a maximum of 8%. The SEA bar has a fatigue life longer than the high strength steel bar. In general, the energy dissipation capacity and ultimate strength of base Dou system have been increased by this simple technique. The SEA bar is more suitable for being used in the seismic application since the constant damping behaviour can resist both the main shock and aftershocks of the earthquake.
- The digital image correlation (DIC) results showed that the base Dou with a conventional wood peg connection has experienced a maximum of 3.5% compressive strain and 1.5% tensile strain when the bracket complex has a rotation of 6.77% radians. No tensile strain has been detected in the base Dou when using a high strength steel bar or super-elastic alloy bar connection. The base Dou could be assumed as a rigid body when it is connected by a pre-strained super-elastic bar since it still has elastic deformation.

The Dou-Gon system that has been studied in this research is a two-layers Dou-Gon. The static push over test and dynamic test have been performed on to the two-layers structure. A dynamic test has been performed by inputting Northridge seismic waves. The seismic wave has been scaled down to present frequent and rare earthquakes. Conventional wooden peg, high strength steel, super-elastic alloy and pre-strained super-elastic alloy has been used for the connection in both the static and dynamic tests. Three different dead loads of 4kN, 7kN and 10kN have been applied to the top of the structure. The following conclusions have been derived from the tests:

- The ultimate strength increased rapidly with the increase in the weight applied on top of the structure when using conventional wooden peg connections; the wooden peg was

pulled out from the hole without any damage and the lateral load was most overcoming the weight on top. The P-Delta effect showed higher impact for increasing weight and results in a lower stiffness of Dou-Gon set.

- Both high strength steel and super-elastic alloy give to the Dou-Gon system a much higher ultimate stiffness than the conventional wooden peg connections. The high strength steel bar connections provided the Dou-Gon system with a highest equivalent damping ratio and stiffness in the first loading cycle. In the second and third loading cycles, the structure experienced a nearly zero stiffness stage before reaching the ultimate strength due to the permanent deformation of the steel bar. Furthermore, the high strength steel bar has a higher risk of fracture during repeated loading cycles.
- Four stages of stiffness have been noticed in the non-prestrained loading cases of Dou-Gon system with super-elastic alloy bar connections. The first two stiffness are regarded as the stiffness of the Dou-Gon system itself and super-elastic alloy provide the latter two stiffness. The first two stiffness disappeared when pre-strain applied on the super-elastic alloy bars. The super-elastic alloy with 3% pre-strain showed hysteresis loops with greater area than non-prestrained loading cases which means it can dissipate more energy. The higher pre-strain level can provide the Dou-Gon structure a higher equivalent damping ratio.
- The seismic behaviour of Dou-Gon is more sensitive to the roof weight when using metal bar as the connection material than conventional wooden peg connections. A heavier roof provides more stability to the structure. It seems reasonable to assume that using metal bars to replace the wooden pegs can provide the structure with a better anti-seismic performance because of the roof is heavier in the real structures than the experiments. Higher pre-strain level of super-elastic alloy bar can give the structure a better anti-seismic performance under rare earthquakes when access by the maximum acceleration and RMS. Releasing the pre-strain of super-elastic alloy bar in the upper layer Dou gives small reductions in maximum acceleration and RMS under frequent earthquake but it is not effective under rare earthquake. The damping ratio is not affected by the dead loads when Dou-Gon with conventional wooden peg connections are adopted. For Dou-Gon with high strength steel bars, the damping ratios are in the range of 2-4%; these values are independent from the dead loads and amplitudes. Heavier roofs lead to higher damping ratio of 4-5% if super-elastic alloy bars are used, and when these bars are pre-strained to 3% strain level, the damping ratios increase to

6-7%. These values are significant higher for the case without pre-strain and the specimens with conventional wood peg. For Dou-Gon with super-elastic alloy bar connections, dead loads dominate the structure's damping ratios and a trend of increasing damping ratios can be observed with the increase of moving amplitudes. This effect cannot be observed when used conventional wooden pegs or high strength steel bars.

Analytical models have been built using the software Open System for Earthquake Engineering Simulation (OpenSEES). The parametric study has been carried out and the output acceleration spectrums have been recorded by inputting three full scaled seismic waves (Northridge earthquake, Kobe earthquake, ElCentro earthquake). The results of the parametric study showed that super-elastic alloy with 3% pre-strain could provide a better structural performance due to the faster vibration decay speed. No significant difference in RMS can be observed under the three different connection conditions. However, the peak response frequency increases when using super-elastic alloy bars instead of wooden pegs and increases when applying the pre-strain on them, due to the increased stiffness of the structure.

From the results of static push over, dynamic tests and parametric study, it appears that using super-elastic alloy bar to substitute conventional wooden peg connections provides the Dou-Gon system with a higher stiffness and ultimate strength. Pre-strain of super-elastic alloy bars can also increase the damping ratios and lead to a greater energy dissipation, not only during the main earthquake shock but also for several aftershocks.

As mentioned in Chapter 1.1.3, there are three main reinforce methods of the traditional timber structures. The technique proposed in this research is not suitable for the structures without significant damage after the earthquake or enhance the structure who has not experience any earthquake yet. Because the super-elastic alloy bar need to be embedded into the structure and such structures do not need to move any components apart. This technique is made for those structures who need reinforcement by taking every component apart. It can be also used for a single column by temporary supporting the upper structure and remove the column to put the super-elastic alloy bar in. The super-elastic alloy bar can also be used in the new build traditional timber structures since it will not change the exterior of the structure.

8.2 Future works

The outcome of this research has been the development of a new connection technique which can enhance the seismic performance of the Dou-Gon system. The Dou-Gon system used in this work reproduces the system used in ancient structures from Henan Province in China. There are many more different types and combinations of Dou-Gon system in Asia. In the future, it is recommended for the proposed connection technique to be tested on other Dou-Gon systems.

Due to the limitations of the dynamic actuator used in the Structural Laboratory at the University of Bath, the input excitations have been scaled down. In the future, shaking table tests with full scaled seismic waves and higher amplitude excitations input are also recommended. Greater dead loads can be applied to the structure to evaluate potential variations in the seismic performance with the variation of the roof weights. Shaking table tests of full scaled portal frames with Dou-Gon systems and super-elastic alloy bar connection should also be performed to evaluate the response of the entire building and the global failure mechanism of the structure after strengthening of Dou-Gon systems. The other important connection of traditional timber structure is column footing joint (Qin et al., 2018). Appling the super-elastic alloy bar to the column footing joint could also take consideration into the full scaled portal frame shaking table test.

The analytical models of a two-layers Dou-Gon system have been developed in this research based on the push over test results, and applied to a parametric study. Further parametric studies should focus on the behaviours of Dou-Gon system with super-elastic alloy bar connections with the entire building, e.g. single portal frame, multi-storey portal frames, portal frames connected by purlins and multi-bay portal frames. Such parametric studies can evaluate which connections govern the building response, guiding the selection of connections to enhance.

Reference

Andrawes, B. and DesRoches, R., 2007. Effect of ambient temperature on the hinge opening in bridges with shape memory alloy seismic restrainers. *Engineering structures*, *29*(9), pp.2294-2301.

Araki, Y., Endo, T., Omori, T., Sutou, Y., Koetaka, Y., Kainuma, R. and Ishida, K., 2011. Potential of superelastic Cu–Al–Mn alloy bars for seismic applications. *Earthquake Engineering & Structural Dynamics*, *40*(1), pp.107-115.

Araki, Y., Maekawa, N., Omori, T., Sutou, Y., Kainuma, R. & Ishida, K., 2012, Rate-dependent response of superelastic Cu-Al-Mn alloy rods to tensile cyclic loads, *Smart Materials and Structures*, Vol. 21, No. 3

Araya, R., Marivil, M., Mir, C., Moroni, O. and Sepúlveda, A., 2008. Temperature and grain size effects on the behavior of CuAlBe SMA wires under cyclic loading. *Materials Science and Engineering: A*, *496*(1-2), pp.209-213.

BS EN ISO 204, Metallic materials-Uniaxial creep testing in tension-Method of test, *British Standard Institution*, June 2009

BS EN ISO 6892-1, Metallic materials-Tensile testing-Part 1: Method of test at room temperature, *British Standard Institution*, August 2009

Chang, B.C., Shaw, J.A. and Iadicola, M.A., 2006. Thermodynamics of shape memory alloy wire: modeling, experiments, and application. *Continuum Mechanics and Thermodynamics*, *18*(1-2), pp.83-118.

Chang, W.S., 2005. On rotational performance of traditional Chuan-Dou timber joints in Taiwan. *Ph. D. dissertation, National Cheng Kung University*.

Chang, W.S., Hsu, M.F. and Chen, C.J., 2004. Estimating rotational stiffness of timber joints by using fractional factorial experiments combined with computer simulation. In *8th World Conference on Timber Engineering, Lathi, Finland*.

Chang, W.S. and Hsu, M.F., 2005. Mechanical characteristics of traditional Go-Dou and stepped dovetail timber connections in Taiwan. *Taiwan Journal of Forest Science*, *20*(1), pp.61-71.

Chang, W.S., Hsu, M.F. and Komatsu, K., 2006. Rotational performance of traditional Nuki joints with gap I: theory and verification. *Journal of wood science*, *52*(1), pp.58-62.

Chang, W.S. and Hsu, M.F., 2007. Rotational performance of traditional Nuki joints with gap II: the behavior of butted Nuki joint and its comparison with continuous Nuki joint. *Journal of Wood Science*, *53*(5), pp.401-407.

Chang, W.S. and Araki, Y., 2016. Use of shape-memory alloys in construction: a critical review. In *Proceedings of the Institution of Civil Engineers-Civil Engineering* (Vol. 169, No. 2, pp. 87-95). ICE Publishing.

Che, A.-L., He, Y., Ge, X.-R., Iwatate, T. & Oda, Y., 2006, Study on the dynamic structural characteristics of an ancient timber — yingxian wooden pagoda, *Soil and Rock Behavior and Modeling*, pp. 390-398

Chen, S.-Y., 2003, Structure of ancient Chinese architects. August 23rd 2003, http://www.china001.com/show_hdr.php?xname=PPDDMV0&dname=KLDNB41&xpos=9, Accessed: 7th May 2014. (in simplified Chinese)

Chinese Academy of Culture Heritage, 2014, accessed 1 February 2019, http://www.cach.org.cn/tabid/76/InfoID/1629/frtid/78/Default.aspx. (in simplified Chinese)

Chinese Academy of Culture Heritage, 2013, accessed 1 February 2019, http://www.cach.org.cn/tabid/80/ctl/InfoDetail/InfoID/1505/mid/385/Default.aspx?ContainerSrc=%5bG%5dContainers%2f_default%2fNo+Container. (in simplified Chinese)

Choi, E., Nam, T.-H. & Chung, Y.-S., 2010, Variation of mechanical properties of shape memory alloy bars in tension under cyclic loadings, *Materials Science and Engineering A*, Vol. 527, pp. 4412-4417

D'Ayala, D.F. & Tsai, P.-H., 2008, Seismic vulnerability of historic Dieh-Dou timber structures in Taiwan, *Engineering Structures*, Vol. 30(8), pp 2101-2113

DesRoches, R. and B. Smith, 2004, Shape memory alloys in seismic resistant design and retrofit: a critical review of their potential and limitations. *Journal of Earthquake Engineering*, Vol. 8, Issue 3, pp. 415-429.

DesRoches, R., McCormick, J. & Delemont, M., 2004, Cyclic properties of superelastic shape memory alloy wires and bars, *Journal of Structural Engineering*, Vol. 130, No. 1, pp. 38-46

Dolce, M., Cardone, D. & Marnetto, R., 2000, Implementation and testing of passive control devices based on shape memory alloys, *Earthquake Engineering and Structural Dynamics*, Vol. 29, pp. 945-968

Dolce, M. & Cardone, D., 2001, Mechanical behaviour of shape memory alloys for seismic applications 2. Austenite NiTi wires subjected to tension, *International Journal of Mechanical Sciences*, Vol. 43, pp. 2657-2677

Dolce, M., Cardone, D. & Marnetto, R., 2001, SMA re-centering devices for seismic isolation of civil structures, *Smart Structures and Materials*, Vol. 4330, pp. 238-249

Dusicka, P., Itani, A.M. & Buckle, I.G., 2007, Cyclic response of plate steels under large inelastic strain, *Journal of Constructional Steel Research*, Vol. 63, pp. 156-164

Fang, D.-P., Iwasaki, S., Yu, M.-H., Shen, Q.-P., Miyamoto, Y.& Hikosaka, H., 2001a, Ancient Chinese timber architecture. I: Experimental study, *Journal of Structural Engineering*, November, pp 1348-1357

Fang, D.-P., Iwasaki, S., Yu, M.-H., Shen, Q.-P., Miyamoto, Y.& Hikosaka, H., 2001b, Ancient Chinese timber architecture. II: Dynamic charactetistics, *Journal of Structural Engineering*, November, pp 1358-1364

Feilden, B.M., 1982, *"Conservation of historic buildings"*, Architectural Press, UK

Fujita, K., Kimura, M., Ohashi, Y. and Sakamoto, I., 1999, Shaking table test of 'Kumimono' used in traditional wooden architecture part 5 static lateral loading test of DEGUMI bracket complex, *Summaries of technical papers of Architectural Institute of Japan annual meeting*, Sep 1999, Tokyo, Japan, pp. 159-160 (In Japanese).

Fujita, K., Sakamoto, I., Ohashi, Y. & Kimura, M., 2000, Static and dynamic loading tests of bracket complexes used in traditional timber structures in Japan, *12th World Conference on Earthquake Engineering*, 30th Jan-4th Feb 2000, New Zeland

Fujita, K., Sakamoto, I., Ohashi, Y. & Kimura, M., 2001, Hysteresis model and stiffness evaluation of bracket complexes used in traditional timber structures based on static lateral loading tests, *Journal of Structural Construction Engineering, Vol. 66, Issue 543, pp. 121-127 (In Japanese).*

Fujita, K., Hanazato, T., Sakamoto, I., 2004, Earthquake response monitoring and seismic performance of five-storied timber pagoda, *13th World Conference on Earthquake Engineering*, 1st-6th Aug 2004, Canada

Fujita, K., Kawai, N., Minowa, C., Koshihara, M. & Chiba, K., 2006, Shaking table test and earthquake response monitoring of traditional Japanese timber pagoda, *9th World Conference on Timber Engineering*, 6th-10th Aug 2006, USA

Fujita, K., Chiba, K., Kawai, N., Kshihara, M., Minowa, C. and Hanazato, T., 2008. Earthquake response analysis of traditional Japanese timber pagoda. In *10th World Conference on Timber Engineering, CDR*.

Gao, D.F., Zhao, H.T., Xue, J.Y. and Zhang, P.C., 2003a. Experimental study on seismic behavior and strengthened effects of Chinese ancient timber structure. *World Information on Earthquake Engineering*, *19*(2), pp.1-10.

Gao, D.-F., Zhao, H.-T., Xue, J.-Y. and Zhang, P.-C., 2003b, Experimental study on structural behaviour of Dougong under the vertical action in Chinese ancient timber structure. *World Information on Earthquake Engineering*, Vol, 19(3), pp. 56–61. (in simplified Chinese)

Gao, T., 2011, Renovation of the Main Hall of Nanchan Temple and the Development of Historical Preservation since the Initial Period of Establishment of China, *Traditional Chinese Architecture and Gardens*, ISSN：1000-7237, Vol. 2, pp. 15-19. (in simplified Chinese)

Gencturk, B., Araki, Y., Kusama, T., Omori, T., Kainuma, R. & Medina, F., 2014, Loading rate and temperature dependency of superelastic Cu-Al-Mn alloys, *Construction and Building Materials*, Vol. 53, pp. 555-560

Guo, Q.-H., 1999, *"The structure of Chinese timber architecture"*, Minerva Press, UK

Han, Y.-L., Li, Q.S., Li, A.-Q., Leung, A.Y.T. & Lin, P.-H., 2003, Structural vibration control by shape memory alloy damper, *Earthquake Engineering and Structural Dynamics*, Vol. 32, pp. 483-494

Hayashi, T., 1998. 'Restoring properties of Japanese traditional wooden frame. *In Proc., World Conf. on Timber Engrg*, pp. 750-751.

Hwang, J.K., Hong, S.G., Kim, N.H., Lee, Y.W., Jeong, S.J. and Joo, S.J., 2008. The effect of friction joint and Gongpo (bracket set) as an energy dissipation in Korean traditional wooden

structure. In *Proceedings of the sixth International Conference on Structural Analysis of Historic Construction*, pp. 861-866.

Huang, H., 2017. *A Temperature Controlled Semi-active Tuned Mass Damper using Shape Memory Alloy for Vibration Reduction Applications* (Doctoral dissertation, University of Bath).

Indirli, M., Castellano, M.G., Clemente, P. & Martelli, A., 2001, Demo application of shape memory alloy devices: the rehabilitation of S. Georgio Church Bell Tower, *Smart Structures and Materials*, Vol. 4330, pp. 262-272

Janke, L., Czaderski, C., Motavalli, M. & Ruth, J., 2005, Applications of shape memory alloys in civil engineering structures-Overview, limits and new ideas, *Materials and Structures*, Vol. 38, pp. 578-592

King, W.S., Yen, J.R. and Yen, Y.A., 1996. Joint characteristics of traditional Chinese wooden frames. *Engineering Structures*, 18(8), pp.635-644.

Kitamor, A., Jung, K., Hassel, I., Chang, W., Komatsu, K. and Suzuki, Y., 2010, June. Mechanical analysis of lateral loading behavior on Japanese traditional frame structure depending on the vertical load. In *11th World Conference on Timber Engineering, Riva del Garda*.

Kusunoki, T., Nagase, T., Kibayashi, M., Hayashi, Y. and Ueda, T., 2005. Experimental study on the structural behaviour of traditional architectural component "masugumi". *Japan Structural Construction Engineering*, *70*(592), pp.129-136. (In Japanese)

Kyuke, H., Kusunoki, T., Yamamoto, M., Minewaki, S. and Kibayashi, M., 2007, Shaking table tests of 'MASUGUMI' used in traditional wooden architectures. *AIJ Journal of Technology and Design* 13 (26):535–38.

Lam, F., He, M.-J. & Yao, Ch.-Ch., 2008, Example of traditional tall timber buildings in China-the Yingxian Pagoda. *Structural Engineering International*, February, pp 126-129

Li, J., 1103, *"Yingzao Fashi"*, Royal Press, Kaifeng, China, (in ancient Chinese)

Li, T.-Y., Wei, J.-W., Zhang, S.-Y. and Li, S.-W., 2004, Double-parameter seismic damage criterion on wooden structure and seismic response appraisement on Yingxian wooden tower. *Journal of Building Structures*, Vol. 25(2), pp. 91-98. (in simplified Chinese)

Li, T.-Y., Wei, J.-W., Zhang, S.-Y. and Li, S.-W., 2005, Appraisal on the structure of the Yingxian Wooden Tower. *China Civil Engineering Journal*, Vol. 38(2), pp. 51-58. (in simplified Chinese)

Li, Z., Que, Y., Zhang, X., Teng, Q., Hou, T., Liu, Y., Wang, X., Que, Z. and Komatsu, K., 2018. Shaking Table Tests of Dou-gong Brackets on Chinese Traditional Wooden Structure: A Case Study of Tianwang Hall, Luzhi, and Ming Dynasty. *BioResources*, 13(4), pp.9079-9091.

Li, Z.-Y., 2010, The characteristic analysis of Kaiyuan Temple in Chaozhou, *Sichuan Building Science*, 1008-1933 (in simplified Chinese)

Liang, S.-C., 1984, *A Pictorial History of Chinese Architecture: A Study of the Development of Its Structural System and the Evolution of Its Type.* MIT Press.

Liu, Y., Xie, Z.-L., Humbeeck, J.V. & Delaey, L., 1998, Asymmetry of stress-strain curves under tension and compression for NiTi shape memory alloys. *Acta Materialia*, Vol. 46, No. 12, pp. 4325-4338

Liu, Y., Xie, Z.-L. & Humbeeck, J.V., 1999, Cyclic deformation of NiTi shape memory alloys. *Materials Science and Engineering*, Vol. 273-275, December, pp. 673-678

Lv, Y.-Q., 2017, Investigation and Analysis on the Present Situation of the Conservation of Historic Buildings - Take Shanxi for Example. *Chinese and Overseas Architecture*, ISSN：1008-0422, Vol. 06, pp. 53-55. (in simplified Chinese)

Maeno, M., Suzuki, Y., Ohshita, T. & Kitahara, A., 2004, Seismic response characteristics of traditional wooden frame by full-scale dynamic and static tests, *13th World Conference on Earthquake Engineering,* 1st-6th Aug 2004, Canada

McCullough, K.Y.G., Fleck, N.A. & Ashby, M.F., 1999, Uniaxial stress-strain behaviour of aluminium alloy foams, *Acta Materialia*, Vol. 47, No. 8, pp. 2323-2330

Ministry of Construction of the People's Republic of China, 2010. Code for seismic design of buildings GB 50011-2010. s.l.: s.n.

Miyazaki, S., Imai, T., Otsuka, K. & Suzuki, Y., 1981, Luders-like deformation observed in the transformation pseudoelasticity of Ti-Ni Alloy, *Scripta Metallurgica*, Vol. 15, No. 8, pp. 853-856

Miyazaki, S., Imai, T., Igo,Y. & Otsuka, K., 1986, Effect of cyclic deformation on the pseudoelasticity characteristics of Ti-Ni alloys, *Metallurgical Transactions*, Vol. 17A, January, pp. 115-120

Miyazaki, S., Duerig, T.W. and Melton, K.N., 1990. Engineering aspects of shape memory alloys.

Moroni, M.O., Saldivia, R., Sarrazin, M. and Sepúlveda, A., 2002. Damping characteristics of a CuZnAlNi shape memory alloy. *Materials Science and Engineering: A*, *335*(1-2), pp.313-319.

Muller, I. & Xu, H., 1991, On the pseudo-elastic hysteresis, *Acta Metallurgica et Materialia*, Vol. 39, No. 2, pp. 263-271

Niitsu, K., Omori, T. and Kainuma, R., 2011. Superelasticity at low temperatures in Cu-17Al-15Mn (at%) shape memory alloy. *Materials transactions*, *52*(8), pp.1713-1715.

Omori, T. & Kainuma, R., 2013, Alloys with long memories, *Nature*, Vol. 502, 3rd October, pp. 42-44

Omori, T., Kusama, T., Kawata, S., Ohnuma, I., Sutou, Y., Araki, Y., Ishida, K. and Kainuma, R., 2013. Abnormal grain growth induced by cyclic heat treatment. *Science*, *341*(6153), pp.1500-1502.

Peng, Q.-Sh., 2013, Earthquake resistant performance of Chinese traditional architecture, MSc dissertation of University of Bath, UK

Piedboeuf, M.C. & Gauvin, R., 1998, Damping behaviour of shape memory alloys: strain amplitude, frequency and temperature effects, *Journal of Sound and Vibration*, Vol. 214, No. 5, pp. 885-901

Priestley, M.N., Seismic design and retrofit of bridges. 1996: John Wiley & Sons.

Principles for the Conservation of Heritage Sites in China, 2004, ICOMOS China, Getty Conservation Institude, Los Angeles

Principles for the Preservation of Historic Timber Structures, 1999, ICOMOS, 12th General Assembly, Mexico

Qi, Y.-T. and Chai, Z.-J., 1980, Renovation of the Main Hall of Nanchan Temple. *Cultural Relics*, ISSN：0511-4772, Vol. 11, pp. 61-75. (in simplified Chinese)

Qian, H., Li, H., Song, G. and Guo, W., 2013a. A constitutive model for superelastic shape memory alloys considering the influence of strain rate. *Mathematical Problems in Engineering*, *2013*.

Qian, H., Li, H.-N., Song, G.-B. & Guo, W., 2013b, Recentering shape memory alloy passive damper for structural vibration control, *Mathematical Problems in Engineering*, Vol. 2013, Article ID 963530

Qin S. and Yang N., 2016 "Investigation of damage condition of Chinese ancient timber buildings," *in Proceedings of the 14th International Symposium on Structural Engineering*, pp. 1390– 1395.

Qin, S., Yang, N. and Dai, L., 2018. Rotational behavior of column footing joint and its effect on the dynamic characteristics of traditional Chinese timber structure. *Shock and Vibration*, Vol 2018, pp. 1-13.

Saadat, S., Salichs, J., Noori, M., Hou, Z., Davoodi, H., Bar-on, I., Suzuki, Y. & Masuda, A., 2002, An overview of vibration and seismic applications of NiTi shape memory alloy, *Smart Materials and Structures*, Vol. 11, pp. 218-229

Saidi, I., Haritos, N., Gad, E.F. and Wilson, J.L., 2006. Floor vibrations due to human excitation-damping perspective. *Earthquake Engineering in Australia*, pp.257-264.

Seo, J.M., Choi, I.K. and Lee, J.R., 1999. Static and cyclic behavior of wooden frames with tenon joints under lateral load. *Journal of Structural Engineering*, *125*(3), pp.344-349.

Shaw, J.A. and Kyriakides, S., 1995. Thermomechanical aspects of NiTi. *Journal of the Mechanics and Physics of Solids*, *43*(8), pp.1243-1281.

Shi, Zh.-L., 1992, *"Field investigation of earthquakes in china"*, Earthquake Press, China

Singh, B. and Nanda, B.K., 2012. Estimation of damping in layered welded structures with unequal thickness. *Shock and Vibration*, *19*(6), pp.1463-1475.

Singh, N.K., Cadoni, E., Singha, M.K. and Gupta, N.K., Dynamic tensile and compressive behaviours of mild steel at wide range of strain rates, *Journal of Engineering Mechanics*, Vol. 139, pp. 1197-1206

Strnadel, B., Ohashi, S., Ohtsuka, H., Ishihara, T. and Miyazaki, S., 1995. Cyclic stress-strain characteristics of Ti-Ni and Ti-Ni-Cu shape memory alloys. *Materials Science and Engineering: A*, *202*(1-2), pp.148-156.

Song, G., Ma, N. & Li,H.-N., 2006, Applications of shape memory alloys in civil structures, *Engineering Structures*, Vol. 28, pp. 1266-1274

Soul, H., Isalgue, A., Yawny, A., Torra, V. and Lovey, F.C., 2010. Pseudoelastic fatigue of NiTi wires: frequency and size effects on damping capacity. *Smart Materials and Structures*, 19(8), p.085006.

Sutou, Y., Omori, T., Kainuma, R. and Ishida, K., 2008. Ductile Cu–Al–Mn based shape memory alloys: general properties and applications. *Materials Science and Technology*, 24(8), pp.896-901.

Suzuki, Y. and Maeno, M., 2006. Structural mechanism of traditional wooden frames by dynamic and static tests. *Structural Control and Health Monitoring: The Official Journal of the International Association for Structural Control and Monitoring and of the European Association for the Control of Structures*, *13*(1), pp.508-522.

Tamai, H. & Kitagawa, Y., 2002, Pseudoelastic behaviour of shape memory alloy wire and its application to seismic resistance member for building, *Computational Materials Science*, Vol. 25, pp. 218-227

Tanaka,K. & Sasaki,Y., 2000, Hysteretic performance of shear panel dampers of ultra low-yield-strength steel for seismic response control of buildings, *12th World Conference on Earthquake Engineering*, 30th Jan-4th Feb 2000, New Zeland

The origin and evolution of Dou-Gon, 2011, Ministry of Culture of P.R. China.

Thomson, P., Balas, G.J. & Leo, P.H., 1995, The use of shape memory alloys for passive structural damping, *Smart Materials and Structures*, Vol. 4, pp. 36-42

Tian, P.-G. and Zhang, F.-L., 2014, Seismic damage analysis and strengthening methods of ancient timber structures. *World Earthquake Engineering*, Vol. 30 (3), pp. 126-133. (in simplified Chinese)

Torra, V., Isalgue, A., Auguet, C., Carreras, G., Lovey, F.C., Soul, H. & Terriault, P., 2009, Damping in civil engineering using SMA. The fatigue behaviour and stability of CuAlBe and NiTi alloys, *Journal of Materials Engineering and Performance*, Vol. 18, pp. 738-745

Tsai, P.-H., 2009, *Seismic evaluation of traditional timber structures in Taiwan*, PhD dissertation of University of Bath, UK

Tsai, P.-H. & D'Ayala, D., 2011, Performance-based seismic assessment method for Taiwanese historic Dieh-Dou timber structures, *Earthquake Engineering and Structural Dynamics*, Vol. 40, pp 709-729

Tsuwa, I., Koshihara, M., Fujita, K. and Sakamoto, I., 2008, A study on the size effect of bracket complexes used in traditional timber structures on the vibration characteristics, *In: Proceedings of 10th World Conference on Timber Engineering,* Miyazaki, Japan.

Wolons, D., Gandhi, F., Malovrh, B., 1998, Experimental investigation of the pseudoelastic hysteresis damping characteristics of shape memory alloy wires, *Journal of Intelligent Material Systems and Structures*, Vol. 9, pp. 116–126

Xie, Q.-F., Zhao, H.-T., Xue, J.-Y., Yao, K. and Sui, Y., 2008, An Experimental Study on the Strengthening of mortise-tenon Joints in Ancient Chinese Wooden Buildings. *China Civil Engineering Journal*, Vol. 41(1), pp. 28-34. (in simplified Chinese)

Xie, W.-J., 2012, Seismic performance under static loadings of complex brackets as used in traditional oriental timber temples, MEng Dissertation of University of Bath, UK

Xue, J.Y., Wu, Z.J., Zhang, F.L. and Zhao, H.T., 2015. Seismic damage evaluation model of Chinese ancient timber buildings. *Advances in Structural Engineering*, *18*(10), pp.1671-1683.

Yeo, S.Y., Hsu, M.F., Komatsu, K., Chung, Y.L. and Chang, W.S., 2016a. Shaking table test of the Taiwanese traditional Dieh-Dou timber frame. *International Journal of Architectural Heritage*, *10*(5), pp.539-557.

Yeo, S.Y., Komatsu, K., Hsu, M.F. and Que, Z., 2016b. Mechanical model for complex brackets system of the Taiwanese traditional Dieh-Dou timber structures. *Advances in Structural Engineering*, *19*(1), pp.65-85.

Yin, Y.-J. & Li, D., 2010, Evolvement of bucket arch and Chinese traditional buildings forms, *Interior Architecture of China*, Vol. 5, pp 198-200, (in simplified Chinese)

Yu, M.-H., Liu, X.-D. & Fang, D.-Q., 1986, On-site pulsating and sinusoidal excitation test of arrow tower, *Science and Technology Report of Xi'an Jiaotong Univercity*, (in simplified Chinese)

Yu, M.-H., Liu, X.-D. & Fang, D.-Q., 1991, An experimental study of static and dynamic characteristics on the Front Tower over the Ancient Xi'an City Wall, *Journal of Xi'an Jiaotong Univercity*, Vol. 25, No. 3, pp 55-62, (in simplified Chinese)

Yu, M.-H., Oda, Y., Fang, D.-P. & Zhao, J.-H., 2008, Advances in structural mechanics of Chinese ancient architectures, *Frontiers of Structural and Civil Engineering*, Vol. 2, No. 1, pp 1-25

Zhang, Ch.-F., Zhang, Zh.-Sh. & Zhang, Q.-J., 2012, Static and dynamic cyclic performance of a low-yield-strength steel shear panel damper, *Journal of Constructional Steel Research*, Vol. 79, pp. 195-203

Zhang, F.-L. 2013, Research on Strengthening and Its Performance of Chinese Ancient Timber Structures. *PhD dissertation, Xi'an University of Architecture & Technology*. (in simplified Chinese)

Zhang, X.C., Xue, J.Y., Zhao, H.T. and Sui, Y., 2011. Experimental study on Chinese ancient timber-frame building by shaking table test. *Structural Engineering and Mechanics*, *40*(4), pp.453-469.

Zhang, X.-F., Zhang, J., Qiao,L., Shi, A.-S., Zhang, Y.-G., He, Y. and Guan,Z.-W., 2013, Experimental study of the compression properties of Al/W/PTFE granular composites under elevated strain rates, *Material Science and Engineering A*, Vol. 581, pp. 48-55

Zhao, J.-H., Yu, M.-H. and Yang, S.-Y., 1999, An experimental study for the dynamic characteristics of 'Dougong' one of the wooden structure parts in ancient architecture of China. *Journal of Experimental Mechanics*, Vol, 14(1), pp. 106–112 (in simplified Chinese)

Zhou, Y.-L., 2007, An analysis on the ancient construction Dougong's characteristic, *Journal of Hunan International Economics University*, Vol. 7, No. 2, June, 2007, pp 75-77, (in simplified Chinese)

Appendix A: Statement of Authorship

<table>
<tr><th colspan="10">This declaration concerns the article entitled:</th></tr>
<tr><td colspan="10">Enhancing the seismic performance of historic timber buildings in Asia by applying super-elastic alloy to a Chinese complex bracket system</td></tr>
<tr><td colspan="10">Publication status (tick one)</td></tr>
<tr><td>Draft manuscript</td><td></td><td>Submitted</td><td></td><td>In review</td><td></td><td>Accepted</td><td></td><td>Published</td><td>✓</td></tr>
<tr><td>Publication details (reference)</td><td colspan="9">Xie, W., Araki, Y. and Chang, W.S., 2018. Enhancing the seismic performance of historic timber buildings in Asia by applying super-elastic alloy to a Chinese complex bracket system. International Journal of Architectural Heritage, 12(4), pp.734-748.</td></tr>
<tr><td>Candidate's contribution to the paper (detailed, and also given as a percentage).</td><td colspan="9">The candidate contributed to/ considerably contributed to/predominantly executed the…

Formulation of ideas: 90%
I formulated the idea of this paper and discussed with other co-authors.

Design of methodology: 90%
10% of the work is from the discussion with other co-authors.

Experimental work: 100%
I conducted the experimental tests in the lab at University of Bath.

Presentation of data in journal format: 90%
I wrote the academic paper, and other co-authors improved the quality.</td></tr>
<tr><td>Statement from Candidate</td><td colspan="9">This paper reports on original research I conducted during the period of my Higher Degree by Research candidature.</td></tr>
<tr><td>Signed</td><td colspan="5"></td><td>Date</td><td colspan="3"></td></tr>
</table>

This declaration concerns the article entitled:									
Static Experimental Study of Two-Layer Dou-Gon System by Using Super-Elastic Alloy as A Connection Material									
Publication status (tick one)									
Draft manuscript		**Submitted**		**In review**		**Accepted**	✓	**Published**	
Publication details (reference)	**Xie, W.** and Chang, W.S., 2018. Static Experimental Study of Two-Layer Dou-Gon System by Using Super-Elastic Alloy as A Connection Material. Submitted to Engineering History and Heritage.								
Candidate's contribution to the paper (detailed, and also given as a percentage).	The candidate contributed to/ considerably contributed to/predominantly executed the… Formulation of ideas: 90% I formulated the idea of this paper and discussed with co-author. Design of methodology: 90% 10% of the work is from the discussion with co-author. Experimental work: 100% I conducted the experimental tests in the lab at University of Bath. Presentation of data in journal format: 95% I wrote the academic paper, and the co-author improved the quality.								
Statement from Candidate	This paper reports on original research I conducted during the period of my Higher Degree by Research candidature.								
Signed						**Date**			

This declaration concerns the article entitled:									
Dynamic experimental and parametric studies of two-layer Dou-Gon system by using super-elastic alloy as a connection material									
Publication status (tick one)									
Draft manuscript		**Submitted**		**In review**	✓	**Accepted**		**Published**	
Publication details (reference)	**Xie, W.** and Chang, W.S., Dynamic experimental and parametric studies of two-layer Dou-Gon system by using super-elastic alloy as a connection material. Submitted to Proceedings of the Institution of Civil Engineers - Civil Engineering.								
Candidate's contribution to the paper (detailed, and also given as a percentage).	The candidate contributed to/ considerably contributed to/predominantly executed the… Formulation of ideas: 90% I formulated the idea of this paper and discussed with co-author. Design of methodology: 90% 10% of the work is from the discussion with co-author. Experimental work: 100% I conducted the experimental tests in the lab at University of Bath. Presentation of data in journal format: 95% I wrote the academic paper, and the co-author improved the quality.								
Statement from Candidate	This paper reports on original research I conducted during the period of my Higher Degree by Research candidature.								
Signed						**Date**			

Appendix II: Permission to use the published academic paper

Copyright Clearance Center RightsLink®

Home | Account Info | Help

Taylor & Francis
Taylor & Francis Group

Journal Reprints

Title: Enhancing the seismic performance of historic timber buildings in Asia by applying super-elastic alloy to a Chinese complex bracket system

Author: Wenjun Xie, , Yoshikazu Araki, et al

Publication: International Journal of Architectural Heritage

Publisher: Taylor & Francis

Date: May 19, 2018

Rights managed by Taylor & Francis

Logged in as:
Wenjun Xie
LOGOUT

Thesis/Dissertation Reuse Request

Taylor & Francis is pleased to offer reuses of its content for a thesis or dissertation free of charge contingent on resubmission of permission request if work is published.

BACK | CLOSE WINDOW